A STUDY ON THE IMPACT OF TRANSIENT SEEPAGE ON TIDAL FRONT EMBANKMENT

THESIS WORK (PG/CE/TH/21)

SUBMITTED IN THE PARTIAL FULFILLMENT FOR THE AWARD OF DEGREE IN MASTER OF CIVIL ENGINEERING IN "SOIL MECHANICS & FOUNDATION ENGINEERING"

Submitted by:

KAUSTUV BHATTACHARYA
Class Roll No: 001410402002
Exam Roll : M4CIV1603
Registration No. 128859 Of 14-15

Under the Supervision of

DR. GUPINATH BHANDARI, Associate Professor

DEPARTMENT OF CIVIL ENGINEERING
JADAVPUR UNIVERSITY
KOLKATA-700032

2016

DEPARTMENT OF CIVIL ENGINEERING
FACULTY OF ENGINEERING & TECHNOLOGY
JADAVPUR UNIVERSITY, KOLKATA-700-032

DECLARATION

This is to declare that the thesis work titled **"A STUDY ON THE IMPACT OF TRANSIENT SEEPAGE ON TIDAL FRONT EMBANKMENT"** submitted in the partial fulfillment for the award of degree in Master of Civil Engineering in "Soil Mechanics & Foundation Engineering" is an original piece of research work presented in accordance with academic rules and ethical conduct. I also declare that all references used in the formulation of this work has been cited to the best of my knowledge.

KAUSTUV BHATTACHARYA
ROLL NO.001410402002
EXAM ROLL : M4CIV1603
REGISTRATION NO. 128859 OF 14-15

DATE :
PLACE :

DEPARTMENT OF CIVIL ENGINEERING
FACULTY OF ENGINEERING & TECHNOLOGY
JADAVPUR UNIVERSITY, KOLKATA-700-032

CERTIFICATE OF RECOMMENDATION

This is to certify that the following thesis prepared under my supervision titled **"A STUDY ON THE IMPACT OF TRANSIENT SEEPAGE ON TIDAL FRONT EMBANKMENT"** presented by **SHRI KAUSTUV BHATTACHARYA** be accepted as a partial fulfillment to the requirements for the Degree of Master of Civil Engineering in Soil Mechanics & Foundation Engineering from this University.

- ----------

DR. GUPINATH BHANDARI
ASSOCIATE PROFESSOR
DEPARTMENT OF CIVIL ENGINEERING
FACULTY OF ENGINEERING AND TECHNOLOGY
JADAVPUR UNIVERSITY

COUNTERSIGNED:

- ----------

DR. R.B.SAHU
HEAD OF THE DEPARTMENT
DEPARTMENT OF CIVIL ENGINEERING
FACULTY OF ENGINEERING AND TECHNOLOGY
JADAVPUR UNIVERSITY

- ----------

DEAN
FACULTY OF ENGINEERING AND TECHNOLOGY
JADAVPUR UNIVERSITY

DEPARTMENT OF CIVIL ENGINEERING
FACULTY OF ENGINEERING & TECHNOLOGY
JADAVPUR UNIVERSITY, KOLKATA-700-032

CERTIFICATE OF APPROVAL

The foregoing thesis entitled **"A STUDY ON THE IMPACT OF TRANSIENT SEEPAGE ON TIDAL FRONT EMBANKMENT"** was presented satisfactorily to warrant its acceptance as a pre-requisite to the Degree of Master of Civil Engineering in Soil Mechanics & Foundation Engineering from this University. It is understood that by this approval, the undersigned do not necessarily approve of any statement expressed or any conclusion drawn, but approve this thesis for the purpose for which it is submitted.

BOARD OF EXAMINERS:

- ----------

- ----------

- ----------

(SIGNATURE OF EXAMINERS)

PREFACE

This research document is the result of my dissertation work to complete my Master's in Soil Mechanics and Foundation Engineering from Jadavpur University, Kolkata, India. I have tried my level best to remain scientific in my methods and approach of the problem and sincerely apologize for any inadvertent error that might have crept in.

I would like to express my gratitude to Dr. G Bhandari, Associate Professor, Civil Engineering Department, Jadavpur University, for his introduction of this thesis problem which sparked a general interest within me from the very first day. His constant guidance and moral support throughout the course of this dissertation helped me in several ways.

I am indebted to Dr. S.P Mukherjee for his constant guidance in this project. I would like to thank him for his patient hearing of all the problems I faced during both the laboratory testing and numerical analysis of the problem and for also arranging site data and materials for testing, organizing a discussion panel on this topic at IIT-Kharagpur.

I would like to thank the Irrigation Works Department, Government of West Bengal, for arranging site materials for development of the experimental model.

I would like to thank Dr. R.B. Sahu, Head of Civil Engineering Department, Jadavpur University for his back up and support during this project.

I would like to thank Prof. S.Ghosh, Prof. S.K.Biswas, and Prof. P. Aitch for their guidance and inspiration.

A special word of thanks to Mr. Amitava Chakroborty for his constant guidance. From our workshop visit days to Banshdroni during fabrication of the experimental model, to the Indian Geotechnical Conference-2015, Pune to the entire laboratory testing stage, each and every moment problems faced were discussed and solutions worked out to the best of our knowledge.

I would like to thank Mr. Robin Pal, Mr. Apurba Banerjee, Mr. Ranjit Kushari, Mr. Bidyut Ghosh for their immense support in laboratory aspect of this project.

Very special thanks to my parents for their constant motivation, moral support and guidance throughout this project. Even back home, I had discussions with them on various aspects of the project and received invaluable advice.

Last but certainly not the least my classmates of PG (2014-16) and Research Scholars of the Geotechnical Section, Jadavpur University also deserve a special mention.

KAUSTUV BHATTACHARYA

CONTENTS

SUBJECT	PAGE NO.
LIST OF TABLES	**i**
LIST OF FIGURES	**ii-v**
ABBREVIATIONS AND NOTATIONS USED	**vi-vii**
ABSTRACT	**viii**
1 CHAPTER ONE : INTRODUCTION	**1- 40**
1.1 TOPIC INTRODUCTION	**1**
1.2 PRESENTATION OF CONTENTS	**1**
1.3 GENERAL THEORETICAL BACKGROUND	**2**
1.3.1 Embankment Types	2
1.3.2 General Seepage Theory	4
1.3.2.1 Steady State	*6*
1.3.2.2 Boundary Conditions	*8*
1.3.2.3 Transient State	*9*
1.3.3 Tidal Variations : Rise-Up and Draw-Down Conditions	10
1.3.4 Soil Water Characteristics Curve	11
1.3.4.1 Volumetric Water Content Function and its Estimation	*12*
1.3.4.1.1 General	*12*
1.3.4.1.2 Estimation Techniques for VWC Function	*14*
1.3.4.2 Hydraulic Conductivity Function and its Estimation	*17*
1.3.4.2.1 General	*17*
1.3.4.2.2 Estimation Techniques for Hydraulic Conductivity Function	*18*
1.3.5 Slope Stability Analysis of Earthen Embankments	20
1.3.5.1 General	*20*
1.3.5.2 Methodology	*21*
1.3.6 Applications of Finite Element Method in Geotechnical Engineering	23
1.3.6.1 General	*23*
1.3.6.1.1 Governing Principles and Terminologies	*26*
1.3.6.1.2 Procedural Description	*29*
1.3.6.2 Application of F.E.M in Seepage Related Problems	*30*
1.3.6.2.1 Mathematical Background	*31*
1.3.6.3 Numerical Modeling using F.E.M based Computer Software	*33*
1.3.6.3.1 Modeling with SEEP/W	*34*

SUBJECT **PAGE NO.**

1.3.6.3.2 Modeling with SIGMA/W 37

1.3.6.3.3 Modeling with SLOPE/W 38

1.3.7 Experimental Modeling Techniques 39

1.3.7.1 General *39*

1.3.7.2 Scaling for Model and Prototype *39*

2 CHAPTER TWO : LITERATURE REVIEW **41- 51**

2.1 STEADY STATE SEEPAGE **41**

2.2 TRANSIENT STATE SEEPAGE **42**

2.3 SOIL WATER CHARACTERISTICS CURVE **47**

2.4 HYDRAULIC AND GEOTECHNICAL SCALING **48**

2.5 SLOPE STABILITY ANALYSIS **49**

2.6 RELEVANCE OF PAST STUDIES **51**

3 CHAPTER THREE : OBJECTIVE AND SCOPE OF PRESENT STUDY **52**

3.1 OBJECTIVE OF PRESENT STUDY **52**

3.2 SCOPE OF PRESENT STUDY **52**

4 CHAPTER FOUR : STUDY AREA **53- 56**

4.1 GENERAL INFORMATION ON SUNDERBAN REGION **53**

4.2 TYPICAL SOIL PROFILE OF SUNDERBAN REGION **54**

4.3 DETAILS OF TYPICAL SUNDERBAN EMBANKMENT **55**

4.4 STUDY AREA PICTURE TEMPLATE **56**

5 CHAPTER FIVE : NUMERICAL ANALYSIS BY FINITE ELEMENT METHOD **57- 110**

5.1 GENERAL **57**

5.2 METHODOLOGY **57**

5.2.1 Geometry 57

5.2.2 Material Properties 58

5.2.3 Boundary Conditions 61

5.2.4 Mesh Properties 63

5.2.5 Convergance and Time Stepping 64

5.2.6 Deformation based Coupled Analysis 65

5.3 FLOWCHART REPRESENTATION OF METHODOLOGY **66**

5.3.1 Flowchart defining Methodology followed during Uncoupled Analysis 66

5.3.2 Flowchart defining Methodology followed during Coupled Analysis 67

5.4 PARAMETRIC STUDY **68**

5.5 RESULTS AND DISCUSSIONS FOR MODEL $SDBN_0$ **68**

SUBJECT **PAGE NO.**

5.5.1 Phreatic Line and its Dynamics 68
5.5.2 Flux Distribution at Various Sections 71
5.5.3 Distribution of Equipotential Line Contours 73
5.5.4 Pore Water Pressure Distribution 78
5.5.5 Deformation based Analysis 81
5.5.6 Slope Stability Analysis 85
5.6 RESULTS AND DISCUSSIONS FOR MODEL $SDBN_{3.5}$ 90
5.6.1 Phreatic Line and its Dynamics 90
5.6.2 Flux Distribution at Various Sections 93
5.6.3 Distribution of Equipotential Line Contours 94
5.6.4 Pore Pressure Distribution 100
5.6.5 Deformation based Analysis 102
5.6.6 Slope Stability Analysis 106

6 CHAPTER SIX : EXPERIMENTAL PROGRAMME AND RESULTS 111- 124
6.1 GENERAL 111
6.2 METHODOLOGY 111
6.3 DEVELOPMENT AND COMMISSIONING OF SEEPAGE SET-UP 112
6.3.1 Development of Seepage Tank 112
6.3.2 Soil Properties 112
6.3.3 Construction of Embankment 114
6.3.4 Piezometer Set-Up 114
6.4 SCHEME OF EXPERIMENTAL SET-UP 117
6.5 PARAMETRIC STUDY 117
6.6 RESULTS AND DISCUSSIONS 118

7 CHAPTER SEVEN : VALIDATION AND DISCUSSIONS 125- 128
7.1 METHODOLOGY 125
7.2 VALIDATION 125
7.3 DISCUSSION ON THE SUNDERBAN PROBLEM 128

8 CHAPTER EIGHT : CONCLUSIONS AND FUTURE SCOPE OF WORK 129- 130
8.1 CONCLUSIONS 129
8.2 FUTURE SCOPE OF WORK 130

REFERENCES 131- 134

LIST OF TABLES

TABLE NO.	NOMENCLATURE	PAGE NO.
1.1	Classification Of Finite Element Methods In Solid Mechanics	28
1.2	Generalization Of Finite Element Methods pertaining to Seepage	30
1.3	Parameter Scale Ratio as per Froude Model Law	40
4.1	Details of Borehole–I, Pathar-Pratima (Government 283 ICDS Centre, Kuimuri)	54
4.2	Dimension Details Of Typical Sunderban Embankment	55
5.1	Material Properties of the Models $SDBN_0$ and $SDBN_{3.5}$ used in F.E.M analysis	60
5.2	Boundary Conditions of the Models $SDBN_0$ and $SDBN_{3.5}$	63
5.3	Slip Surface Location, Minimum Factor of Safety, Safety Map for Model $SDBN_0$ during Rise-Up Stage (t = 1 hr to t = 6 hrs) of Single Tidal Cycle	88
5.4	Slip Surface Location, Minimum Factor of Safety, Safety Map for Model $SDBN_0$ during Draw-down Stage (t = 7 hrs to t = 12 hrs) of Single Tidal Cycle	89
5.5	Slip Surface Location, Minimum Factor of Safety, Safety Map for Model $SDBN_{3.5}$ during Rise-Up Stage (t = 1 hr to t = 6 hrs) of Single Tidal Cycle	108
5.6	Slip Surface Location, Minimum Factor of Safety, Safety Map for Model $SDBN_{3.5}$ during Draw-down Stage (t = 7 hrs to t = 12 hrs) of Single Tidal Cycle	109
6.1	Soil Properties for Experimental Model	113
6.2	Piezometer Positions Inside Embankment constructed in Laboratory	115
6.3	Parametric Study Tests Conducted in the Laboratory	118
7.1	Scaling Ratio as per Froude Scaling Methodology	125

LIST OF FIGURES

FIGURE NO.	NOMENCLATURE	PAGE NO.
1.1	General Arrangement of Homogenous Earthen Embankment showing Phreatic Surface	3
1.2	General Arrangement of Zone Embankment	3
1.3	Casagrande Method for Determination of Phreatic Surface	8
1.4	A typical VWC v/s Pore water pressure plot	13
1.5	Plot showing Best estimate of VWC function for El-Paso sand (Zapata etal 2006)	13
1.6	Plot showing Best estimate of VWC function for Price Club silt (Zapata etal 2006)	13
1.7	Plot showing Best estimate of VWC function for Fountain Hills clay (Zapata etal 2006)	14
1.8	Plot showing Specified Hydraulic conductivity functions as per Thieu etal (2001)	17
1.9	Force distribution on a slice within the sliding wedge with a circular slip surface	22
1.10	General Limit Equilibrium Plot showing Factor of Safety v/s Lambda	22
1.11	The enhanced Burland Triangle (after Anon. 1999)	23
1.12	Built in sample set of VWC functions in SEEP/W, Geostudio	35
4.1	Typical Sunderbans Embankment With Tidal Head Variation Of 4 Meters	55
4.2	Map Of Sunderbans Region	56
4.3	Picture showing Sonakhali Site During Rise-Up	56
4.4	Picture showing Sonakhali Site During Draw-Down	56
4.5 (a) (b) (c)	3D Model for Typical Sunderbans Embankment showing Tidal Phase	56
5.1	Geometry of the Finite Element Model for Sunderban embankment model $SDBN_0$	58
5.2	Geometry of the Finite Element Model for Sunderban embankment model $SDBN_{3.5}$	58
5.3	Grain Size Distribution for Sunderban Clayey Silt with percentage components	59
5.4	Volumetric Water Content function for Sunderban Clayey Silt	60
5.5	Volumetric Water Content versus Pore Water Pressure for Sunderban Clayey Silt	61
5.6	Hydraulic Conductivity function for Sunderban Clayey Silt	61
5.7	Tidal Boundary Condition – Sunderbans Rise-Up Curve for a Single Tidal cycle	62
5.8	Tidal Boundary Condition – Sunderbans Draw-down Curve for a Single Tidal Cycle	62
5.9	Tidal Boundary Condition for Multiple Cycles (120 cycles over a duration of 2 months)	62
5.10	Mesh arrangement showing nodes and elements for both the models $SDBN_0$ and $SDBN_{3.5}$	64
5.11(a)	Flowchart of Sequence of Uncoupled Analysis for a Single Tidal Cycle	66
5.11(b)	Flowchart of Sequence of Coupled Analysis for a Single Tidal Cycle	67
5.12	Steady State Phreatic Surface for $SDBN_0$	69
5.13	Dynamics of Phreatic Surface during Rise-Up Condition of a Single Cycle for $SDBN_0$	69
5.14	Dynamics of Phreatic Surface during Draw-down Condition of a Single Cycle for $SDBN_0$	70
5.15	Dynamics of Phreatic Surface during Multiple Cycles for $SDBN_0$	70
5.16	Magnified Image showing Dynamics of Phreatic Line with tidal cycles for $SDBN_0$	71
5.17	Location of Flux Sections for Monitoring flux rate in $SDBN_0$	71

FIGURE NO.	NOMENCLATURE	PAGE NO.
5.18	Variation of flux across sections with Rise up and Draw-down for $SDBN_0$	72
5.19	Effect of Multiple Tidal Cycles on Flux across sections for $SDBN_0$	72
5.20	Steady State Equipotential Lines for LTL position at t = 0 hr for $SDBN_0$.	74
5.21, 5.22, 5.23, 5.24, 5.25, 5.26	Equipotential Line Contour during Rise-Up condition of a Single Cycle at t = 1, 2, 3, 4, 5, 6 hrs for $SDBN_0$	74-75
5.27, 5.28, 5.29, 5.30, 5.31, 5.32	Equipotential Line Contour during Draw-down condition of a Single Cycle at t = 7, 8, 9, 10, 11, 12 hrs for $SDBN_0$	75-76
5.33, 5.34, 5.35, 5.36, 5.37, 5.38	Equipotential Line Contour at the end of Multiple Tidal cycles, n = 2, 5, 10, 50, 70, 120 for $SDBN_0$	77-78
5.39	PWP Variation by Uncoupled Analysis during Single Tidal Cycle in Lower Slope region of *$SDBN_0$*	79
5.40	PWP Variation by Uncoupled Analysis during Single Tidal Cycle in Berm portion of *$SDBN_0$*	79
5.41	PWP Variation by Uncoupled Analysis during Single Tidal Cycle in Upper Slope Region of *$SDBN_0$*	80
5.42	PWP Variation by Uncoupled Analysis during Single Tidal Cycle in Interior of Embankment of *$SDBN_0$*	80
5.43	Pore Water Pressure Contour at Steady State Condition for *$SDBN_0$*	80
5.44	Pore Water Pressure Contour at end of 1st Cycle for *$SDBN_0$*	80
5.45, 5.46, 5.47, 5.48	Pore Water Pressure Contour at end of n = 5, 10, 60, 120 cycles for *$SDBN_0$*	81
5.49	PWP Variation by Coupled Analysis during Single Cycle in the Lower Slope of *$SDBN_0$*	83
5.50	Vertical deformation during Single Cycle in the Lower Slope of *$SDBN_0$*	83
5.51	PWP Variation by Coupled Analysis during Single Cycle in the Berm Region of *$SDBN_0$*	84
5.52	Vertical deformation during Single Cycle in the Berm Region of *$SDBN_0$*	84
5.53	PWP Variation by Coupled Analysis during Single Cycle in the Upper Slope Region of *$SDBN_0$*	84
5.54	Vertical deformation during Single Cycle in the Upper Slope Region of *$SDBN_0$*	84
5.55	PWP Variation by Coupled Analysis during Multiple Cycles in the Lower Slope of *$SDBN_0$*	84
5.56	Variation in Vertical Deformation during Multiple Cycles in the Lower Slope of *$SDBN_0$*	84
5.57	PWP Variation by Coupled Analysis during Multiple Cycles in the Berm region of model *$SDBN_0$*	85
5.58	Variation in Vertical Deformation during Multiple Cycles in the Berm region of model *$SDBN_0$*	85
5.59	PWP Variation by Coupled Analysis during Multiple Cycles in the Upper Slope of *$SDBN_0$*	85
5.60	Variation in Vertical Deformation during Multiple Cycles in the Upper Slope of *$SDBN_0$*	85
5.61	Slip surfaces, Minimum F.O.S and Safety Map during Steady State conditions for *$SDBN_0$*	86
5.62, 5.63, 5.64, 5.65, 5.66, 5.67	Slip Surface Location, Minimum Factor of Safety, Safety Map for $SDBN_0$ during Rise-Up Stage (t = 1, 2, 3, 4, 5, 6 hrs) of Single Tidal Cycle	88

FIGURE NO.	NOMENCLATURE	PAGE NO.
5.68, 5.69, 5.70, 5.71, 5.72, 5.73	Slip Surface Location, Minimum Factor of Safety, Safety Map for $SDBN_0$ during Draw-down Stage (t = 7, 8, 9, 10, 11, 12hrs) of Single Tidal Cycle	89
5.74	A plot of the F.O.S against Time during a Single Tidal Cycle in Uncoupled and Coupled Analysis respectively for $SDBN_0$	90
5.75	A plot of the Minimum F.O.S against Number of Tidal Cycles for $SDBN_0$	90
5.76	Steady State Phreatic Surface for $SDBN_{3.5}$	91
5.77	Dynamics of Phreatic Surface during Rise-Up Condition of a Single Cycle for $SDBN_{3.5}$	91
5.78	Dynamics of Phreatic Surface during Draw-down Condition of a Single Cycle for $SDBN_{3.5}$	92
5.79	Dynamics of Phreatic Surface during Multiple Cycles for $SDBN_{3.5}$	92
5.80	Magnified Image showing Dynamics of Phreatic Line with tidal cycles for $SDBN_{3.5}$	93
5.81	Location of Flux Sections for Monitoring flux rate in $SDBN_{3.5}$	93
5.82	Variation of flux across sections with Rise up and Draw-down for $SDBN_{3.5}$	94
5.83	Effect of Multiple Tidal Cycles on Flux across sections for $SDBN_{3.5}$	94
5.84	Steady State Equipotential Lines for LTL position at t = 0 hr for $SDBN_{3.5}$.	96
5.85, 5.86, 5.87, 5.88, 5.89, 5.90	Equipotential Line Contour during Rise-Up condition of a Single Cycle at t = 1, 2, 3, 4, 5, 6 hrs for $SDBN_{3.5}$	96-97
5.91, 5.92, 5.93, 5.94, 5.95, 5.96	Equipotential Line Contour during Draw-down condition of a Single Cycle at t = 7, 8, 9, 10, 11, 12 hrs for $SDBN_{3.5}$	97-98
5.97, 5.98, 5.99, 5.100, 5.101, 5.102	Equipotential Line Contour at the end of Multiple Tidal cycles, n = 2, 5, 10, 50, 70, 120 for $SDBN_{3.5}$	98-99
5.103	PWP Variation by Uncoupled Analysis during Single Tidal Cycle in Lower Slope region of $SDBN_{3.5}$	100
5.104	PWP Variation by Uncoupled Analysis during Single Tidal Cycle in Berm portion of $SDBN_{3.5}$	100
5.105	PWP Variation by Uncoupled Analysis during Single Tidal Cycle in Upper Slope Region of $SDBN_{3.5}$	101
5.106	PWP Variation by Uncoupled Analysis during Single Tidal Cycle in Interior of Embankment of $SDBN_{3.5}$	101
5.107	Pore Water Pressure Contour at Steady State Condition for $SDBN_{3.5}$	101
5.108	Pore Water Pressure Contour at end of 1st Cycle for $SDBN_{3.5}$	101
5.109, 5.110, 5.111, 5.112	Pore Water Pressure Contour at end of n = 5, 10, 60, 120 cycles for $SDBN_{3.5}$	102
5.113	PWP Variation by Coupled Analysis during Single Cycle in the Lower Slope of $SDBN_{3.5}$	104
5.114	Vertical deformation during Single Cycle in the Lower Slope of $SDBN_{3.5}$	104
5.115	PWP Variation by Coupled Analysis during Single Cycle in the Berm Region of $SDBN_{3.5}$	104
5.116	Vertical deformation during Single Cycle in the Berm Region of $SDBN_{3.5}$	104
5.117	PWP Variation by Coupled Analysis during Single Cycle in the Upper Slope Region of $SDBN_{3.5}$	105
5.118	Vertical deformation during Single Cycle in the Upper Slope Region of $SDBN_{3.5}$	105

FIGURE NO.	NOMENCLATURE	PAGE NO.
5.119	PWP Variation by Coupled Analysis during Multiple Cycles in the Lower Slope of *SDBN$_{3.5}$*	105
5.120	Variation in Vertical Deformation during Multiple Cycles in the Lower Slope of *SDBN$_{3.5}$*	105
5.121	PWP Variation by Coupled Analysis during Multiple Cycles in the Berm region of *SDBN$_{3.5}$*	105
5.122	Variation in Vertical Deformation during Multiple Cycles in the Berm region of *SDBN$_{3.5}$*	105
5.123	PWP Variation by Coupled Analysis during Multiple Cycles in the Upper Slope of *SDBN$_{3.5}$*	106
5.124	Variation in Vertical Deformation during Multiple Cycles in the Upper Slope of *SDBN$_{3.5}$*	106
5.125	Slip surfaces, Minimum F.O.S and Safety Map during Steady State conditions for *SDBN$_{3.5}$*	106
5.126, 5.127, 5.128, 5.129, 5.130, 5.131	Slip Surface Location, Minimum Factor of Safety, Safety Map for SDBN$_{3.5}$ during Rise-Up Stage (t = 1, 2, 3, 4, 5, 6 hrs) of Single Tidal Cycle	108
5.132, 5.133, 5.134, 5.135, 5.136, 5.137	Slip Surface Location, Minimum Factor of Safety, Safety Map for SDBN$_{3.5}$ during Draw-down Stage (t = 7, 8, 9, 10, 11, 12hrs) of Single Tidal Cycle	109
5.138	A plot of the F.O.S against Time during a Single Tidal Cycle in Uncoupled and Coupled Analysis respectively for SDBN$_{3.5}$	110
5.139	A plot of the Minimum F.O.S against Number of Tidal Cycles for Model SDBN$_{3.5}$	110
6.1	Grain Size distribution of Sunderban Soil Sample used in Laboratory tests	113
6.2	Stress – Strain Plot obtained from UU test for Laboratory Model Embankment	113
6.3, 6.4, 6.5, 6.6, 6.7, 6.8, 6.9	Construction Stages of the Laboratory Embankment Model	116
6.10	Seepage Set-up developed at Geotechnical Engineering Laboratory, Jadavpur University	117
6.11, 6.12, 6.13, 6.14, 6.15, 6.16, 6.17	Excess PWP Head v/s Tidal Cycle Time for 1R$_{30}$D$_{30}$, 1R$_{45}$D$_{45}$, 1R$_{60}$D$_{60}$, 1R$_{90}$D$_{90}$, 1R$_{120}$D$_{120}$, 1R$_{150}$D$_{150}$, 1R$_{180}$D$_{180}$	121-122
6.18	Effect of Tidal Rate on the Excess PWP developed in the Lower Slope	122
6.19	Effect of Tidal Rate on the Excess PWP developed in the Berm Region	122
6.20	Effect of Tidal Rate on the Excess PWP developed in the Upper Slope	123
6.21	Effect of Tidal Rate on the Excess PWP developed in the Embankment Interior	123
6.22, 6.23, 6.24	Excess PWP Head during Multiple Cycles for 3R$_{30}$D$_{30}$, 3R$_{60}$D$_{60}$, 3R$_{90}$D$_{90}$	123
6.25	Low Tide Position with Excess River Water Head = 0 cm	124
6.26	High Tide Position with Excess River Water Head = 20 cm	124
6.27	Flowlines due to Transient seepage during Tidal Cycle	124
6.28 (a)	Magnified view of Lower Slope showing development of cracks after multiple tidal cycles	124
6.28 (b)	Magnified view of Lower Slope	124
7.1	Comparison of Results for Excess PWP in Lower Slope for Single Cycle	127
7.2	Comparison of Results for Excess PWP in Berm Region for Single Cycle	127
7.3	Comparison of Results for Excess PWP in Upper Slope for Single Cycle	127

ABBREVIATIONS AND NOTATIONS USED

ABBREVIATIONS

HTL – High Tide Level
LTL – Low Tide Level
SWCC – Soil water characteristic curve
EGL – Existing Ground Level
LGWT –Land Side Groundwater table
FEM – Finite Element Method
VWC – Volumetric Water Content function
AEV – Air Entry Value
FEM – Finite Element Method
FDM – Finite Difference Method
ZIR – Zone of Influence of Rise-Up
PWP – Pore Water Pressure

NOTATIONS

x , y = *Abscissa and Ordinate of a point*
v = *Velocity of seepage flow*
$k_{x,y}$= *Co-efficient of soil permeability for water flow in the –x, -y directions respectively*
$k_{\theta i}$ = Calculated hydraulic conductivity for a specified volumetric water content or at a negative pore water pressure (in cm/min)
(k_S/ k_{SC}) = Matching factor given by the ratio of measured saturated conductivity to calculated saturated conductivity
k_W = *Hydraulic conductivity at volumetric water content, w*
i = *Hydraulic gradient*
i_K= *The last water content class on the wet end. (Green and Corey 1971)*
m_W = *Slope of volumetric water content function*
m_V = *Co-efficient of volume compressibility*
$[K]$ = *Characteristic matrix containing hydraulic conductivity*
$\{H\}$ = *Vector of Unknown Head*
h – *Total head difference for flow*
h_{iK} = The negative pore water pressure head for a given class of water filled pores (in cm of water)
h_{CO} = *Mean capillary rise*
$\{Q\}$ = *Flow Vector*
Q – *Volumetric source/ sink*
q = *Total flow per unit length of cross-section*
$\frac{\partial \theta}{\partial t}$ – *Rate of change of soil water storage w.r.t time*
γ_W –*Unit weight of water*
$\Phi\ (x,y)$ - *Potential function*
$\psi\ (x,y)$ - *Stream function*
N_d = *Number of equipotential drops,*
N_q = *Number of flow channels,*
Δt = *Time increment,*

[M] = Mass matrix (accounts for storage during time increment and is a function of the volumetric water content function)
$\{H_0\}$, $\{H_1\}$ = Initial head at start of time step and new head at the end of time step, respectively
$\{Q_1\}$ = Transient boundary condition
η = Soil porosity
S = Degree of Saturation
S_A, S_C= Degree of Saturation due to adhesion and capillary forces respectively
θ_W = Volumetric water content
S_r or θ_R = Residual water content
θ_S = Saturated water content
ψ_O = Negative pore water pressure
ψ_i = Suction pressure corresponding to the water content at inflection point
ψ_R = Soil parameter which is a function of the suction at which residual water content occurs (in kPa)
θ_P *= Volumetric water content at the halfway point between saturated and residual water content respectively.*
ψ_P = Matric suction at the halfway point between saturated and residual water content respectively.
$C_{\psi O}$ = Correction factor in Fredlund and Xing method (1994)
e *= exp (1) = 2.71828*
s = Slope of the line tangent to the function that passes through the inflection point in Fredlund and Xing method (1994)
D_{10} *= particle diameter size (in cm) corresponding to 10 % passing on a grain size curve*
C_U = Co-efficient of uniformity
w_L *= Liquid Limit*
T = surface tension of water (in dyne /cm)
μ = Viscosity of water (in gm/cm.sec)
ρ = Density of water (in gm/cm^3)
g = Gravity co-efficient (in cm/s^2)
p = a parameter that accounts for the interaction between pore classes
σ_x, σ_y = The Normal stress components in –x and –y directions respectively
τ_{xy} *= Shear Stress component in the –xy plane*
ϵ_x, ϵ_y = The Normal strain components in –x and –y directions respectively
γ_{xy} *= Shear strain in –xy plane.*
E = Modulus of Elasticity of material
H = Unsaturated Soil Modulus for Soil structure with respect to matric suction
μ = Poisson ratio of the material
[F] = Force Matrix in F.E.M
[k] = Stiffness Matrix in F.E.M
[δ] = Displacement Matrix in F.E.M
[ϵ] = Strain Matrix in F.E.M
[B] = Strain transformation matrix in F.E.M and is a function of nodal co-ordinates .
H_δ = Head difference between LTL and HTL
t_{RU} – Rise-Up Half Cycle Time
t_{DD} – Draw-Down Half Cycle Time
t_F – Full Cycle Time

ABSTRACT

Earthen embankments are one of the most efficient and economic water retaining structures. Apart from its utility in the irrigation, navigation and transportation sectors, it is also used extensively in protective structures along rivers, coasts, etc. One of the main problems that affect the design life of an earthen embankment is seepage. Seepage may be in the form of steady and transient seepage. Usually, the embankments that are used as protective structures along the river banks are exposed to transient seepage induced by cyclic tidal heads. A tidal cycle generally consists of Rise-Up and Draw-down half cycles, which denote the rising and falling of the tidal water as per cycle time, respectively. Although, a lot of publication is available for both steady and transient seepage in embankments, however literature explaining the effect of transient seepage induced by tidal cycles is scarce. The present study has taken up a field problem in the Sunderban region of West-Bengal, India where 3520 kms of earthen embankments used as protective structures along rivers and creeks are exposed to diurnal tidal head variation of 4-6 metres in 6 hours.

A numerical model based on the finite element method has been developed based on the field problem. The soil water characteristic curve for Sunderban clayey silt has been developed by estimating techniques based on grain size distribution and other basic soil parameters. The volumetric water content curve was developed by the modified Kovacs method whereas the hydraulic conductivity function was estimated from the saturated permeability using the Van Genuchten method. The tidal head is modeled by appropriate hydraulic boundary conditions which is a function of cycle time. The transient seepage analysis is done by both uncoupled and coupled methodology, where the latter is used to find out both deformation and pore water pressure simultaneously. The dynamics of the phreatic line during Rise-Up and Draw-Down half cycles was also determined. The effect of multiple cycles was also investigated for all the important seepage parameters. An experimental model was additionally developed in the laboratory and the effect of cycle time, rate of rise-up, rate of draw-down, effect of multiple cycles was investigated.

The results have shown that transient seepage induced by tidal head has a significant impact on the phreatic line, the pore water head distribution and is limited to a certain zone within the embankment termed as the Zone of Influence of Rise-Up (ZIR). The Factor of Safety for stability was seen to increase during rise-up and decrease during draw-down for a single tidal cycle. The same remains constant more or less after multiple cycles. The coupled deformation analysis showed that portions of the embankment within the ZIR that experienced both build up and release of pore water pressure during the multiple tidal cycles were prone to serviceability failure as they encountered cyclic settlement and rebound, leading to permanent deformation due to plastic behavior of soil. Such instances have also been recorded in the field. The numerical findings were validated by the experimental results. This study brings out the effect of tide induced transient seepage on earthen embankments.

Keywords : Unsaturated permeability, Transient seepage, Earthen embankment, Soil Water Characteristic Curve, Tidal cycles, Finite Element Method, Laboratory Model.

CHAPTER ONE
INTRODUCTION

CHAPTER ONE
INTRODUCTION

1.1 : TOPIC INTRODUCTION

It is known that embankments have been used as an efficient water retaining structure since very early times. One of the key advantages of these type of structures are that they can be constructed in relatively weaker foundation bases. Though the purpose for retention may vary from place to place, but their popularity is based on the fact that the material for construction is easily available locally, hence making the process easier and economic. The material for construction can be selected as per local topography, soil profile, purpose of construction, etc.

Embankment dams are constructed across rivers for water retention and application on a large scale. The utility are in the sectors of irrigation, agriculture, power, navigation, etc. India is home to the longest earthen embankment dam in Asia in the form of Hirakud Dam at Sambalpur district of Odisha. Medium to Small scale embankment levees are popular throughout the country catering to local needs. The construction of earthen embankments for the Transportation sector such as highways and railway tracks are also quite popular. In several areas they are also used in the form of protective structures along river banks to prevent flooding of human settlement during tides, storm surges, etc.

Although embankments are much easier to construct and have a moderate life span, yet the design life may be cut short due to various factors attributed to improper construction methodology, external forces like seismic, hydrostatic, hydrodynamic, weathering actions, etc. Hydrostatic force induced failures include failure due to seepage, piping failure, failure due to uplift forces ,etc.

This study revolves around the hydrostatic factor and to be more precise the effect of steady and transient seepage on the stability of an Unconfined, Partially Saturated Riverfront Earthen Embankment prone to tidal fluctuations. A site based case study has been taken up and analyzed to solve a real life problem affecting the general population of the study area.

1.2 : PRESENTATION OF CONTENTS

The relevant theory pertaining to this thesis have been discussed in Chapter-1 – Introduction, which is followed by Chapter-2 – Literature Review. The objective and scope has been defined in Chapter-3. The study area based on which the experimental set-up is developed and numerical analysis done has been highlighted in Chapter-4. Chapter-5 and 6 deals with the numerical and laboratory experimentation models respectively. The general discussions and trends obtained

between the numerical and experimental models have been laid out in Chapter-7, followed by conclusions and future scope of work in Chapter-8.

1.3 : GENERAL THEORETICAL BACKGROUND

1.3.1 : Embankment Types

Embankment dams may be broadly classified under - (i) Earthen dams, (ii) Rockfill dams and (iii) Composite sections

It is to be noted that while rigid dams can withstand bending moments, the embankment dams depend on their shear strength for stability. In view of the above statement, a few characteristics of embankment dams have been listed as under –

(i) These dams are mainly constructed with locally available materials. There is less use of manufactured/ transported materials. Thus, it is of major economic importance in developing countries like India.

(ii) The soil requirement for foundation is less demanding .i.e. the design of foundations can be suited to local soil conditions , with or without soil treatment.

(iii) They are more conveniently adaptable to stage construction. Stage construction may have economic advantages .It also helps in improvement of soil conditions.

(iv) Embankment dams are economically viable compared to Gravity dams.

The materials mainly used for construction of embankment dams may vary from rocks to silty soils to clays. On the basis of construction , earthen embankment dams may be classified as under**:**

(i) *Homogenous embankment* : Usually consist of a single material , homogenous throughout the dam . As huge quantities of materials are required, it is essential that bulk of the material is available locally. The main problem encountered by these type of embankments is seepage. Moreover, a huge section is required for stability. These dams are usually provided with bottom drainage filter to withstand piping effects. Typical section is shown in **Figure – 1.1**.

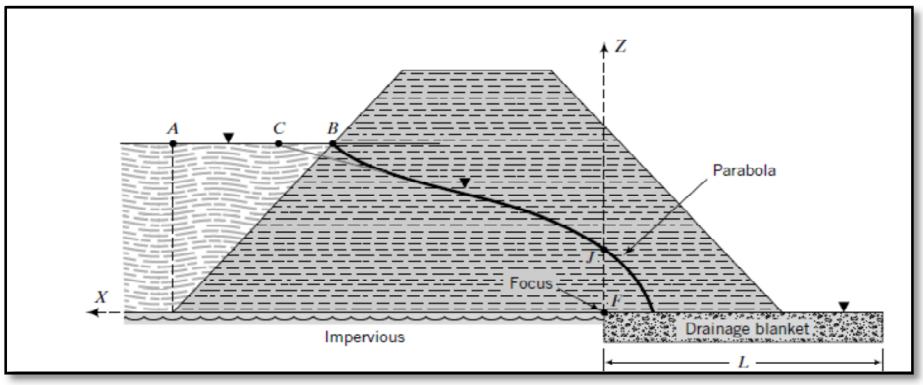

Figure - 1.1 - General Arrangement of Homogenous Earthen Embankment showing Phreatic Surface, with toe drain. (Picture courtesy - Soil Mechanics & Foundation Engineering 3rd edition 2010 , by Muni Budhu)

(ii) *Zone Embankment* :They usually have a central impervious core, with a comparatively pervious transition zone , followed by a much pervious outer zone. The central core prevents internal seepage. The transition zone prevents building up of pore pressure due to sudden drawdown conditions, whereas the outer zone gives stability to the dam section. Typical section is shown in **Figure – 1.2**.

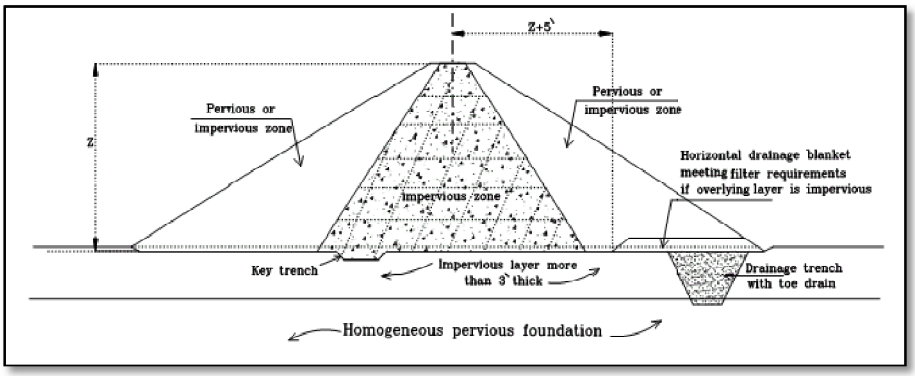

Figure - 1.2 - General Arrangement of Zone Embankment (Picture Courtesy : Internet)

The main types of failure usually associated with earthen embankments are -

(i) Overtopping of Dam due to water pressure , uplift forces.

(ii) Erosion of upstream & downstream faces by scouring , wave action , water currents , rain water action

(iii) Upstream face failure due to pore pressure buildup during sudden drawdown condition

(iv) Piping of dam base at downstream in absence of drainage filter. Sloughing is the progressive removal of soil from the wet downstream face.

1.3.2 : General Seepage Theory

In general, Seepage is caused due to the flow of water under a hydraulic gradient within the interconnected pores due to its permeable nature of the saturated soil mass. Thereby, in seepage, the difference in energy states from one end to other depends on the soil resistance to flow of water. For analysis, the basic assumptions are that both soil & water are incompressible**.** As the velocity & gradient varies from section to section in direction of flow, Darcy (1856) derived the relation between velocity of seepage flow (v), co-efficient of soil permeability (k) and hydraulic gradient (i) as in **equation (1.1)**

$$v = k.i$$

where , v = velocity of seepage flow,
$k_{x,y}$ = co-efficient of soil permeability for water flow in the –x, -y directions respectively,
i = hydraulic gradient

Darcy's law is applicable to both steady and transient states (Richards 1931, Thieu etal 2001) . Moreover, from conservation of mass for a representative volume element, flow through a heterogeneous, anisotropic, saturated-unsaturated soil mass, for 2D flow, the governing partial differential equation is given by **equation (1.2)**

$$\frac{\partial}{\partial x}\left(k_x \frac{\partial h}{\partial x}\right) + \frac{\partial}{\partial y}\left(k_y \frac{\partial h}{\partial y}\right) + Q = m_w \gamma_w \frac{\partial h}{\partial t}$$

where, m_W = slope of volumetric water content function
Q – volumetric source/ sink
h – total head difference for flow
$\frac{\partial \theta}{\partial t}$ – Rate of change of soil water storage w.r.t time
γ_W –Unit weight of water

Equation (1.2) indicates that the sum of rate of change of gradient, with distance, in –x and –y directions respectively plus sink/source boundary condition equates to the rate of change of volumetric water content with respect to time.

Although non-linear laws may describe the relation between velocity and hydraulic gradient more suitably, linear Darcy's law is used for simplification.

As per the U.S Army Corps of Engineers, Radhakrishnan (1978), seepage analysis may be carried out by the following methods -

(a) **Development of flownets** : These may be obtained by solving Laplace equation for seepage. The solution is in the form of sets of orthogonal curves.

(b) **Experimentation models** :

(i) Electrical analogy

(ii) Sand box experiments with dyes, tracing flowlines and piezometers measuring potential heads

(iii) Viscous flow models (e.g. Hele Shaw model), have been used extensively to study transient flow in fluids using oil / glycerine to simulate laminar flow.

(c) **Analytical methods :**

(i) Mapping and transformation (Harr,1962) have been used where the geometry of a problem is transferred from a plane where the solution is unknown to another complex plane where the solution is known. It requires the use of complex variable theory and proper choice of transformation functions

(ii) Semi-empirical Method (Pavlovsky, 1936) involves the method of fragments, where complicated seepage problems are solved by breaking them down into parts, analyzing flow patterns individually and then re-assembling the parts to obtain overall solution

(iii) Closed form solutions exist for simpler problems like flow to a fully penetrating well with a radial source (Musket 1946)

(d) **Numerical and computer based analysis** :

(i) Finite Difference method solves the Laplacian equations by approximating them with a set of linear algebra equations. The flow region is divided into discrete rectangular grid with nodal points which are assigned values of head i.e.- known head values along fixed head boundaries or points, estimated heads for nodal points that do not have initially known head values. Then applying Darcy's law and with the assumption that the head at a given node is the average of the surrounding nodes, a set of N-linear algebraic equations with N-unknown values of head are developed, where N is the number of nodes. For large number of grids and multiple iterations, the help of computer is taken for solving the problem.

(ii) Finite Element method is a numerical approach based on grid pattern, which is not necessarily rectangular, and divides the flow region into discrete elements and provides N equations with N unknowns to solve the problem. The inputs may be in the form of geometry, material properties and boundary conditions.

In brief comparison between Finite Difference method (FDM) and Finite Element method (FEM) , though the former uses iterative techniques such as successive over relaxation which converge to the correct solution allowing it to be more economical for simpler problems, the latter is generally preferred for complex geometries where the shape and size of mesh elements may be varied to obtain accuracy and even sloping layers of materials may be accommodated. In brief, FDM is more a mathematical approach rather than physical compared to FEM which is more a physical approach rather than mathematical.

1.3.2.1 : Steady State :

It is the state, when the controlling parameters do not change with respect to time. Assuming isotropic condition ($k_x = k_y$) and no storage or loss, equation (1.2) takes a Laplacian form given in **equation (1.3)**

$$\frac{\partial^2 h}{\partial x^2} + \frac{\partial^2 h}{\partial y^2} = 0$$

Equation (1.3) indicates that during steady state, the pore pressure distribution depends solely on the hydraulic head and is independent of any material properties.

On solving the above equation ,we get the potential function Φ (x, y) ,as in **equation (1.4)**, **(1.5)**, and stream function ψ(x, y) , as in **equation (1.6)**, **(1.7)**.

$$\frac{\partial \Phi}{\partial x} = v_x = -k\frac{\partial h}{\partial x}$$

$$\frac{\partial \Phi}{\partial y} = v_y = -k\frac{\partial h}{\partial y}$$

$$\frac{\partial \psi}{\partial y} = v_x = -k\frac{\partial h}{\partial y}$$

$$-\frac{\partial \psi}{\partial x} = v_y = -k\frac{\partial h}{\partial x}$$

where, Φ (x,y) - potential function
ψ (x,y) - stream function

The relation between flow & equipotential lines can be summarized as follows –

(1) Flow lines are in the direction of seepage velocity . Consecutive flow lines do not intersect each other.

(2) Equi-potential lines denote the head drop along the section . Consecutive lines do not intersect.

(3) Flowlines & Equipotential lines form the flow net . They intersect orthogonally.

Usually flownets are drawn by and rectified in iterative processes by trial & error, with the basic concept that the intersection must be orthogonal with the flow elements as approximate squares. The amount of seepage was then calculated using Darcy's law **.**

Total flow per unit length of cross-section, given in **equation (1.8)**,

$$q = k\ H\ N_q / N_d$$

where, N_d = Number of equipotential drops,
N_q = Number of flow channels,
q = Total flow per unit length of cross-section

According to Casagrande (1940), the following rules should be obeyed in drawing flow nets:

(1) Flow lines and equi potentials should always be perpendicular to each other, in a homogeneous isotropic system, and form curvilinear squares.

(2) Flow lines should always be parallel to an impermeable boundary, and Equipotential lines are always perpendicular to it.

(3) Flow lines should always be perpendicular to a constant head boundary, and Equipotential lines are always parallel to it

A point of interest for all researchers' is the location of the zero pore pressure line or the phreatic surface during both steady and transient seepage. Several scientists' like Dupuit, Schnaffernak (1917), Casagrande (1932), Pavlovsky (1931) have given mathematical or graphical approach for the determination of phreatic surfaces in earthen embankment dams during steady state condition. The most popular or widely used approach is that of L. Casagrande (1932), who obtained the same on basis of Dupuit's assumption of hydraulic gradient with slight modifications over slope. He found out that the phreatic surface closely resembles a base parabola, hence developed equations, with corrections at entry point and exit point as shown in **Figure-1.3**.

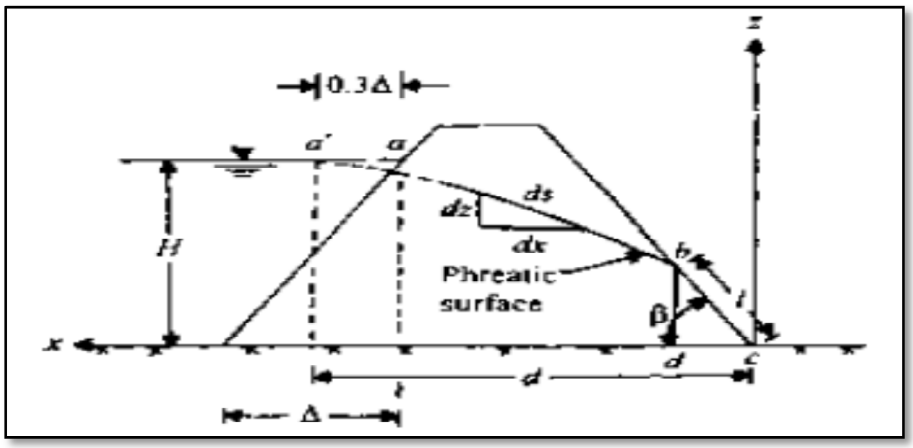

Figure - 1.3 – Casagrande Method for Determination of Phreatic Surface. (Picture Courtesy : Advanced Soil Mechanics & Foundations – B.M.Das)

Charts were developed for corrections depending on side slopes and the quantity of seepage can be calculated on this basis as per **equation (1.9)** and **(1.10)**.

$$l = \sqrt{d^2 + H^2} - \sqrt{(d^2 + H^2 \cot^2 \beta)}$$

$$q = klsin^2\beta$$

where the terms are self explanatory from figure-1.3

1.3.2.2 : Boundary Conditions

Usually flow in dams and embankments are categorized as

(1) Confined flow, which represents the class of problems with all boundary conditions of flow domain completely defined. e.g. Concrete dams with sheet piles

(2) Unconfined flow, where at least one boundary of the flow domain is a free surface and not rigidly defined. e.g. Motion of groundwater in any flow system

General seepage problems in an Unconfined flow problem are associated with four types of boundaries as per Harr (1962)

(i) Impervious Boundaries :The interface between saturated pervious soil mass and adjacent materials of very low permeability are taken as Impervious Boundaries. No normal flow is assumed to take place across this interface as the velocity component normal to any point must be zero. Hence it may be used to define the locus of the lowest streamline. The boundary condition is given as in **equation (1.11)** and **(1.12)**

$$\frac{\partial \Phi}{\partial y} = \frac{\partial \psi}{\partial x} = 0$$

$$\psi = constant$$

(ii) *Entrance / Exit* :The lines where the water enters or exits the earthen dam surface. Flow is usually perpendicular to entrances / exits. These are also called reservoir boundaries. Along these lines are the equipotential lines with same piezometric level at all points on the line. The boundary condition is given as in **equation (1.13)**

$$\Phi = constant$$

(iii) *Seepage Surface* :The saturated pervious soil mass having a boundary exposed to atmosphere such that it is neither a flow line nor an equipotential line. The pressure on this surface is constant and atmospheric. The boundary condition is given as in **equation (1.14)**

$$\Phi + k.y = constant$$

(iv) *Line of Seepage* :The pore pressure along this line is zero and the pressure is atmospheric. It is the uppermost stream-line of the flow domain. The boundary condition is given as in **equation (1.15)** and **(1.16)**

$$\Phi + k.y = constant$$

$$\psi = constant$$

1.3.2.3 : Transient State

It is the state, when the controlling parameters change with respect to time and equation (1.2) can be written as **equation (1.17)**

$$\frac{\partial}{\partial x}\left(k_x \frac{\partial h}{\partial x}\right) + \frac{\partial}{\partial y}\left(k_y \frac{\partial h}{\partial y}\right) = m_w \gamma_w \frac{\partial h}{\partial t}$$

During transient state analysis, additional parameters like soil water storage function, unsaturated permeability come into action for the analysis of the problem. Both the soil storage function and unsaturated permeability function depend on the matric suction developed. Usually for high saturation values the air phase may be excluded as per Freeze and Cherry (1979).

Henceforth both saturated and unsaturated permeability shall be referred in terms of hydraulic conductivity function.

The soil water storage function is an indication of the amount of water stored or released by the soil due to change in pore water pressure and is defined by the slope of the volumetric water content function. The hydraulic conductivity value is constant at saturated conditions, but becomes a

function of the negative pore water pressure in the unsaturated region and may be derived from the volumetric water content function.

The assumption of a rigid soil skeleton in conventional seepage may be too restrictive, as in certain site conditions, where deformations are also significant during seepage. The analysis can be carried out by using coupled approach in these situations. Biot's theory of flow through deformable media may be used, where both displacements and pore water pressures are assumed to be unknowns in finite element method. The non-linear stress analysis is carried out simply by superimposing on it known seepage forces caused by steady or transient seepage

1.3.3 : Tidal Variations : Rise-Up And Draw-Down Conditions

It is established that due to the gravitational effect of the Sun & Moon on the rotating Earth, water-bodies face a gravitational pull resulting in periodic rise and fall of surface water levels, called 'tides'. The condition in which there is a rise in water level is called flow tide (Bengali term : Jowar), whereas the falling tide is termed as ebb tide (Bengali term : Bhata). These tides have predominant effects in case of shallow depth water bodies with constrained landmasses & when astronomical occurrences of New Moon or Full Moon happen. The time period for each tidal half cycle, defined as the time taken by river water level to rise from Low Tide Level (LTL) to High Tide Level (HTL) defined as Rise-Up, and from High Tide Level down to Low Tide Level defined as Draw-down, given as six hours each. A single Rise-Up and Draw-Down constitute a complete Tidal cycle. It has also been observed that in a country like India, normally the time period for one complete cycle of Low Tide to High Tide and back to Low Tide is about 12 hours , thereby producing two cycles per day.

The above described phenomenon has its effects on water-front structures, imposing a additional stability criteria, especially for earthen dams. During the low tides, as the water levels fall from their initial position, the condition is termed as Drawdown – a state in which the rate of receding water level and the permeability of the associated earthen dam is vital, as due to rapid drawdown in low permeability soils (e.g. clays), pore pressure induced may cause slope failure. An additional problem usually encountered during the drawdown phase is the probability of piping failure in which fine soil particles find passage through the soil pores along the outgoing water, loosening the interparticle soils and making the hole bigger in size with subsequent movement. The other half of the tidal cycle consists of Rise-Up – a state during which the water levels go up, thereby seepage occurs as per transient hydraulic gradient. Usually as, during rise-up, the rising water imparts an additional lateral stability to the upstream face of the earthen embankment, failure chances are

minimum for seepage. However, the position of landside groundwater table (LGWT) has an important role to play to determine the steady state conditions which form the basis for transient state analysis.

1.3.4 : Soil Water Characteristics Curve

In transient seepage analysis, the pore pressures and quantity of flow are functions of time, hence apart from inclusion of time parameter, time dependant boundary conditions, additional functions also need to be defined in the form of Volumetric Water Content function (VWC), hydraulic conductivity function. Numerous literature is available where the latter can be derived from the former.

As per Johari etal (2006), the determination of Soil Water Characteristics Curve may be done as per-

(1) Laboratory tests – (a) Pressure Plate (b) Buchner Funnel (c) Tensiometer (d) Pressure membrane

(2) Indirect methods – (a) Filter paper (b) Porous stone (c) Heat dissipation sensor

Laboratory tests are usually very costly, hence several researchers favor development of empirical methodology for determination of Soil Water Characteristics Curve. These methods can be broadly classified as –

(i) *Type-I* : Hutson and Cass (1987), Aubertin etal (1998) correlated the water contents at individual matric suction with specific soil properties like porosity, effective grain size, etc. The process involves regression analysis followed by curve fitting technique.

(ii) *Type-II* : Cresswell and Paydar (1996), Tomasella and Hodnett (1998) used regression analysis involving analytical equations for correlation of SWCC parameters with basic soil properties such as grain size distribution and dry density using regression analysis.

(iii) *Type-III* : Fredlund etal (1997), Zapata etal (2003) developed a physio-empirical modeling of SWCC, where the grain size distribution is converted into a pore size distribution, which in turn is related to the distribution of water content and associated pore pressure.

(iv) *Type-IV* : In this method, artificial intelligence is used for development of SWCC. Neural networks, genetic programming is utilized.

1.3.4.1 : Volumetric Water Content Function And Its Estimation

1.3.4.1.1 : General

In an unsaturated soil, the volumetric water content (θ_W) is given as in **equation (1.18)**

$$\theta_W = \eta S$$

where, η = soil porosity
S = Degree of Saturation

The Volumetric Water Content Function (VWC) defines the capability of the soil to store water under changes in matric pressure. The VWC function describes what portion or volume of the voids remain water filled as the soil drainage takes place. It depends on the following parameters-

(i) *Air Entry Value (AEV)* : It corresponds to the magnitude of the negative pore water pressure when the largest voids start draining freely by virtue of gravity only. It is generally a function of the pore size distribution and maximum pore size in a soil. Soils with large, uniformly shaped pores have relatively low AEV.

(ii) *Slope of the function for both positive and negative pore water pressures (m_V, m_W)*

(iii) *Residual water content (S_r or θ_R)*: It is the minimum volumetric water content that remains in the soil even after full drainage by virtue of gravity has taken place. A water content lower than this may occur due to evaporation or osmotic forces.

The importance of Air Entry Value and Residual Water Content, in the development of VWC have been shown in **Figure - 1.4**. The value of the volumetric water content at zero pore pressure corresponds to the porosity. Moreover, in the positive pore pressure region, the drainage occurs by external load application. The slope of the VWC in unsaturated region represents the rate at which the volume of water stored within the soil changes with pressure from Air Entry Value to Residual Water Content.

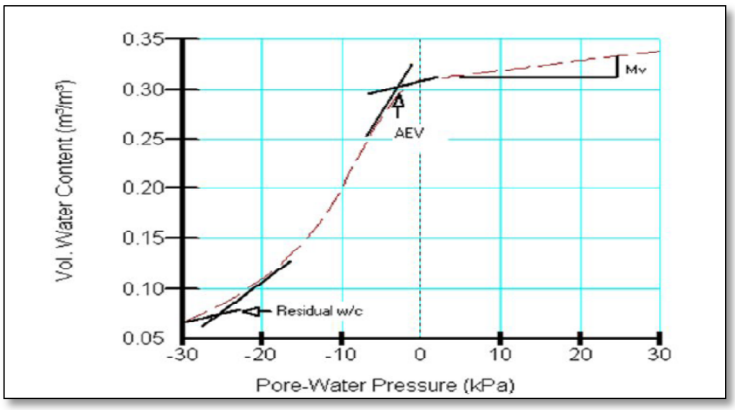

Figure - 1.4 – A typical VWC v/s Pore water pressure plot showing Air entrant value, Residual water content and Co-efficient of volume compressibility. (Picture courtesy: GEO-SLOPE International Ltd, "Seepage Modeling with SEEP/W, an engineering methodology", July 2012 edition)

Typical VWC curves developed by Zapata etal (2006) for El-Paso sand, Price Club silt and Fountain Hills clay have been shown in **figures (1.5, 1.6, 1.7)** . It can be seen that in case of uniform sand where particles are relatively large, water can be removed under relatively smaller negative pressures, compared to silt and clay. The uniform size of particles ensure that all pores drain over a small range of negative pore pressure, hence giving a steep slope function compared to silt and clay. For silt, a higher negative pore pressure is required for drainage thereby increasing the AEV. The slope of the function becomes less steep as drainage occurs over a large range of matric suction. In clay, the individual grain size is so small that it is difficult to identify a specific air entry value. Moreover, consolidation changes the structure of the system , water can be released over a significant range of matric suction before air actually enters the pores. Also, as clay is compressible, the co-efficient of volume compressibility also plays a major role in the derivation of the VWC function.

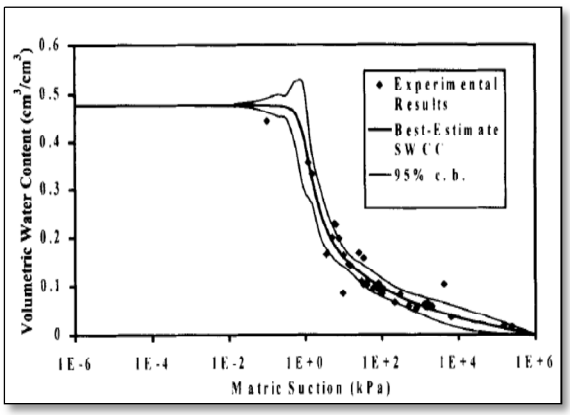

Figure - 1.5 – Best estimate of VWC function for El-Paso sand (Picture Courtesy : Zapata etal (2006))

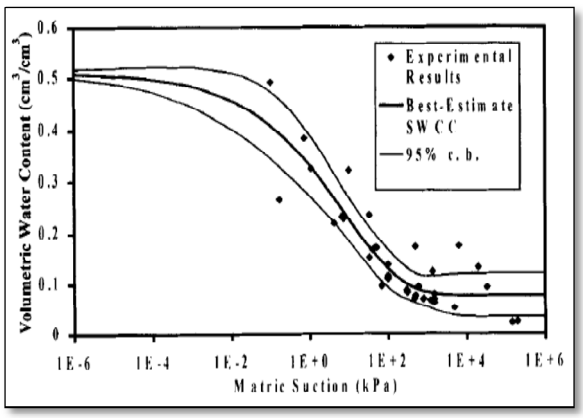

Figure -1.6 – Best estimate of VWC function for Price Club silt (Picture Courtesy : Zapata etal (2006))

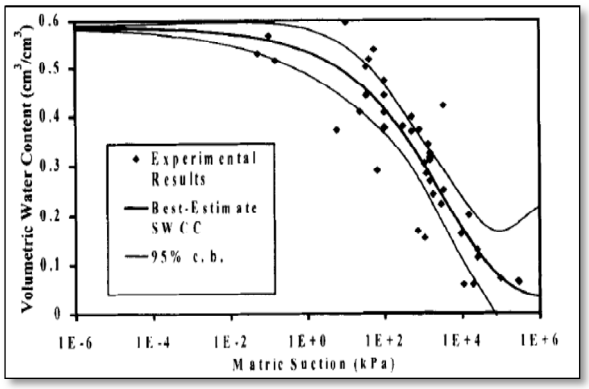

Figure - 1.7 – Best estimate of VWC function for Fountain Hills clay (Picture Courtesy : Zapata etal (2006))

1.3.4.1.2 : Estimation Techniques For VWC Function

Notable finding on SWCC has been given by researchers like Gardener (1958), Brooks and Corey(1964), Farrel and Larson (1972), Van Genuchten (1980), Van Genuchten and Burdine (1980), Kovacs (1981), Williams etal (1983), Mckee and Bumb (1987), Fredlund and Xing (1994), Aubertin etal(2003).

In the following segment, the methodology developed by Van Genuchten (1980), Fredlund and Xing (1994) and Aubertin etal (2003) shall be discussed in detail.

(a) Van Genuchten (1980) Method-

A closed form solution was developed for prediction of VWC function, based on four parameter equations given as in **equation (1.19)**

$$\theta_W = \theta_R + \frac{(\theta_S - \theta_R)}{(1 + \left(\frac{\psi_O}{a}\right)^n)^m}$$

where, θ_W, θ_R, θ_S = The Volumetric water content, the Residual water content and the Saturated water content respectively.
ψ_O = Negative pore water pressure
a = Parameter which is a function of air entry value of the soil (in kPa)
n = Soil Parameter depending on rate of water extraction from soil once the AEV is exceeded
m = Parameter which is a function of the Residual water content of soil

(b) Fredlund and Xing (1994) Method-

An estimating solution was developed for prediction of VWC function based on **equations (1.20)**, **(1.21)**, **(1.22) and (1.23)**

$$\theta_W = C_{\psi_O} \frac{\theta_S}{(\ln\left[e + \left(\frac{\psi_O}{a_1}\right)^{n_1}\right])^{m_1}}$$

$$C_{\psi_O} = \left[1 - \frac{\ln\left(1 + \left(\frac{\psi_O}{\psi_R}\right)\right)}{\ln\left(1 + \left(\frac{10^6}{\psi_R}\right)\right)}\right]$$

$$n = \frac{1.31^{m_1+1}}{m_1\,\theta_S}(3.72\,s\psi_i)$$

$$m_1 = 3.67 \ln\left[\frac{\theta_S}{\theta_i}\right]$$

where, θ_W, θ_S = The Volumetric water content and the Saturated water content respectively.
$C_{\psi O}$ = Correction factor
ψ_O , ψ_i = Negative pore water pressure, Suction pressure corresponding to the water content at inflection point, respectively.
ψ_R = Soil parameter which is a function of the suction at which residual water content occurs (in kPa)
e = exp (1) = 2.71828
a_1 = ψ_i in kPa (It is given by the inflection point of the VWC function. It generally is slightly larger than the AEV)
n_1 = Parameter controlling slope of the VWC function
m_1 = Parameter which is a function of the Residual water content of soil
s = Slope of the line tangent to the function that passes through the inflection point

A few interesting observations in this method is given below-

(i) This method is applicable when the parameters a_1, m_1, n_1 are known.

(ii) The method cannot be used to estimate a VWC function from a grain size distribution

(iii) The function is developed smoothly over a range of matric suction such that at a negative pore water pressure of 1 million kPa, the volumetric water content tends to zero value.

(c) Modified Kovacs Method-

This method was proposed by Aubertin etal (2003) is a modified form including clay type of soils, to the one proposed by Kovacs (1981). The VWC function is estimated on basic material properties like grain size distribution, Liquid limit, etc.

The function is determined initially as a Degree of Saturation (S) which is divided into two components –

(i) The first component (S_C) contributes to the amount of water stored in the soil by capillary forces at small negative pore water pressures. It depends on the pore diameter and pore size distribution and given as in **equation (1.24)**

$$S_C = 1 - \left[\left(\frac{h_{CO}}{\psi}\right)^2 + 1\right]^m exp\left[-m\left(\frac{h_{CO}}{\psi}\right)^2\right]$$

where, m = a parameter that takes into account the pore size distribution and controls the shape and position of the VWC function in the capillary zone.

In plastic cohesive soils , $m = 3 \times 10^{-5}$, $a = 7 \times 10^{-4}$

In capillary based soils , $m = 1$, $a = 0.01$

(ii) The second component (S_A) is a function of adhesion, where the water is stored at high negative pore water pressure. This is guided by a bounded function (S_A^*) and its contribution is significant to the development of the VWC function. It is associated with the thin film of water that covers the surface of soil grain and depends on basic material properties such as (a) Negative Pore water pressure in soil (b) Particle size, shape co-efficient and porosity of soil. It is given by **equations (1.25)**, **(1.26)**, **(1.27)**, **(1.28)**

$$S_A = a_0 C_{\psi o} \frac{\left[\frac{h_{CO}}{\psi_n}\right]^{2/3}}{e^{1/3}\left[\frac{\psi_O}{\psi_n}\right]^{1/6}}$$

$$For\ Cohesionless\ soils, h_{CO} = \frac{b}{eD_{10}}$$

$$For\ Cohesive\ soils, h_{CO} = \frac{\zeta {w_L}^{1.75}}{e}$$

$$b\ (in\ cm^2) = \frac{0.75}{1.17 \log C_U + 1}$$

where, a_0 = curve fitting parameter
e = void ratio
h_{CO} = mean capillary rise
ψ_n = Suction term introduced to ensure dimensionless component
D_{10} = particle diameter size (in cm) corresponding to 10 % passing on a grain size curve
C_U = Co-efficient of uniformity = (D_{60}/D_{10})
w_L = Liquid Limit
ζ = constant = 402.2 cm^2

$C_{\psi O}$ = Correction factor as per Fredlund and Xing (1994)

This method gave a empirical equation for the Suction corresponding to the residual water content (ψ_R) component in Fredlund and Xing (1994) as in **equation (1.29)**

$$\psi_R = 0.86 \left[\frac{\zeta}{e}\right]^{1.2} {w_L}^{1.74}$$

Equation (1.18) can be extended to form **equation (1.30)**

$$S = S_C + {S_A}^*(1 - S_C)$$

Bounded function (${S_A}^*$) is given by

$${S_A}^* = 1 , \qquad if\ S_A > 1$$

$${S_A}^* = S_A , \qquad if\ S_A \leq 1$$

1.3.4.2: Hydraulic Conductivity Function And Its Estimation

1.3.4.2.1 : General

As soil starts to drain freely by virtue of gravity, air enters the largest pores and make them non-conductive, thereby increasing the tortuosity of the flow path. Hence, in the analysis of an unsaturated soil system, the hydraulic conductivity which is a function of the matric suction, must be properly defined over a suitable range. In cases where there are chances of negative surface fluxes like evaporation, the negative pore water pressure range defined must be increased to cover some thousands of kPa. For coarse grained materials, the hydraulic conductivity becomes infinitely low and can be neglected, once desaturated (i.e. at zero or negative pore pressure). A typical hydraulic conductivity plot has been shown in **figure 1.8**

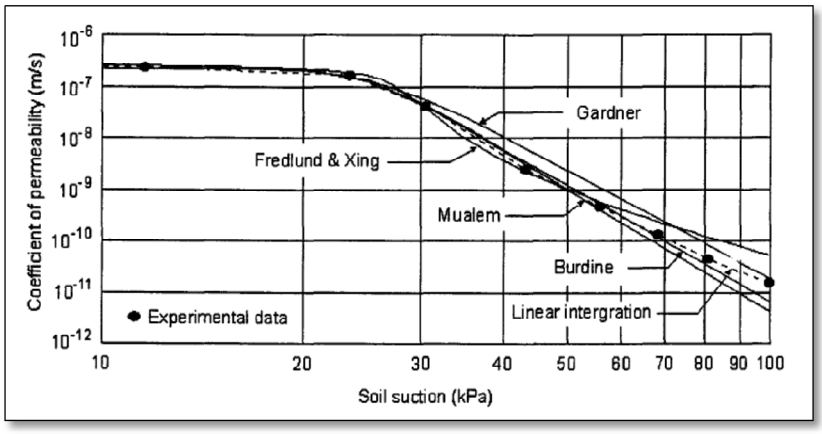

Figure -1.8 – Specified Hydraulic conductivity functions as per Thieu etal (2001)

1.3.4.2.2 : Estimation Techniques For Conductivity Function

The estimation of saturated hydraulic conductivity may be done by appropriate permeability tests. The conductivity values for the unsaturated regions of the soil may be obtained from the Hydraulic Conductivity functions, which may be estimated from –

(i) Volumetric Water Content function and (ii) Saturated hydraulic conductivity

A few methodologies have been described in the forthcoming sections for the development of the same.

(a) Green and Corey Method (1971) –

The **equation (1.31)** was proposed for the development of the hydraulic conductivity function.

$$k_{\theta_i} = \left(\frac{k_S}{k_{SC}}\right)\left(\frac{30T^2}{\mu g \rho}\right)\left(\frac{\eta^p}{{n_O}^2}\right)\left[\sum_{j=i_K}^{m}(2j + 1 - 2i_K){h_{iK}}^{-2}\right]$$

where, $k_{\theta i}$ = Calculated hydraulic conductivity for a specified volumetric water content or at a negative pore water pressure (in cm/min)
(k_S/ k_{SC}) = Matching factor given by the ratio of measured saturated conductivity (k_S) to calculated saturated conductivity (k_{SC})
i_K = The last water content class on the wet end. (e.g. i=1 defines the pore class corresponding to the lowest water content, i=m defines the pore class corresponding to the saturated water content)
h_{iK} = The negative pore water pressure head for a given class of water filled pores (in cm of water)
n_O = total number of pore classes between i and m
T = surface tension of water (in dyne /cm)
μ = Viscosity of water (in gm/cm.sec)
ρ = Density of water (in gm/cm^3)
η = saturated porosity
g = Gravity co-efficient (in cm/s^2)
p = a parameter that accounts for the interaction between pore classes and is given as Marshall (1958) : 2, Millington and Quirk (1961) : 1.3, Kunze etal (1968) : 1.0

(b) Van Genuchten Method (1980) –

A closed form equation was introduced to develop the hydraulic conductivity of a soil as a function of matric suction. The following **equation (1.32)** is given as

$$k_W = k_S\left[\frac{[1 - (a\psi^{n-1})(1 + ((a\psi^n)^{-m})]^2}{((1 + a\psi)^n)^{\frac{m}{2}}}\right]$$

The slope of the VWC function (S_P) is given by **equation (1.33)** -

$$S_P = \frac{1}{(\theta_S - \theta_R)} Mod\left[\frac{d\theta_P}{d(\log \psi_P)}\right]$$

where, *a, n, m* are curve fitting parameters
k_W = Hydraulic conductivity at volumetric water content, w
θ_P = Volumetric water content at the halfway point between saturated and residual water content respectively.
ψ_P = Matric suction at the above mentioned point
Other terminologies bear the same meaning as defined in earlier sections

As per this method, the parameters a, m can be estimated graphically from the VWC function of the soil. These are as per **equations (1.34)**, **(1.35)**, **(1.36), (1.37)** and depend upon the slope of the VWC function (S_P). The appropriate point to evaluate the same is the halfway point between the saturated water content and residual water content of the VWC function.

$$n = \frac{1}{1-m}$$

$$m = 1 - \exp(-0.8 S_P) \quad for\ 0 \le S_P \le 1$$

$$m = 1 - \frac{0.5755}{S_P} + \frac{0.1}{{S_P}^2} + \frac{0.025}{{S_P}^3} \quad for\ S_P > 1$$

$$a = \frac{1}{\psi}\left[2^{\frac{1}{m}} - 1\right]^{1-m}$$

(c) Fredlund etal Methodology (1994) –

The hydraulic conductivity function in the unsaturated zone is obtained by integrating along the VWC function and given as per **equation (1.38)**

$$k_W = k_S \frac{\sum_{i=j}^{N} \frac{[\theta_F(e^y) - \theta_F \psi]\theta_F{}'(e^{y_i})}{e^{y_i}}}{\sum_{i=1}^{N} \frac{[\theta_F(e^y) - \theta_S]\theta_F{}'(e^{y_i})}{e^{y_i}}}$$

$\theta_F{}'$ = First derivative of **equation (1.39)**

$$\theta_F = C(\psi) \frac{\theta_S}{\left[\ln\left(e + \left(\frac{\psi}{a}\right)^n\right)\right]^m}$$

C(ψ) is a correction function defined as per **equation (1.40)**

$$C(\psi) = 1 - \frac{\ln\left(1 + \frac{\psi}{C_r}\right)}{\ln\left(1 + \frac{10^6}{C_r}\right)}$$

where, k_W = The calculated hydraulic conductivity at a certain volumetric water content or matric suction (in m/s)
e = 2.71828
y = Dummy variable of integration which represents the logarithm of negative pore water pressure
j, N = Least and maximum negative pore water pressure respectively, to be described by final function
ψ = Suction at j^{th} interval
a = AEV value of soil
m = A parameter related to the residual water content of the soil
n = A parameter depending on the slope of the inflection point of the VWC curve
C_r = A Constant related to the matric suction at residual water content and a typical value is about 1500 kPa

1.3.5 : Slope Stability Analysis Of Earthen Embankments

1.3.5.1 : General

The stability analysis of slope forms the backbone of any design associated with earthen embankments. The Limit equilibrium method of stability analysis is one of the oldest and best known techniques, which comprises the idea of dividing a potential sliding failure mass into several divisions called slices and analyzing the same on the laws of statics, i.e. the summation of moments, horizontal and vertical forces about a stationary body is zero. The same is repeated with numerous potential slip surfaces until the one with the Minimum Factor of Safety is determined. This value is selected as the Factor of Safety for entire structure. Here, the Factor of safety is defined as the factor by which the soil strength must be reduced so that the potential sliding mass is at the point of limit equilibrium.

Researchers like Fellenius (1936), Janbu (1954), Bishop (1955), Morgenstern-Price (1965), Spencer (1967) made significant contribution in the development of the Limit Equilibrium Method. Bishop Simplified Method (1950) considered interslice normal forces and satisfied overall moment equilibrium, whereas Janbu Simplified method (1954) considered the normal interslice force and satisfied the overall horizontal force equilibrium. Later, in the methods introduced by Morgenstern-Price (1965), Spencer (1967) introduced the interslice shear force in addition to the interslice normal forces and solved the same by static equilibrium.

This Limit Equilibrium method has its own limitations as it is based solely on the physics of static equilibrium. All the slices selected have the same Factor of Safety. Moreover, the stress – strain behavior cannot be modeled in this approach, hence the actual field condition may not be represented by this method which is popular for its simplicity. With the advent of computers which can handle complex mathematical functions, the Finite Element Method became popular for stability analysis of slopes. In this method, the stress – strain behavior can be easily modeled.

1.3.5.2 : Methodology

As discussed in previous section, there are several methods for analysis of slope stability and computation of Factor of Safety. The general theory pertaining to the General Limit Equilibrium (GLE) Method, Spencer Method and Finite Element Stress Method has been briefly discussed in this section. In the forthcoming chapters, the Spencer method and Finite Element method has been utilized in slope stability analysis of an model using Uncoupled and Coupled approach respectively.

(a) General Limit Equilibrium Method – The method was developed by Fredlund etal. It is based on two factor of safety (F.O.S) equations based on moment equilibrium (F_M) and horizontal force equilibrium (F_F). Both the interslice normal and shear forces have been considered. The interslice shear forces (X) were given in the form of **equation (1.41)** as proposed by Morgenstern and Price (1965).

$$X = E\,\lambda f(x)$$

where, *E* = interslice normal forces,
f(x) = a distribution or shape function (e.g.: constant, half sine). It is unity in the Spencer method.
λ = Scaling factor, given by the ratio of Interslice Shear and Interslice Normal, at unit shape function. The arctan (λ) gives the angle of the resultant of X and E with the horizontal.

The F.O.S for moment equilibrium and force equilibrium have been shown in **equation (1.42)** and **(1.43)** respectively

$$F_{M=}\ \frac{\sum[c'\beta R + (N - u\beta)Rtan\emptyset']}{\sum Wx - \sum Nf \pm Dd}$$

$$F_{F=}\ \frac{\sum[c'\beta cos\alpha + (N - u\beta)tan\emptyset' cos\alpha]}{\sum(Nsin\alpha) - Dcos\omega}$$

The Interslice Base normal (N) is determined by the **equation (1.44)**.

$$N = \frac{W + (X_R - X_L) - \frac{c'\beta sin\alpha + u\beta sin\alpha\ tan\emptyset'}{F}}{cos\alpha + \frac{sin\alpha\ tan\emptyset'}{F}}$$

where, c', Φ' = effective cohesion and effective friction angle respectively
u = Pore Water Pressure
X_R, X_L = Interslice shear forces on right and left side respectively of the concerned slice
W, N = slice weight and slice base normal force respectively
D = concentrated point load
α = inclination of slice base
β, R, x, f, d, ω – geometry parameters
F = F_M or F_F as applicable

Multiple iterations are made such that the value obtained satisfies both the above equations or in other words the Normal obtained by the force and moment equilibrium methods must be the same.

The Force distribution on a slice within the sliding wedge with a circular slip surface and a typical G.L.E plot is shown in **figure - 1.9, 1.10**

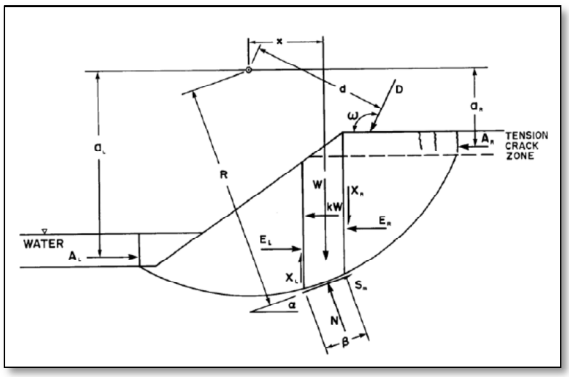

Figure - 1.9 – Force distribution on a slice within the sliding wedge with a circular slip surface

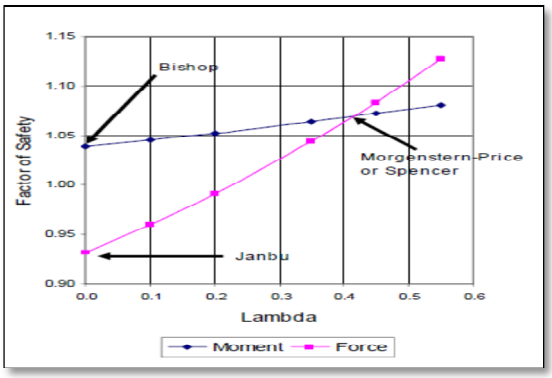

Figure -1.10 – General Limit Equilibrium Plot showing Factor of Safety v/s Lambda

(Courtesy **:** "Stress and Deformation Modeling with SIGMA/W – An Engineering Methodology")

(b) Spencer Method – Similar to the General Limit Equilibrium method, with f(x) = 1 in the equation (1.41). The resultant interslice forces are of constant slope throughout the sliding mass. Here, both the force and moment equilibrium equations must be satisfied simultaneously. This is done in an iterative procedure to reach a particular value of lambda, such that the normal and shear forces computed give the same F.O.S for moment and forces respectively. The value of lambda at this point is shown in figure -1.10 for a particular problem.

(c) Finite Element Method : To overcome the limitations of the limit equilibrium method, the stress – strain approach is incorporated in the finite element stress method. Here, the normal and shear stress distribution are found out. Then these are utilized to determine the local factor of safety or the stability factor given as the ratio of Total Shear resistance to the Shear Mobilized along the entire length of slip surface. Hence, unlike limit equilibrium method, here the F.O.S varies from slice to slice. Thus the displacement criteria is also fulfilled and the stress generated resembles field conditions.

1.3.6 : Applications Of Finite Element Method In Geotechnical Engineering

1.3.6.1 : General

The importance of numerical modeling in geotechnical engineering was illustrated by Professor John Burland, Imperial College, U.K. In his famous Nash lecture in 1987, he explained the role of the three fundamental elements – (1) Ground profile (site characterization and site conditions) (2) Soil behavior (obtained from laboratory tests, field measurements, etc) and (3) Modeling (may be conceptual/ analytical/ physical), by means of the Burland triangle (refer **figure 1.11**)

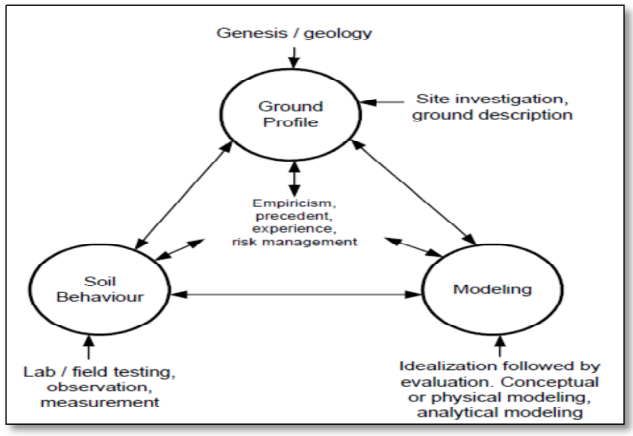

Figure – 1.11 : The enhanced Burland Triangle (after Anon. 1999) (Picture courtesy: GEO-SLOPE International Ltd, "Seepage Modeling with SEEP/W, an engineering methodology", July 2012 edition)

In the recent past, considering advancement in computer engineering, numerical methods applying longer and complicated computations has become possible and time friendly. Hence, the finite element method, which operates on the basic principle of discretization of a structure into finite number of small elements and carrying out analysis on these individual units thereby applying the results to the system as a whole, is a popular tool for simulating complex site conditions and analyzing them

The entire structure can be idealized as an assembly of finite number of discrete elements connected at finite number of nodes. The properties of individual elements are adjusted so that the assembly behaves in the same manner as the original continuum. The most common element for 2D analysis is a simple triangular element with three nos. primary external nodes and in some cases three additional secondary nodes for better solution providing higher number of knowns. Other common types of 2D elements are rectangular and quadrilateral shapes.

The most common method of 2D analysis for structures with lengths very high compared to the other two dimensions is Plane Strain (e.g. Embankments), whereas for structures with lengths very

small compared to the other two dimensions, Plane Stress (e.g. Thin walled plate loaded in its plane) method is opted.

One of the important expressions for plane strain condition in simplified matrix form is given as in **equation (1.45)** -

$$\begin{Bmatrix} \sigma_x \\ \sigma_y \\ \tau_{xy} \end{Bmatrix} = \frac{E}{(1+\mu)(1-2\mu)} \begin{bmatrix} 1-\mu & \mu & 0 \\ \mu & 1-\mu & 0 \\ 0 & 0 & \frac{1-2\mu}{2} \end{bmatrix} \begin{bmatrix} \epsilon_x \\ \epsilon_y \\ \gamma_{xy} \end{bmatrix}$$

where, σ_x, σ_y = The Normal stress components in –x and –y directions respectively
τ_{xy} = Shear Stress component in the –xy plane
ϵ_x, ϵ_y = The Normal strain components in –x and –y directions respectively
γ_{xy} = Shear strain in –xy plane.
E = Modulus of Elasticity of material
μ = Poisson ratio of the material

In a coupled stress – pore water pressure analysis, certain modifications are made to equation (1.45) to get **equation (1.45a)** which gives the incremental stress – strain relationship for an unsaturated soil medium (Fredlund and Rahardjo, 1993) which is similar on the lines of Biot's equation.

$$\begin{Bmatrix} \Delta\sigma_x - u_a \\ \Delta\sigma_y - u_a \\ \Delta\tau_{xy} \end{Bmatrix} = \frac{E\,(1-\mu)}{(1+\mu)(1-2\mu)} \begin{bmatrix} 1 & 0 & 0 \\ 0 & 1 & 0 \\ 0 & 0 & \frac{1-2\mu}{2(1+\mu)} \end{bmatrix} \begin{Bmatrix} \Delta(\epsilon_x - \frac{(u_a - u_w)}{H}) \\ \Delta(\epsilon_y - \frac{(u_a - u_w)}{H}) \\ \Delta\gamma_{xy} \end{Bmatrix}$$

with H = Unsaturated Soil Modulus for Soil structure with respect to matric suction ($u_a - u_w$).

For saturated soil conditions and considering linear elastic material, we have **equation (1.45b)**

$$H = \frac{E}{1-2\mu}$$

The equation (1.45) used above may be used for analysis of 2D earthen embankments in plane strain condition with Mohr-Coulomb or Tresca failure criteria, where the Force matrix is given as in **equation (1.46)**

$$[F] = [k][\delta]$$

The Strain matrix is given as in **equation (1.47)**

$$[\epsilon] = [B][\delta]$$

where, *[F]* = Force Matrix,
[k] = Stiffness Matrix
[δ] = Displacement Matrix
[ϵ] = Strain Matrix
[B] = Strain transformation matrix and is a function of nodal co-ordinates .

After the piecewise discretization has taken place, a relatively simpler function describing the solution of approximate displacement of individual element must also be defined. The most important requirements which the displacement function must satisfy are

(1) Continuity within the element which is usually satisfied by choosing polynomial forms

(2) Compatibility between adjacent element such that deformation should not lead to opening, overlap or discontinuity between them .

In case of a two dimensional problem with triangular element with nodes **i** (x_i, y_i), **j** (x_j, y_j), **m** (x_m, y_m), the displacement of each node in -x , -y direction given as u, v is described in linear model form as in **equations (1.48**, **1.49**, **1.50**, **1.51**, **1.52**, **1.53)**

$$u_i = a_1 + a_2 x_i + a_3 y_i$$

$$u_j = a_1 + a_2 x_j + a_3 y_j$$

$$u_m = a_1 + a_2 x_m + a_3 y_m$$

$$v_i = b_1 + b_2 x_i + b_3 y_i$$

$$v_j = b_1 + b_2 x_j + b_3 y_j$$

$$v_m = b_1 + b_2 x_m + b_3 y_m$$

For the above 2D problem, the linear displacement model may be replaced by various n- degree polynomial approximations in the form of **equation (1.54)**, **(1.55)** at a particular node

$$u(x, y) = a_1 + a_2 x + a_3 y + a_4 x^2 + a_5 xy + a_6 y^2 + \cdots + a_k y^n$$

$$v(x, y) = b_1 + b_2 x + b_3 y + b_4 x^2 + b_5 xy + b_6 y^2 + \cdots + b_k y^n$$

where, a_k *and* b_k in the above equations are termed as *generalized co-ordinates* or *generalized displacement amplitudes.*

The equations (1.54), (1.55) may be simplified into a matrix form as in **equation (1.56)**, **(1.57)**

$$\{u\ (x,y)\} = \begin{bmatrix} \{\emptyset_1\}^T & \{0\}^T \\ \{0\}^T & \{\emptyset_1\}^T \end{bmatrix} \{a_k\}$$

$$\{v\ (x,y)\} = \begin{bmatrix} \{\emptyset_1\}^T & \{0\}^T \\ \{0\}^T & \{\emptyset_1\}^T \end{bmatrix} \{b_k\}$$

where, $\{\emptyset_1\}^T = [\ 1\ x\ y\ \ x^2\ xy\ y^2 \ldots y^n\ ]$

$\{\ a_k\ \}^T = [a_1\ \ a_2\ \ a_3\ \ldots\ \ a_n]$

$\{\ b_k\ \}^T = [b_1\ \ b_2\ \ b_3 \ldots\ \ b_n]$

It has been observed that greater the number of terms included in the approximation, the more closer it gets to the exact solution. The procedure for analysis of these type of structures for deformation model involve :

(i) Idealization of structure into finite number of elements & nodes at appropriate locations established on a global co-ordinate scale.

(ii) Calculation of nodal force vector by distribution of load

(iii) Calculation of stiffness matrix for all elements

(iv) Application of boundary conditions to get modified stiffness matrix.

(v) Strains and Stresses are computed from nodal displacements based on above section.

1.3.6.1.1 : Governing Principles And Terminologies

As we shift more towards the application of F.E.M in Geotechnical Engineering, several notions associated specifically with Solid Mechanics and displacement method has to be modified. One of these is the concept of *continuum* which must be broadened to include fluids, soil media, etc in addition to structural definitions. As per Desai and Abel, commonly used in Solid Mechanics - *Material Subdivision* or subdividing a continuum into an assemblage of finite elements, it was previously envisioned to be either a physical subdivision of the material of the body, or the inscription of dividing lines or planes onto the material, where the nodal points in the assemblage actually move and the assemblage mesh is deformed. However, Material Subdivision may not stand relevant in other fluids. For example in Fluid Mechanics, the assemblage represents a *Spatial Subdivision*, where the finite element doesnot represent the fluid, but the space through which it flows. The velocity potential is a typical unknown in fluid mechanics, which is to be solved at nodes

of an assemblage that is fixed in space. In coupled problems such as fluid flow through a porous deformable medium, the displacements and potentials have to be simultaneously solved, hence a combined point of view of the assemblage may be taken. However, the concept is satisfactory for small displacement of nodes.

The principal unknowns of a problem are the *Field Variables*. These may be in the form of displacements, potentials, temperature, stresses, etc. A *Field Variable Model* is the assumed function which approximates the distribution of the field variable over a finite element, example – displacement model discussed in earlier sections. The *Amplitude of a Field Variable* is the magnitude of the variable at a node or at a particular location. The term *Nodal Field Variable Vector* denotes the vector of unknown amplitudes at the nodal points. The *Gradients of a Field Variable* refers to the derivatives or rates of change of variables, e.g.: Rate of change corresponding to strains, slopes in displacement model.

As seen in earlier sections, in the displacement model, a set of equilibrium equations is used to relate nodal displacements to nodal forces through a Stiffness Matrix. The general algebraic equations that result from the element analysis are the *Finite Element Equations*. The vector of forcing parameters analogous to loads is called the *Nodal Action Vector* or the *Nodal Force Parameter Vector*. These may be in the form of fluid flux, prescribed displacements, applied temperatures, etc. One of the essential components of the finite element equations is the matrix of co-efficients which characterizes the properties of the matter or material considered in the problem and is termed as *Property Matrix* or *Characteristics Matrix*, e.g. – stiffness for displacement method. These may also include hydraulic conductivity, flexibility, etc, for other model types.

In the formulation of finite element equations, *a variational principle or energy theorem* is generally used, e.g.- principle of minimum potential energy used in displacement method. The functional used in such a formulation is known as *Associated Variational Functional*. Examples are the complimentary energy for equilibrium method and total potential for displacement method. It is possible to obtain an associated functional without knowledge of the specific energy theorem governing the problem. For example, the differential equation associated with Laplace equation in 3D given in **equation (1.58)**

$$\frac{\partial^2 u}{\partial x^2} + \frac{\partial^2 u}{\partial y^2} + \frac{\partial^2 u}{\partial z^2} = 0$$

It has a associated functional *A*, obtained from variational calculus as in **equation (1.59)**

$$A = \iiint \frac{1}{2}\left[\left(\frac{\partial u}{\partial x}\right)^2 + \left(\frac{\partial u}{\partial y}\right)^2 + \left(\frac{\partial u}{\partial z}\right)^2\right] dV$$

where u is the field variable.

Seepage through porous media is governed by the Laplace and Poisson equations depending on nature of the problem. A generalized associated functional often employed for finite element equations are given as in **equation (1.60)**

$$A = \iiint_V \frac{1}{2}\left[k_x\left(\frac{\partial \psi}{\partial x}\right)^2 + k_y\left(\frac{\partial \psi}{\partial y}\right)^2 + k_z\left(\frac{\partial \psi}{\partial z}\right)^2 - C\psi\right] dV$$

where, C, k_x, k_y, k_z are known functions of –x, -y, -z. When C = 0, the above Eulerian equation becomes a Laplace equation, otherwise it becomes an Poisson equation.

However, it is not necessary for the finite element formulations to have a associated functional. In addition to the Direct Method, General Energy Balance Concepts and Residual Concepts (Collocation, Least Squares and Galerkin methods) may be also be used for generation of finite element equations. The classification of finite element methods in solid mechanics is given as per **Table -1.1**

TABLE-1.1 : Classification Of Finite Element Methods In Solid Mechanics

(Courtesy**:** Numerical Methods in Engineering, Vol-1, No.1,1969, Wiley Interscience, London)

Methods	**Variational Principle**	**Assumption inside each element**	**Assumption along Inter-element boundary**	**Unknowns in final equations**
Displacement	Minimum Potential Energy	Smooth displacement distribution	Continuos displacement	Nodal displacement
Equilibrium	Minimum Complimentary Energy	Smooth and Equilibrating Stress distribution	Equilibrium of Boundary tractions	(a) Generalized Nodal displacement (b) Stress function parameters.
Hybrid Equilibrium	Modified Complimentary Energy	Smooth and Equilibrating Stress distribution	Assumed compatible displacements	Nodal displacements
Hybrid displacement	Modified potential energy	Smooth displacement distribution	Assumed equilibrating boundary tractions	Boundary redundant forces

1.3.6.1.2 : Procedural Description

A six step procedure for finite element analysis of Seepage through a rigid porous medium is given below (Desai and Abel) –

(i) *Discretization of the continuum* : The continuum is divided into an equivalent system of finite elements according to the principles of displacement method, such that the elements are fixed in space and do not change in size or shape while the fluid seeps through them.

(ii) *Selection of the field variable models* : Assumed patterns of the field variables within each element are selected, usually in polynomial form. The unknowns of the system thereby become the amplitudes of the field variables at the nodes. For seepage, the field variable is the Hydraulic Head (H), which is a scalar quantity compared to displacements which is a vector quantity.

(iii) *Derivation of the finite element equations* : The derivation of the finite element equations may be achieved by Direct methods, variational methods or Residual methods. The associated functional for the steady state seepage problem is in **equation (1.61)**

$$A = \iiint_V \frac{1}{2}\left[k_x\left(\frac{\partial H}{\partial x}\right)^2 + k_y\left(\frac{\partial H}{\partial y}\right)^2 + k_z\left(\frac{\partial H}{\partial z}\right)^2\right] dV$$

with *k* being the hydraulic conductivity, making the characteristic matrix as the hydraulic conductivity matrix.

(iv) *Assembly of the algebraic equations for the overall discretized continuum* : The assembly process is exactly analogous to the displacement method, that is the direct stiffness method is used to obtain an overall hydraulic conductivity matrix.

(v) *Solution for the nodal field variable vector* : The solution of the overall methods is described by the matrix methods.

(vi) *Computation of the element resultants from the nodal field variable amplitudes* : The element resultants or the secondary field variables are governed by the type of problem analyzed. The process is analogous to the calculations of stresses, strains in displacement type problems. In seepage problems, the element resultants desired are the fluid velocities and / or flow rates.

As per Desai and Abel, the finite element approach for seepage related issues encountered in practical geotechnical conditions is given as per **Table - 1.2**

TABLE - 1.2 : Generalization Of Finite Element Methods pertaining to Seepage

Field of Application	Field Variables	Actions	Properties
Seepage in Rigid Media	Hydraulic head or fluid potential	Sources, flux	Permeability, porosity
Seepage in deformable media			
Uncoupled	Displacements and/ or Stress	Mechanical loads, applied displacements, pore pressure	Elastic or elastic plastic stiffness plus porosity
Coupled	Displacements and/ or Stress plus Pore Pressure	Mechanical loads, applied displacements, fluid flow	Elastic or elastic plastic stiffness plus permeability and porosity

1.3.6.2 : Application Of F.E.M In Seepage Related Problems

Both steady and transient state fluid flow in porous media are significant problems belonging to the class known as field problems. Typical applications in this field are given as –

(i) *Steady Confined Seepage* : The fluid potentials at all pervious external boundaries are constant and known. e.g. Seepage through a confined permeable foundation under constant head.

(ii) *Steady Unconfined Seepage* : These problems involve a free or phreatic surface, whose boundary is not known in advance and its location is governed by non-linear law. e.g. Seepage through a permeable foundation under constant head.

(iii) *Unsteady Unconfined Seepage* : These problems also involve a free or phreatic surface, whose boundary is not known in advance, however, the boundary conditions are not constant and are a function of time. e.g. Seepage in Earthen embankments under tidal head variation.

(iv) *Unsteady Confined Seepage* : It involves transient or unsteady seepage in confined conditions. e.g. Flow towards wells in saturated confined aquifers.

The basic mathematical equations for seepage related problems by the finite element method are given in the subsequent sub-sections.

1.3.6.2.1 : Mathematical Background

The basic differential equation governing two dimensional seepage, which is on the lines of equation (1.2) may be expressed as in **equation (1.62)**

$$\frac{\partial}{\partial x}\left(k_x \frac{\partial \psi}{\partial x}\right) + \frac{\partial}{\partial y}\left(k_y \frac{\partial \psi}{\partial y}\right) + \overline{Q} = c\frac{\partial \psi}{\partial t}$$

where, $\overline{Q}$ = The applied fluid flux per unit volume
c = porosity,
ψ = Fluid Potential or total head, which is the sum of pressure head and elevation head (Unknown field variable in seepage problems).
$k_{x,y}$= Co-efficient of soil permeability for water flow in the –x, -y directions respectively

If the time dependant term on the right is removed, the above equation takes the form of Poisson equation, which is a form of steady state.

The boundary conditions for the above problem is given as per **equation (1.63)**, **(1.64)**

$$\psi = \overline{\psi}(t) \ \ on \ \ S_1$$

$$k_x \frac{\partial \psi}{\partial x} l_x + k_y \frac{\partial \psi}{\partial y} l_y + \overline{q}(t) = 0 \ on \ \ S_2$$

where, S_1 is the part of the boundary on which ψ is prescribed. S_2 is the part of boundary on which $\overline{q}$,being the flow intensity on the surface of the element, is applied.

l_x, l_y = Direction cosines of the outward normal to the boundary

The associated functional corresponding to above type of problems is given by **equation (1.65)** -

$$A = \iiint_V \frac{1}{2}\left[k_x\left(\frac{\partial \psi}{\partial x}\right)^2 + k_y\left(\frac{\partial \psi}{\partial y}\right)^2 + k_z\left(\frac{\partial \psi}{\partial z}\right)^2 - 2(\overline{Q} - c\frac{\partial \psi}{\partial t})\psi\right] dV - \iint_{S2} \overline{q}\,\psi \, dS_2$$

The boundary condition in equation (1.63), (1.64) must also be satisfied. Alternative functional proposed by Gurtin or residual approach method by Galerkin may also be utilized.

The potential may be written as in **equation (1.66)**

$$\psi = \{N\}^T\{\psi_n\}$$

where, $\{\psi_n\}$ = Vector of nodal potentials
$\{N\}^T$ = Matrix of Interpolation / Shape functions

If a linear model for a triangular element is adopted, there shall be three nodal potentials and hence $\{\psi_n\}$ shall be 3 X 1. The differentiation of ψ in above equation with respect to the x and y co-ordinates gives the vector of gradients, $\{g\}$ as in **equation (1.67)**

$$\{g\}_{2\ X\ 1} = \begin{Bmatrix} \partial\psi/\partial x \\ \partial\psi/\partial y \end{Bmatrix} = \frac{1}{2A}\begin{bmatrix} b_1 & b_2 & b_3 \\ a_1 & a_2 & a_3 \end{bmatrix}\begin{Bmatrix} \psi_1 \\ \psi_2 \\ \psi_3 \end{Bmatrix} = [B]\{\psi_n\}$$

with a_i , b_i are defined as per **equations (1.68)**, **(1.69)**, **(1.70)**, **(1.71)**, **(1.72)**, **(1.73)** where **1** (x_1,y_1), **2** (x_2,y_2), **3** (x_3,y_3) denote the nodes of the triangular element.

$$a_1 = x_3 - x_2, \qquad a_2 = x_1 - x_3, \qquad a_3 = x_2 - x_1$$

$$b_1 = y_2 - y_3, \qquad b_2 = y_3 - y_1, \qquad b_3 = y_1 - y_2$$

The matrix of permeabilities in the principal directions [R] is given as in **equation (1.74)** -

$$[R] = \begin{bmatrix} k_x & 0 & 0 \\ 0 & k_y & 0 \\ 0 & 0 & k_z \end{bmatrix}$$

The following finite element **equation (1.75)** is formed –

$$[p]\{\psi_n\} + [k]\{\psi_n\} = \{f\}$$

where the respective terms are defined in **equations (1.76), (1.77), (1.78)**

$$[p] = c\iiint_V \{N\}^T\{N\}\,dV$$

$$[k] = \iiint_V [B]^T[R][B]\,dV$$

$$[f] = \iiint_V \{N\}^T\{\overline{Q}\}\,dV + \iint_{S2} \{N\}^T\{\overline{q}\}\,dS_2$$

where, *[N]* denoting the field variable interpolation model
[B] denoting the corresponding field variable gradient model
[p] denoting the element porosity matrix
[k] denoting the element permeability matrix
[f] denoting the element nodal vector of applied flow
n denotes the nodal values.

The direct stiffness method is used to obtain the equations for the assemblage **equation (1.79)**,

$$[P]\{\psi_n\} + [K]\{\psi_n\} = \{F\}$$

where the applied potentials are introduced and the time dependant equations are solved as propagation problems. The solutions of equation (1.79) give the values of nodal fluid heads as primary quantities. Once these heads are known, fluid velocities and quantities of flow may be evaluated as element resultants. The velocity and discharge components can be obtained as per **equations (1.80), (1.81)**

$$\{v\} = \begin{Bmatrix} v_x \\ v_y \end{Bmatrix} = -[R] \begin{Bmatrix} \frac{\partial \psi}{\partial x} \\ \frac{\partial \psi}{\partial y} \end{Bmatrix} = -[R][B]\{\psi_n\}$$

$$\begin{Bmatrix} Q_{x1} \\ Q_{x2} \\ Q_{x3} \\ Q_{x4} \\ Q_{x5} \\ Q_{x6} \end{Bmatrix} = -\frac{1}{2} \begin{bmatrix} b_1 & 0 \\ b_2 & 0 \\ b_3 & 0 \\ 0 & a_1 \\ 0 & a_2 \\ 0 & a_3 \end{bmatrix} \{v\}$$

1.3.6.3 : Numerical Modeling Using F.E.M Based Computer Software

The fundamentals of modeling in any F.E.M based software is –

(i) Creation of numerical domain: Preparation of model geometry and discretization of the mesh elements

(ii) Specification of material properties

(iii) Generation of finite element mesh

(iv) Application of boundary conditions

The general technique during numerical modeling is to start simple with the estimated soil parameters, add complexities in stages to make analysis less cumbersome, make a guess about the probable results of the problem and then try and match the outcomes from the analysis, leave out any components if seem unnecessary.

The basic equation used for solving steady state seepage problems is given by **equation (1.82)**

$$[K]\{H\} = \{Q\}$$

where, *[K]* = Characteristic matrix containing hydraulic conductivity / Element Property Matrix
{H} = Vector of Unknown Head / Nodal Total Head

{Q} = Flow Vector / Nodal flow

The equation is solved for either the unknown vector head or the unknown flow vector, as per suitable boundary conditions

The finite element equation for transient conditions, in terms of a "Backward Difference" finite difference form leads to the **equation (1.83)** (Segerlind,1984)

$$\Delta t\,[K] + [M]\{H_1\} = \Delta t\,\{Q_1\} + [M]\{H_0\}$$

where, Δt = time increment,
[M] = Mass matrix (accounts for storage during time increment and is a function of the volumetric water content function)
{H_0}, {H_1} = Initial head at start of time step and new head at the end of time step, respectively
{Q_1} = Transient boundary condition

One of the major concerns during analysis of partially saturated soils is the hydraulic conductivity, which no longer remains a constant and becomes a function of the matric suction. Since the matric suction itself depends on the water head which must be computed, hence the entire non-linear problem must be solved by iterative numerical techniques.

Computer softwares have made life easy for geotechnical engineers when handling of numerous elements and solving individual elements in an iteration based analysis, comes into play. One of the popular finite element based software for seepage analysis is SEEP/W, a product of GeoStudio. The associated slope stability analysis can be carried out using SLOPE/W, another package of GeoStudio.

The fundamentals of modeling in the above mentioned softwares have been discussed in the sections below.

1.3.6.3.1 : Modeling With Seep/W

Material Modeling Types

Usually four types of soil behavior models are available in SEEP/W-

(i) *None* : To model inactive regions

(ii) *Saturated/ Unsaturated* : This is used for partially saturated models, where the range of input varies from hydraulic conductivity function with ratio and direction, water content function, air conductivity function.

(iii) *Saturated Only*: This is used for model portions which lie permanently below the phreatic line. The range of input are Saturated hydraulic conductivity with ratio and direction, saturated water content, co-efficient of volume compressibility

(iv) *Interface model*: It is used to model geo-membranes, wick drains, cutoff walls, etc. The input parameters are hydraulic normal and tangent conductivity, air conductivity, etc.

Development of Storage Function

One of the major input parameters for transient seepage analysis is the volumetric water content function. It may be estimated by –

(i) A closed form solution that requires user specified curve fitting parameters.

(ii) To use a predictive method that uses a measured grain size distribution curve.

SEEP/W has three methodologies available to develop a volumetric water content function, as -

(a) Estimation of a data point function using a predictive method based on grain size (e.g. – Modified Kovacs method)

(b) Based on a sample set of functions already built within the software (shown in **Figure 1.12**)

(c) Based on closed form equations using curve fitting parameters (e.g.- Fredlund and Xing method, Van Genuchten method)

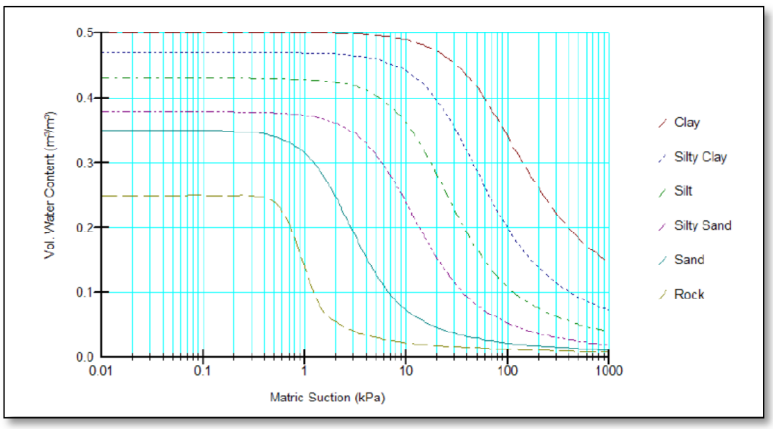

Figure : 1.12 – Built in sample set of VWC functions in SEEP/W, GeoStudio (Picture courtesy: GEO-SLOPE International Ltd, "Seepage Modeling with SEEP/W, an engineering methodology", July 2012 edition)

Development of Conductivity Function

The hydraulic conductivity function may be developed in SEEP/W based on methodologies discussed in earlier sections.

When the Green and Corey (1971) method is used, the term $\left(\frac{30T^2}{\mu g \rho}\right)\left(\frac{\eta^p}{{n_O}^2}\right)$ in equation(1.31) is taken as unity. The hydraulic conductivity at zero pressure is calculated using the **equation (1.84)**

$$k_{SC} = \left[\sum_{j=i_K}^{m} (2j + 1 - 2i_K){h_{iK}}^{-2}\right]$$

The saturated conductivity (K_S) is user defined. After the basic plot is obtained, it is refined by using the matching factor, so that the function passes through the point, K_S.

Mesh and Convergance

Generally in 2D Uncoupled analysis, the degree of freedom associated with each node is one, i.e. Head or Pore Water Pressure. In case of 2D Coupled analysis the degree of freedom associated with each node becomes three, i.e. deformation in the –X and –Y directions and Pore Water Pressure. Another important criteria in mesh analysis is the selection of field variable distribution, which may be linear or curved. Generally, in linear variation, nodes at the corners of the elements are sufficient for the analysis and are termed as First Order Elements. The derivative of the field variable with respect to distance is a constant in the above case and is suitable for seepage problems. When three nodes are defined along an edge (i.e. additional node at each edge compared to the First Order Elements), the distribution of field variable is defined by a quadratic solution, with a linear equation gradient. Such elements are termed as Second Order Elements. These are effective in case of Stress – Deformation analyses with multiple degrees of freedom for field variables. Element and mesh compatibility also play a vital role in the finite element analysis. Connected elements must have common nodes and the distribution of field variable must be the same for an edge common to two elements. The mixing of elements of different orders may create incompatibility. In GeoStudio, additional Gauss Integration Points are generated within an element where sampling is done individually during development of the Characteristics matrix and solved data is stored accordingly after completion of analysis.

Time stepping / Temporal Integration

The time increment should be sufficiently large to allow the moving particle to move a significant distance relative to the element size, while it should not be so large so as to allow the particle jump

across several elements resulting in less data. To be more precise, if the migration of wetting front is too rapid, then time steps need to be decreased and if the migration is too slow, they must be increased. Each time step is basically a miniature steady state analysis. It has been observed that element size is directly proportional to the time step size. Thus, when the element size is increased / decreased, the time step must be increased/ decreased accordingly.

Boundary Conditions

For modeling a transient phenomenon, the boundary condition may be imposed as a Hydraulic Head function which changes with respect to time.

1.3.6.3.2 : Modeling With Sigma/W

Apart from the stability criteria, it is also important to look into the serviceability criteria in order to get a full picture of the problem. In other words, the deformation under working loads must also be checked to satisfy the serviceability criteria. The deformation based analysis can be performed using SIGMA/W.

Some of the constitutive models available are (i) Linear Elastic Model (ii) Mohr-Coulomb Model (iii) Modified Cam-Clay Model, etc.

The material parameters are in the form of (i) Total Stress, where the total stress parameters are selected ignoring pore water pressures (ii) Effective Drained, where the effective stress parameters are considered, however the excess pore water pressure is dissipated as soon as it develops as in granular soils (iii) Effective Undrained or Effective with PWP change. where the effective stresses are considered with analysis of the excess pore water pressure (e.g. Coupled Consolidation analysis)

The basic finite element equation used for coupled analysis in SIGMA/W where both the deformation and pore water pressures are unknowns and can be simultaneously determined is given in **equation (1.85).** It is interesting to note that it is the combined action of the force equilibrium equation and the flow continuity equation.

$$\begin{bmatrix} [K_S] & [L] \\ [L]^T & [K_W] \end{bmatrix} \begin{Bmatrix} \Delta d \\ \Delta u \end{Bmatrix} = \begin{Bmatrix} \Delta F \\ \Delta Q \end{Bmatrix}$$

where, *[L]* = coupling matrix,
[K] = Matrix containing material properties (conductivity, stiffness, etc)
[F] = Force matrix
{d} = deformation vector

{u} = Pore Water Pressure vector
[Q] = Flow matrix

However, the computed known values of pore water change can also be imported from parent SEEP/W analysis, if possible. In that case, only the deformation is computed.

In this type of coupled analysis, it is mandatory to provide both hydraulic and stress- strain boundary conditions.

A important property which may be used for calculation of deformation is the Modulus of Elasticity (E). A simple relation between the modulus of volume compressibility (m_v), Bulk modulus (K_b) and the Modulus of Elasticity is given in **equation (1.86)**

$$m_V = \frac{1}{K_b} = \frac{3(1-2\mu)}{E}$$

For Poisson ratio, μ =0.333 which is very common for soils, we get **equation (1.87)**

$$m_V = \frac{1}{E}$$

1.3.6.3.3 : Modeling With Slope/W

The slope stability analysis can be performed with SLOPE/W using the Limit Equilibrium method for Uncoupled analysis, where the pore water pressures can be imported from SEEP/W analysis. The various methods under the Limit equilibrium domain available are – GLE, Bishop simplified, Janbu simplified, Morgenstern - Price, Spencer, Lowe-Karafiath, Corps of Engineers , Sarma, etc. Additionally, a Finite Element Stress based slope stability analysis can be performed with stress distribution imported from SIGMA/W analysis.

The trial slip surfaces can be selected by various methods such as (i) Entry and Exit method (ii) Grid and radius for circular slips (iii) Composite slip surfaces (iv) Specified Slip surfaces (v) Block slip surfaces, etc. The F.O.S is computed separately for each trial slip surface and the same is repeated as per user input of number of trials. The minimum F.O.S is selected for evaluation. SLOPE/W additionally provides a safety map, which shows the contour of slip surfaces with similar values of F.O.S

1.3.7 : Experimental Modeling Techniques

1.3.7.1 : General

The basic requirement of any laboratory model developed on the basis of the field prototype is to simulate site conditions in a controlled environment and study the influence of the suspected parameters on the same. The Laboratory model has its limitations and the entire site conditions especially in the geotechnical domain can never be modeled with 100 percent accuracy. Proper care must be taken about the scaling techniques applied and instrumentation developed as per requirement. The selection of boundary conditions is important in any laboratory model. Moreover, the set-up must be developed on the basis of type of study. For example, for studying a Plane Strain condition, the dimensions of the set-up shall be different compared to a Plane Stress condition.

Laboratory models based on Plane Strain Seepage problems are used throughout the globe to study various parameters like pore pressures, soil movements, soil stresses, etc as and when applicable. The Hampden H- 6510 Drainage & Seepage Tank is a popular commercially available set-up for studying seepage related problems. General laboratory set-up for seepage studies include a tank containing the required soil model, with provisions of entry and exit of water at both ends . A small reservoir is also present with a small pump to control the entry of water. Exit of water is usually done by gravity. A dye chamber is sometimes fitted to study flow lines. A set of piezometers is also required to measure pore water pressures. Some of the common instruments utilized for measurement of pore water pressure are (i) ordinary stand pipe piezometer (ii) Digital transducers

1.3.7.2 : Scaling for Model and Prototype

During modeling, it is important to maintain *Similitude* which is defined as the similarity between the model and the prototype in every aspect. Three types of similarities must exist between the model and prototype –

(a) *Geometric Similarity* : The ratio of all corresponding linear dimension in the model and prototype are equal. It is defined by the Length Scale ratio, L_r given as in **equation (1.88)**

$$L_r = {}^{L_P}/_{L_m}$$

where, L_P and L_m = Corresponding linear dimensions of prototype and model respectively

(b) *Kinematic Similarity* : It defines the similarity of motion between the model and prototype and defined by the ratios of velocity and acceleration at corresponding points in the model and prototype.

(c) *Dynamic Similarity* : The ratio of all corresponding predominant forces both in magnitude and direction must be same for the model and prototype.

The various model laws in hydraulics are – (i) Reynold's Model (where the inertial and viscous forces are predominant), (ii) Froude's Model (where the inertial and gravitational forces are predominant), (iii) Euler's Model (where the inertial and pressure forces are predominant), (iv) Weber's Model (where the inertial and surface tension forces are predominant).

An attempt as been made in forthcoming chapters to model the tidal effect on the riverfront embankment on the basis of Froude's model law, where the predominant forces are Inertia and Gravity. The various parameters have been scaled according to this law for the field (i.e. prototype) and laboratory (i.e. model). The details are discussed below.

The basic formulations as per Froude's Model law is given as in **equations (1.89)**, **(1.90)**. Some other important features of Froude number model are given in **Table -1.3**

$$F_{e(model)} = F_{e(Prototype)}$$

$$V_m \Big/ \sqrt{g_m L_m} = V_P \Big/ \sqrt{g_P L_P}$$

where $F_{e(model)}$, $F_{e(Prototype)}$, g_m, g_P , V_m, V_P are the Froude number, acceleration due to gravity, velocity of model and prototype respectively.

Table -1.3 : **Parameter Scale Ratio as per Froude Model Law**

Serial No.	Parameter	Criteria Ratio
1	Time scale ratio ($T_r = T_p / T_m$)	$\sqrt{L_r}$
2	Acceleration scale ratio ($a_r = a_p / a_m$)	1
3	Velocity scale ratio ($V_r = V_p / V_m$)	$\sqrt{L_r}$
4	Discharge scale ratio ($Q_r = Q_p / Q_m$)	$L_r^{2.5}$

where, a_m, a_P, T_m, T_P, Q_m, Q_P are the acceleration, time, discharge of model and prototype respectively.

CHAPTER TWO
LITERATURE REVIEW

CHAPTER TWO
LITERATURE REVIEW

This part has been sub-divided into five portions in accordance to the relevance of current thesis , viz. Steady State Seepage, Transient State Seepage, Soil Water Characteristics Curve, Hydraulic and Geotechnical Scaling, Slope Stability Analysis. The available literature associated with each of the above mentioned sub-divisions is enormous and only the ones studied extensively by the author during this coursework has been included below.

2.1 : STEADY SEEPAGE –

Steady seepage may be defined as the time independent state of seepage flow, which occurs under a constant head. The general equation for two dimensional steady state flow is given by

$$\frac{\partial}{\partial x}\left(k_x \frac{\partial h}{\partial x}\right) + \frac{\partial}{\partial y}\left(k_y \frac{\partial h}{\partial y}\right) = 0$$

where the terms have their usual meaning.

Li and Desai (1983) : Utilized the FEM approach for seepage & stability analysis of earthen dams. The seepage (based on residual flow schemes in both unsaturated & saturated zones) & external forces are super-imposed , on the same mesh , which remains invariant through the sequential construction stages of the model dam. The residual flow scheme involves solution of a differential equation for incompressible media involving permeability (maximum for saturated condition & pressure dependant one for unsaturated regions) , porosity , fluid head & specific storage The behavior of soil is given by Linear elastic , piecewise linear elastic (Hyperbolic) & Drucker- Prager models . The results were compared with field values.

Boufadel etal (1999) : The effect of capillary flow on steady seepage in trenches and dams was studied. A model was developed & compared with formulation to see the effects of unsaturated zone on seepage face heights & outflows from hypothetical unconfined anisotropic rectangular domains. It was seen that seepage occurred in unconfined groundwater flows as well. The formulation centred along three dimensionless parameters M (product of anisotropy ratio & squared ratio of the vertical length scale to horizontal length scale), n (pore size distribution), α (ratio of vertical length of domain to height of capillary fringe). Nomo graphs were developed for rectangular domains & trapezoidal dams. For trapezoidal domains , the seepage face height decreased first with decreasing M and increased later at low values of M .

Boufadel etal (1999) : This work elucidates the advantages of the dimensionless formulation by discussing issues related to scaling of physical systems and by investigating steady seepage in an anisotropic trapezoidal domain simulating a dam. The requirement of proper scaling down from anisotropic to isotropic is essential, as pointed out by this study, else error in the estimation of seepage was almost 60 percent.

Sachpazis (2014) : By means of a drainage and seepage tank, an experimental flow net system inside the body of a homogenous earth embankment dam model, formed from Leighton Buzzard Silica sand, was developed and studied in this experimental research paper, for Steady State

Shrivastava etal (2015) : The seepage analysis for a model to derive the equation of the phreatic line experimentally and thereafter proposing the best solution to trace the line has been shown. Sandy silt is used as a base material for this case. Phreatic Line for the model is plotted by carrying out 3 iterations each for two cases, earthen dam without filter and with filter. Their corresponding phreatic line curves are traced on the butter paper on one of the longer side of the model. Further, the traced curves are compared with the Analytical solution of Casagrande. Regression modeling had been done to obtain an equation of phreatic line.

2.2 : TRANSIENT SEEPAGE

Transient seepage may be defined as the time dependent state of seepage flow , which may occur due to a varying boundary conditions. The general equation for two dimensional transient state flow is given by

$$\frac{\partial}{\partial x}\left(k_x \frac{\partial h}{\partial x}\right) + \frac{\partial}{\partial y}\left(k_y \frac{\partial h}{\partial y}\right) = \frac{\partial \theta}{\partial t}$$

where the terms have their usual meaning.

Aral and Maslia (1983) : An transient analysis for seepage involving unsaturated – saturated criteria in FEM model , was carried out for the western dyke of Wallace dam (Lake Oconee , Georgia , USA) . The water level fluctuation was about 1.5 ft (0.46 meter). The effect of presence of chimney drain , 1.8 m wide , on this zoned dam was also studied. The unsteady state is given by a partial differential equation , which was numerically solved by Galerkin formulation.. It was observed that the saturated-unsaturated flow model developed in this study is less sensitive to variations in pressure head /volumetric moisture content relations in comparison to variations in other parameters. The flow vector to the chimney drain showed that it was very effective in reducing seepage pressures.

Yang H. Huang (1986) : This research publication has tried to estimate the position of phreatic surface in earthen dams due to unsteady flow, as a function of time. This procedure follows the methodology of Cedergren (1977), where the phreatic surface in impervous horizontal base earthen dams using transient flownets was developed and compared with a viscous fluid model . With time , while the upper end of the phreatic surface remained still at entry point water level , the same moved horizontally along the impervous base towards the downstream end. The same was assumed to be a straight line to be on the conservative side.

Chang (1987) : In this paper , Boundary element method (BEM**)** has been presented for seepage analysis of earthen dams involving drawdown of the water level in the reservoir. It was observed that amongst various numerical techniques, the boundary element method is perhaps the most flexible and efficient tool for solving the seepage problem involving free surface, because the boundary element method requires discretization only on the boundary rather than over the whole region, as required in FEM. Furthermore, some numerical instabilities, related to redefining the finite element mesh after the location of free surface changes at the end of each time step, are also avoided . Though the boundary element method is an efficient tool for analysis, the question often arises regarding the applicability of such an analytical tool to field conditions, in view of the mathematical idealization in the boundary element method, which neglects some factors of the field condition, such as geometrical details, the consolidation effect, the soil capillarity effect, material variation, stress-dependent permeability, etc. This paper reports an evaluation of the applicability of the boundary element method to the seepage analysis of earth dams due to drawdown of the water level in reservoir. Dam heights used in this evaluation range from 15 inches to 100 feet The evaluation is based on comparisons between calculated response and measured results from laboratory model test and field observations, for types of soil ranging from coarse sand to clayey sand.

Desai (1988) : This paper has discussed the various merits & de-merits of seepage analysis in uncoupled mode, coupled analysis with deformation from case studies where field data has been compared with computed data from finite element / finite difference analysis**.** In coupled analysis, both displacement and pore water pressures are assumed to be the unknowns in FEM. In uncoupled analysis , the residual flow procedure (i.e. same mesh is used for stress and seepage) is coupled with an non-linear finite element with elasto-plastic models for soils. Moreover, unlike as in coupled approach , partial saturation may be assumed. Case studies discussed included- (i) Transient Seepage Analysis of River Mississippi (ii) Time dependant head fluctuation analysis of

Sherman Dam (iii) Consolidation & Seepage in deformable soils using Biot's Coupled Approach & Uncoupled approach by Residual flow procedure.

Thieu etal (2001) : Three cases, involving 2D Steady state conditions, transient conditions & 3D steady state conditions have been studied. The role of permeability and water storage with variations in suction pressure have been studied experimentally and compared with available literature. In solving for the flow-nets during both steady and transient conditions, the boundary conditions have been carefully selected and inputted into the Partial Differential Equation for seepage. The values of permeability & water storage has been carefully selected , to cater to the unsaturated soil property functions. The best fit line was taken from mathematical softwares, with a predetermined error margin. Solutions indicate that the phreatic line positions defined are very sensitive to the transient state seepage predictions at early times and in long run they lie significantly close to the that of the steady state

Simulia- Abaqus Technology (2007) : This literature discusses the utility of the Abaqus (a commercially available software based on Finite Element method) to simulate the construction process of an earthen dam , which after completion is subjected to Rapid drawdown & earthquake load. The results from the Abaqus model includes Position of Phreatic surface , pore pressures & slope stability during rapid drawdown

Ozkan and Adrian (2008) : In this paper, transient flownets have been developed for a homogenous, isotropic flow medium with respect to fluctuations in reservoir head. The geometry of the flownets do not change with time, however the numerical values assigned to equipotential lines and flow lines change with time. Two solutions of transient flownets were obtained, one for infinite depth aquifers and one for finite depth aquifers. Modifications were proposed to Polubarinova – Kochina method (1962) of analysis.

Ozkan etal (2008) : Analytical methodology has been developed for transient head conditions (sinusoidally varying boundary conditions), under a levee for confined flow problem. The effect of levee flooding on the uplift forces developed, potential for sand boil on land side with piping through permeable horizontal confined aquifer layer was analyzed and discussed based on Mississippi River model.

Jia etal (2009) : This paper presents a large-scale 1g- Centrifuge model test simulating the performance of a sandy silty soil slope subjected to water level rise and drawdown.

Hansen etal (2012) : In this paper a numerical parametric study of twenty-four flow through rock fill dam geometries was conducted. The nonlinear nature of the p-laplacian–like partial differential equation was dealt with using a finite-difference scheme that directly incorporated the exponent of a power law that replaced Darcy's law. Convergence, use of specialty nodes, nodal density, and boundary condition effects were quantitatively investigated. The flow-field angle of the toe was found to be a useful starting point in studying the potential for unraveling failure. Factors of safety (FS) against this type of failure are then presented for a range of downstream slopes, thus showing which combinations of slope and particle diameter are unsafe . It is shown that the FS tends to drop below unity under the seepage face primarily because of the strength of the exit gradient near the toe of the structure and secondarily because of the overflow velocity. In modeling high Reynold number , non-Darcy flow , apart from finite difference , finite element , finite volume or boundary integral equations , FD (non linear finite difference & best applicable for internal nodes) & NLHC may be used .The paper has compared the two methods applicable for non-Darcy flow (i.e. Non laminar flow). There is very little difference between hydraulic heads found using the PCL approach and the NLHC method of modeling, where both are cases of completely non-Darcy flow shows that there is also little difference between hydraulic heads found for flow governed by Darcy's law & that with non-Darcy flow.

Rakhshandehroo and Pourtouiserkani (2013) : A 3-D finite element model of the Doroodzan Dam on Kor River (Iran) was developed and analyzed for steady and transient conditions. Transient pore water pressure fluctuations were predicted at different piezometer locations for a 21-day rapid drawdown of 23.9m. It was found that seepage through the dam is not sensitive to hydraulic conductivity of downstream dam body, apparently due to the effective hydraulic behavior of the chimney drainage there. Under rapid drown down conditions, a maximum of 11.8m excess pore water pressure on upstream part of the dam was observed (compared to the steady state conditions) while no significant excess pressure was seen at the downstream part of the dam. Dynamics of the phreatic line location during the 21-day rapid drawdown was monitored in four 5.25-day time steps. Phreatic line at the upstream face of the dam closely followed the reservoir level rapid drawdown. However, phreatic line at the interior sections of the dam did not drop as fast. As a result, a gradient towards upstream face of the dam was developed after 10 days which might jeopardize slope stability there. In general, rapid drawdown should be cautiously analyzed in dams, especially those with short emptying times, as it may reverse the seepage direction, endanger the slope stability, and not allow excess pore water pressure to dissipate . A 4-year period (1999 to 2002) field data was used for calibrating the model and the results were verified. It was observed

that unsaturated zone has a considerable effect on slope stability, safety factor, and deformation of dams, however, it does not change overall flow conditions and hydraulic behavior of the dam considerably .

Lopez etal (2013) : The stability of an earthen embankment during drawdown (viz. Fully Slow drawdown, fully rapid drawdown, transient drawdown) was analysed using commercially available FEM softwares Plaxis 2D and Plaxflow. In modeling of fully slow drawdown, uncoupled drained analysis was made, for fully rapid drawdown, uncoupled undrained analysis and for transient drawdown , undrained analysis coupled with deformation was made. The influence of soil permeability, drawdown rate and drawdown ratio on the stability of embankment was also studied, for the three modes mentioned above. Moreover, the selection of type of model, i.e. Mohr-Coulomb , Hardening Soil Model , on the stability analysis has also been discussed

Khalilzad etal (2014) : The research presented in this paper focused on the effect of various parameters (geometry of the embankment and hydraulic loading in terms of intensity, duration, and cycles of loading and unloading as a result of the rise and fall of the water level in the reservoir) on the deformation response of embankment dams and the corresponding performance limit states.. The analysis of a model embankment dam is conducted using the finite-element approach (15 noded triangular plane strain using Plaxis 2D software) and the results are incorporated into simplified deformation-based probabilistic analyses. The effect of the change in geometry on shear strains and horizontal deformations and the corresponding probabilities of exceeding three predefined limit states are presented. The constitutive model of the analysis domain is defined by the hardening soil (HS) model in comparison with the Mohr-Coulomb model.

Vandenberge etal (2015) : This investigation was based on external water level variations, such as rapid drawdown or flood loading, change the internal pore pressures in an embankment as a result of changes in the boundary conditions. Three different effects resulting were : (1) changes in water pressure on the slope change the seepage boundary conditions, (2) changes in the total stress applied by the weight of the water on the slope change the confining pressure on the soil, and (3) changes in the stabilizing load from the reservoir cause changes in shear stress. . In principle, the stability of a slope can be evaluated using either total stress (undrained) or effective stress (drained) strength parameters. Effective stress analyses use drained strengths, which are often easier to measure and tend to be less dependent on the direction of loading or loading stress path. For these reasons, effective stress analyses are attractive for embankments experiencing changing water levels, such as RDD or flood loading. Uncoupled transient seepage analyses, which consider only the change of water pressure on slope, are increasingly being advocated as an

appropriate means to calculate pore pressures for effective stress stability analyses following water level changes. This paper discusses the limitations of uncoupled transient seepage analyses for calculating pore pressures during drawdown, explains the requirements for more appropriate analyses, and gives examples that show the errors incumbent on the use of uncoupled analyses Examples are provided that illustrate the shortcomings of using uncoupled transient seepage for stability analyses

Moayed etal : This paper deals with the effectiveness of different types of drainage filters used in toe of earthen embankment dams. A model was developed in finite element software Abaqus (Simulia) and drawdown was simulated by transient loading in 15 steps (each representing 1m daily drawdown) , in addition to static loading. The mesh was made of 1473 6-noded iso-parametric Quad-Triangular elements. The phreatic line , for different cases of filter was plotted. The conclusion was that chimney drain is most effective , in dissipation of pore pressures.

2.3 : SOIL WATER CHARACTERISTICS CURVE

It is defined as one of the critical tools for analysis of any transient stage seepage problem. A few research work on this topic is enlisted below

Van Genuchten (1980) : An closed form estimation technique for the development of VWC curve was developed with parameters such as saturated porosity, residual water content, air entrant value. A estimation methodology to determine the unsaturated hydraulic conductivity curve from the VWC was also suggested with known saturated conductivity as input.

Fredlund and Xing (1994) : An estimation technique for the development of VWC curve, similar on the lines of Van G method was developed. The method of computation of concerned parameters was different from the Van G method (1980). The function is developed smoothly over a range of matric suction such that at a negative pore water pressure of 1 million kPa, the volumetric water content tends to zero value

Zapata etal (2003) : This paper analyzed the uncertainty and variability in the (i) direct measurement and (ii) indirect estimation (using soil index properties/ GSD) of Soil Water Characteristic Curves(SWCC) used widely in unsaturated soil mechanics. Three different soil profiles (El Paso sand, Price Club silt, Fountain Hills clay) were selected so as to widen the applicability range of analysis. The analysis was based on methods of direct matric suction measurement, equations used to fit in the data, the operator used, the number of points used for development of SWCC and the range of matric suction selected. A model with database of 190 soil

profiles was developed for estimation of SWCC from GSD (grain size distribution)/ Index properties . It was found out that the accuracy was higher for the developed algorithms to be used for estimation of SWCC compared to the complicated direct measurement procedure.

Marinho (2005) : The importance of Soil Water Characteristics Curve (SWCC) has been discussed in this article, especially for plastic soils. It is used for prediction of mechanical and hydraulic properties of unsaturated soils, in an indirect manner. The effect of parameters such as type of soil, liquid limit, stress history of the soil plays an important role in construction of SWCC. Usually a semi-logarithmic plot of water content v/s suction pressure is obtained, depending on above parameters. The shape of the plot (usually S-shaped) depends upon – (i) pore size distribution (ii) compressibility of soil w.r.t suction. The research dealt with the examination of 49 SWCC from 18 soil samples. Based on these a simple plot was obtained which may be used to find out the SWCC of a plastic soil, based on its stress history. Further study of applicability of this method for over-consolidated soils may be studied

Johari etal (2006) : A genetic programming (GP) model was proposed to develop the SWCC of soils with input as initial void ratio, initial water content, normalized matric suction, clay and silt content. The same was based on database of SoilVision and validated by experimental results. As direct laboratory tests for development of SWCC is costly, hence estimation methods based on genetic programming can be used with a high amount of accuracy to determine the same from basic soil parameters.

2.4 : HYDRAULIC AND GEOTECHNICAL SCALING

A publication on Hydraulic and Geotechnical scaling of laboratory models based on field prototype is presented below.

Dupont etal : This research publication deals with the experimental investigation of breaching of an embankment dam. A numerical analysis has also been supplemented to validate the results. The scaling for the developed model with respect to prototype has been done using similarity rules of hydraulics. The important factors for this study was (i) breaching & overtopping of upstream earthen dam (ii) sediment transport from the breached dam downstream. For the first part, since the gravitational & inertial forces are predominant, the scaling has been based on Froude model, i.e. Froude number for both model and prototype must be same. For the sediment transport, the simulation was done based on non-dimensional shear stress for a particular Reynolds number (kept in such a manner that the viscosity does not come into play).

2.5 : SLOPE STABILITY ANALYSIS

Slope Stability Analysis forms one of the most important aspects of any embankment design. A few literature on this topic is enlisted below

Janbu (1954) : A limit equilibrium analysis for slope stability considering interslice normal forces was done. In this analysis, only the overall Horizontal force equilibrium was satisfied. The method of analysis can be used to analyze the influence of partial submergence and draw-down conditions. The effects of tension cracks and surcharges are also included. The shear strength is assumed constant along the entire sliding surface. In case of layered soils, the shear strength is constant in each layer. At the instance of failure, the shear strength is completely mobilized at each point along the sliding surface.

Bishop (1955) : Bishop's method of slices can be used for total as well as effective stress analysis. The limit equilibrium analysis considering interslice normal forces was solved for overall moment equilibrium only. Only the interslice normal forces were considered.

Spencer (1967) : In this limit equilibrium slope stability analysis, both the interslice normal and shear forces were considered and analysed for force and moment equilibrium individually. The Factor of Safety was computed accordingly. The shape function was kept a constant. The resultant interslice forces are of constant slope throughout the sliding mass. The F.O.S for both force and moment were matched by iterations at a particular value of lambda.

Lane etal (2000) : This paper deals with generation of charts , based on FEM , for slope stability analysis on complex geometries and conditions (submergence & drawdown). The finite-element program is for 2D, plane strain, slope stability analysis by finite elements using eight-node quadrilateral elements of elastic-visco-plastic soil with a Mohr-Coulomb failure criterion and a non associated flow rule. In partial submergence / Slow Drawdown (Drained condition), neglecting seepage conditions , FOS of slope in drawdown condition has been computed for various Depth of Drawdown wrt Embankment top to Height of Embankment. In the initial stages of partial submergence slow drawdown ($L/H < 0.7$), the increased weight of the slope has a proportionately greater destabilizing effect than the increased frictional strength and the FOS falls. At higher drawdown levels ($L/H > 0.7$), however, the increased frictional strength starts to have a greater influence than the increased weight and the FOS rises. In the finite-element program rapid drawdown is modeled when the piezometric surface is specified as per the original water level, but the face loads are based on the drawdown reservoir level, which in this case is below that of the

piezometric values. In totality , FOS charts were developed for Slow as well as Rapid drawdown , for different drawdown ratios (L/H) in order to get the minimum FOS to be used in design

Xu etal (2005) : Based on centrifuge (Cap. 400 g ton) experiments on soft ground made from the remolded clay cakes from in-situ soft ground of Huai-He River's levee of a flood channel to Huang sea , in China. The test section with lowest Factor of Safety against stability was taken for the Centrifuge Test. The behavior of the levee at end of construction & sudden drawdown was simulated & analysed in two separate centrifuge tests. The experiment was conducted in plane strain condition with dimensions 1.1 m by 0.4 m wide by 0.55 m height. It is found that concerning the instability behavior of levee on soft foundation at the end of construction, the sliding surface is a deep seated one, which passes through the soft ground. Also it is seen that concerning the mechanism of instability during sudden drawdown of floodwater, a general failure of sliding is preceded with a local failure of slope instability in embankment slope, whose slip surface passes through the toe of slope.

Zeng etal (2005) : During the design of the slope stability in the Three Gorges Reservoir Zone , the methods adopted for determining the ground water table and hydrodynamic forces during reservoir drawdown were mostly empirical and varied from one project to another. To improve the methods, a simplified formula of the phreatic-line in landslide mass was proposed during reservoir drawdown in this article, based on the Boussinesq's differential equation of unsteady-seepage, and deduced by Laplace's transform. In the end, the amended formula was proved by a large-scale model test. The test shows that the value obtained is much close to that by the amended formula, with the error within 5%.

Athania etal (2015) : This paper presents the results of seepage and stability analyses of the considered earth dam using finite element method. The seepage analysis is divided into two categories viz. Steady state and Transient analyses. Based on the parametric sensitivity analysis, both the seepage and stability studies have brought out the importance of considering the coupled effects on the overall stability of the earth dam. The paper presents the results of finite element modelling of the stability and seepage analyses of the earth dam using PLAXIS 3D software. The two main parameters which were varied in the study to indentify the changes in the stability of the earth dam are the Young's modulus (E) and angle of internal friction (φ). The stability of the dam has been checked for the following conditions (1) Full (High) reservoir level of the dam (2) Rapid drawdown (RDD 1 and RDD2) in 5 and 10 days duration (3) Slow drawdown in 50 days duration and (4) Low water level of the dam. The study shows that increase in the Young's modulus of core and shell resulted in the decrease of the maximum crest displacement and the variation in angle of

internal friction plays a vital role in the fulfillment of the overall stability criteria. .The factor of safety (FS) was greater than 1.6 for both the full (high) reservoir condition and low reservoir condition whereas, the FS values were found to be less than the stipulated values for the other stability considerations.

2.6 : RELEVANCE OF PAST STUDIES

A summary of past studies relevant to this study has been presented below -

- Several researchers have worked elaborately on Steady State Seepage Conditions. Both numerical and experimental analyses have been conducted. However, literature pertaining to the experimental analysis have been mainly found for cohesion less type of soils, whereas numerical analyses by Finite Difference, Finite Element and Boundary Element methods have been found for both cohesion less and cohesive soil types.

- Transient stage analysis have been performed by several researchers. A lot of literature, both numerical and experimental was found for transient stage induced by draw-down conditions. Although several publications have brought out numerical analysis for both cohesive and cohesionless type of soils, yet experimentation models based on cohesive soils are not quite popular. Full scale model centrifuge tests are also becoming popular to study such events. However, scarce literature is available for numerical or experimentation analysis of transient seepage conditions induced by continuous rise-up and draw-down conditions with multiple cycles, as in case of embankments exposed to diurnal tidal cycles.

- The importance of Coupled seepage analysis involving both pore water pressure and deformation as opposed to an Uncoupled seepage analysis where only the pore water pressure is determined was also established by several researchers.

- The development of soil water characteristics curve for any soil is a major challenge for any geotechnical engineer. Experimental development of the same is complicated , hence estimation methods are popular. However, the concept of SWCC is critical for any sort of transient seepage analysis.

- Hydraulic scaling has been used by several researchers to simulate field conditions in a controlled laboratory experiment. The usage of Froude model is quite popular for models where the Inertial and gravitational forces are predominant.

CHAPTER THREE
OBJECTIVE AND SCOPE OF PRESENT STUDY

CHAPTER THREE
OBJECTIVE AND SCOPE OF PRESENT STUDY

3.1 : OBJECTIVE OF PRESENT STUDY

The major objectives of the present study are summarized below –

(i) To study the dynamics of the phreatic surface of an earthen embankment during transient stage including rise-up and draw-down condition of a single tidal cycle. The shape and dynamics of the phreatic surface in the embankment after multiple tidal cycles shall also be investigated.

(ii) To estimate the pore water pressure distribution within the embankment during transient stage including rise-up and draw-down condition for a single tidal cycle using uncoupled methodology. The effect of multiple cycles shall also be investigated.

(iii) To estimate the deformation and pore water pressure simultaneously at critical areas within the embankment using coupled methodology both for single and multiple tidal cycles .

(iv) To conduct the slope stability analysis during steady and transient state including rise-up and draw-down condition for model embankment in single and multiple tidal cycles using both uncoupled and coupled methodology.

3.2 : SCOPE OF PRESENT STUDY

The scope of the present study comprises –

(i) Literature review for steady and transient seepage in earthen embankments.

(ii) Analysis of embankment model in any popular finite element method based software. Simulation of rise-up and draw-down condition in single and multiple tidal cycles shall be made, followed by determination of parameters mentioned in Objective portion.

(iii) An experimental model shall be developed in the Geotechnical Engineering Laboratory, to simulate and observe the effects of transient seepage inside an earthen embankment exposed to tidal cycles.

(iv) Data collection and study follow-up from selected sites of research area

(v) Validation of results obtained from field, computer model and laboratory model for parameters mentioned in Objective area.

CHAPTER FOUR
STUDY AREA

CHAPTER FOUR
STUDY AREA

4.1 : GENERAL INFORMATION ON SUNDERBAN REGION

The Sunderban delta (21º 56' 59'' N, 89º 10' 59'' E) is shared by South 24 Parganas, West Bengal, India and Khulna division, Bangladesh with the latter having a major share of about sixty percent. This delta is formed due to the super confluence of the rivers Ganga, Bramhaputra and their distributaries. The whole of the Sunderban comprises intricate network of criss-cross channels which divide the entire area into several small and large islands. Channels and creeks are numerous, which ultimately find their way to the Bay of Bengal through some principal distributaries like Hoogly, Muriganga, Saptamukhi, Thakuran, Matla, Gosaba, Haribhanga and Raimangal. It covers an area of 10,000 square kilometers, mainly saline wetlands comprising largest single block of tidal halophytic mangrove forests. This biosphere is the habitat of the Royal Bengal Tiger and has been declared as an UNESCO world heritage site. The physiography is dominated by deltaic formations that include innumerable drainage lines associated with surface and sub-aqueous levees . There are also marginal marshes above mean tide level along with tidal sandbars which can be seen during Low Tide. The geology mainly comprises proto-delta clays and silt sediments. The floor varies from 0.9 meters to 2.11 meters above MSL.

The deltaic island system is a reclaimed area and has been used for human settlement since the late 18th century. The existing ground level of most of the islands is above the Low Tide Level (LTL), but below the High Tide Level (HTL), hence there is requirement of embankments in order to protect the islands from tidal water inundation. The construction of the same is said to have been done mainly using locally available soil without any engineering analysis. The total length of existing earthen embankments in Indian part of Sunderbans is approximately 3520 km. A typical embankment is shown in **Figure- 4.1.** The geographic map of the area is shown in **Figure- 4.2**. The water head difference due to diurnal tidal cycle is about 4 to 6 meters. Single cycle time is the time-period taken by the river water level to rise from LTL to HTL and then fall back from HTL to LTL. The time period for a single cycle is about 12 hours. Site photographs of tidal cycle and the general tidal mechanism is shown in **Figures- 4.3, 4.4, 4.5**. Site investigations have revealed river side lower slope failure underneath berm region in most of the embankments in this region **(Refer Figure- 4.4)**. A rise in the frequency of failure in embankments is recorded during the monsoon season at the riverfront end. In cases of storm surges (like Aila (2009)), the level difference between LTL and HTL may rise to 8-10 meters, spilling saline water into the landside crop fields, thus rendering the land useless for agricultural purposes for at least for 2-3 years, hence a great

loss in economy is encountered. The economy is contributed by the local population of approximately fifty lacs, comprising mainly fisherman and farmers.

4.2 : TYPICAL SOIL PROFILE OF SUNDERBAN REGION

For studying the Sunderban Soil Profile, data from the following bore-hole at Patharpratima site has been taken

Site : Pathar-Pratima (Government 283 ICDS Centre , Kuimuri)

TABLE- 4.1 : Details of Bore Hole–I, Pathar-Pratima (Government 283 ICDS Centre, Kuimuri)

(Shell/Auger Boring , Wash Boring with 150 mm diameter BH)

DEPTH (BELOW EGL) in metres	PROFILE	SOIL PARAMETERS
4.5	SOFT BROWNISH GREY SILTY CLAY / CLAYEY SILT	N (SPT) = 2
		Cohesion, C = 20 kN/m^2
		Angle of Internal Friction, Φ = 7 degree
		Bulk Density – 18.2 kN/m^3
		Normal Moisture Content = 30.8 %
		Liquid Limit (LL) = 47 %
		Plastic Limit (PL) = 22 %
		Co-efficient of Volume Compressibility, m_v= 0.048 per kPa
		Specific Gravity, G =2.65
7.5	DENSE TO VERY DENSE SILTY FINE SAND WITH MICA	N (SPT) = 6-20
		Angle of Internal Friction, Φ = 30 degree
		Specific Gravity, G =2.65
26	MEDIUM TO DENSE GREY SILTY FINE SAND WITH MICA	N (SPT) = 16-40 ,
		Angle of Internal Friction, Φ = 33 degree
		Bulk wt – 18.5 kN/m^3
		Normal Moisture Content = 24.86 %
		Specific Gravity, G =2.65
28	STIFF GREY SILTY CLAY WITH TRACES OF DECOMPOSED WOOD	N (SPT) = 19-33
		Specific Gravity, G =2.65
30	STIFF TO VERY STIFF , GREY BROWNISH GREY SILTY CLAY	N (SPT) = 18
		Specific Gravity, G =2.65
REMARKS : WATER TABLE IS AT GROUND LEVEL		

After going through bore log data, it was found that it some of the sites in PatharPratima, the Groundwater table (GWT) was situated very close to the Existing Ground Level on the land side (or

the Human Settlement side of the embankment). In other sites, the location of the same varied 2 - 3.5 metres below existing ground level.

4.3 : DETAILS OF TYPICAL SUNDERBAN EMBANKMENT

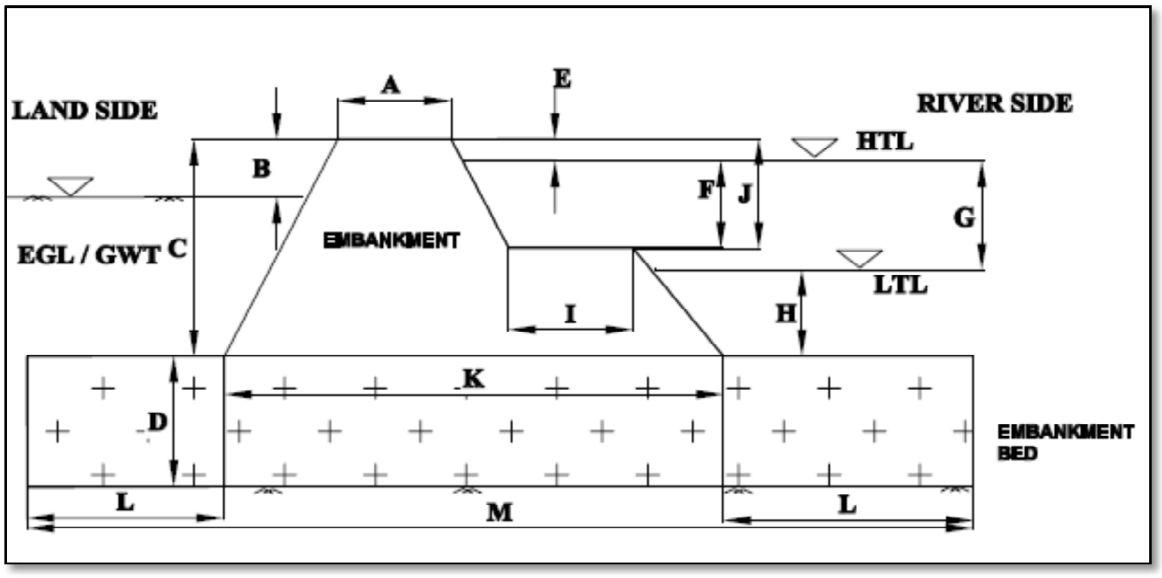

Figure- 4.1 : Typical Sunderbans Embankment With Tidal Head Variation Of 4 Meters, With Dimensions Given In Table 4.2 (Not To Scale)

TABLE- 4.2 : Dimension Details Of Typical Sunderban Embankment

Parameter as per figure	Prototype Dimension (m)
A	2.0
B	2.0
C	5.5
D	5.0
E	0.5
F	3.0
G	4.0
H	1.0
I	2.0
J	3.5
K	21.5
L	5.0
M	31.5

4.4 : STUDY AREA PICTURE TEMPLATE

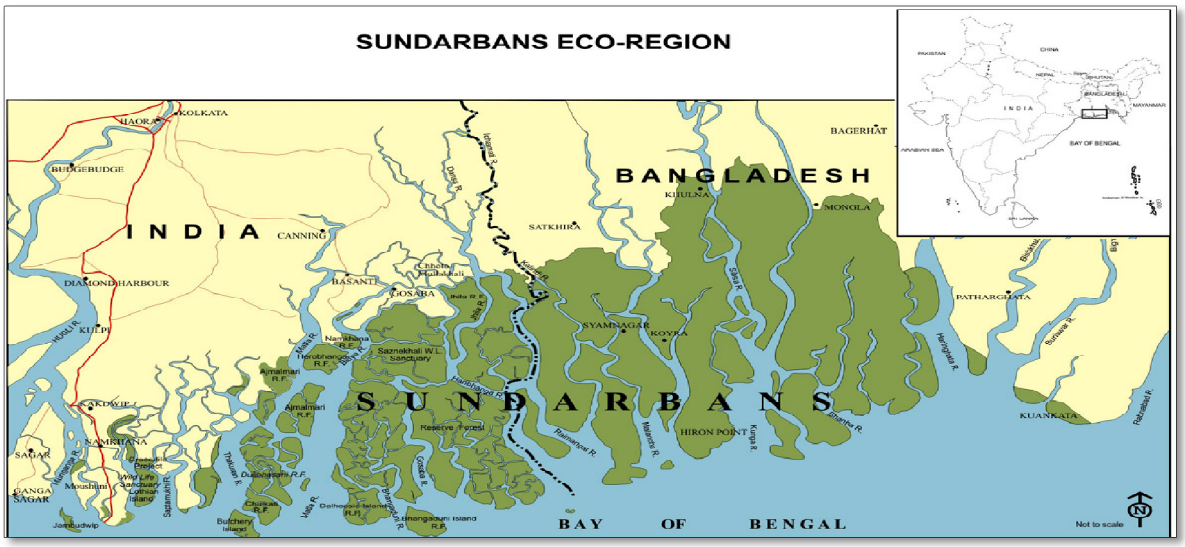

Figure- 4.2 : Map Of Sunderbans Region (Picture Courtesy : Internet)

Figure- 4.3 : Sonakhali Site During Rise-Up

Figure- 4.4 : Sonakhali Site During Draw-Down

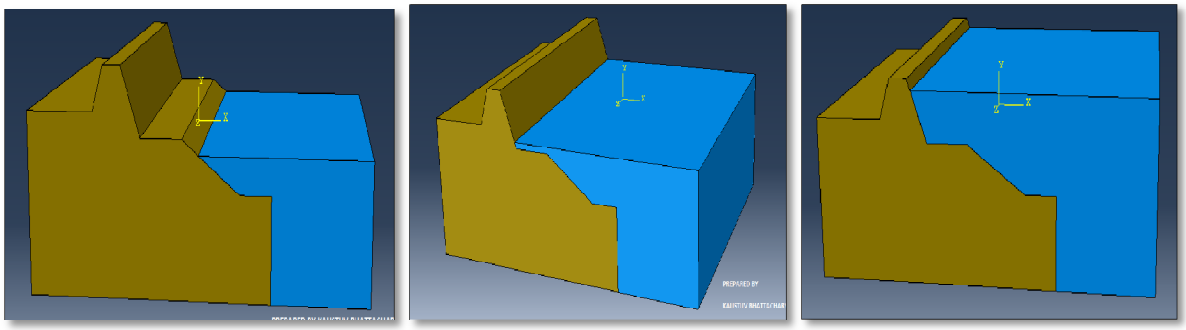

Figure- 4.5 (a), (b), (c) : 3D Model for Typical Sunderban Embankment. Sequence Of Low Tide Level To High Tide Level During Rise Up Condition is shown. The Land side and River side is shown on left and right side respectively. The sequence of High Tide Level to Low Tide Level during Draw-down can be traced by following the picture set in reverse.

CHAPTER FIVE
NUMERICAL ANALYSIS BY FINITE ELEMENT METHOD

CHAPTER FIVE
NUMERICAL ANALYSIS BY FINITE ELEMENT METHOD

5.1 : GENERAL

The finite element methodology has been adopted to study the effect of transient seepage induced by tidal cycle consisting of Rise-up and Draw-down on earthen embankments. The Sunderban Case-Study has been adopted for this project. Details of the Sunderban soil profile and typical Sunderban embankment geometry has been discussed in Chapter-4: Study Area. The available field data has been utilized in the numerical analysis.

The seepage analysis both in steady and transient state has been carried out using SEEP/W, a popular F.E.M based software. The slope stability analysis for each phase has been carried out using SLOPE/W. A deformation analysis was carried out using SIGMA/W to get field oriented results where pore pressure generated due to seepage is accompanied by deformation. All three F.E.M based softwares mentioned above are products of GeoStudio.

5.2 : METHODOLOGY

As discussed in earlier chapters, the main parts of any finite element analysis are the geometry, material properties, boundary conditions and mesh generation. These shall be discussed in the following sub-sections as per developed model. In the seepage analysis, the steady state conditions were first established as per position of Low Tide Level (LTL) and location of Landside Groundwater Table (LGWT). Then, the transient seepage analysis was conducted on the basis of Rise-Up and Draw-down time cycles, with initial parameters from the Steady State results. This has been explained in **Flowcharts in sections - 5.3.1 and 5.3.2**. The effect of multiple cycles have also been studied. The seepage analysis is presented first, followed by deformation and slope stability analysis.

5.2.1 : Geometry

Two models were developed separately for analysis of the seepage analysis during rise up and draw down condition of the tidal cycle. These are-

(i) Typical Sunderban embankment with Landside Groundwater Table (LGWT) at Existing Ground Level (EGL) (Model Code – $SDBN_0$)

(ii) Typical Sunderban embankment with Landside Groundwater Table (LGWT) at 3.5 metres below Existing Ground Level (EGL) (Model Code – $SDBN_{3.5}$)

The reason for selection of two models is that it has been observed that at various sites in Patharpratima, Sunderbans, the land groundwater table (LGWT) is at existing ground level (EGL) , whereas in several other sites it has been observed lying 2 – 3.5 metres below EGL, hence these models $SDBN_0$ and $SDBN_{3.5}$ have been taken up to study the effect of LGWT on steady seepage and tide induced transient seepage . These are shown in **Figures 5.1** and **5.2**. The geometrical dimensions are as per Figure 4.1 and Table-4.2. The geometry can be broadly classified into four segments – (a) Embankment Body (b) Embankment Bed (c) Land Side (d) River Side

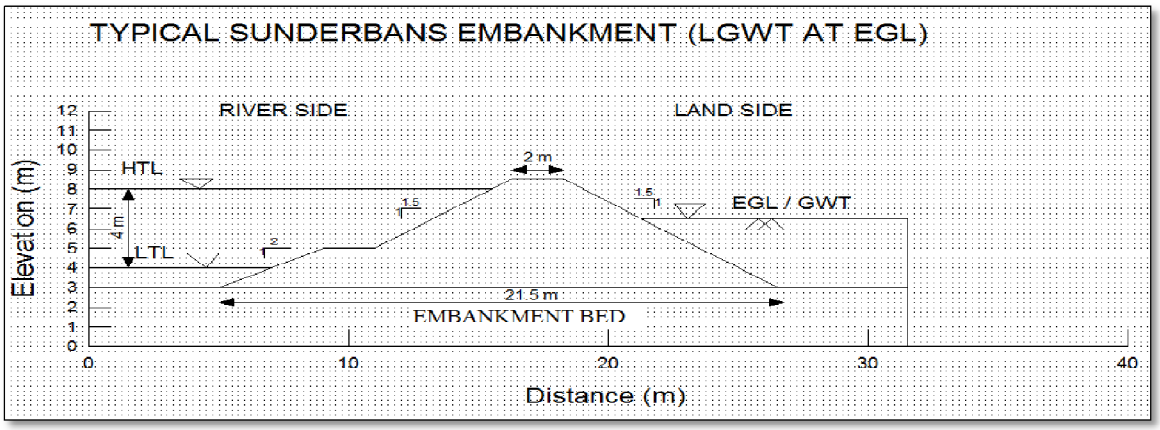

Figure-5.1 : Geometry of the Finite Element Model for Sunderban embankment model $SDBN_0$

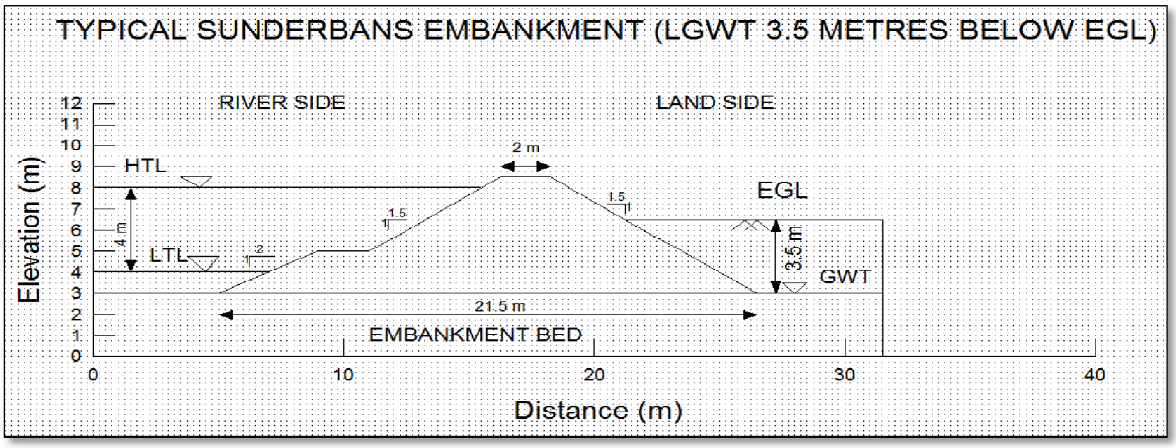

Figure-5.2 : Geometry of the Finite Element Model for Sunderban embankment model $SDBN_{3.5}$

5.2.2: Material Properties

As discussed in earlier chapters, one of the key segments of any transient analysis is the volumetric water content function and the hydraulic conductivity function. It has been recorded from site data, that the embankments in Sunderban have been constructed with the locally available top soil layer. The conductivity properties have been kept the same for the embankment and the embankment bed for both the models.

The volumetric water content function has been developed on the basis of Modified Kovacs method (2003) using grain size distribution, liquid limit, porosity, co-efficient of volume compressibility. The hydraulic conductivity function has been estimated from the VWCC function as a data point function using the Van Genuchten methodology (1980), with saturated permeability and residual water content as the additional input. The air entrant value and residual water content have been obtained from the VWC Curve. The above mentioned data have been selected as per Bore log data given in Table-4.1. Additional data not available in bore log was obtained as per conducted laboratory tests on soil sample brought from site. The methodology for development of above mentioned functions has been vividly discussed in Chapter-1. The material property details along with type of material model has been given in **Table-5.1**. The grain size distribution along with developed VWCC function and hydraulic conductivity function for typical Sunderban Clayey Silt has been shown in **Figures (5.3)**, **(5.4)**, **(5.5)**, **(5.6)** respectively.

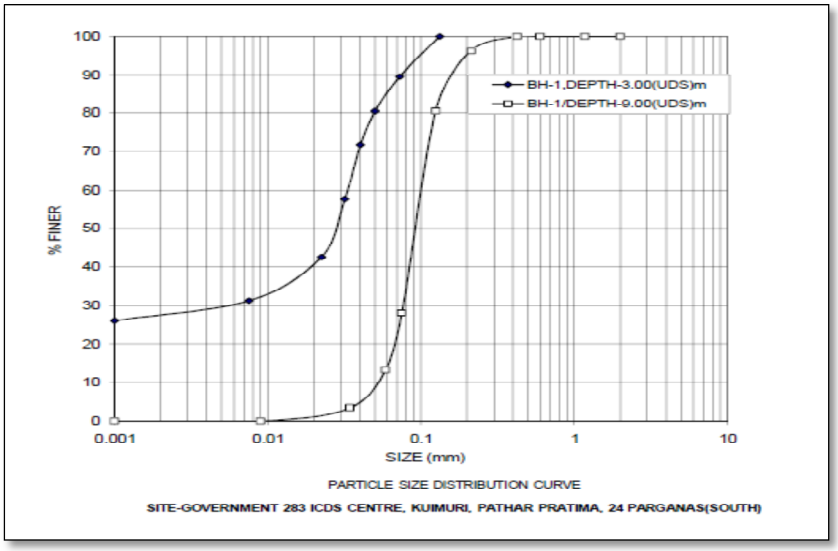

BH-1, Depth – 3.0 m

Percentage of Sand	10
Percentage of Silt	62
Percentage of Clay	28

Figure-5.3 : Grain Size Distribution for Sunderban Clayey Silt with percentage components (as per Soil Report at ICDS Site at Kuimuri, Patharpratima – Bhandari 2011)

TABLE-5.1 : Material Properties of the Models $SDBN_0$ and $SDBN_{3.5}$ used in F.E.M analysis

Segment	*Embankment*	*Embankment Bed*	*Landside Soil*
Properties			
Soil Type	Soft Brownish Grey Clayey Silt	Soft Brownish Grey Clayey Silt	Soft Brownish Grey Clayey Silt
Material model (Hydraulic)	Saturated / Unsaturated	Saturated / Unsaturated	Saturated / Unsaturated
Material model (Stress - Strain)	Mohr-Coulomb	Mohr-Coulomb	Mohr-Coulomb
Co-efficient of volume compressibility (m_v)(per kPa)	0.048	0.048	0.048
Bulk Density (kN/m^3)	18.2	18.2	18.2
Saturated Porosity (m^3/m^3)	0.465	0.465	0.465
D_{10} (mm)	0.001	0.001	0.001
D_{60} (mm)	0.034	0.034	0.034
Liquid Limit (%)	47	47	47
Saturated Hydraulic Conductivity (K_{sat}) (m/s)	10^{-8}	10^{-8}	10^{-8}
Residual Water content (m^3/m^3)	0.18	0.18	0.18
Air Entrant Value (in kPa)	-66.67	-66.67	-66.67
Effective Cohesion, c' (kN/sqm)	5	5	5
Effective Angle of Internal Friction, Φ' (degrees)	25	25	25
Dilation Angle, ψ ((degrees)	0	0	0
Poisson ratio	0.333	0.333	0.333
Effective Young Modulus, E' (kPa)	2083	2083	2083

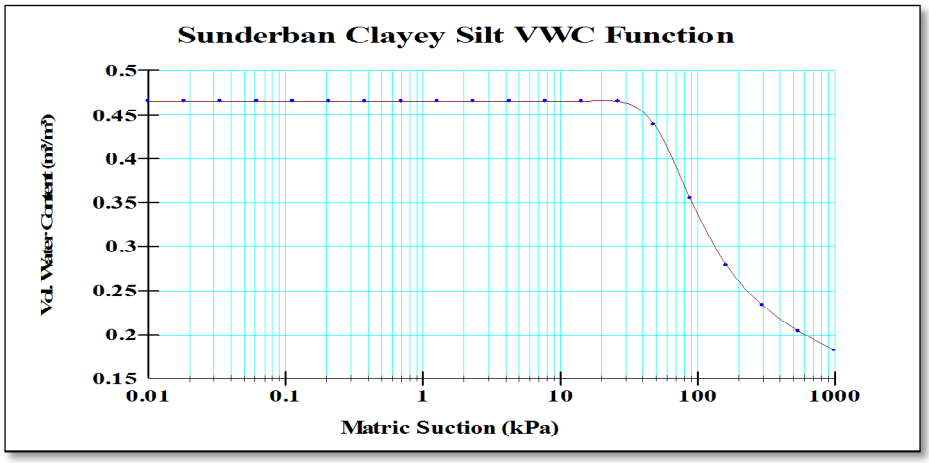

Figure-5.4 : Volumetric Water Content function (as per Modified Kovacs methodology using Grain size distribution) showing plot of Volumetric water content (m^3/m^3) versus Matric Suction (kPa) for Sunderban Clayey Silt

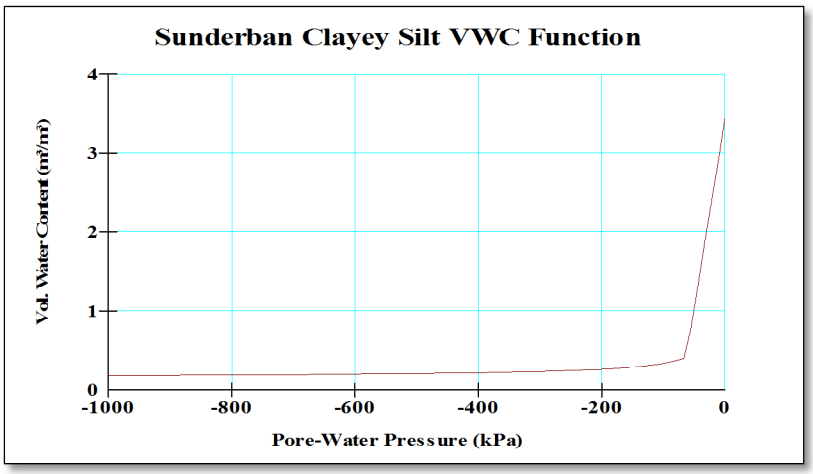

Figure-5.5 : Plot showing Volumetric Water Content (m^3/m^3) versus Pore Water Pressure (kPa) for Sunderban Clayey Silt

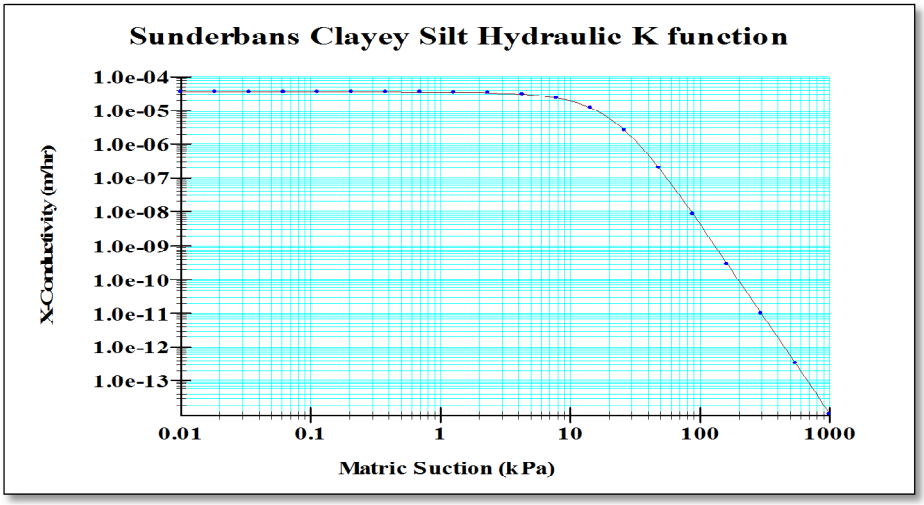

Figure-5.6 : Hydraulic Conductivity function showing plot of Conductivity (m/sec) versus Matric Suction (in kPa) for Sunderban Clayey Silt

The unit weight of water was taken as 9.807 kN/m^3 in all types of analyses.

5.2.3 : Boundary Conditions

Single Cycle

At the river-side, the Low Tide Level has been defined as a constant hydraulic head boundary. The land-side groundwater table has been defined as a constant hydraulic head boundary, as per location which varies in $SDBN_0$ and $SDBN_{3.5}$.

The time period for each tidal half cycle, defined as the time taken by river water level from LTL to HTL defined as Rise-Up, and from HTL back to LTL defined as Draw-down, given as six hours each. A single Rise-Up and Draw-Down constitute a complete Tidal cycle. The Rise-Up and Draw-Down boundary condition has been defined as hydraulic head which is a linear function of tidal

cycle time and shown in **Figure-5.7, 5.8**. A potential seepage review face with a zero flux boundary condition has been imposed on the riverside slope during rise up and drawdown condition. The details of boundary conditions are presented in tabular format in **Table-5.2**.

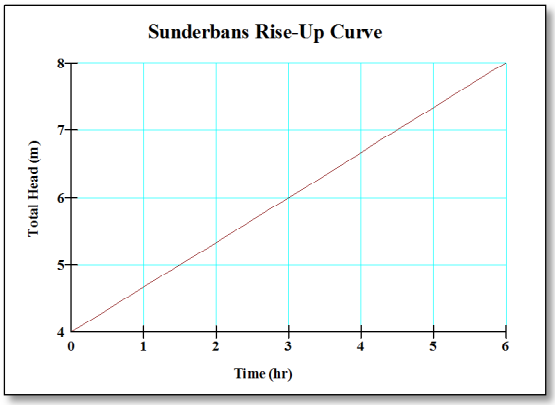

Figure-5.7 : Tidal Boundary Condition – Sunderbans Rise-Up Curve for a Single Tidal cycle

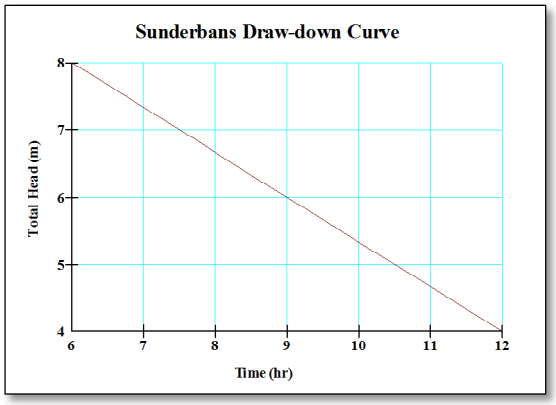

Figure-5.8 :Tidal Boundary Condition – Sunderbans Draw-down Curve for a Single Tidal Cycle

Multiple Cycles

The Rise-Up and Draw-down boundary conditions are defined as hydraulic heads which are linear functions of time in the form of multiple cycles. The potential seepage review face with a zero flux boundary condition has been imposed on the riverside slope during rise up and drawdown condition. In this particular analysis, the number of cycles was taken over two months, i.e. 60 days with 120 cycles. The multiple cycle boundary condition curve has been shown in **Figure-5.9**. All other boundary conditions remain same as per single cycle

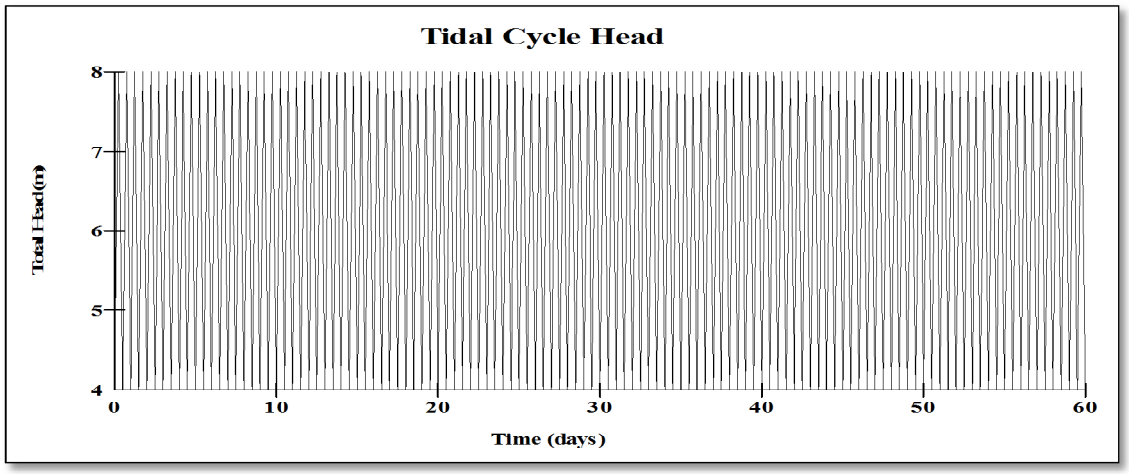

Figure-5.9 : Tidal Boundary Condition for Multiple Cycles (120 cycles over a duration of 2 months)

TABLE-5.2 : Boundary Conditions of the Models $SDBN_0$ and $SDBN_{3.5}$

Model Code		$SDBN_0$	$SDBN_{3.5}$
Type of Analysis : Uncoupled			
Type of Boundary Conditions : (i) Hydraulic Head			
Landside Groundwater Table		Constant Head = 6.5 m	Constant Head = 3.0 m
River Side			
Low Tide Level		Constant Head = 4.0 m	Constant Head = 4.0 m
Single Tidal Cycle	Rise-Up	Head = function (time) as in Figure-5.7	Head = function (time) as in Figure-5.7
	Draw-Down	Head = function (time) as in Figure-5.8	Head = function (time) as in Figure-5.8
Multiple Tidal Cycles		Head = function (time) as in Figure-5.9	Head = function (time) as in Figure-5.9
Type of Analysis : Coupled			
Type of Boundary Conditions : (i) Hydraulic Head (ii) Hydrostatic Pressure defined on basis of Hydraulic head **(iii) Displacement – (a) Bottom** – Fixed (b) **Vertical Sides** – Fixed in – X direction, Free in –Y direction			
Landside Groundwater Table		Constant Head = 6.5 m	Constant Head = 3.0 m
River Side			
Low Tide Level		Constant Head = 4.0 m	Constant Head = 4.0 m
Single Tidal Cycle	Rise-Up	Head = function (time) as in Figure-5.7	Head = function (time) as in Figure-5.7
	Draw-Down	Head = function (time) as in Figure-5.8	Head = function (time) as in Figure-5.8
Multiple Tidal Cycles		Head = function (time) as in Figure-5.9	Head = function (time) as in Figure-5.9
Note : The Potential Seepage face review with total flux = 0, was applied on the River Side slopes during Single and Multiple Tidal cycles for both the model types in both type of analysis			

5.2.4 : Mesh Properties

The entire geometry for both the models $SDBN_0$ and $SDBN_{3.5}$ was divided into 489 nodes and 473 elements. First Order elements, i.e. elements with nodes at the corners only, were selected with a linear field variable distribution. The shape of mesh was unstructured origin family of quadrilaterals

and triangles, with individual element size of 1 m in the embankment bed and landside region. A magnification of 2 indicating mesh element size of 0.5 m was taken within embankment. Thereby the number of nodes for a single triangular and quadrilateral element was taken as 3 and 4 respectively with additional 3 and 4 no.s Gauss integration points respectively. Compatibility matching was done at the boundaries of embankment and embankment bed, embankment and landside soil due to variation in mesh size in these regions. Mesh refining was done after an optimization and lower mesh size did not improve the results but only took additional computer memory space and time for solving. The mesh arrangement has been shown in **Figure.5.10**.

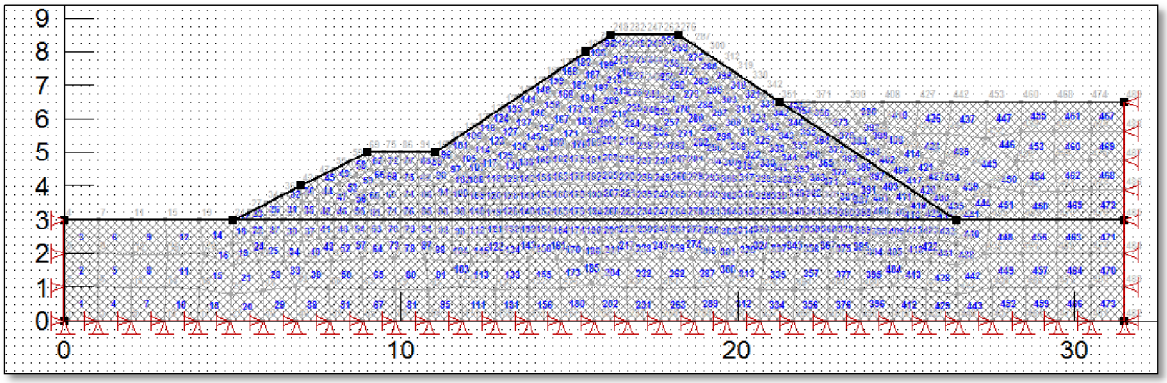

Figure-5.10 : Mesh arrangement showing nodes and elements for both the models $SDBN_0$ and $SDBN_{3.5}$. The displacement boundary conditions have also been shown

5.2.5 : Convergance and Time Stepping

The maximum number of iterations was set to 50, with an tolerance of 0.1 for convergance. For conductivity iterations the minimum and maximum changes allowed was 0.0001 and 1.0, with a rate of change as 1.1. A parallel direct equation solver was used. In case of potential seepage face review, the number of reviews was limited to 10.

For single cycle analysis, the time stepping was taken as 1 hour and increased linearly till 6 hours, separately for rise-up and draw-down respectively.

In case of multiple cycle analysis with approach towards higher number of cycles, the time stepping becomes a critical criteria. The selection of number of time steps, elapsed time and mode of increase of time intervals is quite challenging in the case of dynamic boundary conditions defined as per tidal head. The selection of improper elapsed times may lead to wrong interpretation of results. In both the models $SDBN_0$ and $SDBN_{3.5}$, an optimization technique with several iterations with different number of cycles was done to get an idea of the time step and elapsed time which were finally used for the multiple cycle analysis. An exponential increase in time stepping was adopted.

5.2.6 : Deformation based Coupled Analysis

A stress – strain type in-situ stage was developed as the base for the Coupled analysis in SIGMA/W. The Low Tide Level (LTL) was selected as the parent, simulating initial stress conditions. The hydrostatic pressure (based on fluid head) on the river-side and groundwater table were provided in addition to the hydraulic boundary conditions in both the In-situ stage and the subsequent tidal cycles. A deformation boundary condition with the bottom as fixed and the vertical sides as rollers was also provided (Refer Figure- 5.10). The material type was selected as Effective parameters with PWP change. The Modulus of Elasticity was derived from the Co-efficient of volume compressibility. A Coupled Stress / PWP mode of analysis was selected for the Tidal cycle stage.

5.3: FLOWCHART REPRESENTATION OF METHODOLOGY

5.3.1: Flowchart Defining Methodology followed during Uncoupled Analysis

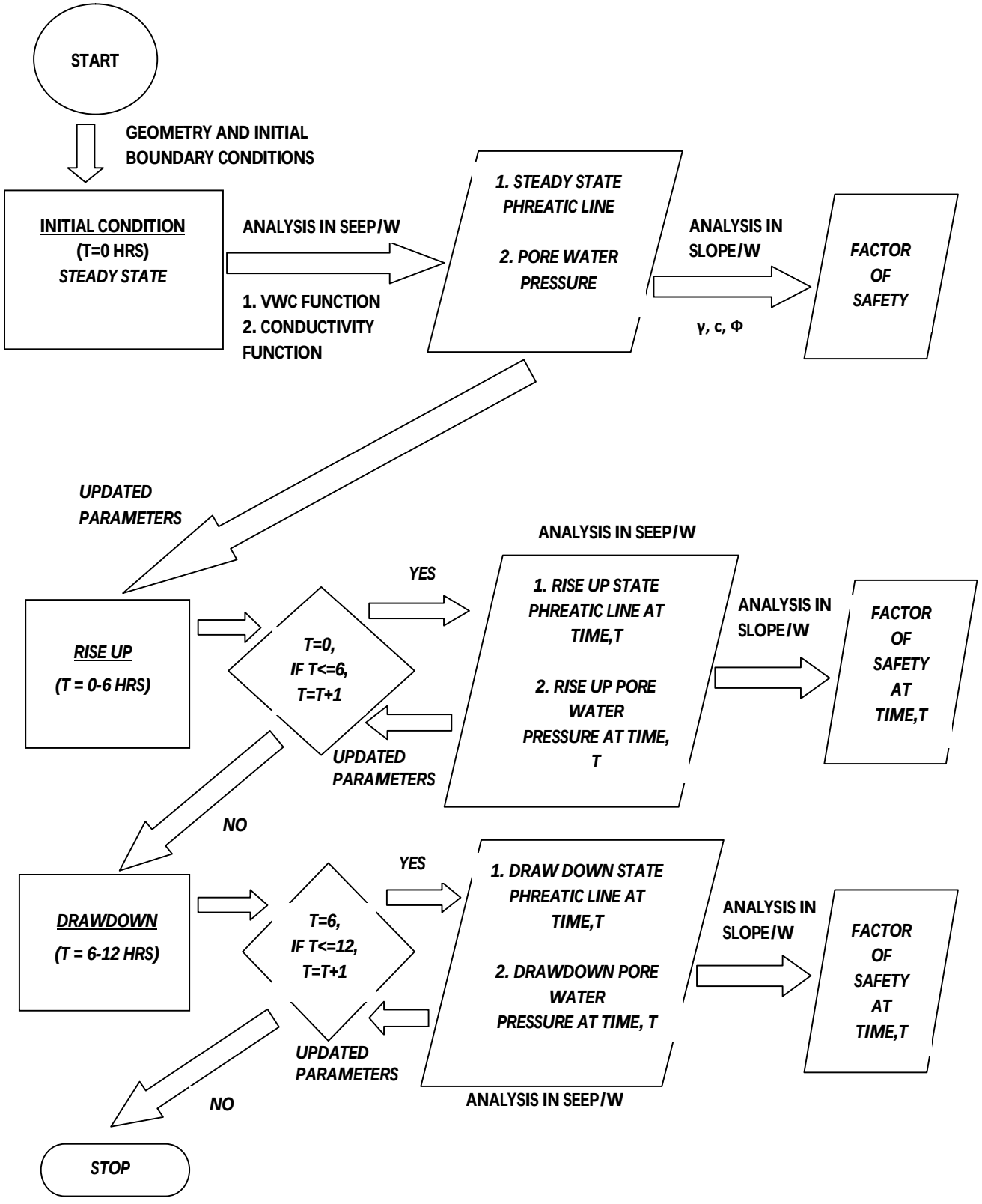

Figure-5.11(a) : Flowchart of Sequence of Uncoupled Analysis for a Single Tidal Cycle

5.3.2 : Flowchart Defining Methodology followed during Coupled Analysis

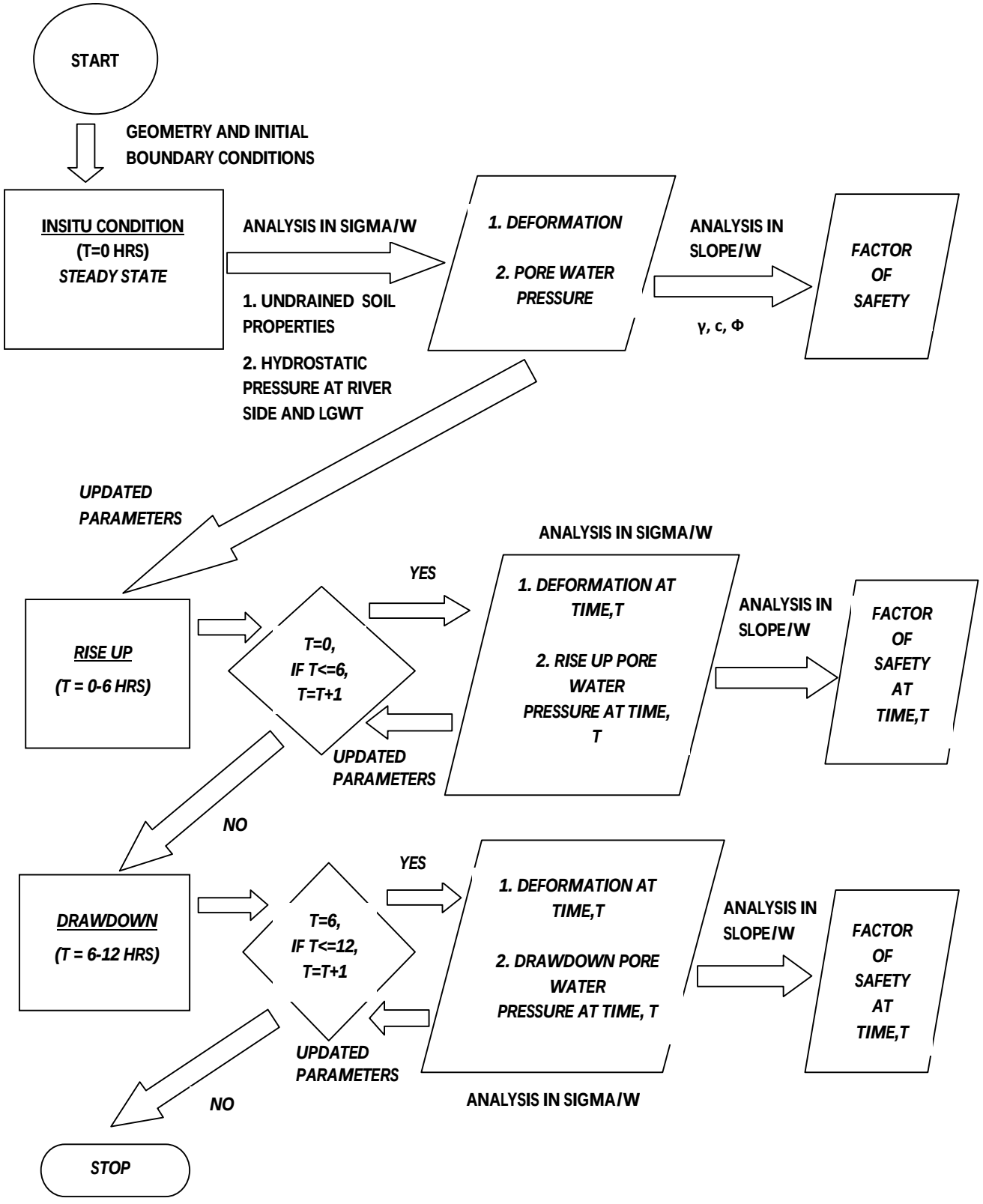

Figure-5.11(b) : Flowchart of Sequence of Coupled Analysis for a Single Tidal Cycle

5.4 : PARAMETRIC STUDY

The models $SDBN_0$ and $SDBN_{3.5}$ were analyzed for transient seepage during tidal cycles acting on the riverfront side of the embankment. An initial steady state condition was developed as per position of Low Tide Level and the Landside Groundwater Table. The latter term varies for the two models mentioned above. After the steady state conditions were developed, the Rise-Up condition (t = 0 to 6 hrs) was simulated in six intervals of one hour each. The results obtained were used in the simulation of the Draw-down condition (t = 6 -12 hrs) also in six intervals of one hour each.

The different parameters determined as per above two case models during this time frame are –

(a) Phreatic line location

(b) Flux quantities at different sections of the embankment

(c) Equipotential total heads

(d) Pore Water Pressure distribution inside the embankment (Uncoupled approach)

(e) Deformation and Pore Water Pressure simultaneously (Coupled approach)

(f) Factor of Safety (F.O.S) for Slope Stability (Both Uncoupled and Coupled approach)

The effect of multiple tidal cycles on the above mentioned parameters was also investigated. 120 number of cycles over a time span of 60 days was simulated on the embankment.

5.5 : RESULTS & DISCUSSIONS FOR MODEL $SDBN_0$

Results and discussions based on Steady and Transient Seepage analysis of Model – $SDBN_0$ has been presented in the following sub-sections

5.5.1: Phreatic Line and its Dynamics

One of the chief interests in any unconfined seepage analysis through an earthen dam is the location of the phreatic line. As mentioned in above sections, the basis of any transient analysis starts from a steady state analysis.

The steady state condition phreatic surface based on the position of land groundwater table at existing ground level and the Low tide level on River side has been shown in **Figure-5.12** for Model $SDBN_0$.

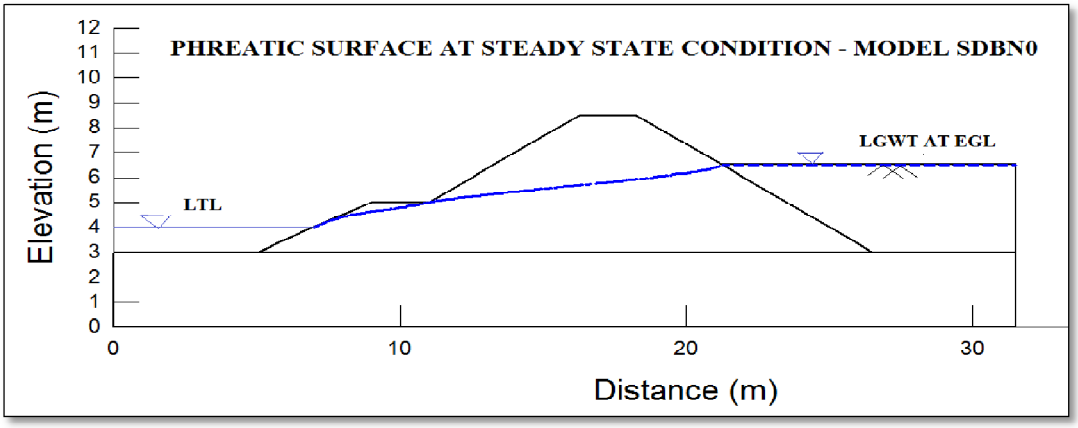

Figure-5.12 : Steady State Phreatic Surface for model *SDBN$_0$* .

Single Tidal Cycle

Along the phenomenon of a single tidal cycle, the dynamics of the phreatic line for the model SDBN$_0$ has been discussed and shown in the following sub-sections.

Rise-Up

The dynamics of the phreatic surface during the Rise-Up phase of the tidal cycle, from t = 0 hr to t = 6 hrs has been shown in **Figure-5.13**. The bold blue dotted line indicates the phreatic surface from steady state condition whereas the firm blue lines indicate the phreatic surface at each time interval.

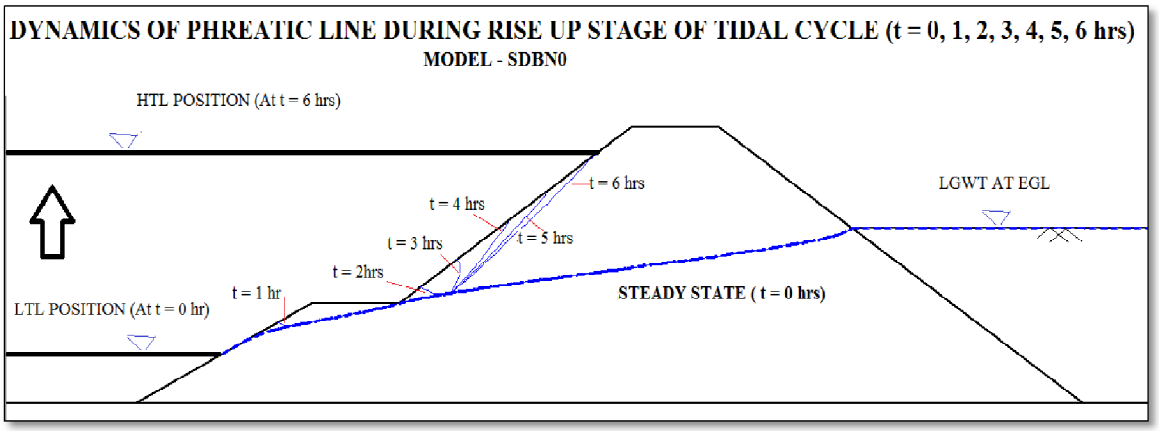

Figure-5.13 : Dynamics of Phreatic Surface during Rise-Up Condition of a Single Cycle for Model SDBN$_0$

Draw-down

The dynamics of the phreatic surface during the Draw-down phase of the tidal cycle, from t = 6 hrs to t = 12 hrs has been shown in **Figure-5.14**. In this Figure, the bold blue dotted line indicates the phreatic surface after a complete tidal cycle at t = 12 hrs. An interesting observation is that the

position of the phreatic surface has shifted from its initial location (before a single cycle) near LTL at t = 0 hr to a new location just above the berm level at t = 12 hrs. Thus, it is expected that the region below this blue dotted line, now encompassing the entire berm region shall remain fully saturated before onset of the immediately next tidal cycle.

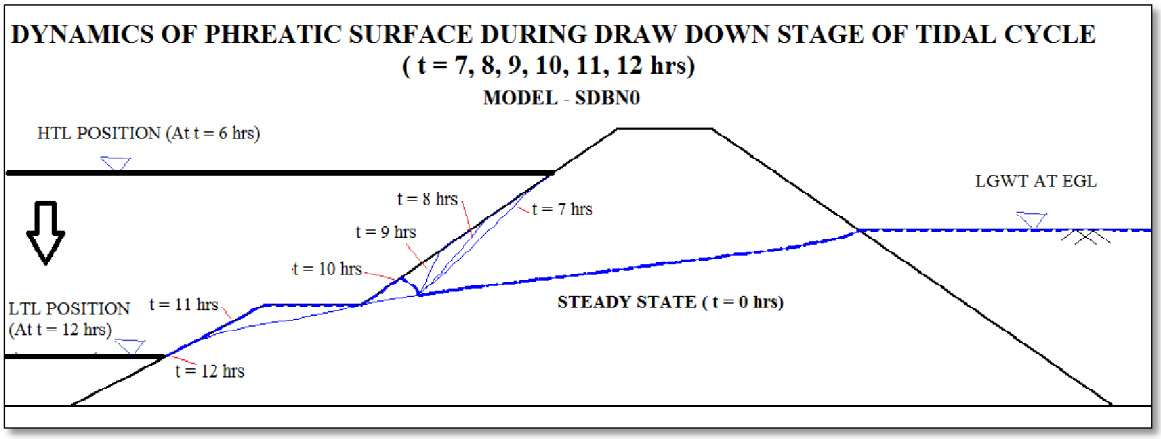

Figure-5.14 : Dynamics of Phreatic Surface during Draw-down Condition of a Single Cycle for Model $SDBN_0$

Effect of Multiple Tidal Cycles

An attempt has been made to study the impact of multiple tidal cycles on the dynamics of the phreatic surface of model $SDBN_0$. The number of tidal cycles selected is based over 60 days time and for 120 cycles. The results have been illustrated in **Figure-5.15**. The bold dotted line indicates the phreatic surface position after running of 120 cycles.

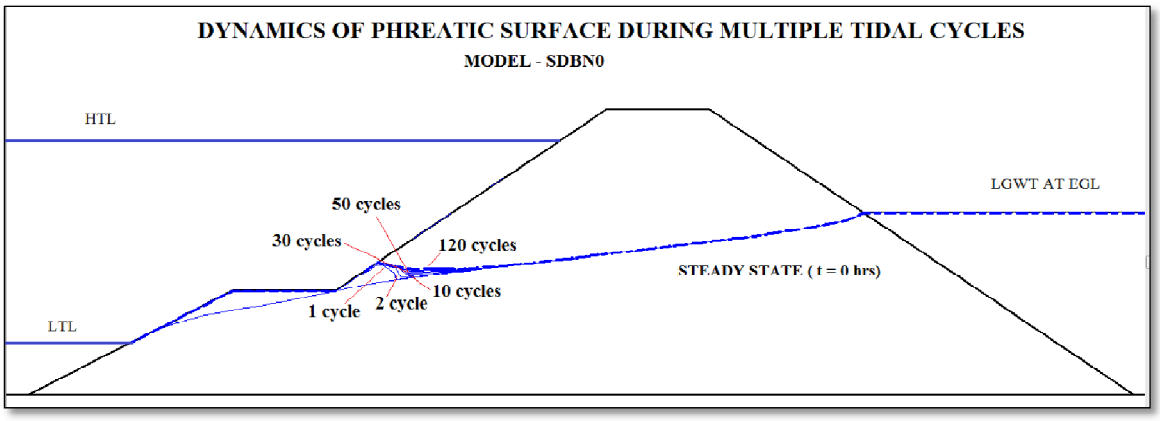

Figure-5.15 : Dynamics of Phreatic Surface during Multiple Cycles for Model $SDBN_0$

It has been observed that the location of the phreatic surface shifts to a slightly higher elevation within a particular zone after each corresponding cycle. The variation is observed upto a certain distance from the River-Embankment interface, beyond which no variation in phreatic line is observed. At the end of 120 cycles, this zone has been measured as 3.5 metres approximately

from the toe of the upper slope for this particular study. However, considering that the material is clayey silt with a very low permeability, the elevational shift in phreatic surface is marginal. A higher magnified image concentrating on the above mentioned zone has been presented in **Figure-5.16** for better understanding.

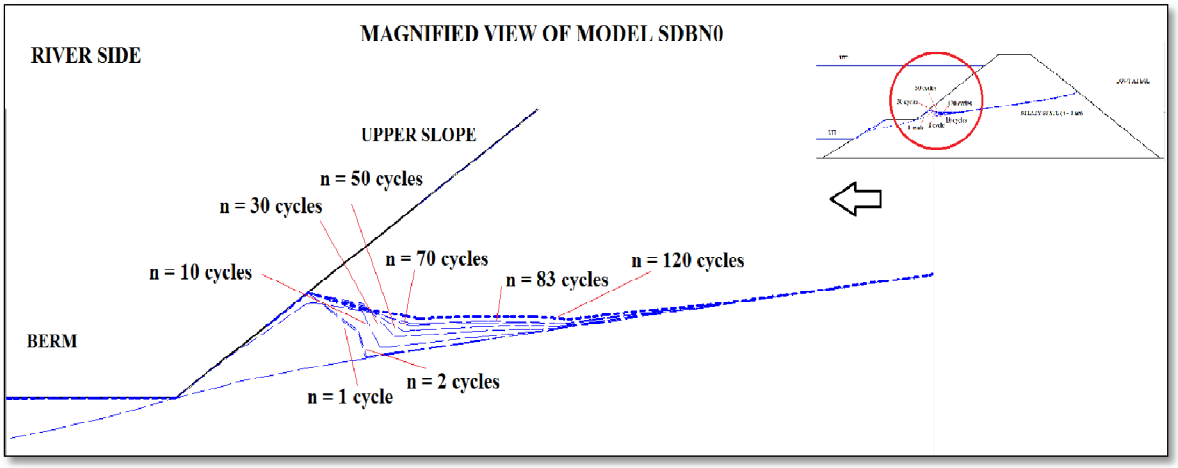

Figure-5.16 : Magnified Image showing Dynamics of Phreatic Line with tidal cycles for Model $SDBN_0$

5.5.2: Flux Distribution at Various Sections

The flux section has been developed at critical areas to monitor the flux rates at these locations during steady and transient stages. These have been shown in the **Figure 5.17**. The five areas selected are the *Berm Toe Section-1* (slope below berm toe), *Berm Section-2* (berm section), *Embankment Section-1* (embankment section exposed to riverfront), *Embankment Section-2(* internal embankment section) and *Embankment Landside Section.*

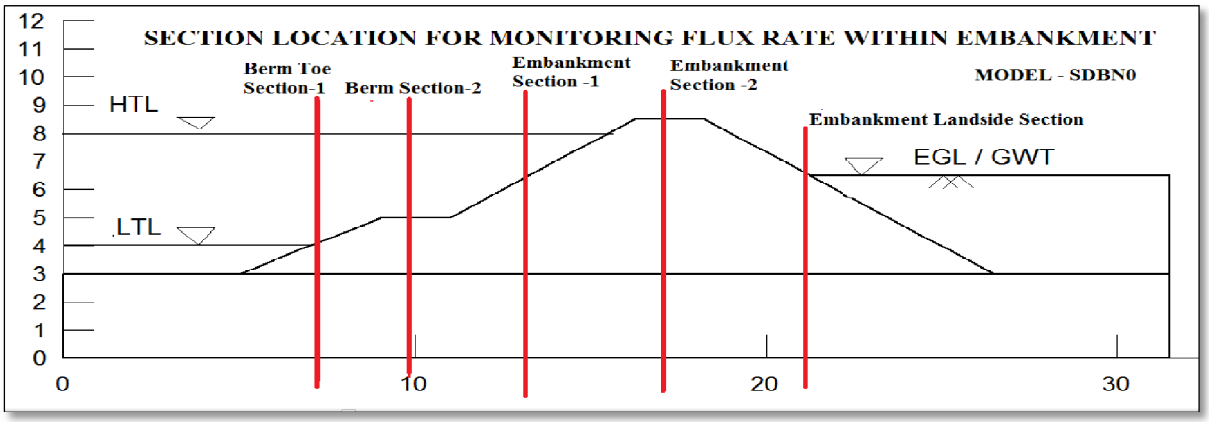

Figure-5.17 : Location of Flux Sections for Monitoring flux rate in Model $SDBN_0$

The flux rate variation for single cycle have been plotted in **Figure-5.18**. Here, t = 0, indicates Steady State values. The maximum variation in flux is observed for Embankment Section-1 followed by Berm Toe Section-1and Berm Section-2. The maximum flux is recorded at t = 6 hrs, at

HTL position, for the above sections. The Embankment Section-2 and Embankment Landside section, being quite far from the riverfront has shown no variation during Rise-Up and Draw-down, recording constant values of flux throughout the single tide cycle.

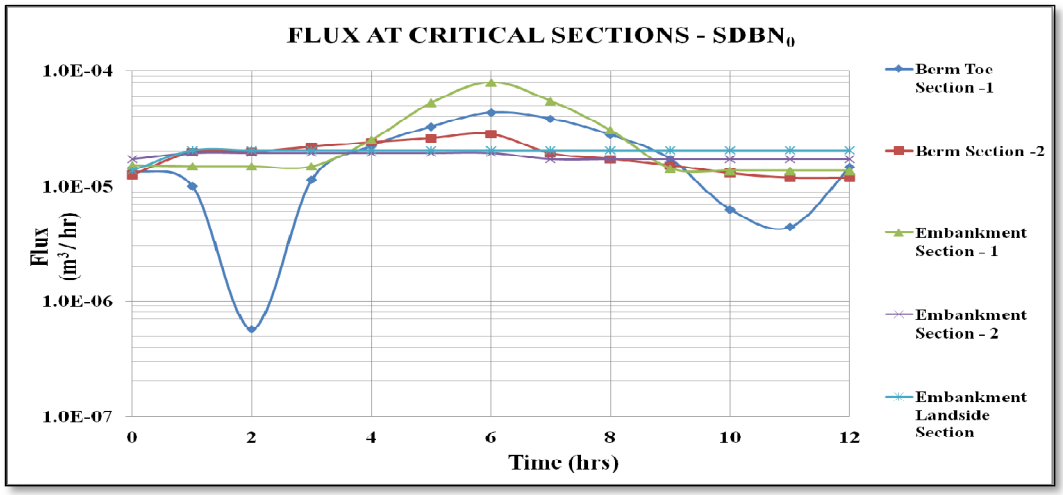

Figure-5.18 : Variation of flux across sections with Rise up and Draw-down for Model $SDBN_0$

Effect of Multiple Tidal Cycles

The impact of multiple cycles on the flux rate at the above mentioned regions have been studied and presented in **Figure-5.19**. It is observed that the flux rates at all sections mentioned above, except from Embankment Section-1, shows a slight increase in flux till the end of the 5th cycle, after which the value remains constant more or less. The variation in flux is maximum for the Embankment Section-1, which shows a gradual decrease in flux with increase in number of cycles. The magnitude of variation is however very small and to the tunes of 10^{-4} m^3/day as is evident from the Figure.

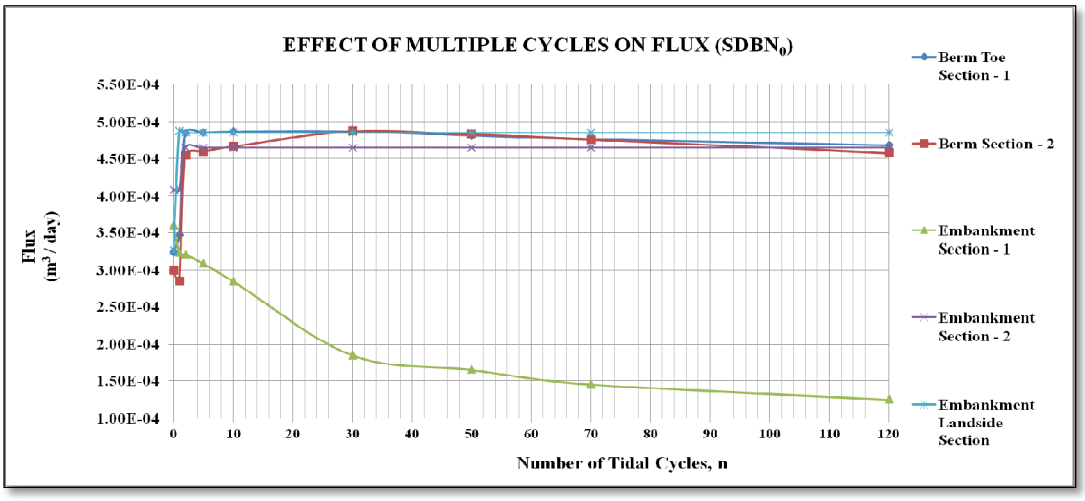

Figure-5.19 : Effect of Multiple Tidal Cycles on Flux across sections for Model $SDBN_0$

5.5.3: Distribution of Equipotential Line Contours

The flow vector and distribution of equipotential lines for steady state condition has been shown in **Figure-5.20**, for $SDBN_0$. The flow vectors have been shown at an magnification of 70000. The maximum hydraulic velocity is about 1.5e-05 m/hr. The transient state results are discussed below.

Single Tidal Cycle

Rise-Up

As the river water level rises from LTL to HTL over t = 0 hrs to t = 6 hrs, the Equipotential Line distribution contours for Model $SDBN_0$ has been shown in **Figures 5.21**, **5.22**, **5.23**, **5.24**, **5.25**, **5.26**. It is seen that only a particular zone at the interface of river – embankment surface is affected by the tidal cycle. This zone has been called the " Zone of Influence of Rise-Up (ZIR)". Other regions within the embankment remains unaffected by the tide induced transient seepage phenomenon. There is an increase in the magnitude of total head, pore water pressure at points within this zone due to the phenomenon. The zone can be identified from the extent of equipotential contour band at each time frame during Rise-Up. It is seen that the zone slowly develops and increases in size along the Lower Slope, Berm and Upper Slope with Rise-Up. The flow vectors (shown by arrows) clearly indicate the inward flow of tidal water into the embankment at this zone, during Rise-Up.

Draw-down

As the river water level recedes from HTL to LTL over t = 6 hrs to t = 12 hrs, the Equipotential Line contour for Model $SDBN_0$ during Draw-down stage of a single tidal cycle has been shown in **Figures. 5.27**, **5.28**, **5.29**, **5.30**, **5.31**, **5.32**. It has been seen that within the ZIR, the total head starts to dissipate during the draw-down phase. It is observed that the river front interface of the embankment has now turned into a seepage surface, with the tidal water that had encroached the embankment during Rise-Up now flowing out of the same, during Draw-Down. This is indicated by the position of flow vectors. Moreover, the ZIR starts diminishing in size during this stage. It is recorded that the rate of diminish of ZIR is maximum in the Lower Slope and Berm Region compared to the Upper Slope of the embankment. At the end of a single cycle, t = 12 hrs (shown in Figure 5.32), the ZIR for a single cycle has almost diminished in the Lower Slope and Berm Regions, however the zone persists in the Upper Slope, where tidal water continues to penetrate inward the embankment, as the next tidal cycle builds up on the river side. Also, there is an net increase in the total head at regions in the lower slope region at t = 12 hrs, compared to its initial steady state stage. (Refer Figure-5.20, 5.32)

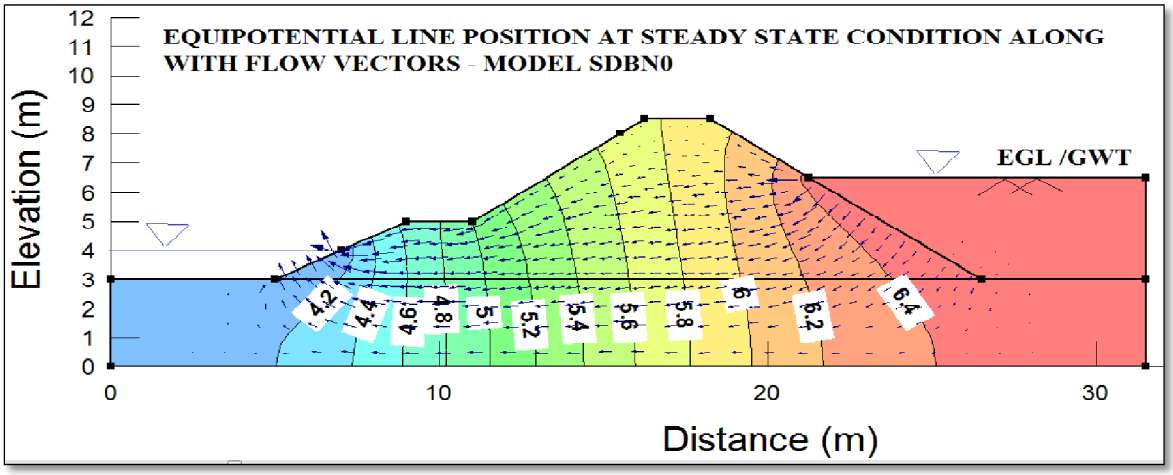

Figure-5.20 : Steady State Equipotential Lines for LTL position at t = 0 hr for *SDBN$_0$*

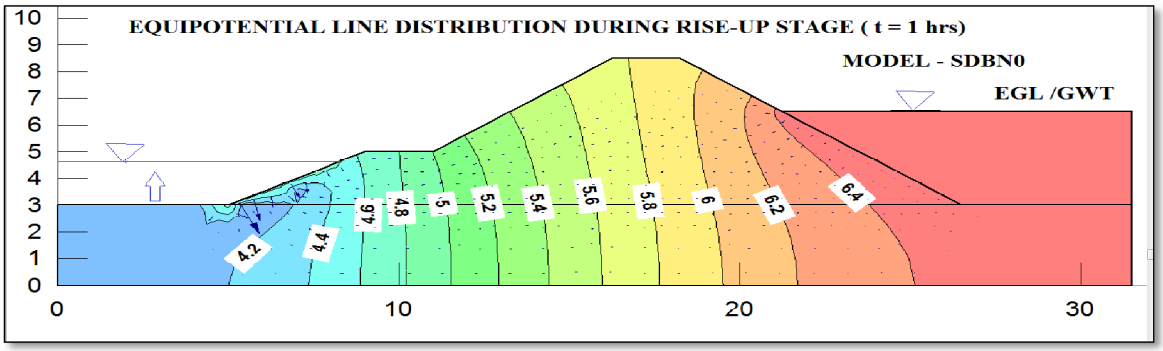

Figure-5.21 : Equipotential Lines during Rise-Up stage (t = 1 hr) at Single Cycle for *SDBN$_0$*

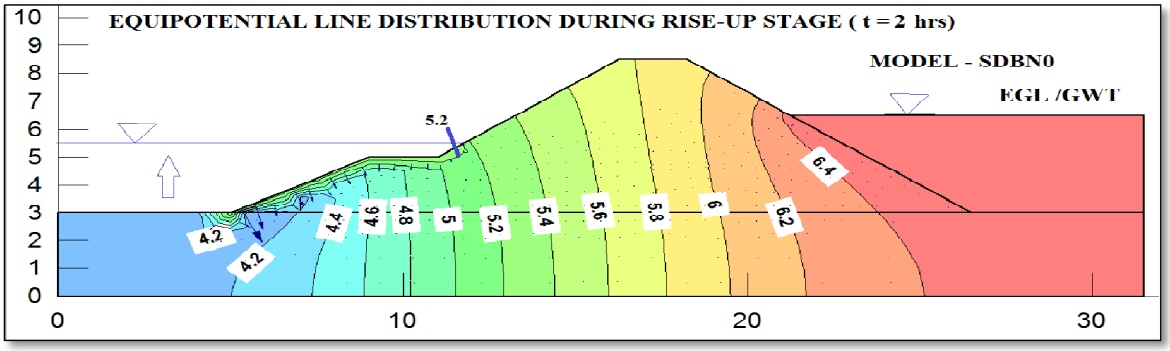

Figure-5.22 : Equipotential Lines during Rise-Up stage (t = 2 hrs) at Single Cycle for *SDBN$_0$*

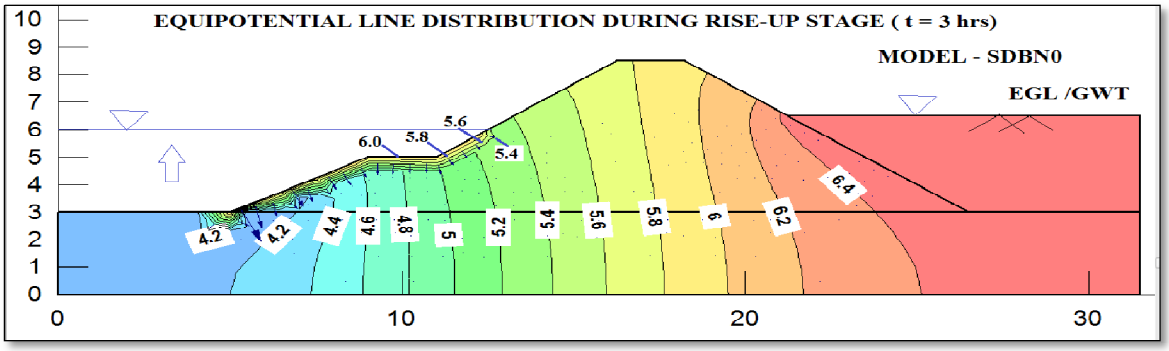

Figure-5.23 : Equipotential Lines during Rise-Up stage (t = 3 hrs) at Single Cycle for *SDBN$_0$*

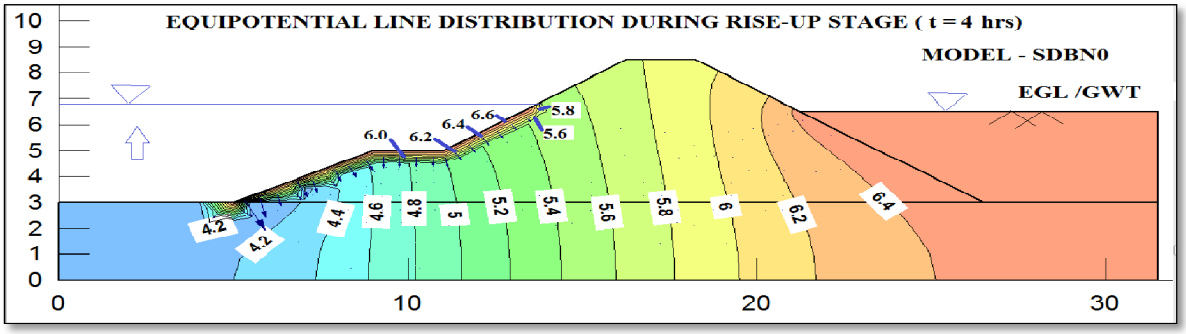

Figure-5.24 : Equipotential Lines during Rise-Up stage (t = 4 hrs) at Single Cycle for *SDBN$_0$*

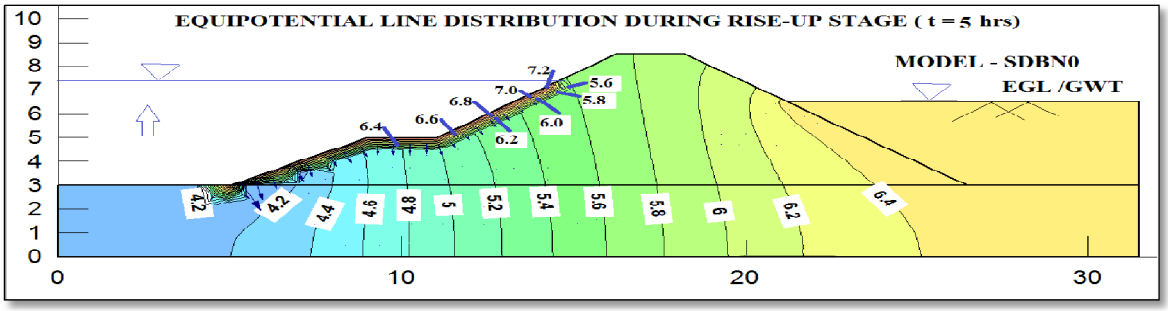

Figure-5.25 : Equipotential Lines during Rise-Up stage (t = 5 hrs) at Single Cycle for *SDBN$_0$*

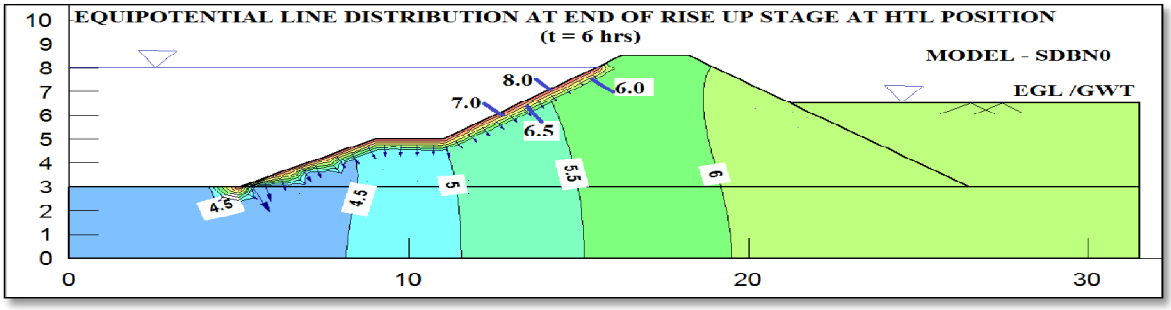

Figure-5.26 : Equipotential Lines at HTL position (t = 6 hrs) for *SDBN$_0$*

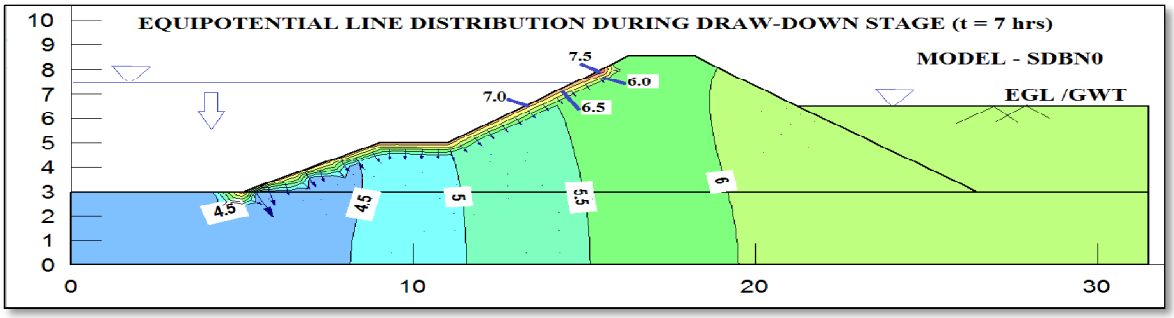

Figure-5.27 : Equipotential Lines during Draw-down stage (t = 7 hrs) at Single Cycle for *SDBN$_0$*

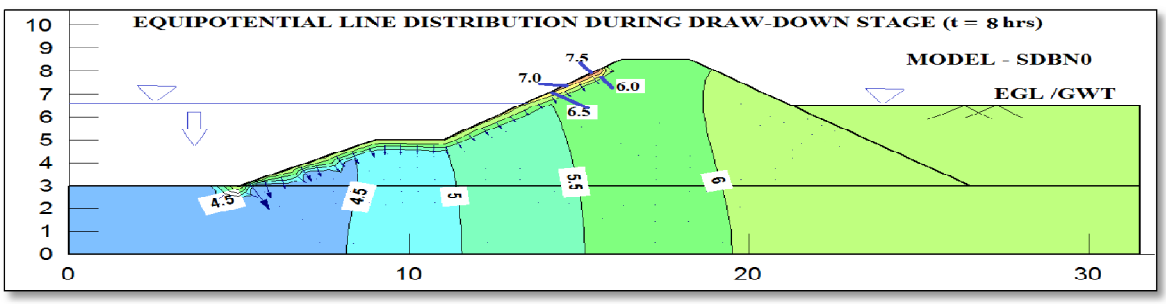

Figure-5.28 : Equipotential Lines during Draw-down stage (t = 8 hrs) at Single Cycle for *SDBN$_0$*

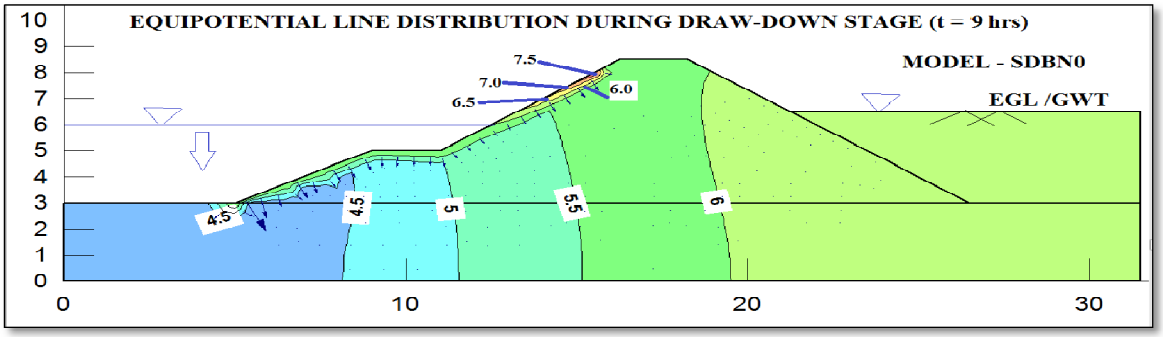

Figure-5.29 : Equipotential Lines during Draw-down stage (t = 9 hrs) at Single Cycle for *SDBN0*

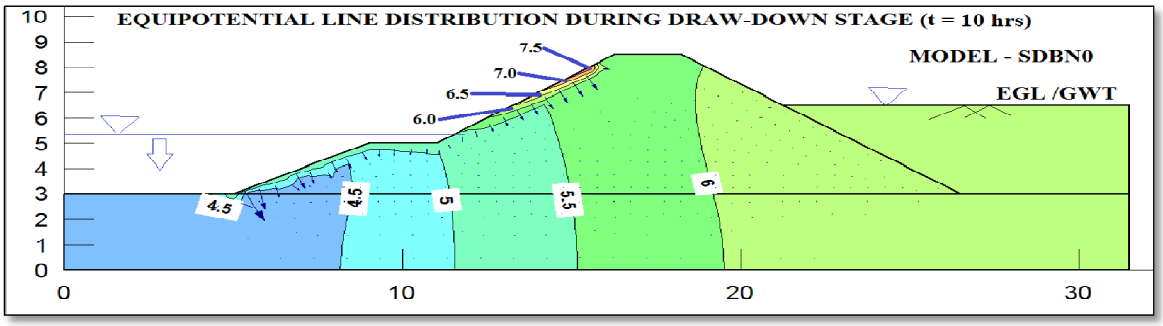

Figure-5.30 : Equipotential Lines during Draw-down stage (t = 10 hrs) at Single Cycle for *SDBN0*

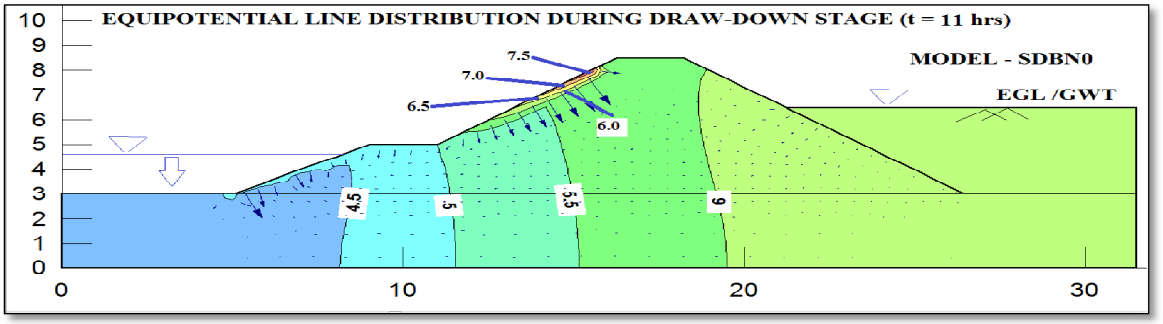

Figure-5.31 : Equipotential Lines during Draw-down stage (t = 11 hrs) at Single Cycle for *SDBN0*

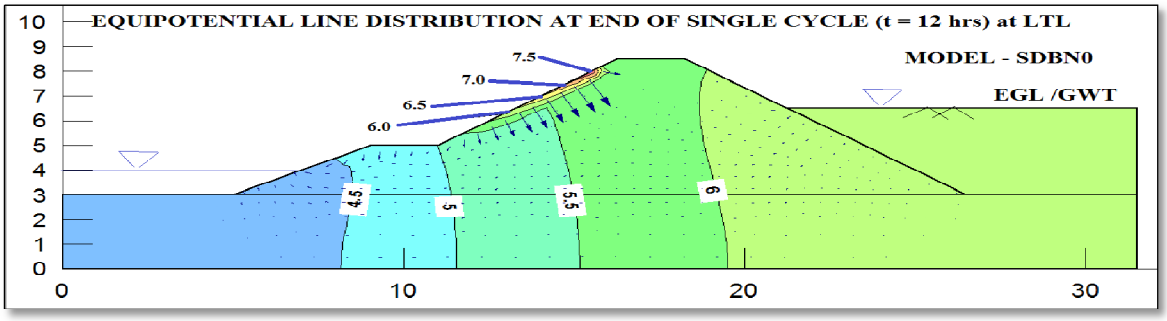

Figure-5.32 : Equipotential Lines at end of Single Cycle Draw-down Stage (t = 12 hrs) for *SDBN0*

Effect of Multiple Tidal Cycles

The distribution of equipotential line contours at the end of multiple tidal cycles have been demonstrated for n = 2, 5, 10, 50, 70, 120 (where n = no. of cycles) in **Figures 5.33**, **5.34**, **5.35**, **5.36**, **5.37**, **5.38.** It has been observed that at the upper slope region, the total head keeps on decreasing with each subsequent tidal cycle. After the end of 1st tidal cycle, the maximum head at

the Upper Slope was 7.5 m and after 120 cycles the same was 6.4 m, indicating a 14.67 percent decrease over this cycle span. This may be attributed to the fact that even after the end of consecutive cycles, there remains a small zone in the Upper Slope where the tide induced excess seepage head had not dissipated and the same continues to dissipate inwards and outwards through a higher time period. Along the Lower Slope and Berm, it has been observed that although majority of the excess tide induced seepage head is dissipated at the end of each cycle, however there is a slight increase in the total head at locations in Lower Slope in comparison to previous cycle.

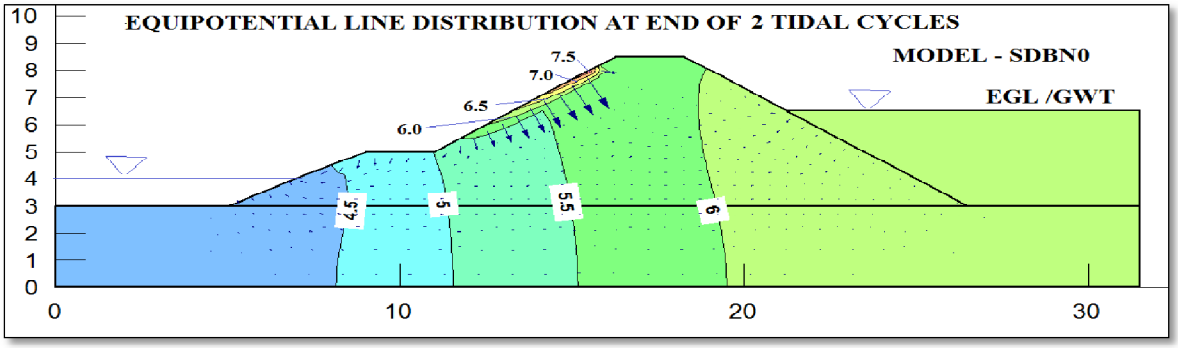

Figure-5.33 : Equipotential Lines at the end of 2nd Cycle for *SDBN$_0$*

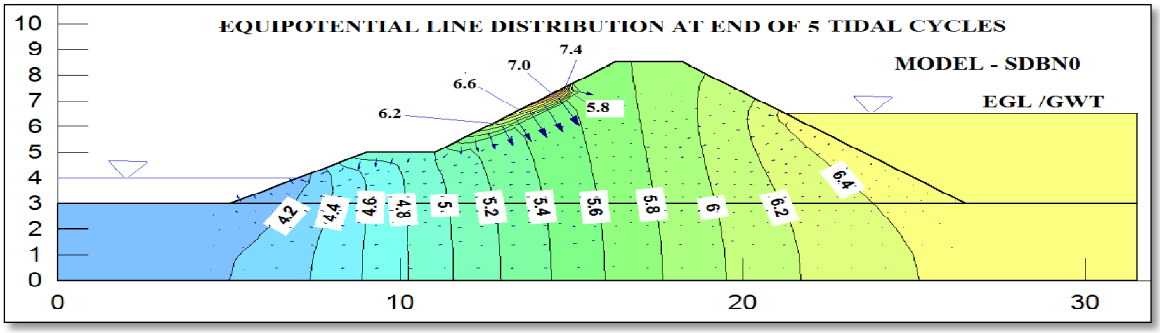

Figure-5.34 : Equipotential Lines at the end of 5th Cycle for *SDBN$_0$*

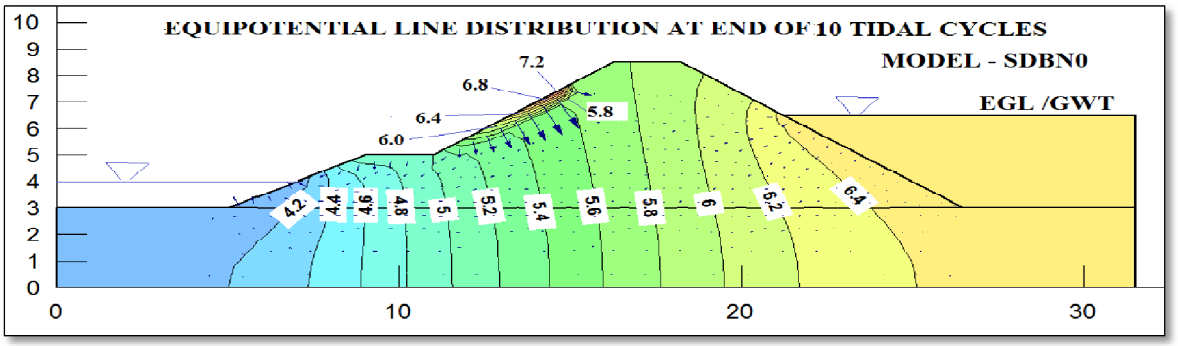

Figure-5.35 : Equipotential Lines at the end of 10th Cycle for *SDBN$_0$*

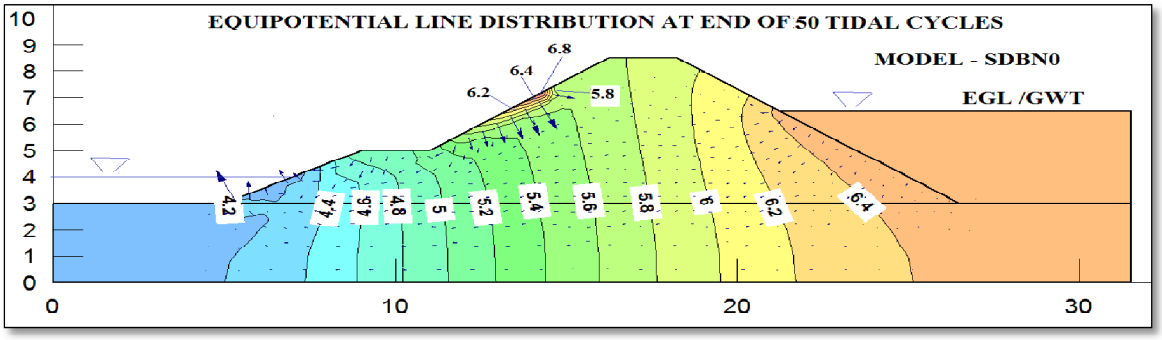

Figure-5.36 : Equipotential Lines at the end of 50th Cycle for *SDBN0*

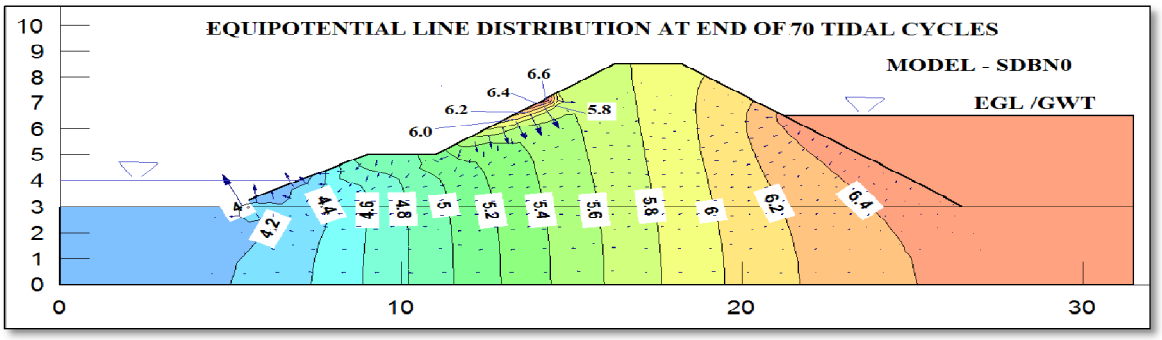

Figure-5.37 : Equipotential Lines at the end of 70th Cycle for *SDBN0*

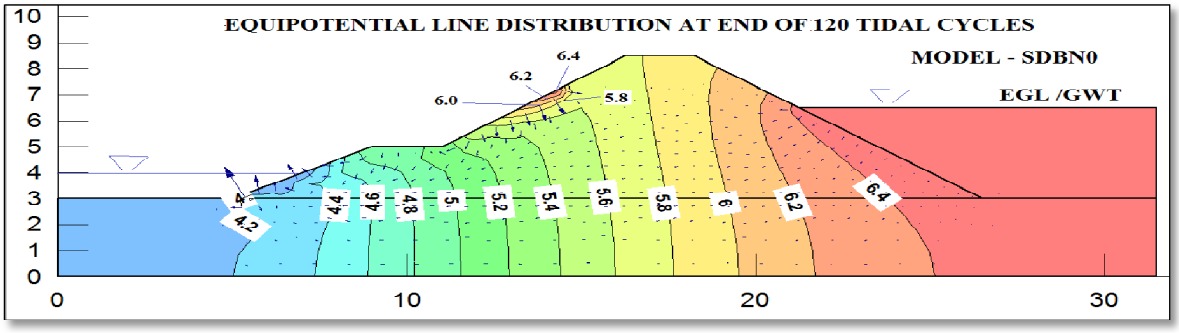

Figure-5.38 : Equipotential Lines at the end of 120th Cycle for *SDBN0*

5.5.4: Pore Water Pressure Distribution

Single Tidal Cycle

Discussions in the previous sub-sections indicate that for transient seepage occurring during a single tidal cycle, the variation of parameters like pore pressure, total head, flux, etc are restricted to River-Embankment interface regions defined by the *Zone of Influence of Rise-Up (ZIR)*. To get a detailed idea about pore pressure variation across the embankment, the entire embankment has been divided into four parts – (i) The Lower Slope Portion (ii) The Berm Portion (iii) The Upper Slope Portion (iv) Interior of embankment upto Landside. A set of points have been taken in each of the above mentioned zones to track the pore water pressure variation during single tidal cycle.

The results obtained during a single tidal cycle are shown in **Figures. 5.39**, **5.40**, **5.41**, **5.42**. A gradual increase in pore water pressure from initial condition at t = 0 hr to a maximum value during Rise-Up phase and then gradual decrease till end of Draw-down at t = 12 hrs, has been observed for majority of points lying within the ZIR. The points where no variation in pore water pressure is observed, lie outside this zone and is unaffected by the single tidal cycle. The maximum percentage variation for pore water pressure is recorded for points in the Lower Slope region in comparison to Berm region and Upper Slope region, during a single cycle. There are regions in the Lower Slope, Berm Region and Upper Slope which were experiencing suction (i.e. points lying above phreatic line) at t = 0 hr and became fully saturated at end of a single tidal cycle, with zero or positive pore water pressure. In the Berm region, the percentage variation in pore water pressure was less in comparison to the Lower slope. The Lower Slope, Berm Region and Upper Slope region have points where variation is zero upto a certain time frame and then the pore water pressure starts increasing till t = 6 hrs and subsequently decrease from t = 6 hrs to t = 12 hrs. These are the regions which were initially out of the ZIR, but with the onset of the tidal cycle, as the river water head increased, more area within the embankment came under the ZIR, thereby encompassing these points. No variation in Pore water pressure was recorded for interior parts of the embankment as they lie outside the ZIR for the entire duration of single cycle.

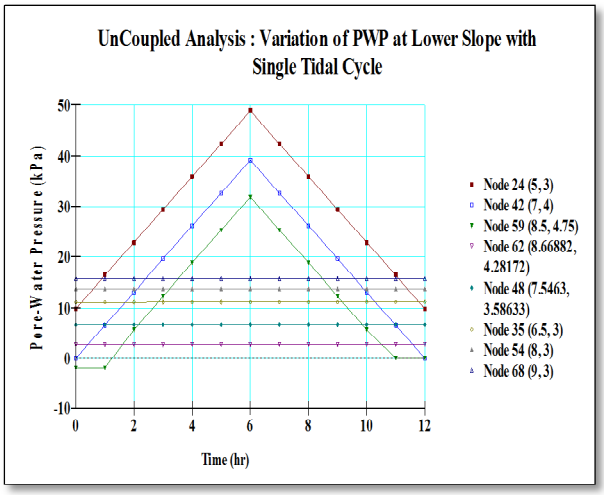

Figure-5.39 : PWP Variation by Uncoupled Analysis during Single Tidal Cycle in Lower Slope region of $SDBN_0$

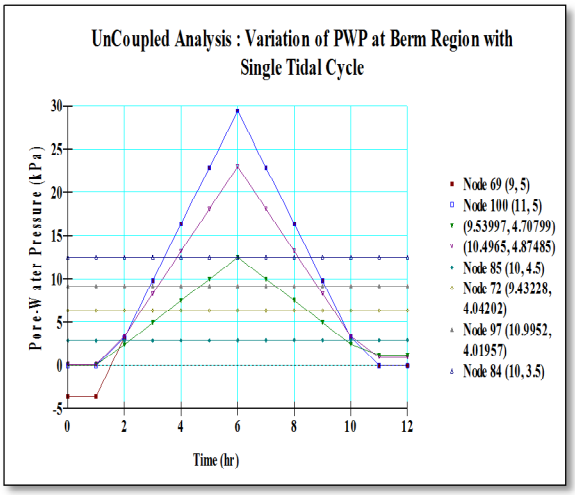

Figure-5.40 : PWP Variation by Uncoupled Analysis during Single Tidal Cycle in Berm portion of $SDBN_0$

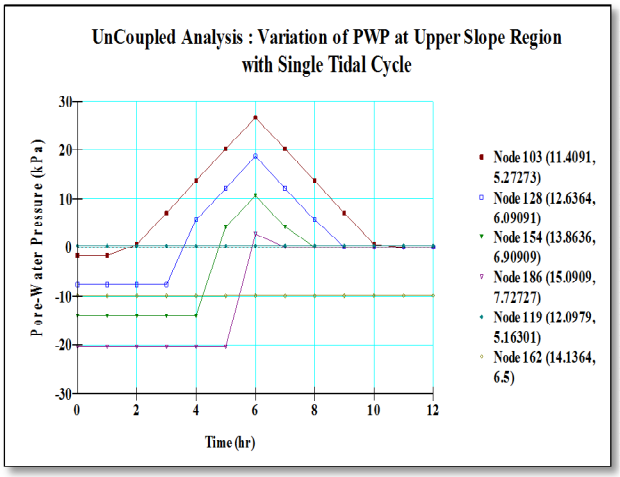

Figure-5.41 : PWP Variation by Uncoupled Analysis during Single Tidal Cycle in Upper Slope Region of *SDBN0*

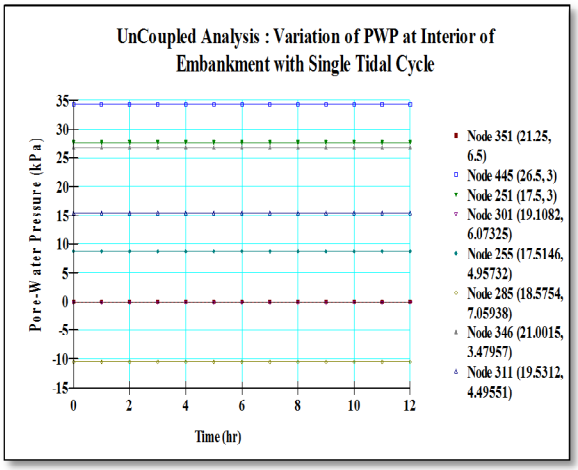

Figure-5.42 : PWP Variation by Uncoupled Analysis during Single Tidal Cycle in Interior of Embankment of *SDBN0*

Effect of Multiple Tidal Cycles

To get an idea about the impact of multiple tidal cycles on the different regions of the embankment, the pore pressure contours at the initial conditions and at the end of 1, 5, 10, 60, 120 cycles have been shown in **Figures – 5.43**, **5.44**, **5.45**, **5.46**, **5.45**, **5.48.** It is recorded that the variations are seen only in the regions of ZIR after initial few consecutive cycles. The rate of variation tends to zero as the number of cycle increases, indicating more or less constant contours.

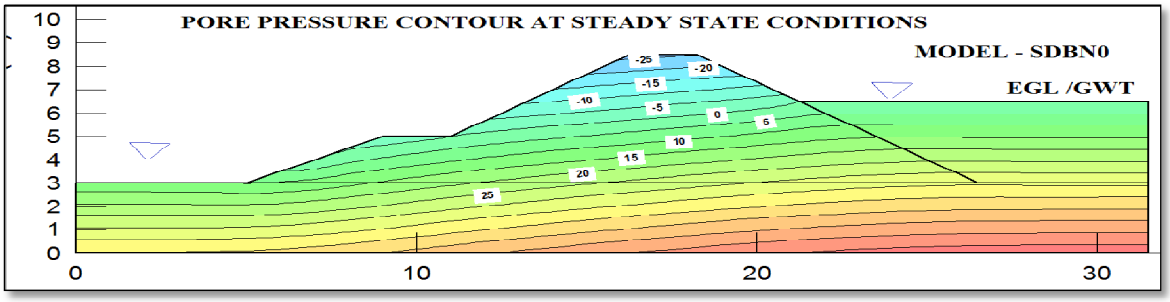

Figure-5.43 : Pore Pressure Contour at Steady State Conditions for *SDBN0*

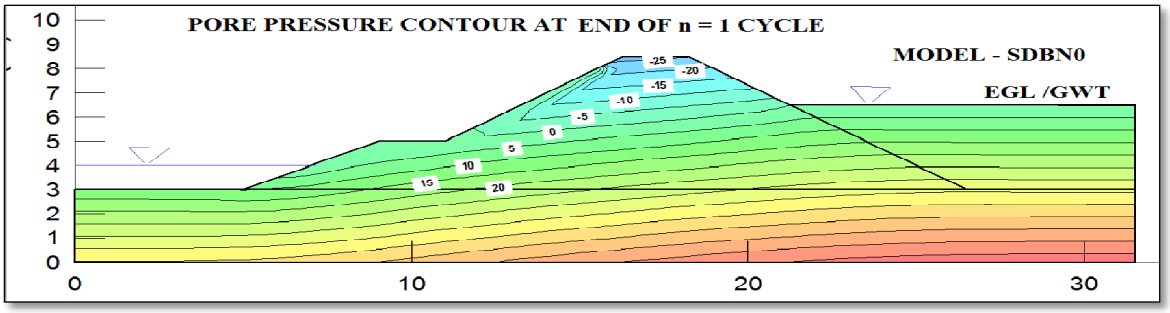

Figure-5.44 : Pore Pressure Contour at end of 1st Cycle for *SDBN0*

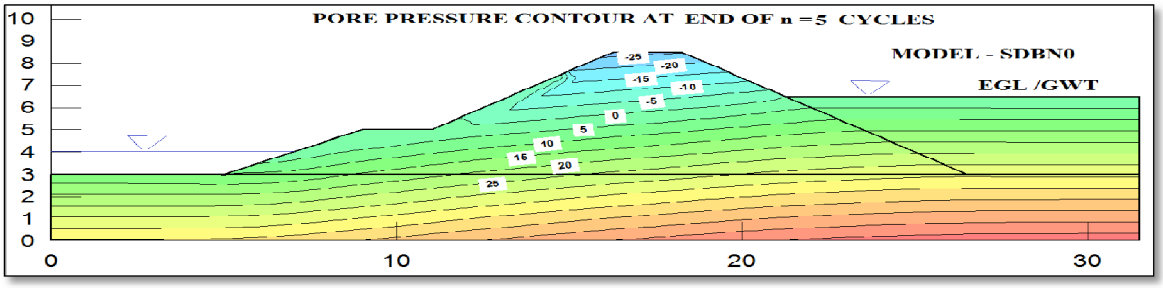

Figure-5.45 : Pore Pressure Contour at end of 5th Cycle for *SDBN0*

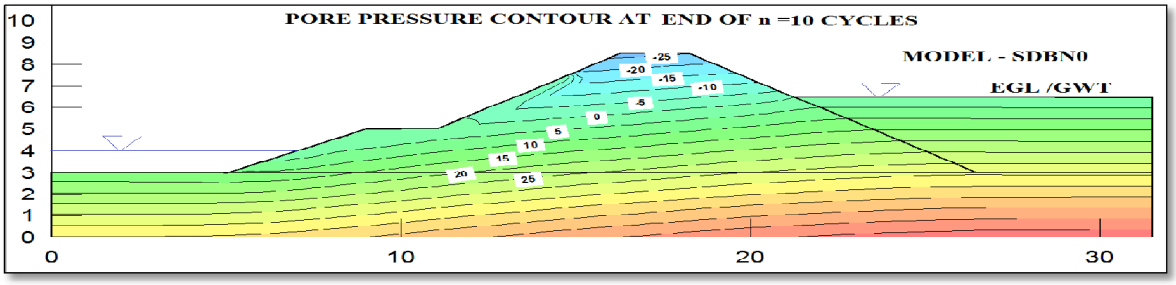

Figure-5.46 : Pore Pressure Contour at end of 10th Cycle for *SDBN0*

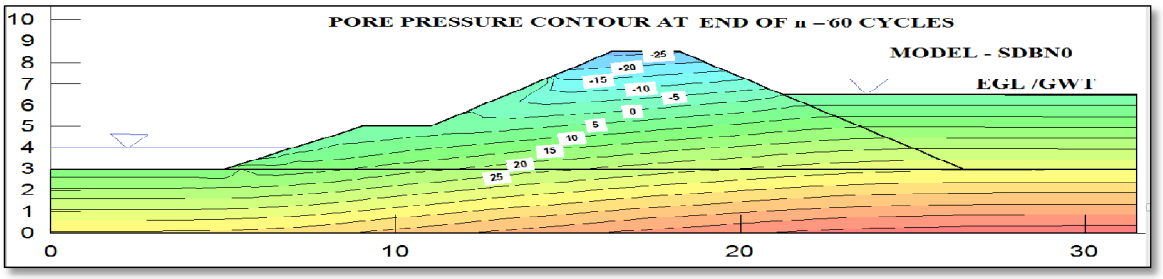

Figure-5.47 : Pore Pressure Contour at end of 60th Cycle for *SDBN0*

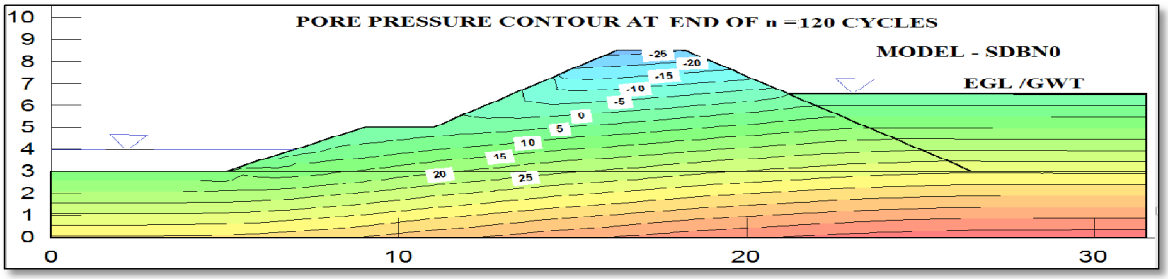

Figure-5.48 : Pore Pressure Contour at end of 120th Cycle for *SDBN0*

5.5.5: Deformation Based Analysis

A coupled analysis was performed to investigate the effect of tidal cycle on the deformation and pore water pressure at critical locations within the embankment. The selection of points was the same as in Uncoupled analysis. The results for Lower Slope, Berm region and Upper Slope during a single tidal cycle has been presented in **Figures - 5.49**, **5.50**, **5.51**, **5.52**, **5.53**, **5.54**. A trend similar to uncoupled analysis was obtained for the interior of the embankment where no variation in pore pressure was seen during the tidal cycle, hence these have not been separately shown. The

effect of multiple cycles on the above mentioned regions for the same parameters have been shown in **Figures – 5.55**, **5.56**, **5.57**, **5.58**, **5.59**, **5.60**.

Deformation

Single Tidal Cycle

It is observed that in Lower Slope, Berm Region and parts of Upper slope, there is vertical settlement which keeps on increasing till t = 6 hrs, during Rise-Up. This is due to the immense hydrostatic pressure of the tidal water head building up during this phase. Thereafter, during Draw-down, there is a rebound of the same points as the tidal water head comes down decreasing the hydrostatic pressure. However, there is a net vertical settlement or rebound at some of the points at the end of a single cycle compared to initial conditions as per ability to dissipate pore water pressure. The points which show a slightly different pattern of encountering rebound during initial stages of Rise-Up followed by vertical settlement have been recognized as points lying initially in the suction zone, which is unsaturated. The same rebounds initially as water is absorbed as it enters this zone which then becomes saturated with zero or positive pore water pressure, then it settles vertically with the remaining Rise-Up phase. The time portion the rebound remains constant before plunging for settlement is the time taken by the point to develop a zero pore water pressure. The opposite happens during the draw-down phase. This pattern is observed more in the Upper Slope compared to the Lower Slope and Berm Region and is justifiable from discussions in previous sections.

Multiple Tidal Cycles

It has been observed that there is an cumulative effect of the tidal cycle on deformation. It has been seen that with increase in number of cycles, the vertical settlement increases. An important aspect is that as the embankment soil is not an elastic material, and it is exposed to continuous multiple tidal cycles consisting of Rise-Up and Draw-down, where as discussed in above sections, the embankment soil encounters cyclic settlement and rebound. It is expected to deform prominently with higher number of cycles. The effect should be a cumulative one and may even result in a serviceability failure. The higher the variation of this cyclic behavior of settlement and rebound, the higher the chances of permanent deformation.

Pore Water Pressure

Single Tidal Cycle

It is seen that with Rise-Up, there is a gradual build up of pore water pressure which dissipates during Draw-down. There is an accumulation of the same at certain points after a single cycle. An observation made compared to uncoupled analysis, is that the pore water pressure at the same points are varying in magnitude for coupled analysis. This is due to the fact that in coupled analysis, as the deformation is considered, the pore pressure develops with vertical deformation and dissipates on rebound. As soil is an elastic plastic material, there is non-linear deformation on increase in hydrostatic pressure and non-linear rebound on release of the same. The pore water pressure is affected accordingly. Moreover, points lying outside the Zone of Rise Up Influence which had not registered a pore water pressure variation in Uncoupled analysis is now showing a variation in Coupled analysis, when the hydrostatic pressure is considered additionally. This indicates the importance of Coupled analysis to get realistic site oriented results.

It has been seen that the maximum variation in pore water pressure during a single cycle is observed for the Lower Slope Region followed by Berm Region and Upper Slope Region.

Multiple Tidal Cycles

With increase in the number of cycles, the variation is small in the first few cycles after which the pore water pressure becomes constant with number of cycles. The observation is seen for Lower Slope, Berm Region and Upper Slope.

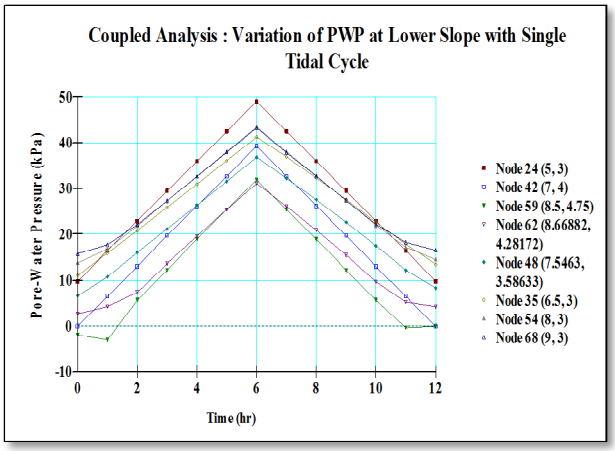

Figure - 5.49 : PWP Variation by Coupled Analysis during Single Cycle in the Lower Slope of $SDBN_0$

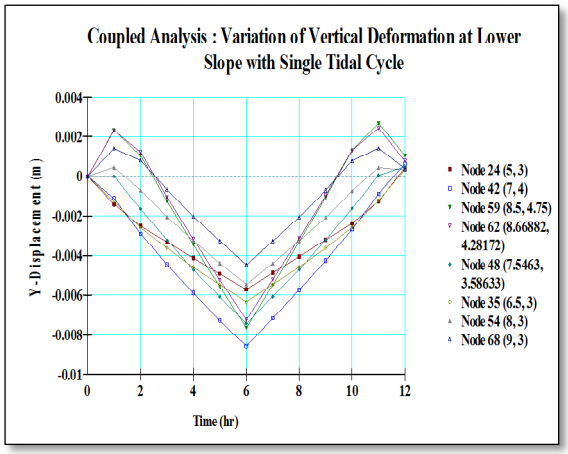

Figure - 5.50 : Vertical deformation during Single Cycle in the Lower Slope of $SDBN_0$

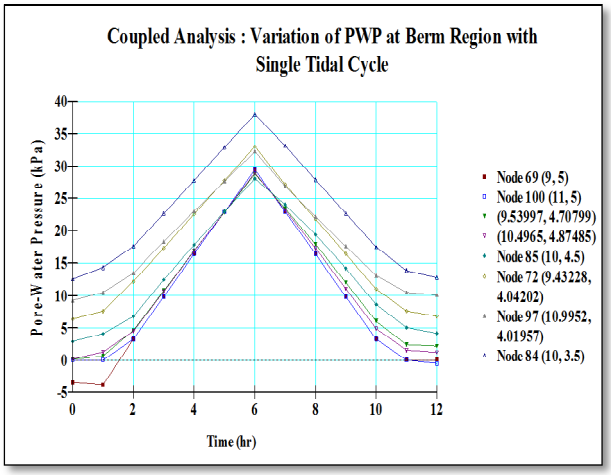

Figure - 5.51 : PWP Variation by Coupled Analysis during Single Cycle in the Berm Region of *SDBN*$_0$

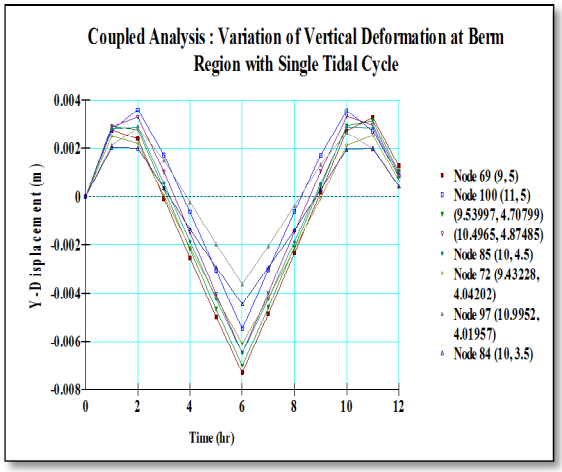

Figure - 5.52 : Vertical deformation during Single Cycle in the Berm Region of *SDBN*$_0$

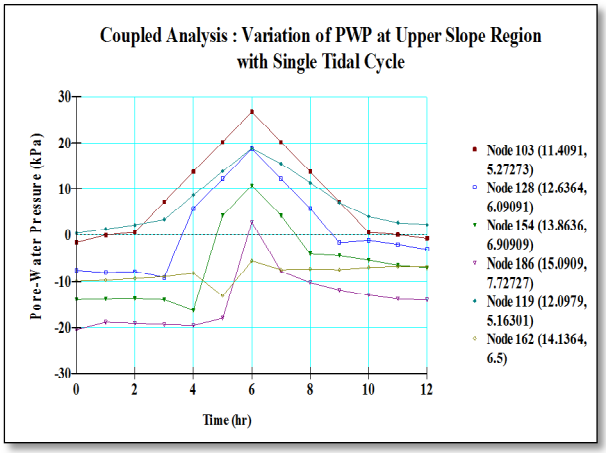

Figure - 5.53 : PWP Variation by Coupled Analysis during Single Cycle in the Upper Slope Region of *SDBN*$_0$

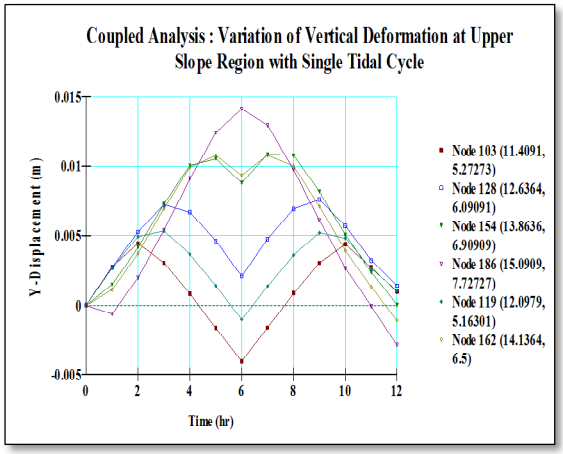

Figure - 5.54 : Vertical deformation during Single Cycle in the Upper Slope Region of *SDBN*$_0$

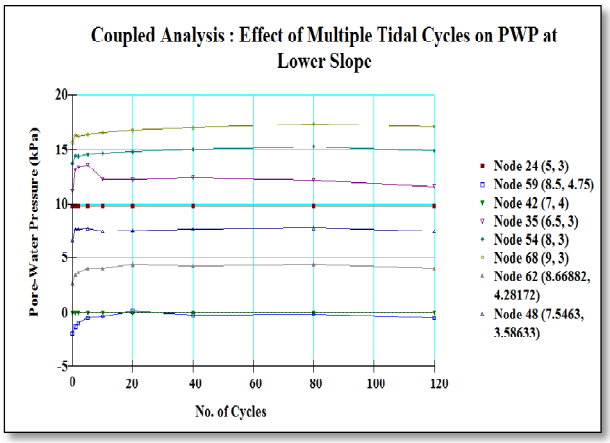

Figure - 5.55 : PWP Variation by Coupled Analysis during Multiple Cycles in the Lower Slope of *SDBN*$_0$

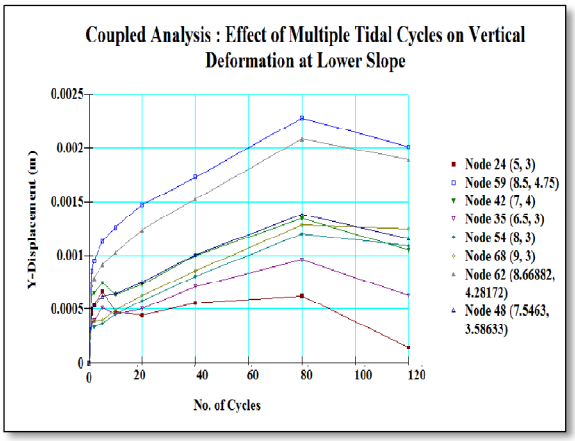

Figure - 5.56 : Variation in Vertical Deformation during Multiple Cycles in the Lower Slope of *SDBN*$_0$

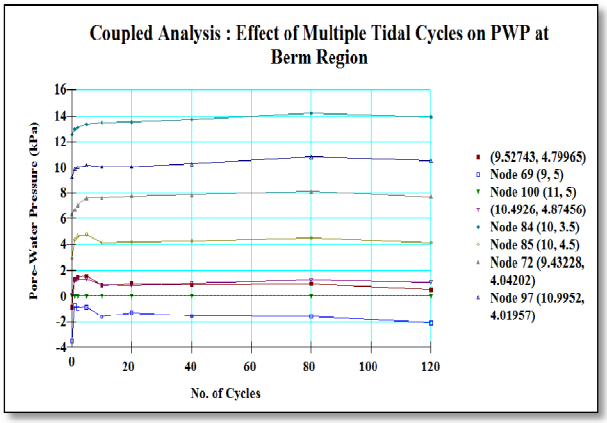

Figure - 5.57 : PWP Variation by Coupled Analysis during Multiple Cycles in the Berm region of *SDBN*$_0$

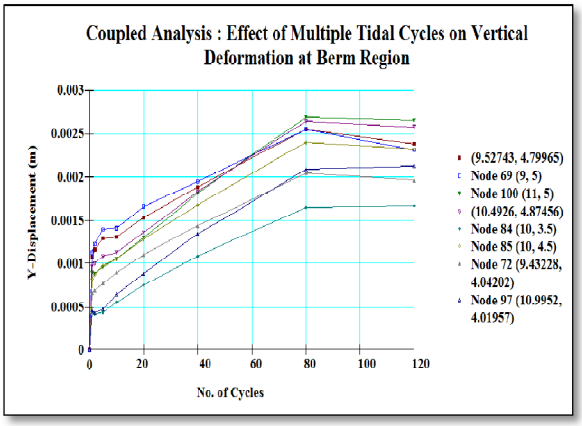

Figure - 5.58 : Variation in Vertical Deformation during Multiple Cycles in the Berm region of *SDBN*$_0$

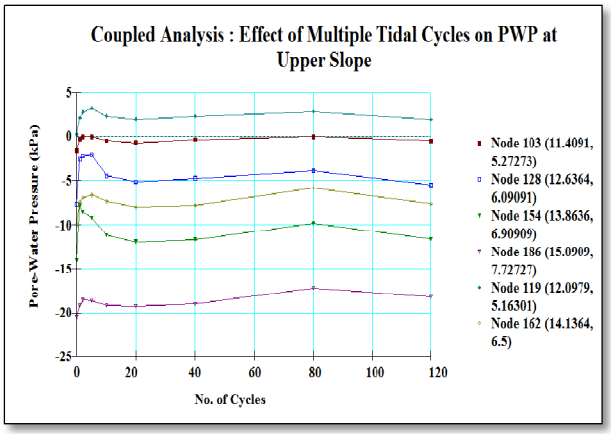

Figure - 5.59 : PWP Variation by Coupled Analysis during Multiple Cycles in the Upper Slope of *SDBN*$_0$

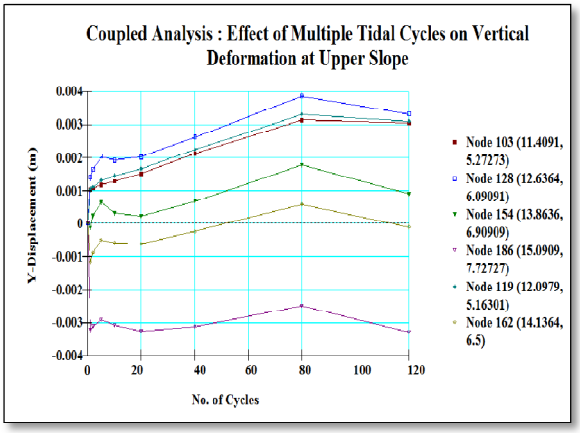

Figure - 5.60 : Variation in Vertical Deformation during Multiple Cycles in the Upper Slope of *SDBN*$_0$

5.5.6: Slope Stability Analysis

Slope Stability analysis has been carried out for both Uncoupled and Coupled methodology during the entire tidal cycle using SLOPE/W. The Limit equilibrium method was followed for the Uncoupled analysis with pore water pressure inputs from SEEP/W. The Spencer method was used for analysis. The Finite Element Slope Stability analysis was utilized for the Coupled analysis. The uncoupled slope stability analysis at steady state conditions have been shown in **Figure -5.61**, where the blue dotted line shows the location of the phreatic surface. The section of trial slip surfaces was done by the Entry and Exit method with gradual radii increments in stages. A total of 726 trial slip surfaces were taken and the minimum Factor of Safety was recorded. A safety map is shown in red band defining al the trial slip surfaces within a certain minimum F.O.S range varying at each stage of tidal cycle. It defines the zone of potential failure, where all the slip surfaces are very

similar. To be on the conservative side, the strength arising due to suction in the unsaturated regions were neglected.

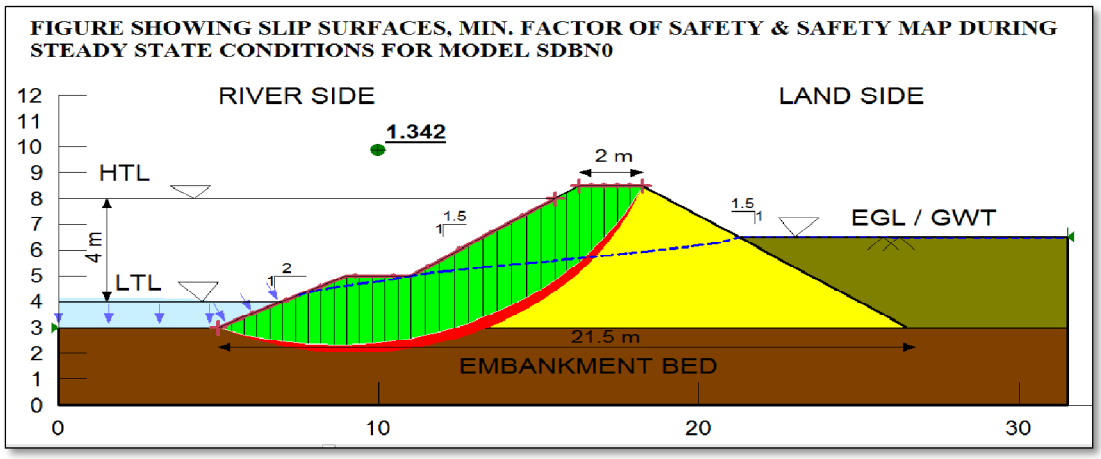

Figure - 5.61 : Slip surfaces, Minimum F.O.S and Safety Map during Steady State conditions (t = 0 hr) for model *SDBN$_0$*

Single Tidal Cycle

The Slip surfaces, F.O.S and Safety map during Rise-Up and Draw-down of a single tidal cycle has been shown in **Table - 5.3, 5.4**. It is seen that the Factor of Safety (F.O.S) increases from t = 0 to t = 6 hrs, throughout the Rise-Up stage. It reaches a maximum value at HTL. Then, with progression of draw-down, it decreases from t = 6 hrs to t = 12 hrs, for a single tidal cycle. It has been seen that the F.O.S value after the completion of a single tidal cycle comes quite close to its initial value from Steady State conditions. A plot of the F.O.S in Uncoupled and Coupled methodology has been shown in **Figure - 5.74**. It is seen that the values obtained in both the methods are almost same throughout the tidal cycle, except from at the HTL position at t = 6 hrs, where the Uncoupled Analysis gives a higher and conservative value of F.O.S. This may be explained as, as the water level rises during Rise-Up condition, there is development of pore water pressure as well as soil deformation (which may be vertical settlement or rebound, depending on location) due to the hydrostatic pressure developed, which is also taken into account by Coupled analysis. At HTL, the vertical settlement is maximum thereby inducing excess pore water pressure which gives lower F.O.S for Coupled analysis. With draw-down as the hydrostatic pressure is released and there is a rebound of soil, the excess pore water pressure dissipates and the soil returns to its original position, thus the F.O.S values suggested by Uncoupled and Coupled analysis are similar.

Multiple Tidal Cycles

The effect of multiple tidal cycles on the F.O.S were determined both in the Uncoupled and Coupled methods. The results have been shown in **Figure - 5.75**. The plotted points indicate the F.O.S at the end of corresponding tidal cycle. It is seen that the F.O.S remains more or less constant throughout multiple cycles, when analyzed by the Uncoupled method. In the Coupled method, an initial decrease in F.O.S is seen for the initial cycles and the same becomes constant after a certain number of cycles. For multiple cycle analysis, the Coupled methodology gives a conservative higher value of F.O.S. This may be attributed to the fact that in coupled methodology, as deformation is simultaneously calculated in addition to pore water pressure, it is known that with consequent deformation and rebound during each cycle, there are chances of permanent settlement or rebound after a certain number of cycles as soil is an inelastic material. The magnitude of net settlement or rebound shall determine whether the excess pore water pressure has been generated or dissipated in accumulation at end of each cycle. The above factor shall decide which F.O.S shall be conservative and which not.

TABLE-5.3 : Slip Surface Location, Minimum Factor of Safety, Safety Map for Model $SDBN_0$ during Rise-Up Stage (t = 1 hr to t = 6 hrs) of Single Tidal Cycle

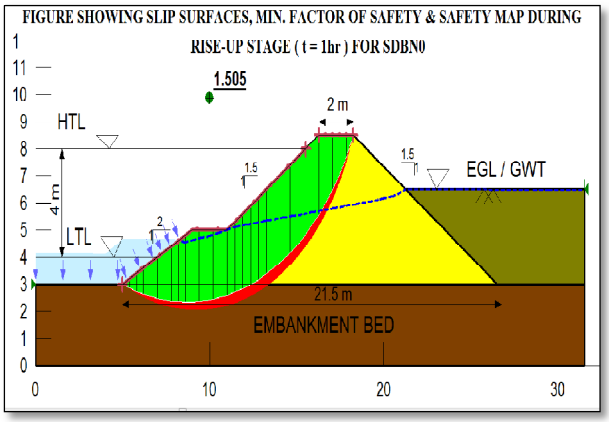

Figure-5.62 : At t = 1 hr, with F.O.S = 1.505

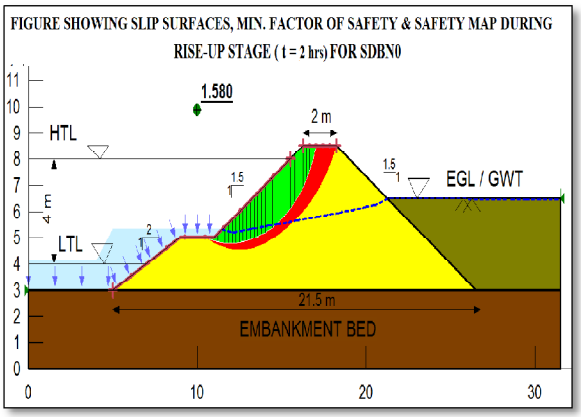

Figure-5.63 : At t = 2 hrs, with F.O.S = 1.580

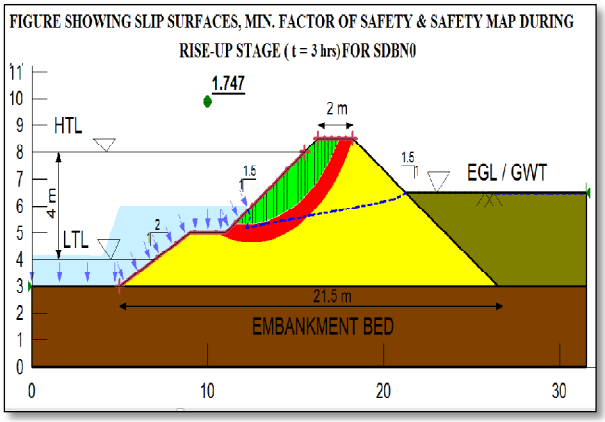

Figure-5.64 : At t = 3 hrs, with F.O.S = 1.747

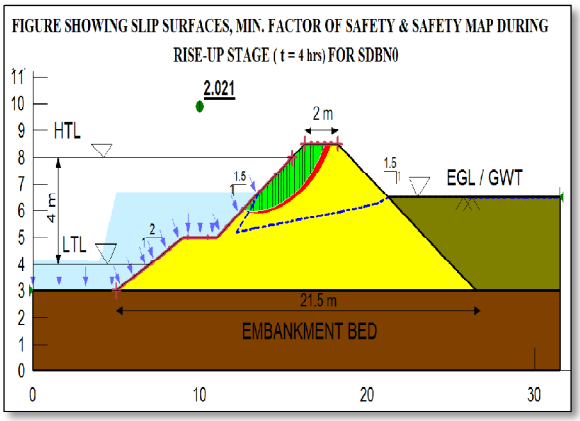

Figure-5.65 : At t = 4 hrs, with F.O.S = 2.021

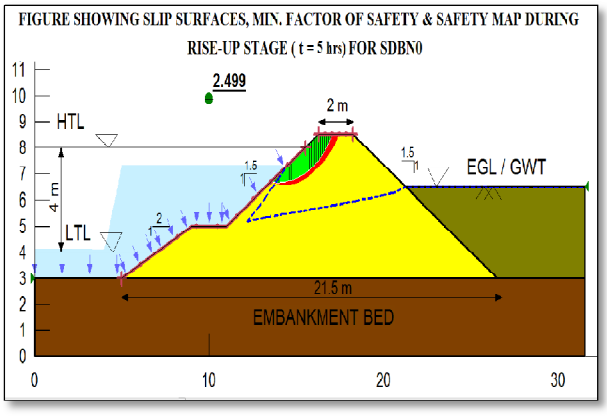

Figure-5.66 : At t = 5 hrs, with F.O.S = 2.499

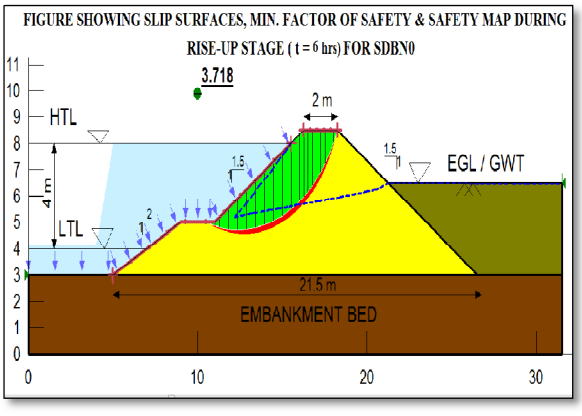

Figure-5.67 : At t = 6 hrs (HTL), with F.O.S = 3.718

TABLE - 5.4: Slip Surface Location, Minimum Factor of Safety, Safety Map for Model $SDBN_0$ during Draw-down Stage (t = 7 hrs to t = 12 hrs) of Single Tidal Cycle

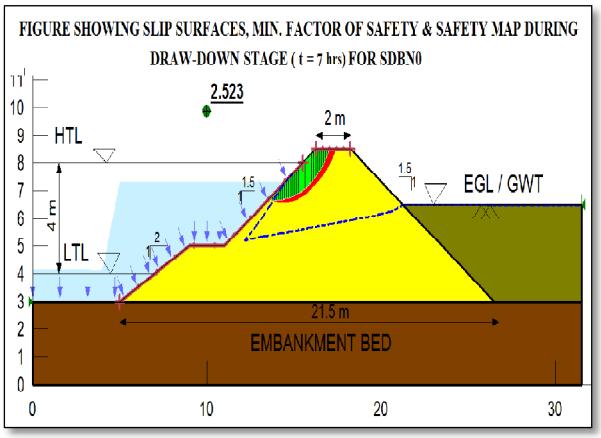

Figure-5.68 : At t = 7 hrs, with F.O.S = 2.523

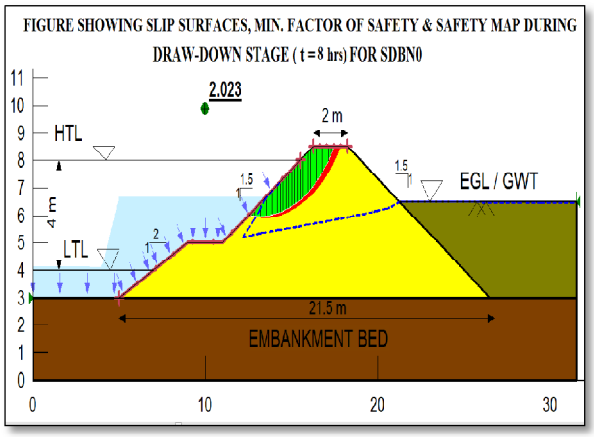

Figure-5.69 : At t = 8 hrs, with F.O.S = 2.023

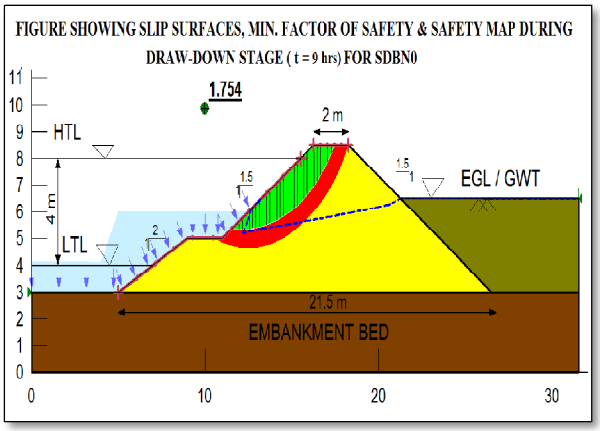

Figure-5.70 : At t = 9 hrs, with F.O.S =1.754

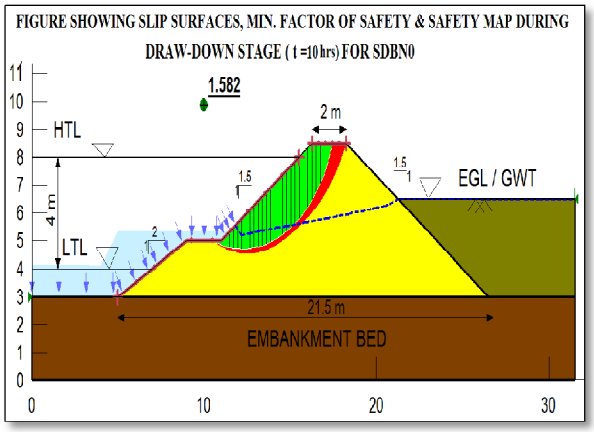

Figure-5.71 : At t = 10 hrs, with F.O.S = 1.582

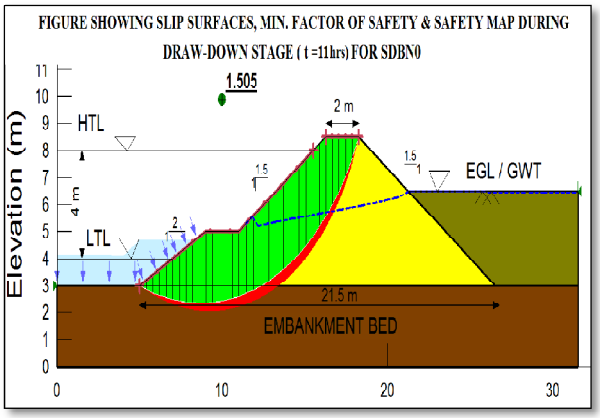

Figure-5.72 : At t = 11 hrs, with F.O.S = 1.505

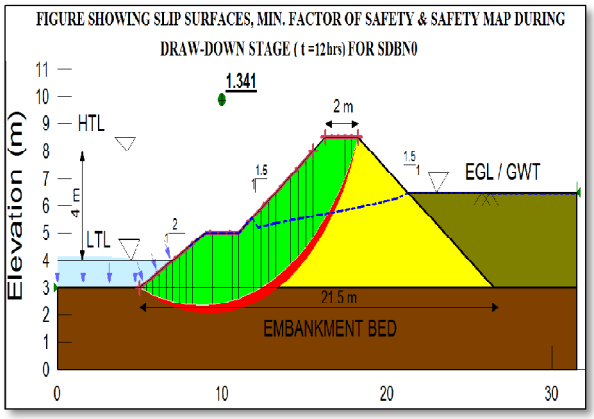

Figure-5.73 : At t = 12 hrs (LTL), with F.O.S =1.341

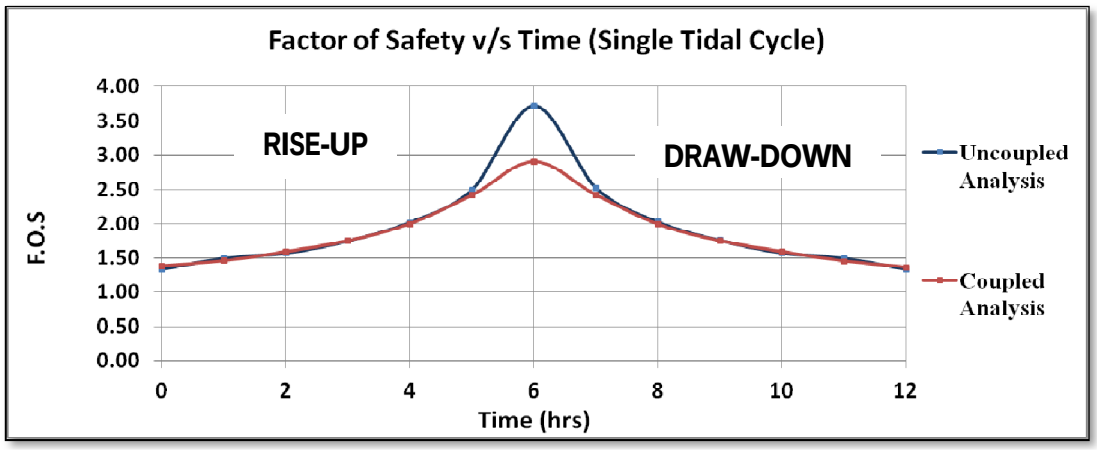

Figure-5.74 : A plot of the F.O.S against Time during a Single Tidal Cycle in Uncoupled and Coupled Analysis respectively for $SDBN_0$

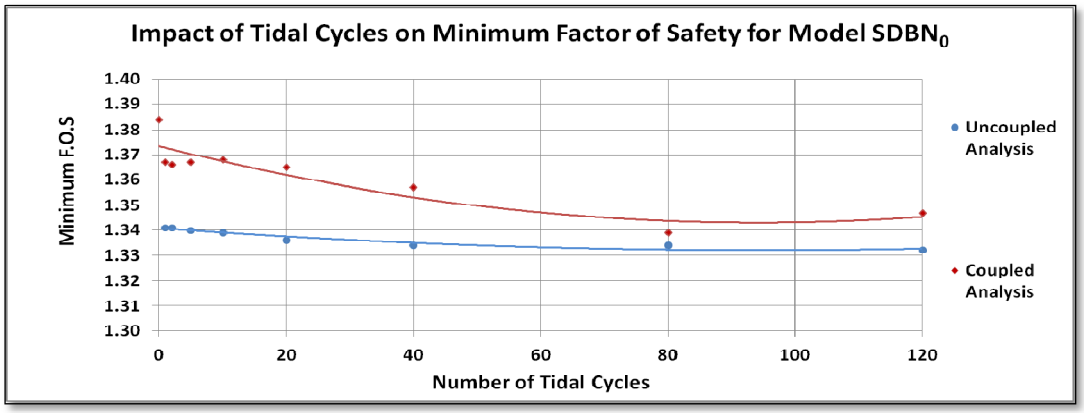

Figure-5.75 : A plot of the Minimum F.O.S against Number of Tidal Cycles for $SDBN_0$

5.6 : Results & Discussions for Model $SDBN_{3.5}$

Results and discussions based on analysis of Model – $SDBN_{3.5}$ has been presented in sub-sections below

5.6.1: Phreatic Line and its Dynamics

The steady state condition phreatic surface based on the position of land groundwater table at 3.5 metres below existing ground level and the Low tide level on River side has been shown in **Figure-5.76** for Model $SDBN_{3.5}$.

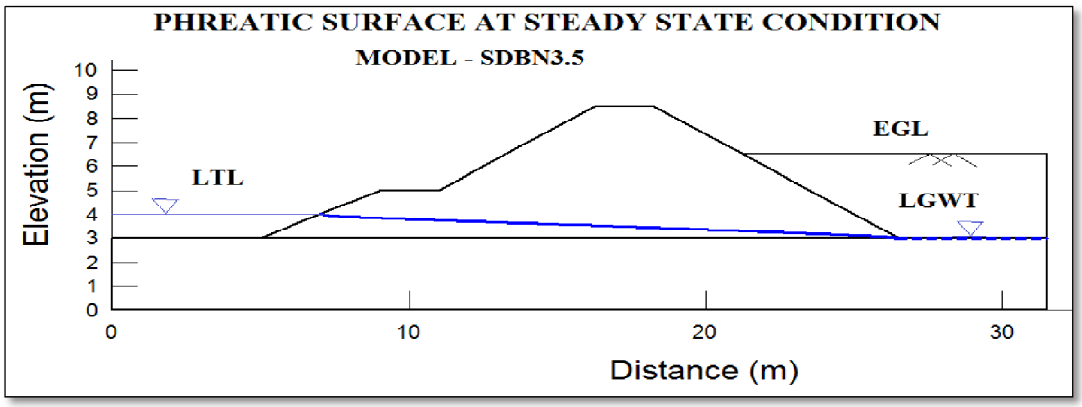

Figure-5.76 : Steady State Phreatic Surface for *SDBN*$_{3.5}$.

Single Tidal Cycle

The dynamics of the phreatic line for the model SDBN$_{3.5}$ has been discussed and shown in the following sub-sections.

Rise-Up

The dynamics of the phreatic surface during the Rise-Up phase of the tidal cycle, from t = 0 hr to t = 6 hrs has been shown in **figure-5.77**. The bold blue dotted line indicates the phreatic surface from steady state condition whereas the firm blue lines indicate the phreatic surface at each time interval.

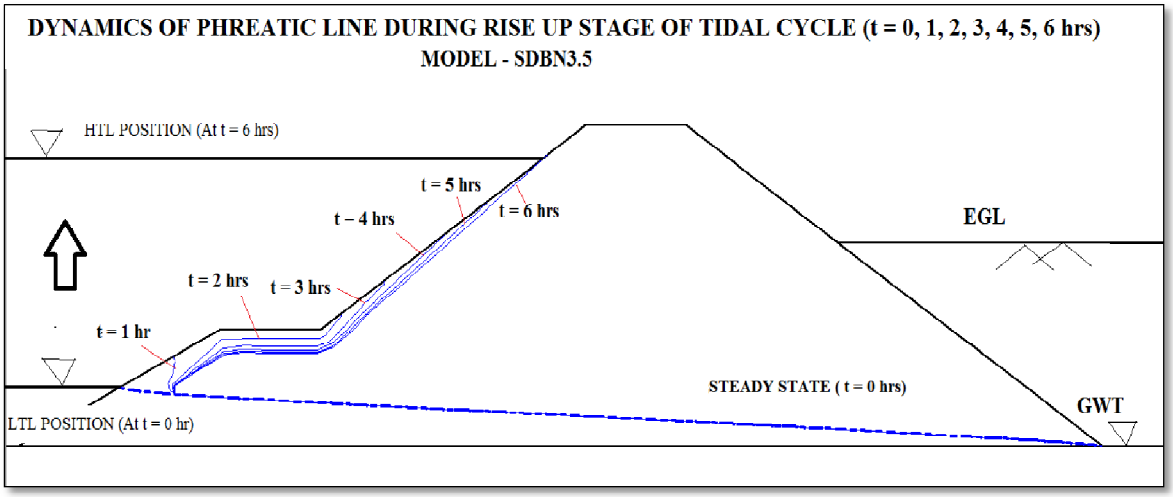

Figure-5.77: Dynamics of Phreatic Surface during Rise-Up Condition of a Single Cycle for SDBN$_{3.5}$

Draw-down

The dynamics of the phreatic surface during the Draw-down phase of the tidal cycle, from t = 6 hrs to t = 12 hrs has been shown in **figure-5.78**. In this figure, the bold blue dotted line indicates the phreatic surface after a complete tidal cycle at t = 12 hrs. It is observed that the position of the

phreatic surface has shifted from its initial location (before a single cycle) near LTL at t = 0 hr to a higher location above the LTL at t = 12 hrs.

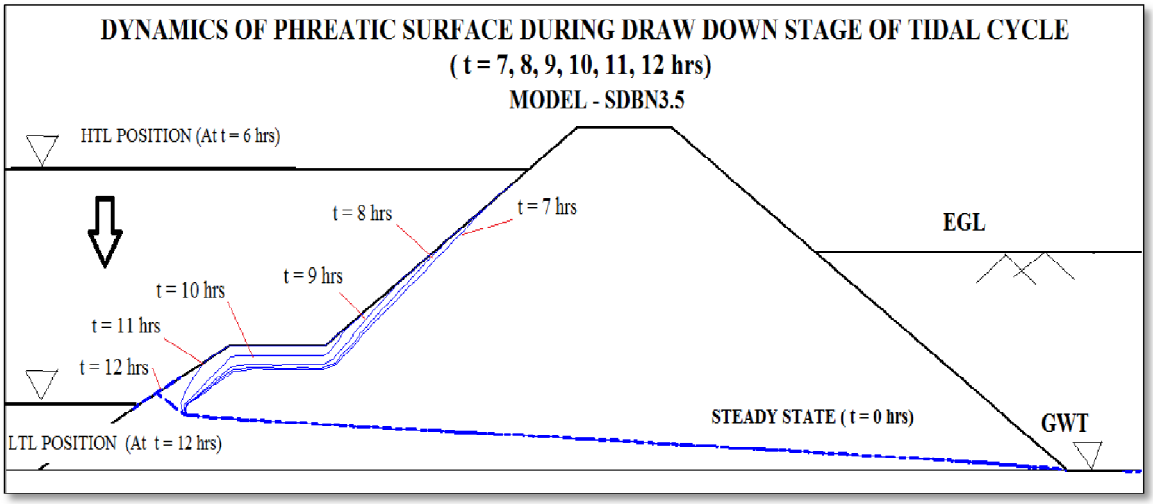

Figure-5.78: Dynamics of Phreatic Surface during Draw-down Condition of a Single Cycle for $SDBN_{3.5}$

Effect of Multiple Tidal Cycles

An attempt has been made to study the impact of multiple tidal cycles on the dynamics of the phreatic surface of model $SDBN_{3.5}$. The number of tidal cycles selected is based over 60 days time and for 120 cycles. The results have been illustrated in **Figure-5.79**. The bold dotted line indicates the phreatic surface position after running of 120 cycles.

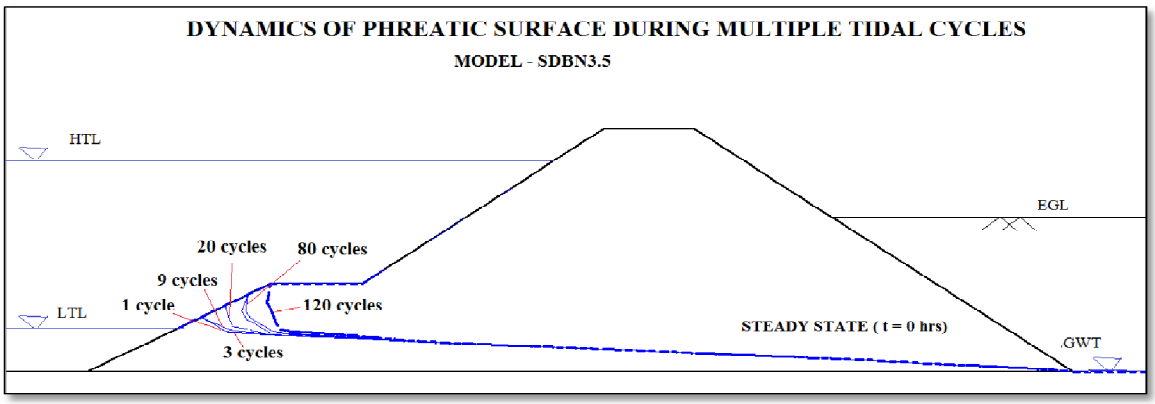

Figure-5.79: Dynamics of Phreatic Surface during Multiple Cycles for $SDBN_{3.5}$

It has been observed that the location of the phreatic surface shifts to a slightly higher elevation within a particular zone after each corresponding cycle. The variation is observed upto a certain distance from the River-Embankment interface, beyond which no variation in phreatic line is observed. At the end of 120 cycles, this zone has been measured as 1.5 metres approximately from the toe of the upper slope for this particular study. However, considering that the material is

clayey silt with a very low permeability, the elevational shift in phreatic surface is marginal. A higher magnified image concentrating on the above mentioned zone has been presented in **Figure-5.80** for better understanding..

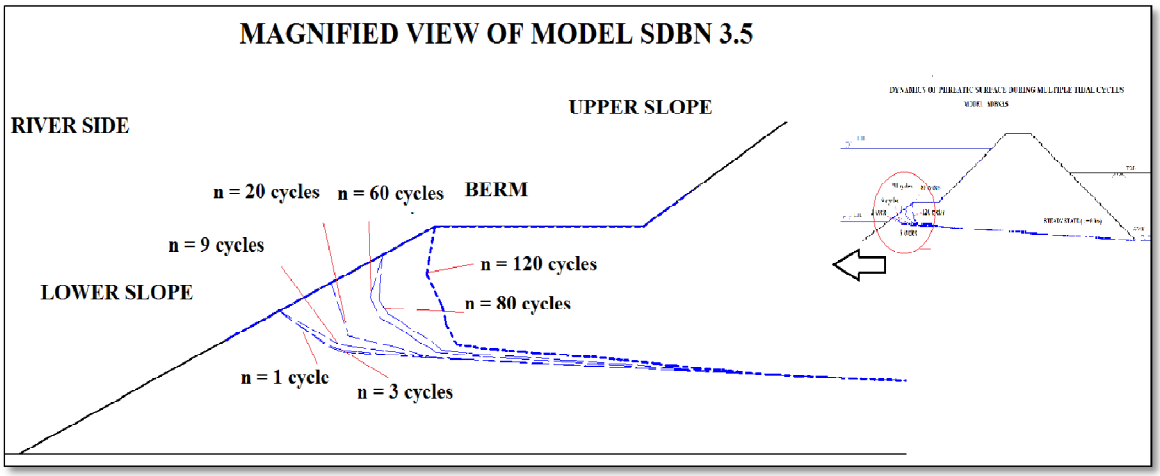

Figure-5.80: Magnified Image showing Dynamics of Phreatic Line with tidal cycles for $SDBN_{3.5}$

5.6.2: Flux Distribution at Various Sections

The flux section has been developed at critical areas to monitor the flux rates at these locations during steady and transient stages. These have been shown in the **Figure.5.81**. The five areas selected are the *Berm Toe Section-1* (slope below berm toe), *Berm Section-2* (berm section), *Embankment Section-1* (embankment section exposed to riverfront), *Embankment Section-2(* internal embankment section) and *Embankment Landside Section.*

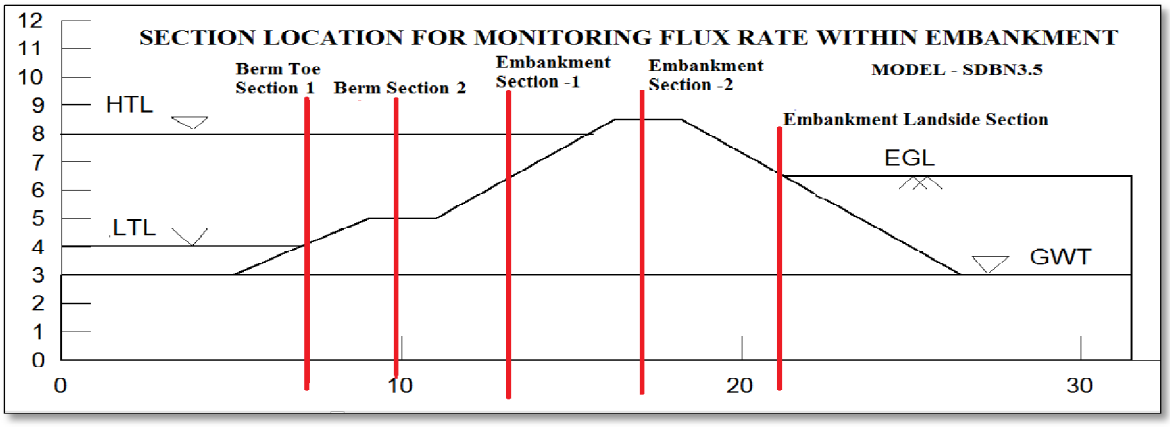

Figure-5.81: Location of Flux Sections for Monitoring flux rate in $SDBN_{3.5}$

The flux rate variation for single cycle have been plotted in **Figure-5.82**. Here, t = 0, indicates Steady State values. The maximum variation in flux is observed for Embankment Section-1 followed by Berm Toe Section-1 and Berm section-2. The maximum flux is recorded at t = 6 hrs, at HTL position, for the above sections. The Embankment Section-2 and Embankment Landside

section, being quite far from the riverfront has shown no variation during Rise-Up and Draw-down, recording constant values of flux throughout the single tide cycle.

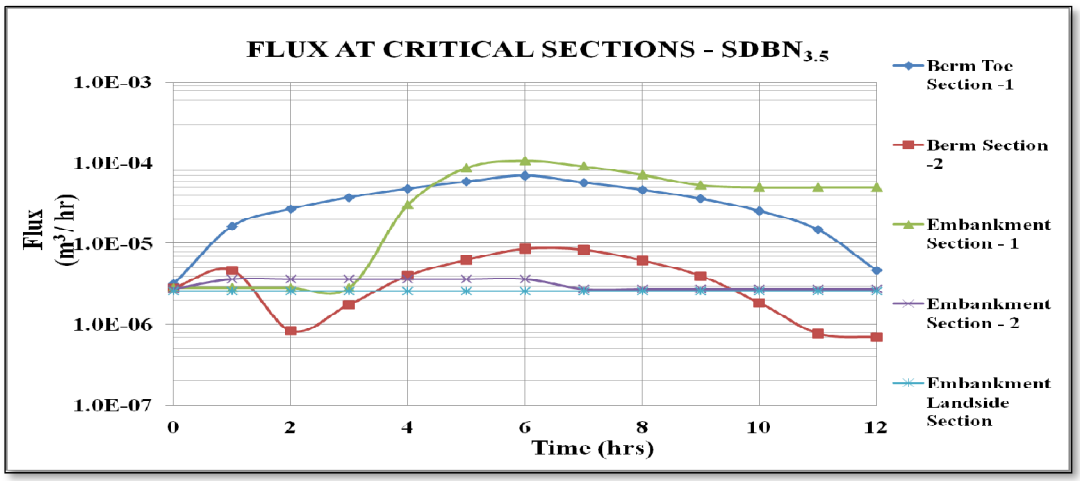

Figure-5.82: Variation of flux across sections with Rise up and Draw-down for $SDBN_{3.5}$

Effect of Multiple Tidal Cycles

The impact of multiple cycles on the flux rate at the above mentioned regions have been studied and presented in **Figure-5.83**. It is observed that the flux rates at all sections mentioned above remain constant more or less, after a few initial cycles.

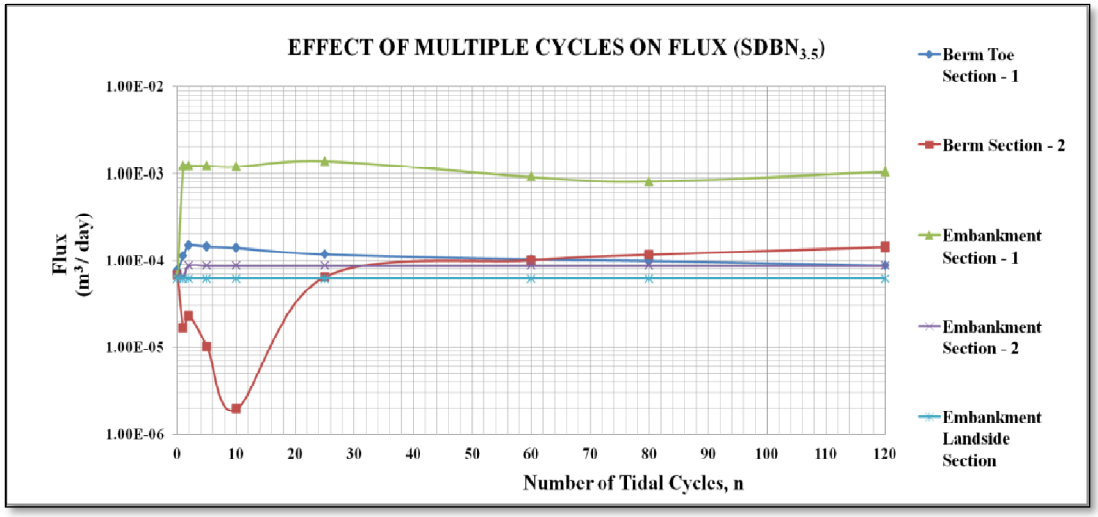

Figure-5.83: Effect of Multiple Tidal Cycles on Flux across sections for $SDBN_{3.5}$

5.6.3: Distribution of Equipotential Line Contours

The Flow Vector and distribution of Equipotential lines for Steady State condition has been shown in **Figure-5.84**, for $SDBN_{3.5}$. The flow vectors have been shown at an magnification of 2.449e+05. The maximum hydraulic velocity is about 4.2884e-06 m/hr.

Single Tidal Cycle

Rise-Up

As the river water level rises from LTL to HTL over t = 0 hrs to t = 6 hrs, the Equipotential Line distribution contours for Model $SDBN_{3.5}$ has been shown in **Figures 5.85**, **5.86**, **5.87**, **5.88**, **5.89**, **5.90**. There is an increase in the magnitude of total head at points within the Zone of Influence of Rise-Up during this period. The zone can be identified from the extent of equipotential contour band at each time frame during Rise-Up. It is seen that the zone slowly develops and increases in size along the lower slope, berm and upper slope with Rise-Up. The flow vectors (shown by arrows) clearly indicate the inward flow of tidal water into the embankment at this zone, during Rise-Up.

Draw-down

As the river water level recedes from HTL to LTL over t = 6 hrs to t = 12 hrs, the Equipotential Line contour for Model $SDBN_{3.5}$ during Draw-down stage of a single tidal cycle has been shown in **Figures. 5.91**, **5.92**, **5.93**, **5.94**, **5.95**, **5.96**. It has been seen that within the ZIR, the total head starts to dissipate during the draw-down phase. It is observed that the river front interface of the embankment has now turned into a seepage surface, with the tidal water that had encroached the embankment during Rise-Up now flowing out of the same, during Draw-Down. This is indicated by the position of flow vectors. Moreover, the ZIR starts diminishing in size during this stage. It is recorded that the rate of diminish of ZIR is maximum in the Lower Slope compared to the Berm Region and Upper Slope of the embankment. At the end of a single cycle, t = 12 hrs (shown in Figure 5.96), the ZIR for a single cycle diminished is more in the Lower Slope, however the zone persists in the Berm Region and Upper Slope, where tidal water continues to penetrate inward the embankment, as the next tidal cycle builds up on the river side. Also, there is an net increase in the total head at regions in the lower slope region at t = 12 hrs, compared to its initial steady state stage. (Refer figure-5.84, 5.96). However, in comparison with $SDBN_0$, the rate at which ZIR is diminished is lower for $SDBN_{3.5}$ resulting in an higher ZIR for $SDBN_{3.5}$ at the end of single cycle when compared to $SDBN_0$.

Effect of Multiple Tidal Cycles

The distribution of equipotential line contours at the end of multiple tidal cycles have been demonstrated for n = 2, 5, 10, 50, 70, 120 (where n = no. of cycles) in **Figures 5.97**, **5.98**, **5.99**, **5.100**, **5.101**, **5.102.** It has been observed that at the upper slope region, the total head keeps on decreasing with each subsequent tidal cycle. After the end of 1st tidal cycle, the maximum head at the upper slope was 7.5 m and after 120 cycles the same was 6.5 m, indicating a 13.33 percent

decrease over this cycle span. Along the Lower Slope, it has been observed that although majority of the excess tide induced seepage head is dissipated at the end of each cycle, however there is a slight increase in the total head at locations in Lower Slope in comparison to previous cycle.

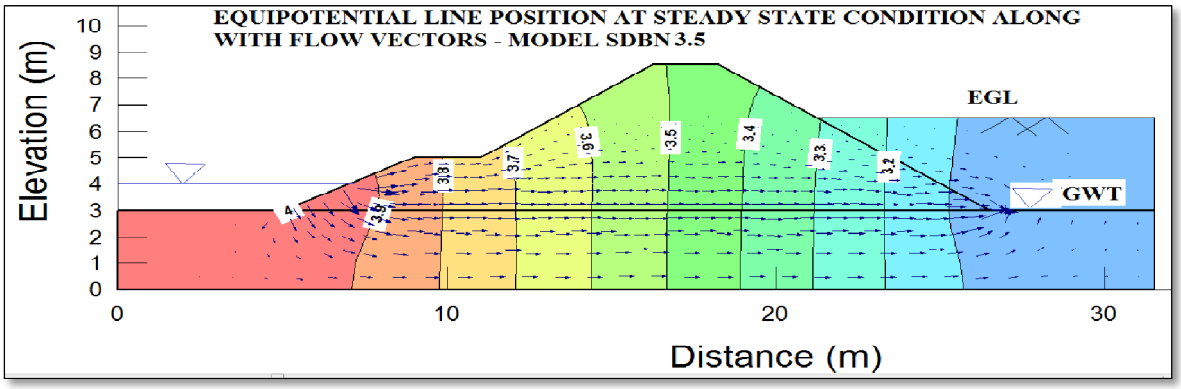

Figure-5.84 : Steady State Equipotential Lines for LTL position at t = 0 hr for *SDBN*$_{3.5}$.

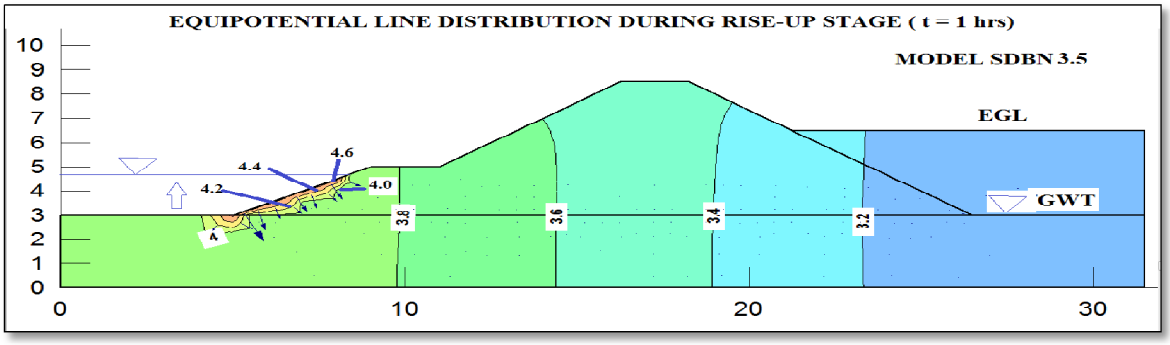

Figure-5.85 : Equipotential Lines during Rise-Up stage (t = 1 hr) at Single Cycle for *SDBN*$_{3.5}$

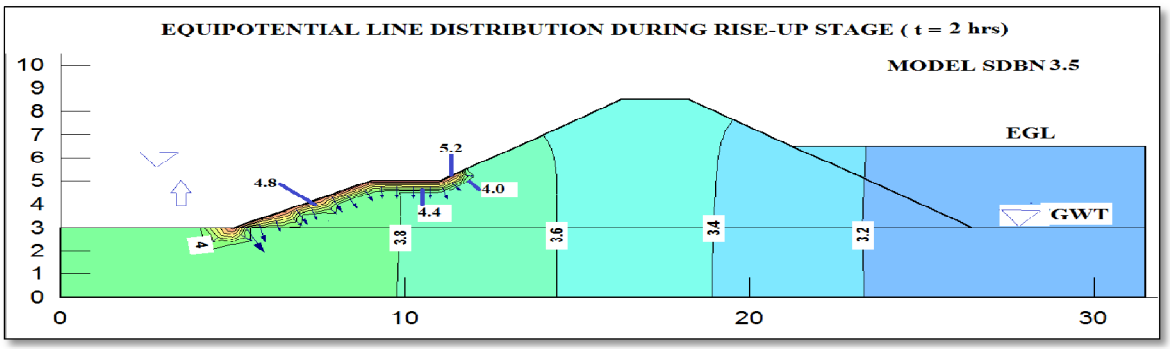

Figure-5.86 : Equipotential Lines during Rise-Up stage (t = 2 hrs) at Single Cycle for *SDBN*$_{3.5}$

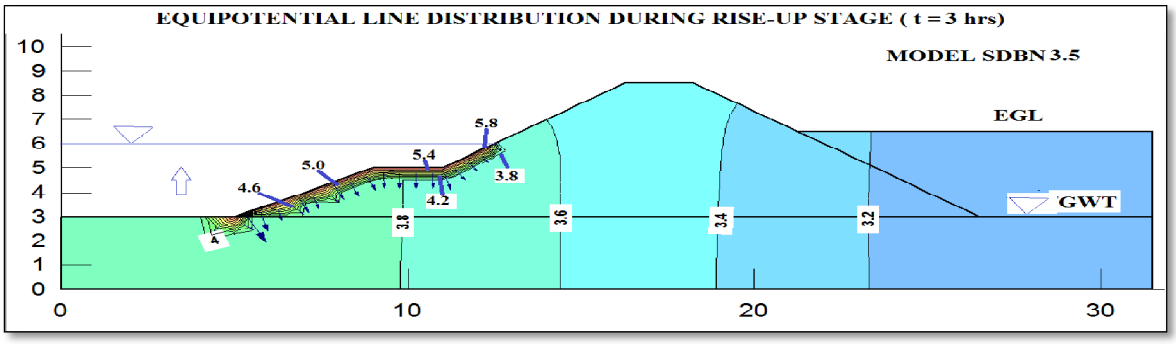

Figure-5.87 : Equipotential Lines during Rise-Up stage (t = 3 hrs) at Single Cycle for *SDBN*$_{3.5}$

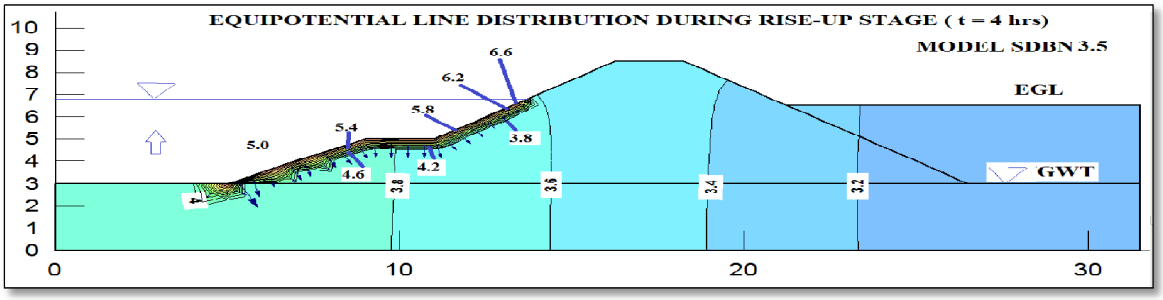

Figure-5.88 : Equipotential Lines during Rise-Up stage (t = 4 hrs) at Single Cycle for $SDBN_{3.5}$

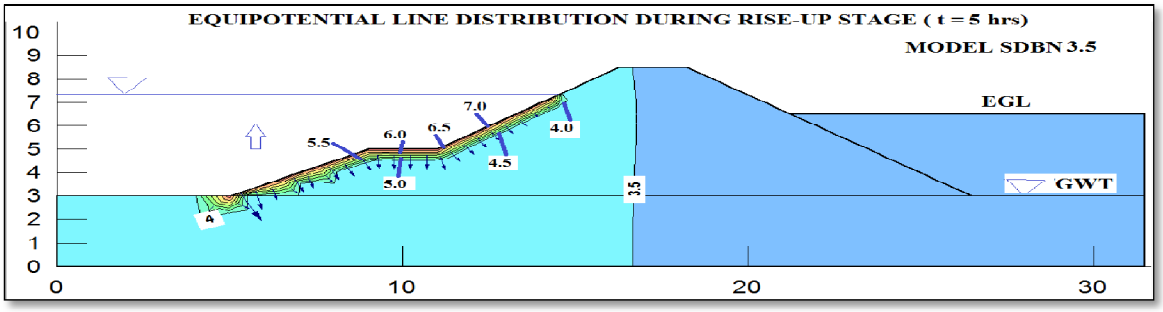

Figure-5.89 : Equipotential Lines during Rise-Up stage (t = 5 hrs) at Single Cycle for $SDBN_{3.5}$

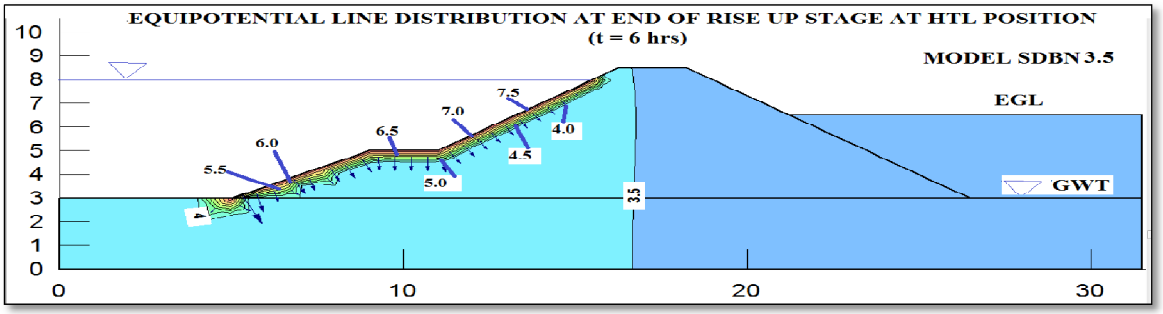

Figure-5.90 : Equipotential Lines at HTL position (t = 6 hrs) for $SDBN_{3.5}$

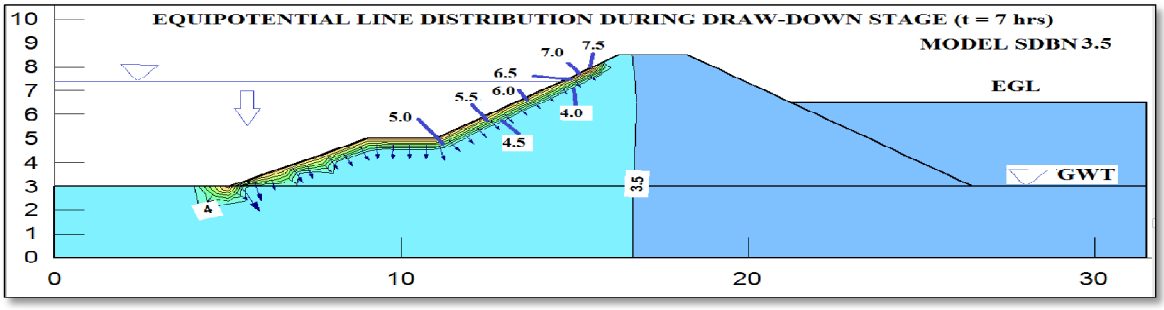

Figure-5.91 : Equipotential Lines during Draw-down stage (t = 7 hrs) at Single Cycle for $SDBN_{3.5}$

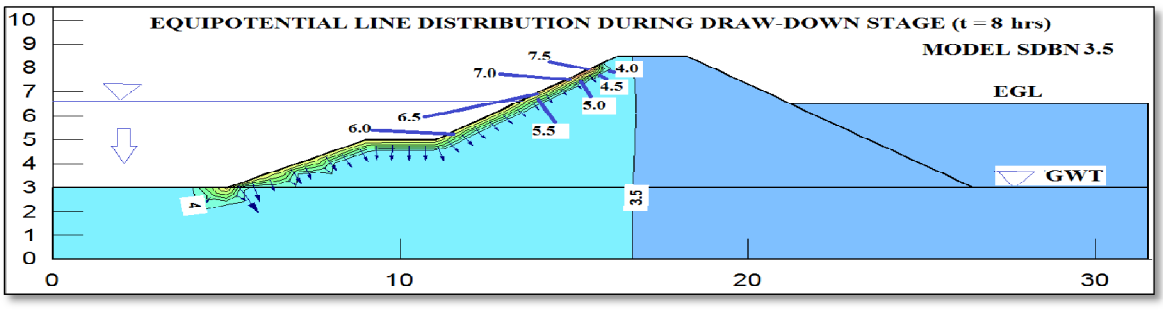

Figure-5.92 : Equipotential Lines during Draw-down stage (t = 8 hrs) at Single Cycle for $SDBN_{3.5}$

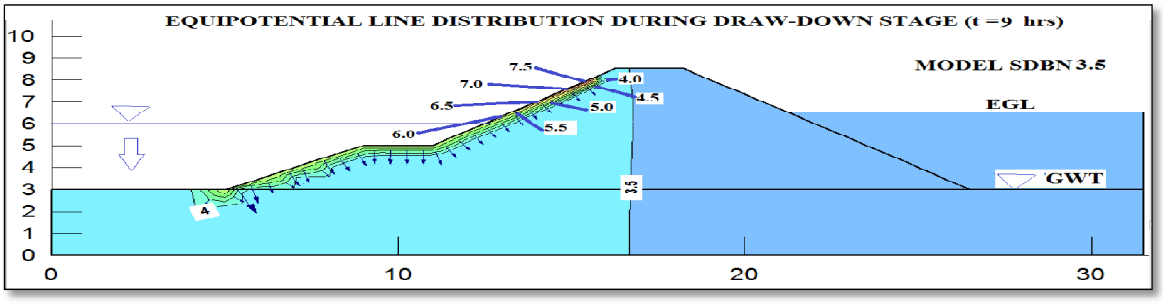

Figure-5.93 : Equipotential Lines during Draw-down stage (t = 9 hrs) at Single Cycle for $SDBN_{3.5}$

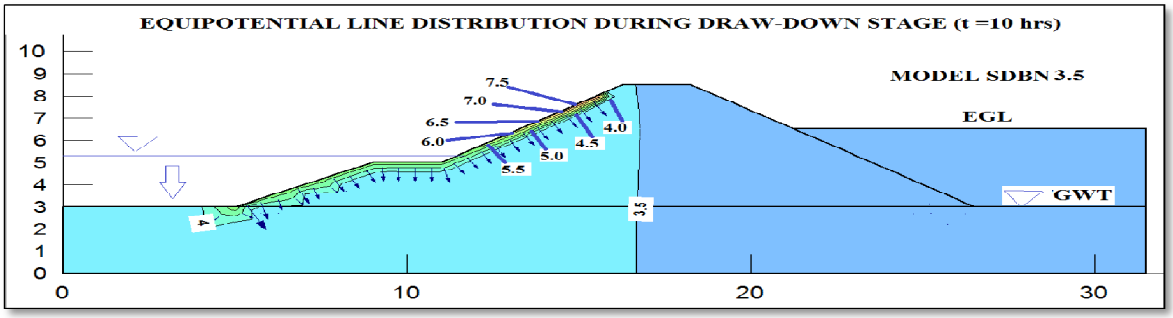

Figure-5.94 : Equipotential Lines during Draw-down stage (t = 10 hrs) at Single Cycle for $SDBN_{3.5}$

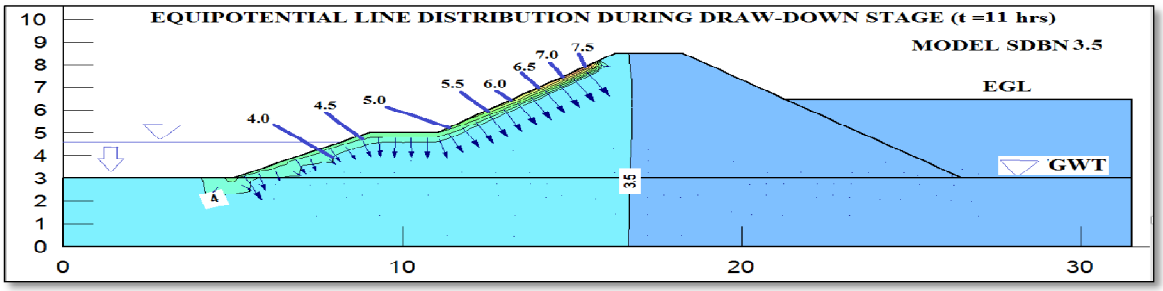

Figure-5.95 : Equipotential Lines during Draw-down stage (t = 11 hrs) at Single Cycle for $SDBN_{3.5}$

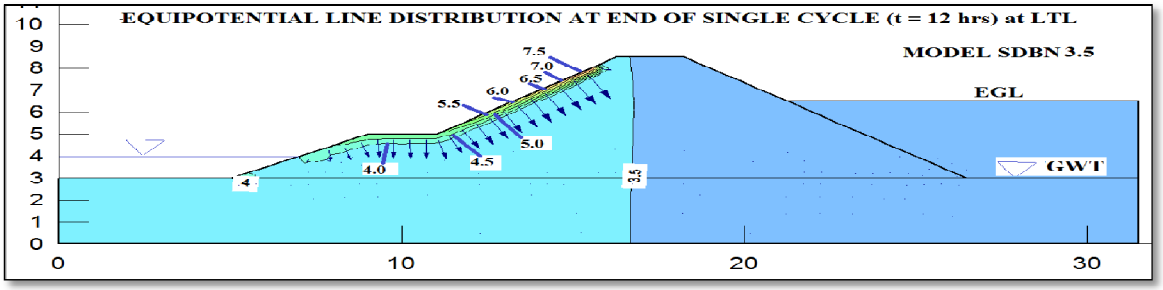

Figure-5.96 : Equipotential Lines at end of Single Cycle Draw-down Stage (t = 12 hrs) for $SDBN_{3.5}$

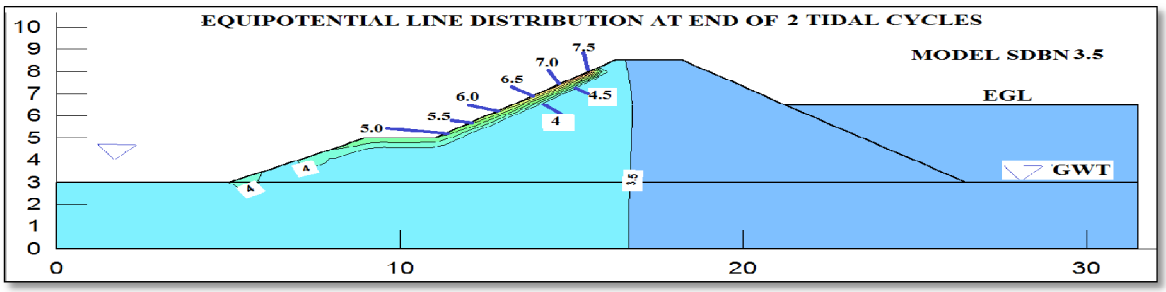

Figure-5.97 : Equipotential Lines at the end of 2nd Cycle for $SDBN_{3.5}$

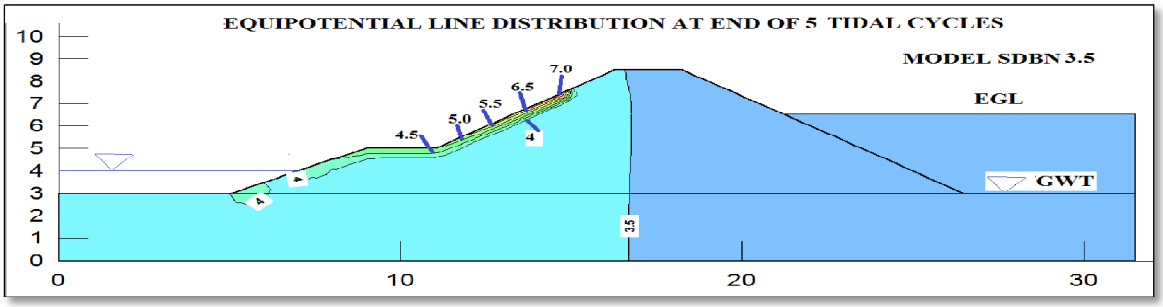

Figure-5.98 : Equipotential Lines at the end of 5th Cycle for $SDBN_{3.5}$

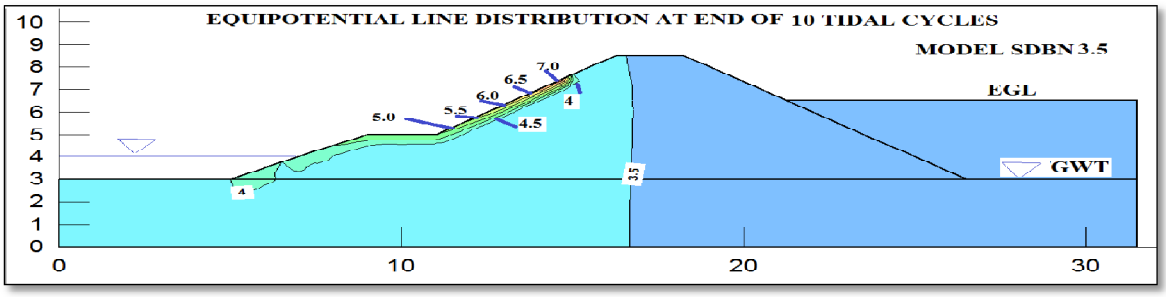

Figure-5.99 : Equipotential Lines at the end of 10th Cycle for model $SDBN_{3.5}$

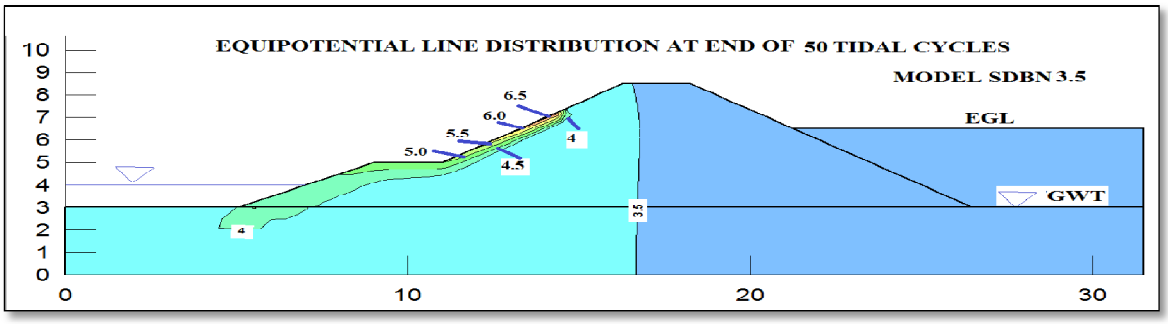

Figure-5.100 : Equipotential Lines at the end of 50th Cycle for $SDBN_{3.5}$

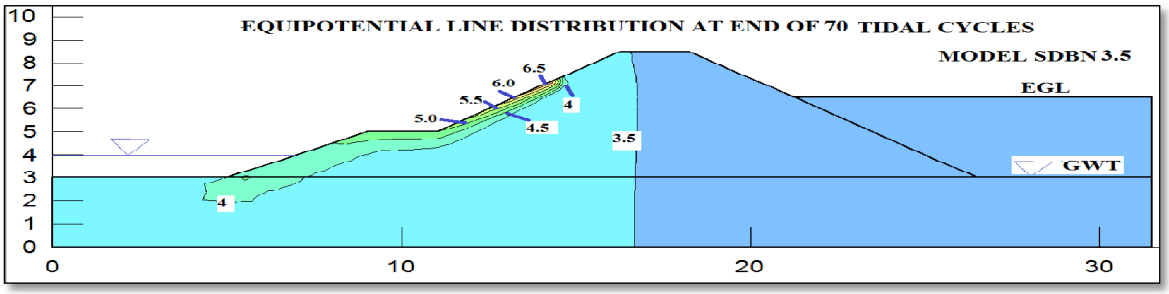

Figure-5.101 : Equipotential Lines at the end of 70th Cycle for $SDBN_{3.5}$

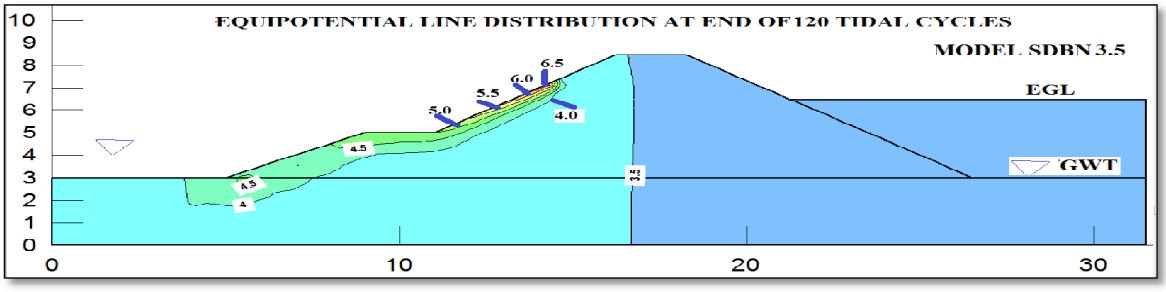

Figure-5.102 : Equipotential Lines at the end of 120th Cycle for $SDBN_{3.5}$

5.6.4: Pore Pressure Distribution

Single Tidal Cycle

To get a detailed idea about pore pressure variation across the embankment, the entire embankment has been divided into four parts – (i) The Lower Slope Portion (ii) The Berm Portion (iii) The Upper Slope Portion (iv) Interior of embankment upto Landside. A set of points have been taken in each of the above mentioned zones to track the pore water pressure variation during single tidal cycle.

The results obtained during a single tidal cycle are shown in **Figures. 5.103**, **5.104**, **5.105**, **5.106**. A gradual increase in pore water pressure from initial condition at t = 0 hr to a maximum value during Rise-Up phase and then gradual decrease till end of Draw-down at t = 12 hrs, has been observed for majority of points lying within the ZIR. The points where no variation in pore water pressure is observed, lie outside this zone and is unaffected by the single tidal cycle. There are regions in the Lower Slope, Berm Region and Upper Slope which were experiencing suction (i.e. points lying above phreatic line) at t = 0 hr and became fully saturated at end of a single tidal cycle, with zero or positive pore water pressure. The Lower Slope, Berm Region and Upper Slope region have points where variation is zero upto a certain time frame and then the pore water pressure starts increasing till t = 6 hrs and subsequently decrease from t = 6 hrs to t = 12 hrs. These are the regions which were initially out of the ZIR, but with the onset of the tidal cycle, as the river water head increased, more area within the embankment came under the ZIR, thereby encompassing these points. No variation in Pore water pressure was recorded for interior parts of the embankment as they lie outside the ZIR for the entire duration of single cycle.

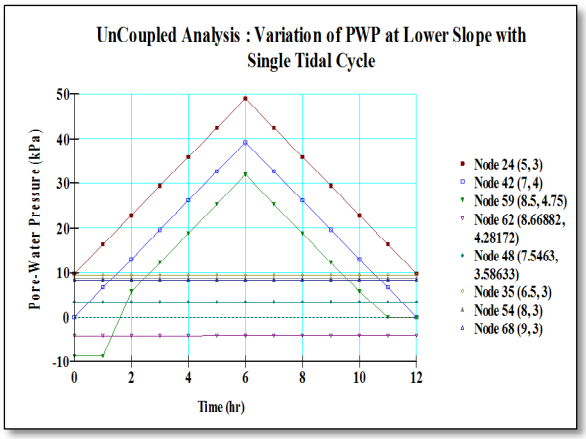

Figure-5.103 : PWP Variation during Single Tidal Cycle in Lower Slope region of $SDBN_{3.5}$

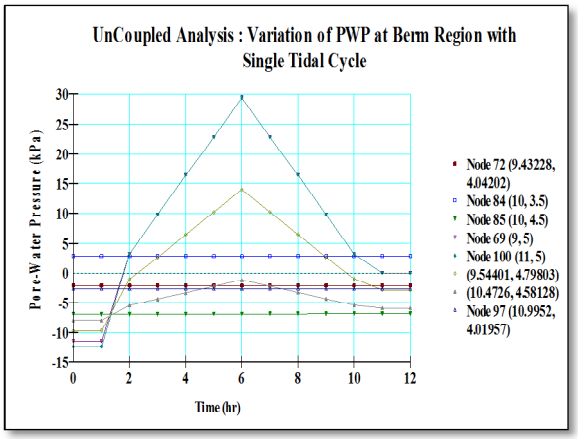

Figure-5.104 : PWP Variation during Single Tidal Cycle in Berm portion of $SDBN_{3.5}$

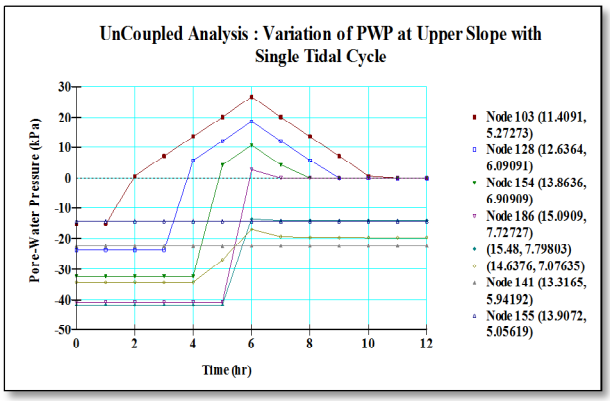

Figure-5.105 : PWP Variation during Single Tidal Cycle in Upper Slope Region of *SDBN*$_{3.5}$

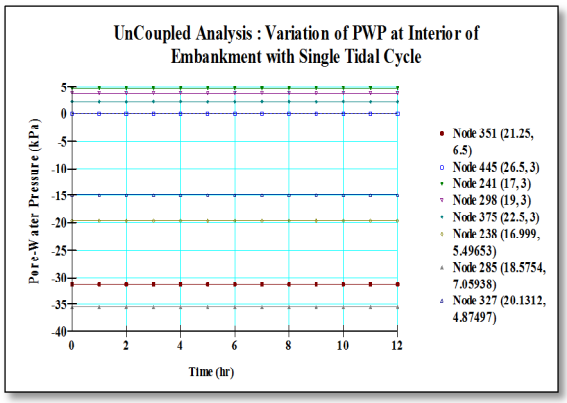

Figure-5.106 : PWP Variation during Single Tidal Cycle in Interior of Embankment of *SDBN*$_{3.5}$

Effect of Multiple Tidal Cycles

The PWP contours at the initial conditions and at the end of 1, 5, 10, 60, 120 cycles have been shown in **Figures – 5.107**, **5.108**, **5.109**, **5.110**, **5.111**, **5.112.** It is recorded that the variations are seen only in the regions of ZIR throughout the multiple cycles. This observation is quite different from the one for SDBN$_0$, where after a few cycles, the variation was more or less insignificant. Also, Significant increase in PWP is seen in Lower Slope at the end of 120 cycles.

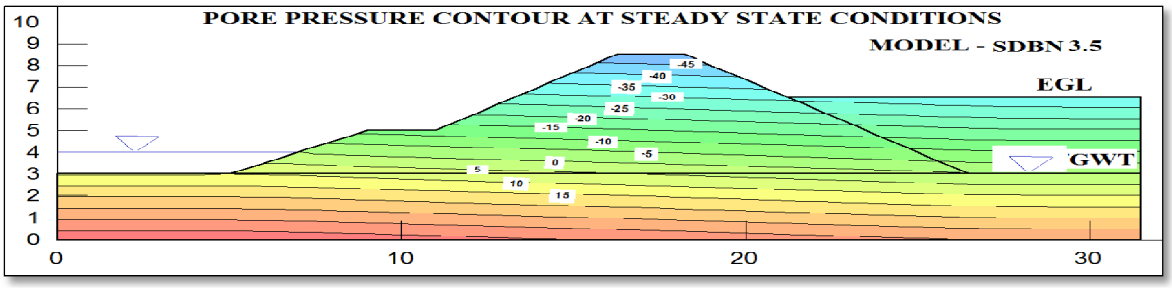

Figure-5.107 : Pore Pressure Contour at Steady State Conditions for *SDBN*$_{3.5}$

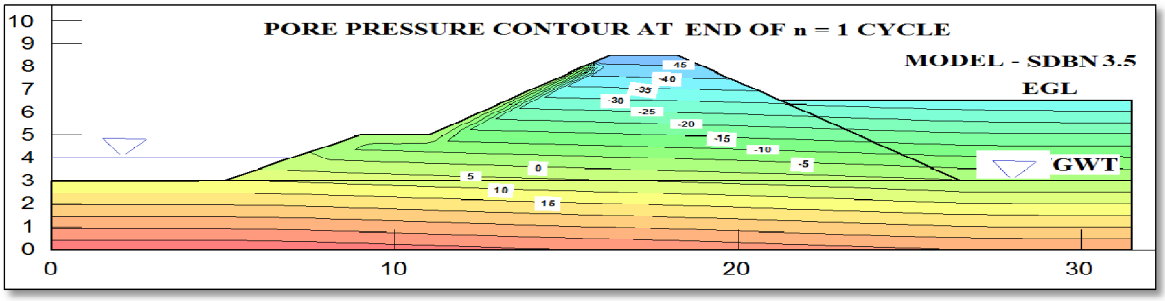

Figure-5.108 : Pore Pressure Contour at end of 1st Cycle for *SDBN*$_{3.5}$

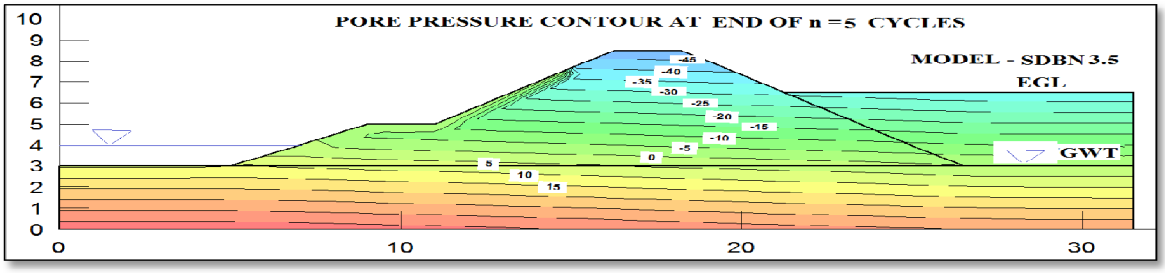

Figure-5.109 : Pore Pressure Contour at end of 5th Cycle for *SDBN3.5*

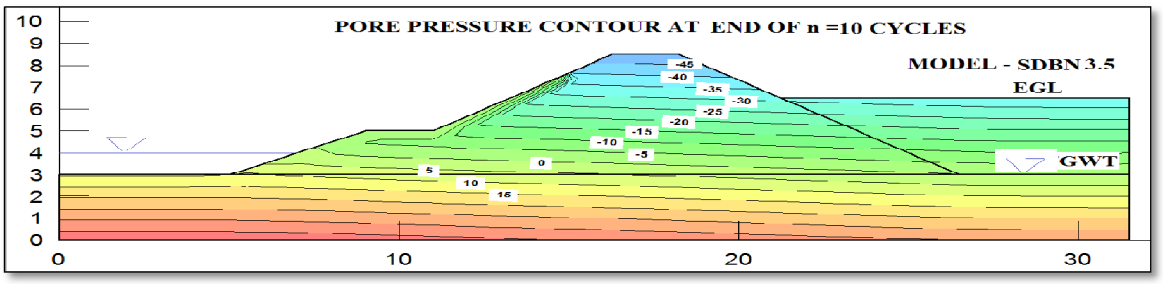

Figure-5.110 : Pore Pressure Contour at end of 10th Cycle for *SDBN3.5*

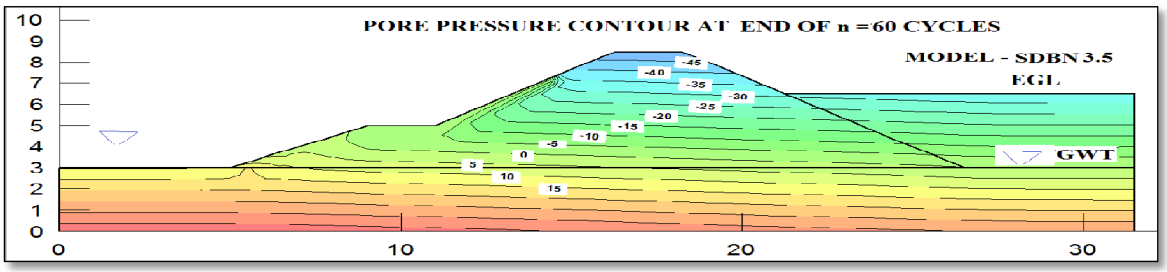

Figure-5.111 : Pore Pressure Contour at end of 60th Cycle for *SDBN3.5*

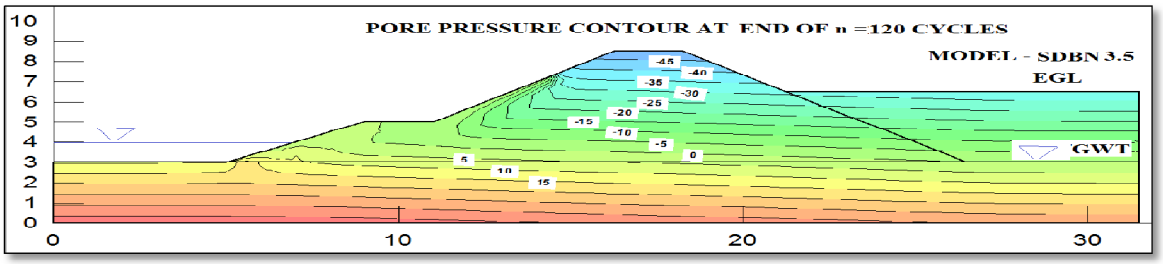

Figure-5.112 : Pore Pressure Contour at end of 120th Cycle for *SDBN3.5*

5.6.5: Deformation Based Analysis

A coupled analysis was performed to investigate the effect of tidal cycle on the deformation and pore water pressure at critical locations within the embankment. The selection of points was the same as in Uncoupled analysis. The results for Lower Slope, Berm region and Upper Slope during a single tidal cycle has been presented in **Figures - 5.113**, **5.114**, **5.115**, **5.116**, **5.117**, **5.118**. A trend similar to uncoupled analysis was obtained for the interior of the embankment where no variation in pore pressure was seen during the tidal cycle, hence these have not been separately

shown. The effect of multiple cycles on the above mentioned regions for the same parameters have been shown in **Figures – 5.119**, **5.120**, **5.121**, **5.122**, **5.123**, **5.124**.

Deformation

Single Tidal Cycle

It is observed that in Lower Slope, Berm Region and parts of Upper slope, there is vertical settlement which keeps on increasing till t = 6 hrs, during Rise-Up. This is due to increase in the hydrostatic pressure of the tidal water head. During Draw-down, there is a rebound of the same points as the tidal water head comes down decreasing the hydrostatic pressure. There is a net vertical settlement or rebound at some of the points at the end of a single cycle compared to initial conditions as per ability to dissipate pore water pressure. The points which show a slightly different pattern of encountering rebound during initial stages of Rise-Up followed by vertical settlement have been recognized as points lying initially in the suction zone, which is unsaturated. The same rebounds initially as water is absorbed as it enters this zone which then becomes saturated with zero or positive pore water pressure, then it settles vertically with the remaining Rise-Up phase. The time portion the rebound remains constant before plunging for settlement is the time taken by the point to develop a zero pore water pressure. The opposite happens during the draw-down phase. This pattern is observed more in the Upper Slope compared to the Lower Slope and Berm Region.

Multiple Tidal Cycles

It has been observed that there is an cumulative effect of the tidal cycle on deformation. It has been seen that with increase in number of cycles, the vertical settlement increases. The reason for the same is given elaborately in Section 5.5.5.

Pore Water Pressure

Single Tidal Cycle

It is seen that with Rise-Up, there is a gradual build up of pore water pressure which dissipates during Draw-down. There is an accumulation of the same at certain points after a single cycle. An observation made compared to uncoupled analysis, is that the pore water pressure at the same points are varying in magnitude for coupled analysis. Moreover, points lying outside the Zone of Rise Up Influence which had not registered a pore water pressure variation in Uncoupled analysis is now showing a variation in Coupled analysis, when the hydrostatic pressure is considered additionally. The variation of PWP across a single cycle is almost same for Lower Slope, Berm

Region and Upper Slope. This is different from the results obtained in $SDBN_0$, where the variation was maximum along the Lower Slope. It may be attributed to the fact that $SDBN_{3.5}$ as a higher area of unsaturation compared to $SDBN_0$.

Multiple Tidal Cycles

With increase in the number of cycles, the variation is small in the first few cycles after which the pore water pressure becomes constant with number of cycles.

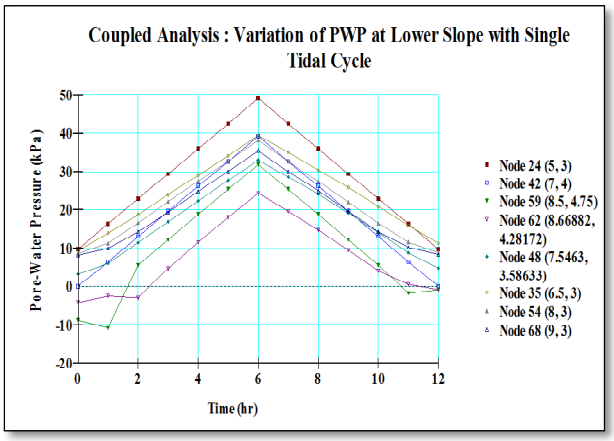

Figure-5.113 : PWP Variation during Single Cycle in the Lower Slope of *SDBN*$_{3.5}$

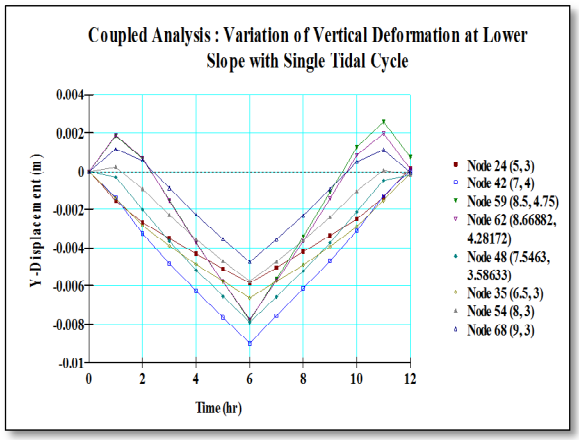

Figure-5.114 : Vertical deformation during Single Cycle in the Lower Slope of *SDBN*$_{3.5}$

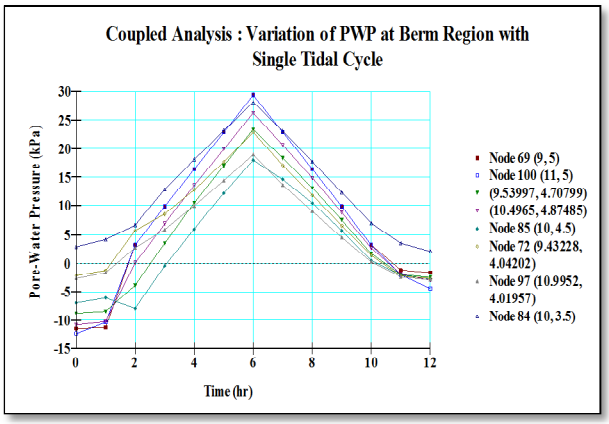

Figure- 5.115 : PWP Variation during Single Cycle in the Berm Region of *SDBN*$_{3.5}$

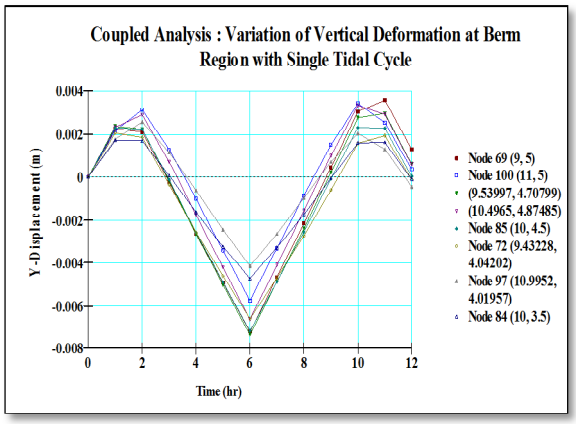

Figure-5.116 : Vertical deformation during Single Cycle in the Berm Region of *SDBN*$_{3.5}$

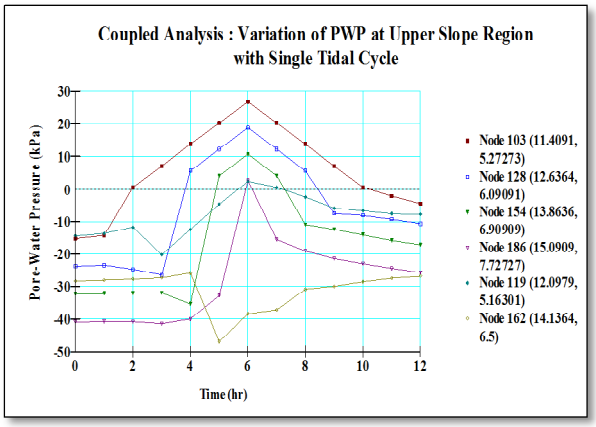

Figure-5.117 : PWP Variation during Single Cycle in the Upper Slope Region of *SDBN*$_{3.5}$

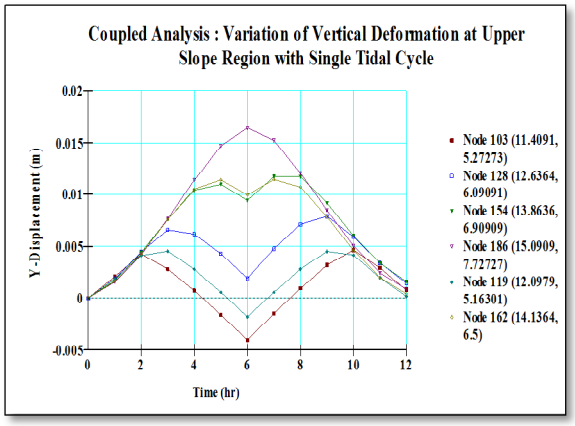

Figure-5.118 : Vertical deformation during Single Cycle in the Upper Slope Region of *SDBN*$_{3.5}$

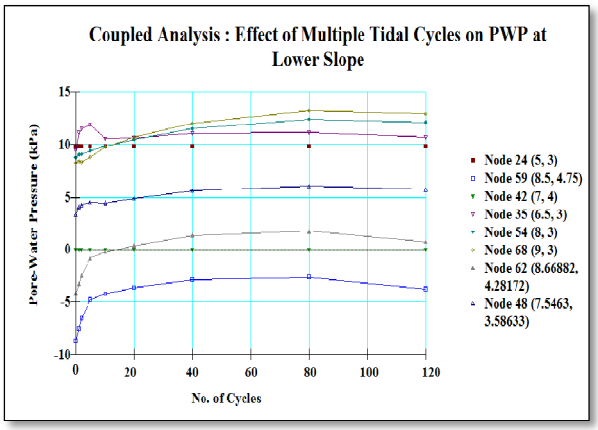

Figure-5.119 : PWP Variation during Multiple Cycles in the Lower Slope of *SDBN*$_{3.5}$

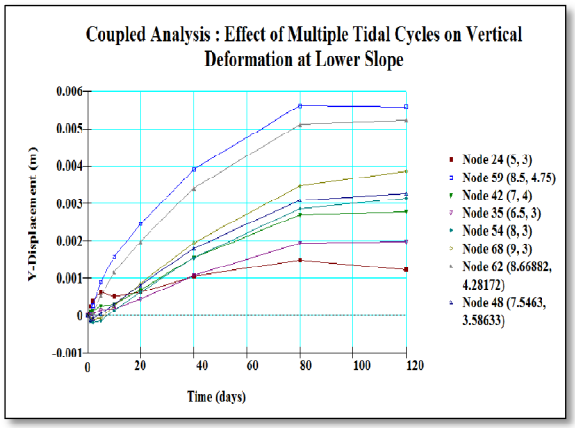

Figure-5.120 : Variation in Vertical Deformation during Multiple Cycles in the Lower Slope of *SDBN*$_{3.5}$

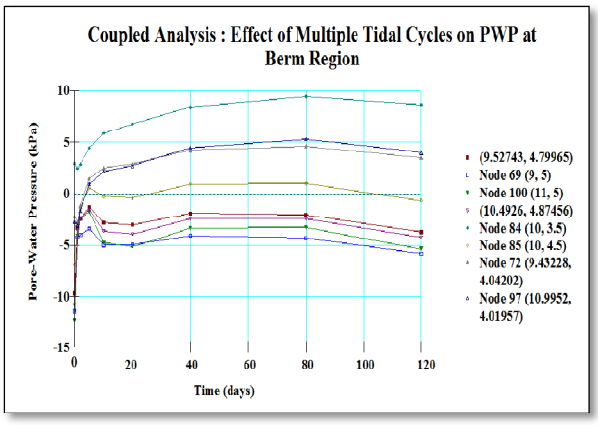

Figure-5.121 : PWP Variation during Multiple Cycles in the Berm region of *SDBN*$_{3.5}$

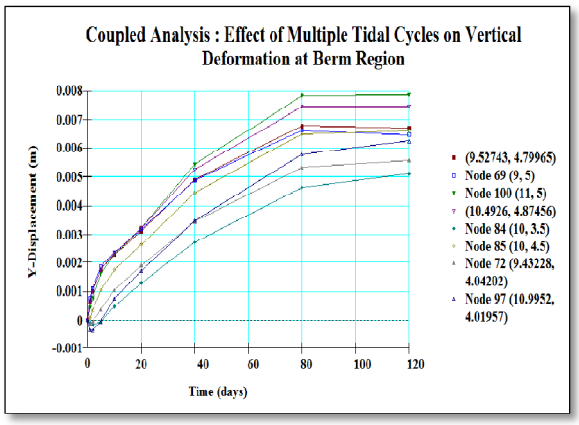

Figure-5.122 : Variation in Vertical Deformation during Multiple Cycles in the Berm region of *SDBN*$_{3.5}$

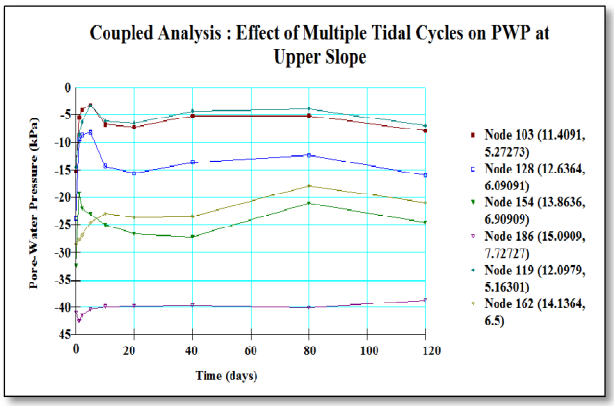

Figure-5.123 : PWP Variation during Multiple Cycles in the Upper Slope of *SDBN*$_{3.5}$

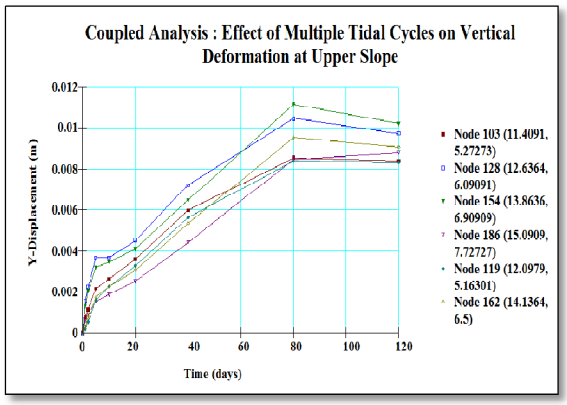

Figure-5.124 : Variation in Vertical Deformation during Multiple Cycles in the Upper Slope of *SDBN*$_{3.5}$

5.6.6: Slope Stability Analysis

Slope Stability analysis has been carried out for both Uncoupled and Coupled methodology during the entire tidal cycle using SLOPE/W. The Pore Water Pressure inputs were received from SEEP/W. The Limit equilibrium method was followed for the Uncoupled analysis, with each slice analysed by the Spencer method. Additionally, the Finite Element Slope Stability analysis was utilized for the Coupled analysis. The uncoupled slope stability analysis at steady state conditions have been shown in **Figure - 5.125**, where the blue dotted line shows the location of the phreatic surface. The section of trial slip surfaces was done by the Entry and Exit method with gradual radii increments in stages. A total of 726 trial slip surfaces were taken and the minimum Factor of Safety was recorded. A safety map, shown in red band defining al the trial slip surfaces within a certain range varying at each stage of tidal cycle, which gives the minimum factor of safety. To be on the conservative side, the strength arising due to suction in the unsaturated regions were neglected.

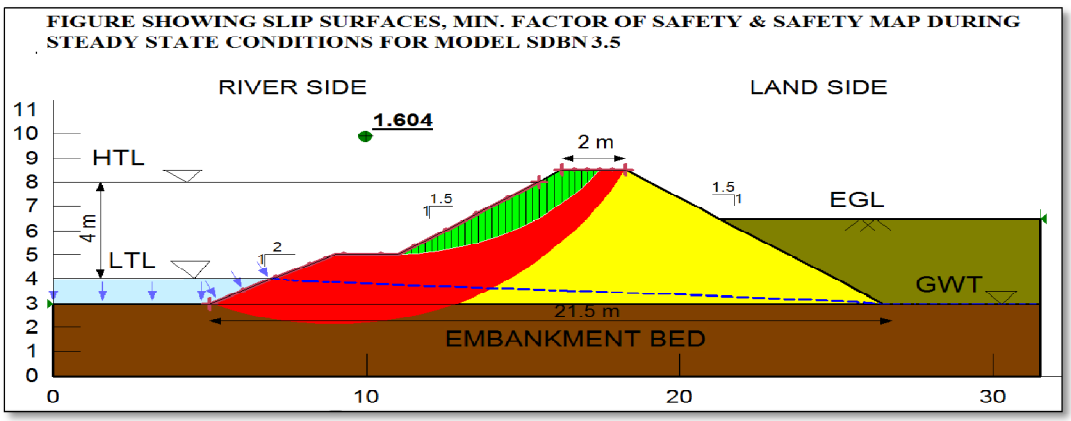

Figure-5.125 : Slip surfaces, Minimum F.O.S and Safety Map during Steady State conditions (t = 0 hr) for *SDBN*$_{3.5}$

Single Tidal Cycle

The Slip surfaces, F.O.S and Safety map during Rise-Up and Draw-down of a single tidal cycle has been shown in **Table-5.5, 5.6**. It is seen that the Factor of Safety (F.O.S) increases from t = 0 to t = 6 hrs, throughout the Rise-Up stage. It reaches a maximum value at HTL. Then, with progression of draw-down, it decreases from t = 6 hrs to t = 12 hrs, for a single tidal cycle. It has been seen that the F.O.S value after the completion of a single tidal cycle comes quite close to its initial value from Steady State conditions. A plot of the F.O.S in Uncoupled and Coupled methodology has been shown in **Figure-5.138**. It is seen that the values obtained in both the methods are different throughout the tidal cycle, with maximum variation at the HTL position at t = 6 hrs, where the Uncoupled Analysis gives a higher and conservative value of F.O.S. At all other stages, the Coupled analysis gives a slightly higher F.O.S on the conservative side.

Multiple Tidal Cycles

The effect of multiple tidal cycles on the F.O.S both in the Uncoupled and Coupled methods have been shown in **Figure-5.139**. It is seen that the F.O.S remains more or less constant throughout multiple cycles, when analyzed by the Uncoupled method. In the Coupled method, an initial decrease in F.O.S is seen for the initial cycles and the same becomes constant after a certain number of cycles. For multiple cycle analysis, the Uncoupled methodology gives a conservative slightly higher value of F.O.S. This pattern is quite different from the ones obtained for model - $SDBN_0$. This may be attributed to the fact that in coupled methodology, as deformation is simultaneously calculated in addition to pore water pressure, it is known that with consequent deformation and rebound during each cycle, there are chances of permanent deformation or rebound after a certain number of cycles as soil is an inelastic material. The magnitude of net deformation or rebound shall determine whether the excess pore water pressure has been generated or dissipated in accumulation at end of each cycle. The above factor shall decide which F.O.S shall be conservative and which not.

The location of groundwater table shall control the degree of saturation and pore water pressures, hence the difference in pattern in F.O.S obtained for both the models by the two different methods, may be attributed to the area of unsaturated zone and magnitude of matric suction developed which differs for both the models.

TABLE - 5.5 : Slip Surface Location, Minimum Factor of Safety, Safety Map for Model $SDBN_{3.5}$ during Rise-Up Stage (t = 1 hr to t = 6 hrs) of Single Tidal Cycle

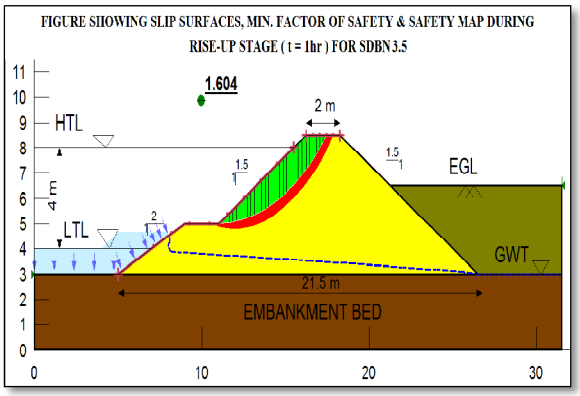

Figure-5.126 : At t = 1 hr, with F.O.S = 1.604

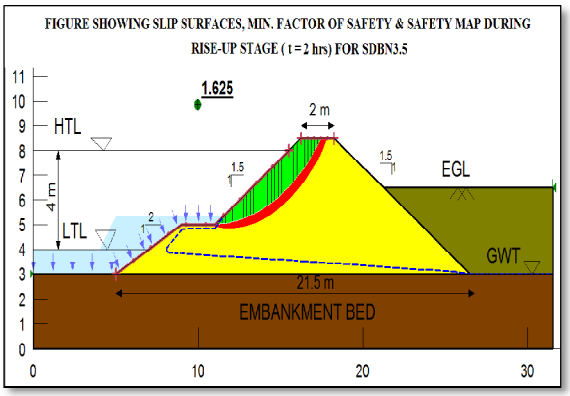

Figure-5.127 : At t = 2 hrs, with F.O.S = 1.625

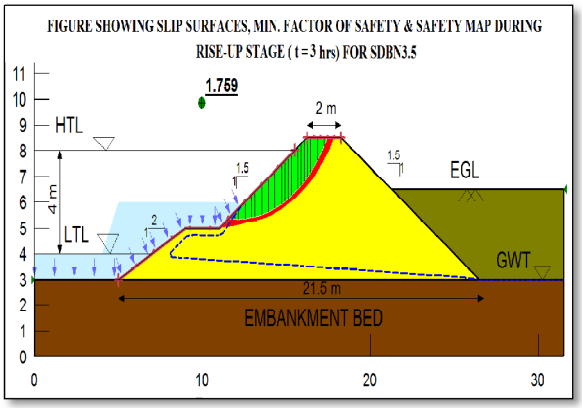

Figure-5.128 : At t = 3 hrs, with F.O.S = 1.759

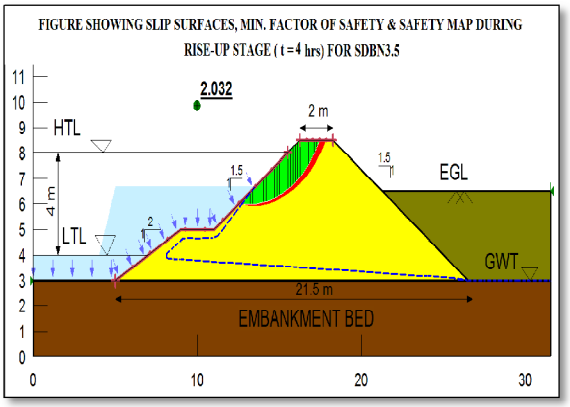

Figure-5.129 : At t = 4 hrs, with F.O.S = 2.032

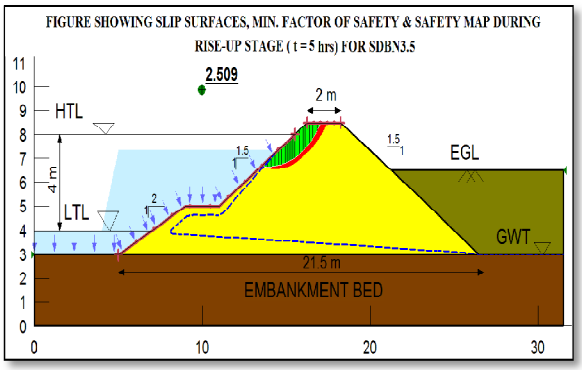

Figure-5.130 : At t = 5 hrs, with F.O.S = 2.509

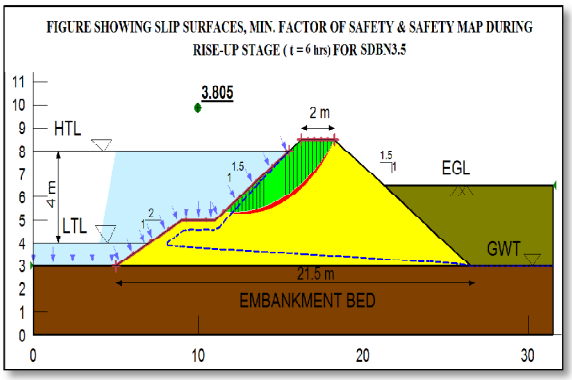

Figure-5.131 : At t = 6 hrs (HTL), with F.O.S = 3.805

TABLE - 5.6 : Slip Surface Location, Minimum Factor of Safety, Safety Map for Model $SDBN_{3.5}$ during Draw-down Stage (t = 7 hrs to t = 12 hrs) of Single Tidal Cycle

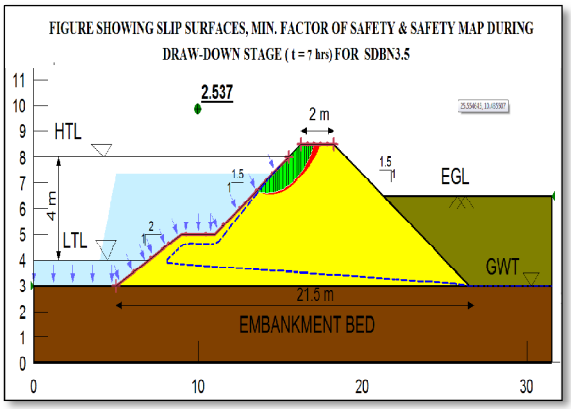

Figure-5.132 : At t = 7 hrs, with F.O.S = 2.537

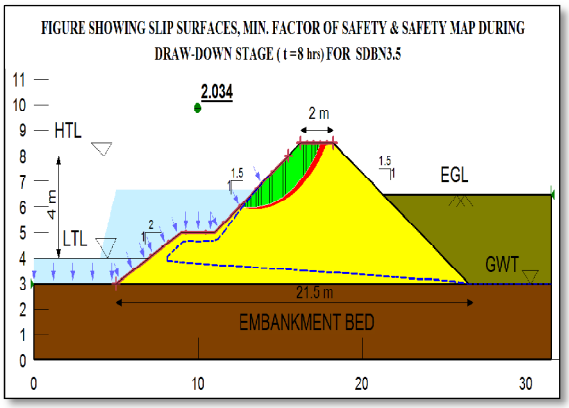

Figure-5.133 : At t = 8 hrs, with F.O.S = 2.034

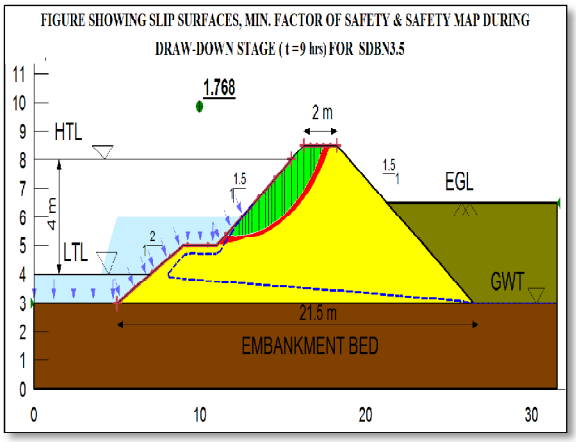

Figure-5.134 : At t = 9 hrs, with F.O.S =1.768

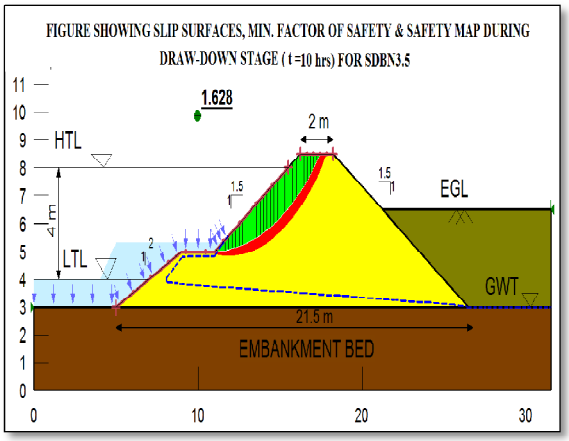

Figure-5.135 : At t = 10 hrs, with F.O.S = 1.628

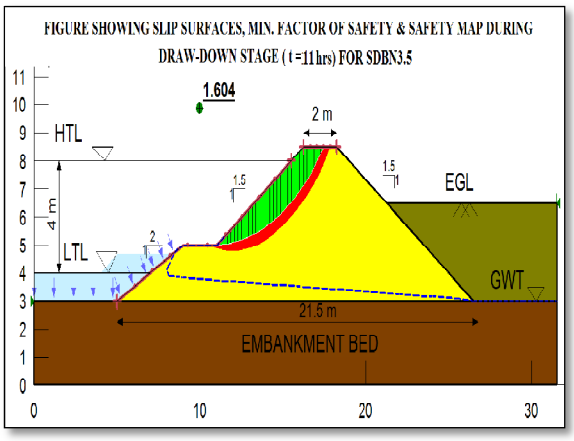

Figure-5.136 : At t = 11 hrs, with F.O.S = 1.604

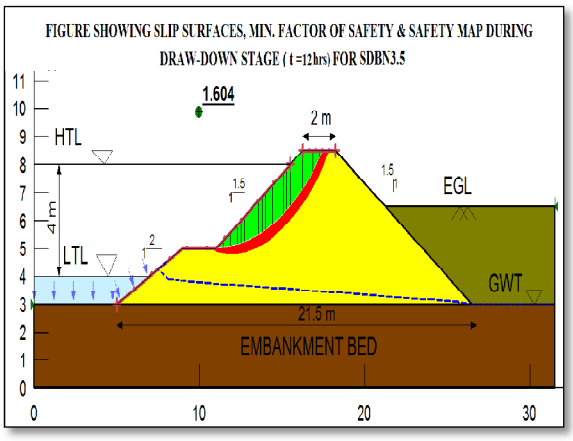

Figure-5.137 : At t = 12 hrs (LTL), with F.O.S =1.604

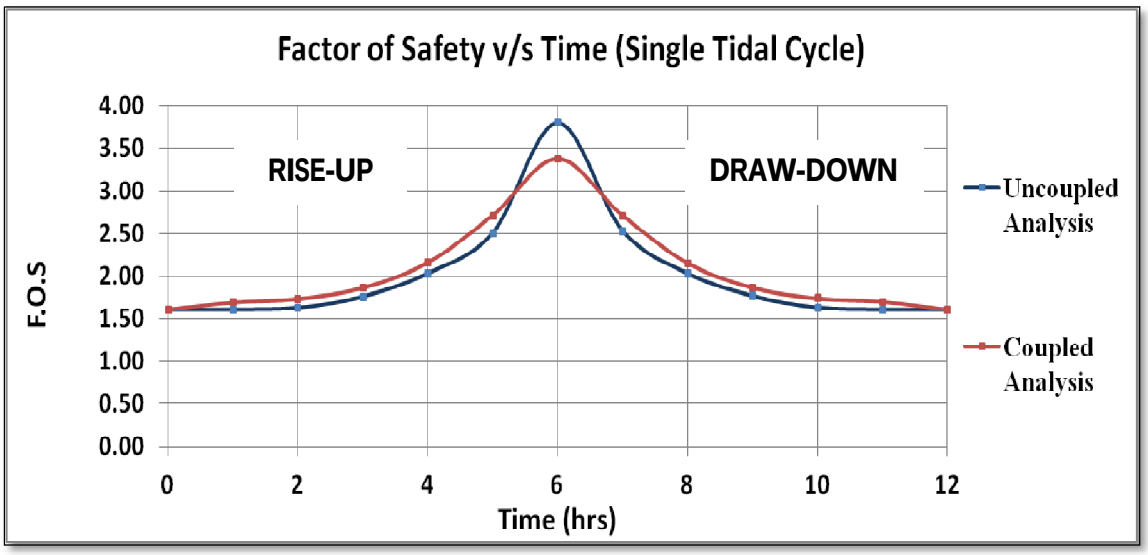

Figure-5.138 : A plot of the F.O.S against Time during a Single Tidal Cycle in Uncoupled and Coupled Analysis respectively for Model $SDBN_{3.5}$

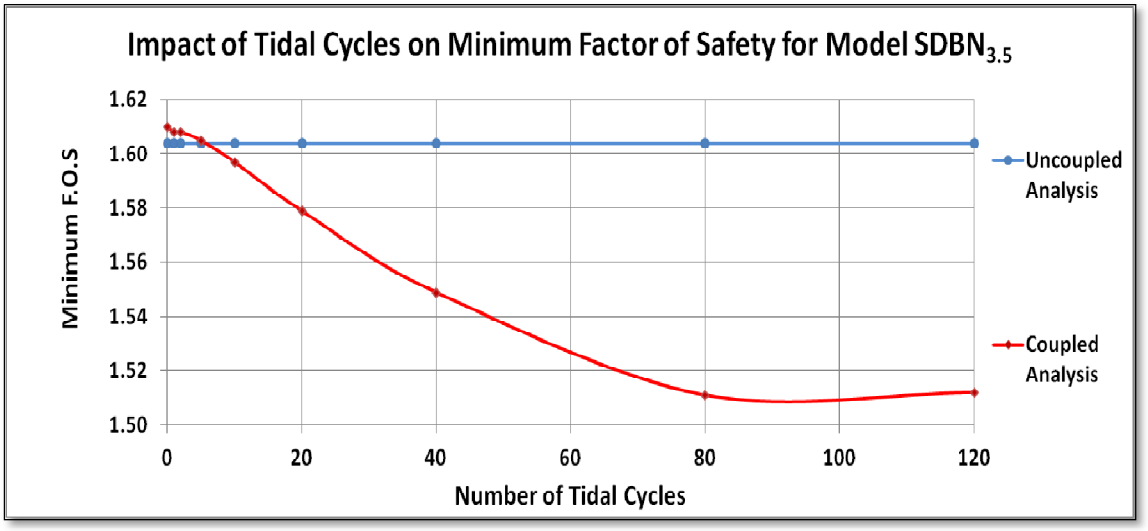

Figure-5.139 : A plot of the Minimum F.O.S against Number of Tidal Cycles for Model $SDBN_{3.5}$

CHAPTER SIX
EXPERIMENTAL PROGRAMME & RESULTS

CHAPTER SIX
EXPERIMENTAL PROGRAMME AND RESULTS

6.1 : GENERAL

An experimental programme was undertaken to study the effect of tide induced transient seepage on earthen embankments. A set-up to study the same was developed and commissioned at the Geotechnical Engineering Laboratory, Civil Engineering Department, Jadavpur University, Kolkata. The details of the set-up are given in the upcoming sub-sections of this chapter. The model selected for study is the typical Sunderban embankment discussed as in Chapter-4.

6.2 : METHODOLOGY

The basics of experimental modeling have been discussed in Chapter-1. The Scale ratio selected for this study is 20. This is based on practical aspects and also controlled by the amount of soil material that could be handled in the laboratory. A seepage tank to simulate plane strain conditions was fabricated accordingly. The details of the tank and method of embankment construction are given in the forthcoming sections.

A Steady State was established between Landside top (EL + 32.5 cm) and the Low Tide Level (EL + 20.0 cm). The riverside tidal effect was simulated on the basis of hydrostatic head which varied with cycle time. The tidal cycle consisting of Rise-Up and Draw-down half cycles were generated by raising and falling the water level from the Low Tide Level (LTL) (EL + 20.0 cm) to the High Tide Level (HTL) (EL + 40.0 cm) and back to the Low Tide Level(EL + 20.0 cm), respectively. This was done with the help of inlet and drainage valves. The time duration of Rise-Up and Draw-down half cycle was varied with subsequent tests. The tidal head was maintained on a linear pattern. Rise-Up Half Cycle time (t_{RU}) is defined as the time duration to complete each Rise-Up half cycle, i.e. time taken by the riverside water to rise from LTL to HTL. Draw-down Half Cycle time (t_{DD}) is defined as the time duration to complete each Draw-down half cycle, i.e. time taken by the riverside water to fall from HTL to LTL. The Full cycle time (t_F) is the summation of the Rise-Up and Draw-Down half cycle time. Cycle Time Ratio is defined as the ratio of the particular time instant to the full cycle time. The Pressure Head was measured at the predefined points at certain time intervals during each tests. Methylene blue Dye was used during the later stage tests to study the flow lines and the Zone of Influence of Rise-Up (ZIR).

6.3 : DEVELOPMENT AND COMMISSIONING OF SEEPAGE SET-UP

6.3.1 : Development of Seepage Tank

A rectangular tank has been fabricated with steel frame, supporting 10 mm thick transparent Perspex sheet on all sides. The dimensions of the tank are 1.4 metre (Length) by 0.15 metre (Width) by 0.525 metre (Height). The main idea was to develop a Plane Strain condition, where the width is very small compared to the length and height of the model, as encountered in 2-D seepage problems. Provision was kept at rear part of the Perspex sheet for insertion of ten number piezometers at specific co-ordinates. The tank was made waterproof by two to three runs of M-Seal followed by GP-Silicone both on the interior and exterior. The water supply to the tank was in the form of a Reservoir of maximum capacity of 30 litres. The reservoir was placed 1.2 metres above the centre of tank and flow from reservoir to tank was by virtue of gravity. A total of three valves – one water inlet valve at river side of tank and two drainage valves - one at the river side and one at the land side of tank respectively were attached to regulate flow in and out of the tank. A linear scale was inked on the sides of the tank for aid during actual construction of the embankment and also during conduction of experiments. The seepage tank has been shown in **Figures** - **6.3, 6.4.**

6.3.2 : Soil Properties

Approximately, 120 kilograms of disturbed soil sample was obtained from Sunderbans embankment site, South 24 Parganas, West-Bengal, courtesy the Irrigation Department, Government of West-Bengal. This soil was utilized for construction of the embankment and preliminary testing for soil properties. The following tests were carried out on this soil between 02.01.2016 to 20.05.2016 –

(i) Attenberg Limit Tests

(ii) Grain Size Distribution and Hydrometer Analysis

(iii) Proctor Density Test

(iv) Falling Head Permeability Test (Conducted at a particular compacted density)

(v) Unconsolidated Undrained Triaxial tests (conducted on undisturbed samples obtained from the constructed embankment at the laboratory)

The properties ascertained by carrying out above mentioned tests on this soil are provided in **Table-6.1**

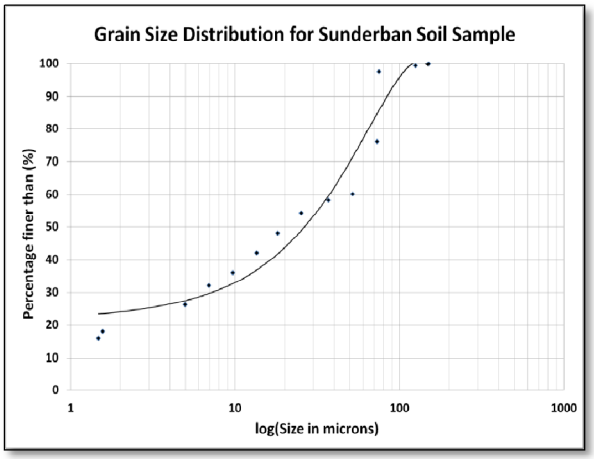

Figure 6.1 – Grain Size distribution of Sunderban Soil Sample used in Laboratory tests

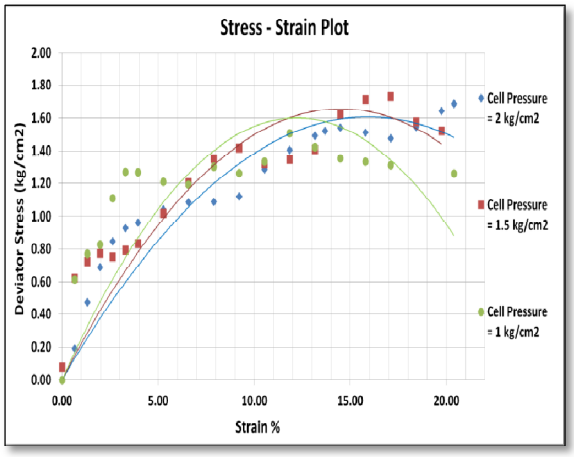

Figure 6.2 – Stress – Strain Plot obtained from UU test for Laboratory Model Embankment

TABLE-6.1 : Soil Properties for Experimental Model

Test Conducted and Property Tested	Result	Remarks
Physical Description	Greyish Silty Clay / Clayey Silt with traces of decomposed wood	Obtained from Sunderban embankment site.
Attenberg Limit Test		
Liquid Limit (%)	40.7	Plasticity Index of 18.6 (greater than 17, Highly Plastic as per IS : 1498-1970
Plastic Limit (%)	22.1	
Shrinkage Limit (%)	19.5	
Wet Sieving and Hydrometer Test		
D_{60} (in microns)	38	**Refer Figure – 6.1** for Grain Size distribution curve
Percentage of Sand (%)	12	
Percentage of Silt (%)	64	
Percentage of Clay (%)	24	
Proctor Density Test		
Maximum Dry Density (kN/m^3)	16.5	
Optimum Moisture Content (%)	17	
Falling Head Permeability Test		
Saturated Hydraulic Conductivity (m/sec)	1.508×10^{-8}	
Unconsolidated Undrained Triaxial Test		
Cohesion, C (kN/m^2)	50	Undisturbed samples collected from the laboratory model
Angle of Internal Friction, Φ (°)	7	
Modulus of Elasticity (kN/m^2)	2397	Obtained by Double tangent method from Stress Strain plot given in **Figure – 6.2**.
Bulk density = 19.52 kN/m^3, Water Content = 26.7 %, Void ratio = 0.71, Porosity = 0.42 (assuming 100 % saturation)		

6.3.3 : Construction of Embankment

The embankment model was developed on the lines of a typical Sunderban earthen Embankment whose dimensions have been discussed in Figure – 4.1 and Table - 4.2. Considering a linear scale of L_r = 20, the embankment was constructed. The embankment was constructed in 5 steps described below, over a span of 1 month.

(i) **Construction of Embankment Bed** : A 15 cm thick bed was constructed in five layers. Initially, the site soil sample including lumps were oven dried. Then the lumps were pulverized and particles with 100 percent passing 4.75 mm sieve were taken. Water was added as per optimum moisture content. Hand mixing was done in small quantities not more than 4 kg of dry soil sample. Compaction was achieved by blows from a Standard Proctor Hammer of 4.5 kg falling over a height of 300 mm. The number of blows was adjusted as per density requirement. The targeted density was as per 95 percent of Proctor density. In places, where dynamic compaction could not be satisfactorily used, static loading in the form of columns of iron block weights were used. In such cases, utmost care was taken to keep the soil layers saturated with water and keeping the side drainage valves open, in order for consolidation and pore pressure dissipation to take place. In such cases, the static loading was kept for 48 hours.

(ii) **Construction of Berm** : As per typical Sunderban embankment model, a berm 10 cm thick was placed at an elevation of 25 cm from base of tank. The side slopes from embankment bed to berm level was kept at 2H : 1V. The density was achieved by methods discussed in above section.

(iii) **Construction of Embankment** : The main embankment was constructed from the berm level to the desired level of 32.5 cm from tank base. The side slopes was kept at 1.5H : 1V. A set of sheet piles were utilized to make the construction process easier. The methods of compaction and consolidation were utilised as discussed above.

The construction stages and the completed embankment have been shown in **Figures 6.5, 6.6, 6.7, 6.8, 6.9**

6.3.4 : Piezometer Set-Up

Ten numbers piezometers were installed for measuring the pore water pressure head. During stage wise construction of the embankment, the mouths of the piezometer pipe connectors embedded in 1 inch diameter sand channels were terminated at pre-determined co-ordinates inside the embankment given in **Table-6.2**. The location of the piezometers have also been shown in **figure-**

6.10. After completion of the embankment construction, scaling graph sheets were attached and developed to the piezometers, with respect to the base of the tank. During conduction of tests, utmost care was taken to rid the piezometer system of air bubbles.

TABLE - 6.2 : Piezometer Positions Inside Embankment constructed in Laboratory

Piezometer Point	Co-ordinates w.r.t tank base (cm)	Remarks
		Origin is left / river side corner at base of tank (Refer Figure – 6.10)
1	(40 , 15)	Riverside portion - Lower Slope Region
2	(60 , 15)	Riverside portion - Berm Region
3	(80 , 15)	Embankment Interior
4	(100 , 15)	Embankment Interior
5	(125 , 15)	Landside portion of embankment
6	(70 , 25)	Riverside portion - Berm Region
7	(90 , 25)	Embankment Interior
8	(110 , 25)	Landside portion of embankment
9	(80 , 32.5)	Riverside portion - Upper Slope Region
10	(100 , 32.5)	Landside portion of embankment

Figure 6.3 – Initial Set-Up of Model Tank

Figure 6.4 – Waterproofing of tank

Figure 6.5 – Stage-1, Construction of Bed

Figure 6.6 – Stage-2, Construction of Berm

Figure 6.7–Stage-3, Construction of Embankment

Figure 6.8 – Completed Embankment

Figure 6.9– 3D view of completed embankment showing river side and land side

6.4 : SCHEME OF EXPERIMENTAL SET UP

The scheme of the set-up has been shown in **Figure -6.10**

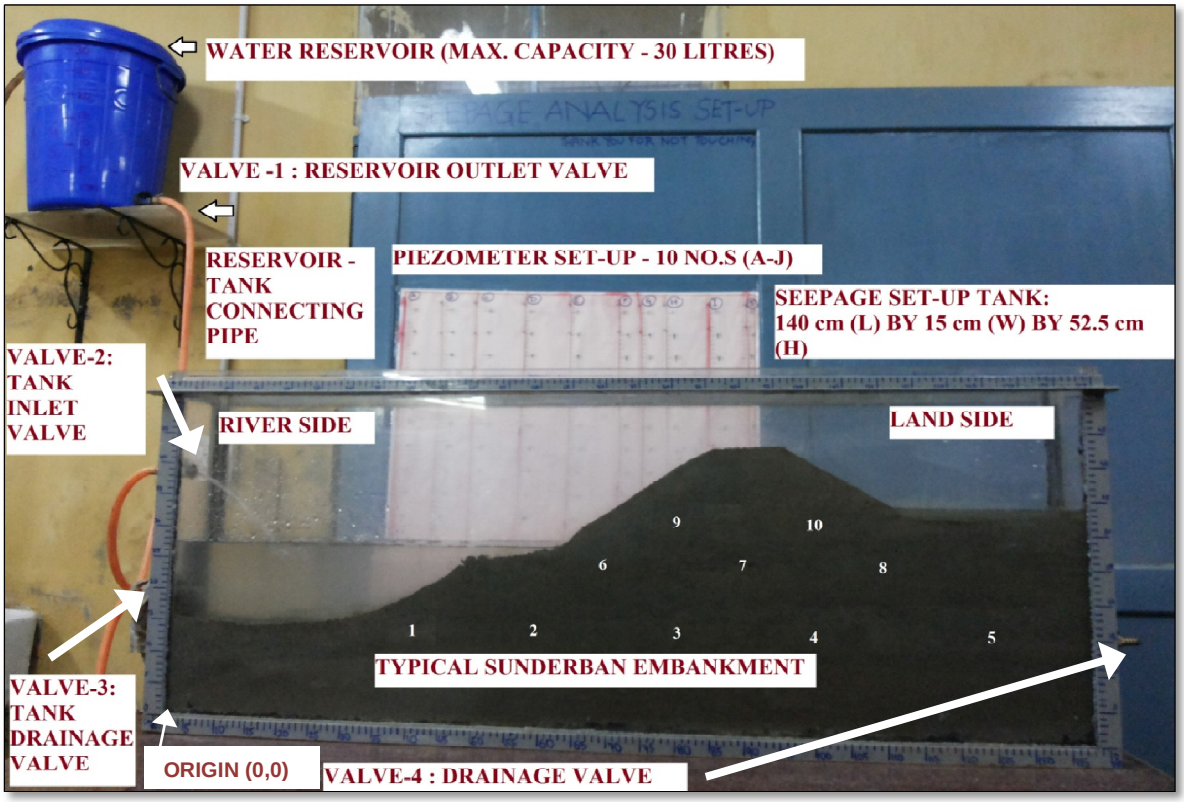

Figure 6.10– Seepage Set-up developed at Geotechnical Engineering Laboratory, Jadavpur University

6.5 : PARAMETRIC STUDY

The main objective of the experimental study was to investigate the effect of the following parameters on the pore water pressure head which was measured at predetermined points 1, 2, 3, 4, 5, 6, 7, 8, 9, 10 (whose co-ordinates have already been discussed in Table – 6.2).

(i) **Rate of Rise-Up and Rate of Draw-Down for Single Cycles**: This was done by varying the Rise-Up Half Cycle time (t_{RU}) and Draw-Down Half Cycle time (t_{DD}) for respective tests. An uniform rate of Rise-Up and Draw-down was maintained for individual tests.

(ii) **Multiple Cycles:** Multiple cycles were performed to study their influence on the pore water pressure head

The details of tests conducted have been shown in **Table – 6.3**

TABLE-6.3 : Parametric Study Tests Conducted in the Laboratory

Serial No.	Nomenclature	Rise-Up Half Cycle Time (t_{RU}) (in minutes)	Draw-Down Half Cycle Time (t_{DD}) (in minutes)	Full Cycle Time (t_F) (in minutes)	Rate of Rise-Up and Draw-Down (cm / min)	Number of Cycles	Remarks
1	$1R_{30}D_{30}$	30	30	60	0.667	1	Single Cycle Tests
2	$1R_{45}D_{45}$	45	45	90	0.444	1	
3	$1R_{60}D_{60}$	60	60	120	0.333	1	
4	$1R_{90}D_{90}$	90	90	180	0.222	1	
5	$1R_{120}D_{120}$	120	120	240	0.167	1	
6	$1R_{150}D_{150}$	150	150	300	0.133	1	
7	$1R_{180}D_{180}$	180	180	360	0.111	1	
8	$3R_{30}D_{30}$	30	30	60	0.667	3	Multiple Cycle Tests
9	$3R_{60}D_{60}$	60	60	120	0.333	3	
10	$3R_{90}D_{90}$	90	90	180	0.222	3	

6.6 : RESULTS AND DISCUSSIONS

The results have been discussed in the sub-sections below

Single Tidal Cycle : Effect of Rise-Up and Draw-Down rate

Zone of Rise-Up Influence (ZIR)

During single cycle tests with different rates of Rise-Up / Draw-Down, the variation in excess pore water head generated has been shown in **Figures – 6.11, 6.12, 6.13, 6.14, 6.15, 6.16, 6.17**. The variation of the Riverside tidal head with respect to cycle time has also been shown in the respective figures. The LTL has been kept at zero position and only the increase and decrease in river water level from LTL to HTL and HTL to LTL is plotted. The Zone of Rise-Up, defined in Chapter-5, can be clearly identified by the co-ordinates of the points which show a variation in pore water pressure (PWP) head during the tidal cycle. It has been seen that portions of the Lower Slope, Berm Region and Upper Slope fall within the ZIR showing variation in PWP head during the tidal cycle, however there are portions in the interior of the embankment which donot show any change as is evident from the figures.

Pore Water Pressure Head

It has been observed that the maximum variation in PWP head has been recorded for the Lower Slope region followed by the Berm Region, Upper Slope and Interior portions of the embankment. It has been seen that in the Lower Slope region, there is an initial gradual increase in PWP head

during Rise-Up, followed by a sharp steep increase near the half cycle time zone, which is followed by a decrease in PWP head during Draw-Down. However, the rate of decline in PWP during Draw-down has been observed to be much lower than its Rise-Up component. The degree of steepness during the half cycle time zone increases with decrease in rate of tidal cycle (which is equal to the rate of Rise-Up and Draw-Down). Moreover, there is a time lag between the HTL and the maximum PWP head developed in the Lower Slope region. The time lag increases with decrease in rate of tidal cycle and is maximum for $1R_{180}D_{180}$. At the end of a single cycle, it has been observed that there is a net gain in PWP head for all portions within the Zone of Rise-Up Influence, compared to the initial condition. The magnitude of net gain in PWP head is maximum for slowest cycle rate.

Separate plots have been developed in **Figures-6.18, 6.19, 6.20, 6.21**, to study the effect of tidal rate on individual embankment zones – Lower Slope, Berm Region, Upper Slope and Interior of Embankment. It has been observed that the maximum variation in PWP head is observed in the Lower Slope Region followed by other zones. The maximum variation in PWP head during a single tidal cycle is observed for $1R_{180}D_{180}$, i.e. the test with the minimum rate of Rise-up and Draw-down. Interestingly, the Lower Slope Region is the only portion where there is a decrease in PWP head after a certain peak value is attained. The same continues till the end of tidal cycle. However, at other points representing Berm Region, Upper Slope, there is continuos increase in PWP head with no decline, throughout the entire tidal cycle. The rate of increase is significantly less compared to the Lower Slope Region.

Multiple Tidal Cycles

Pore Water Pressure Head

The effect of multiple cycles have been shown in **Figures 6.22, 6.23, 6.24**. The Excess River Water Head has also been shown in the figure. It is interesting to note that the point representing the Lower Slope region has shown maximum variation in PWP head, showing cycles of increase and decrease in PWP head with corresponding Rise-Up and Draw-Down half cycles. The magnitude of variation became significantly higher for lower rate of tidal cycle (in this case $3R_{90}D_{90}$). For the Berm Region, Upper Slope there is only increase in PWP head during the entire multiple cycle range, with head building up with each consecutive cycle but at a very small rate compared to the Lower Slope. The Interior of the embankment showed negligible changes during multiple cycles.

In the later stages, blue dye was injected on the riverside to observe the transient flowlines on the River- Embankment Interface. The depth of penetration of dye varied from 3 – 5 mm in the Upper

Slope and Berm Region. The Lower Slope had a higher depth of penetration of 10 – 15 mm which increased with multiple cycles. This has been shown in **Figures -6.27, 6.28(a)(b)**

Deformation

Deformation cracks were observed in the Lower Slope after multiple tests had been conducted. This is shown in Figures - Figures -6.27, 6.28(a)(b). A zone of possible deformation was clearly developing with each subsequent cycle in the above mentioned region. This may be explained by the fact that this region undergoes both build up and release of PWP head during each tidal cycle. This phenomenon is usually accompanied by settlement during build up of PWP and rebound during release of PWP. Consecutive cycles of settlement and rebound can result in formation of cracks in plastic soils, as seen in this region.

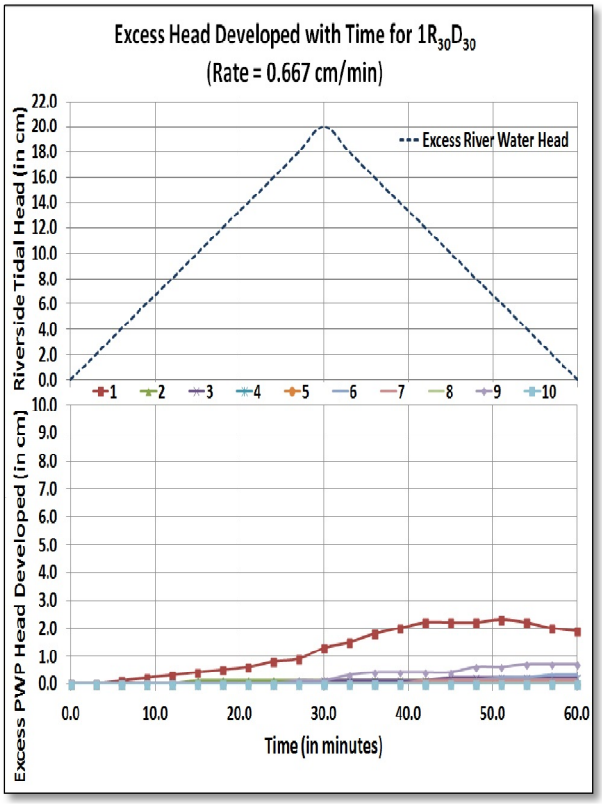

Figure 6.11 – Excess PWP Head v/s Tidal Cycle Time for $1R_{30}D_{30}$

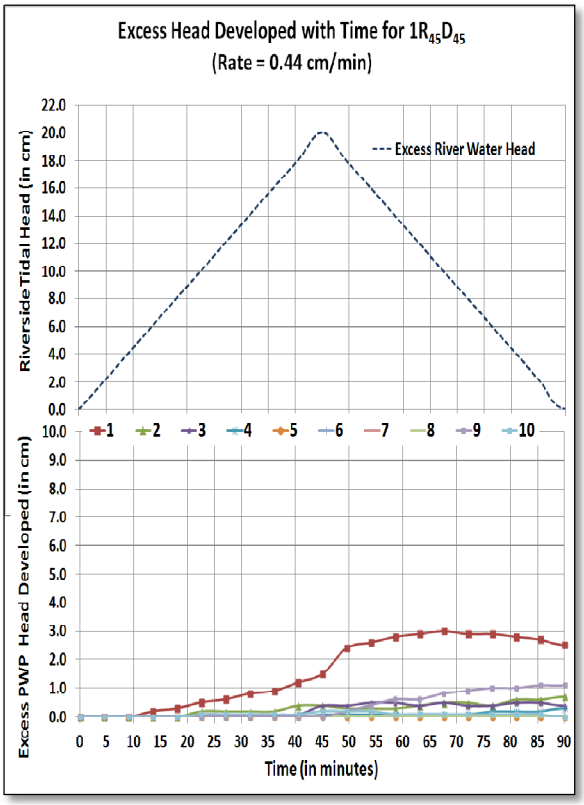

Figure 6.12 – Excess PWP Head v/s Tidal Cycle Time for $1R_{45}D_{45}$

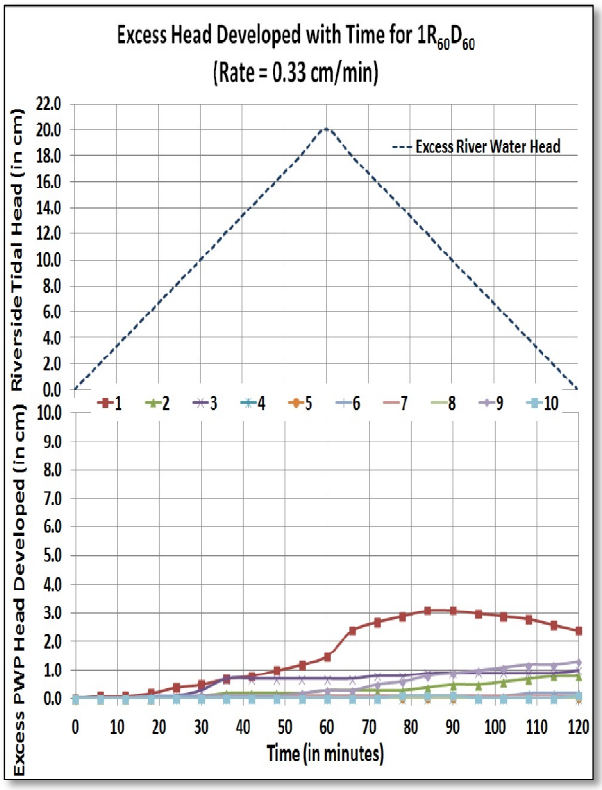

Figure 6.13 – Excess PWP Head v/s Tidal Cycle Time for $1R_{60}D_{60}$

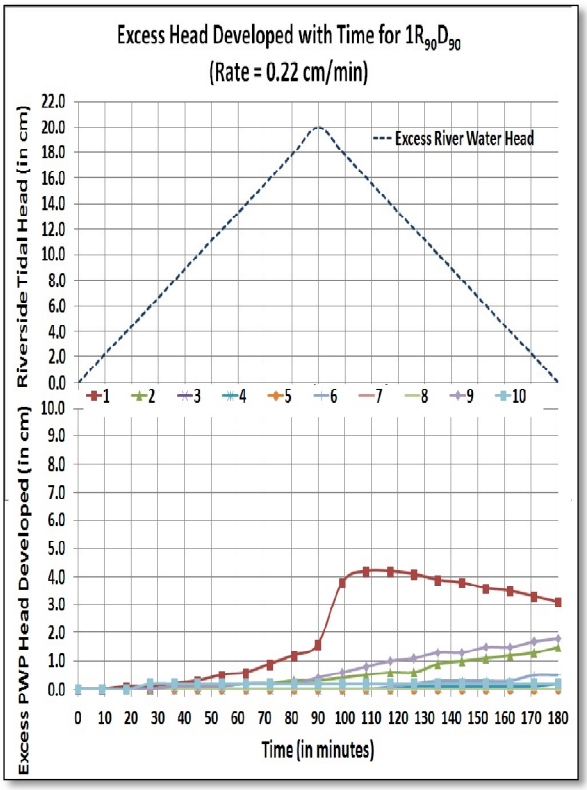

Figure 6.14 – Excess PWP Head v/s Tidal Cycle Time for $1R_{90}D_{90}$

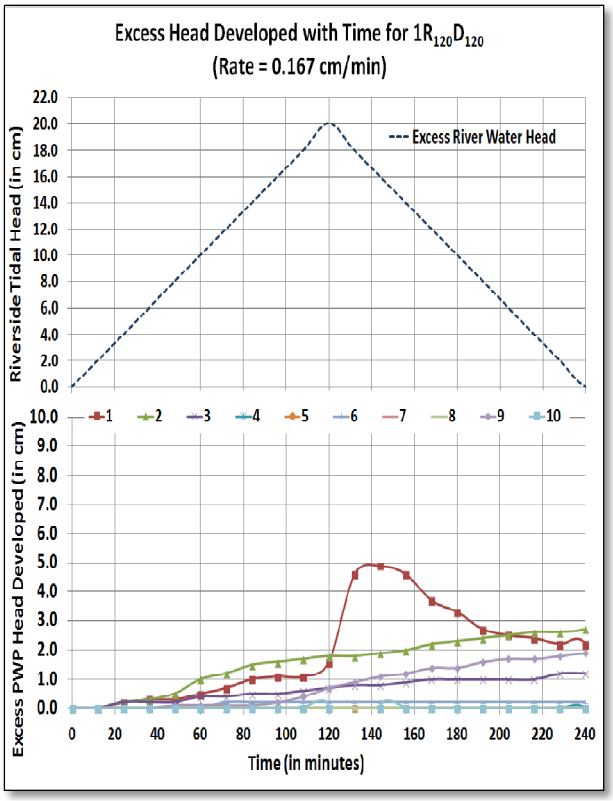

Figure 6.15 – Excess PWP Head v/s Tidal Cycle Time for $1R_{120}D_{120}$

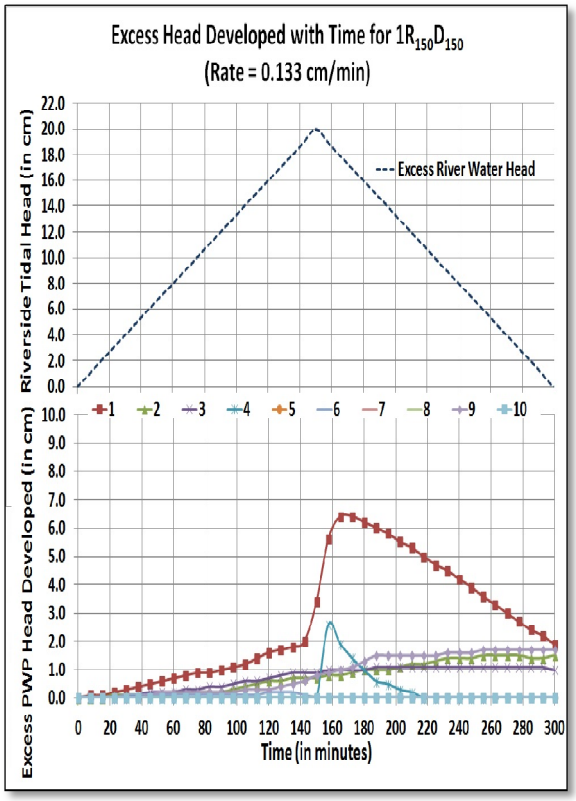

Figure 6.16 – Excess PWP Head v/s Tidal Cycle Time for $1R_{150}D_{150}$

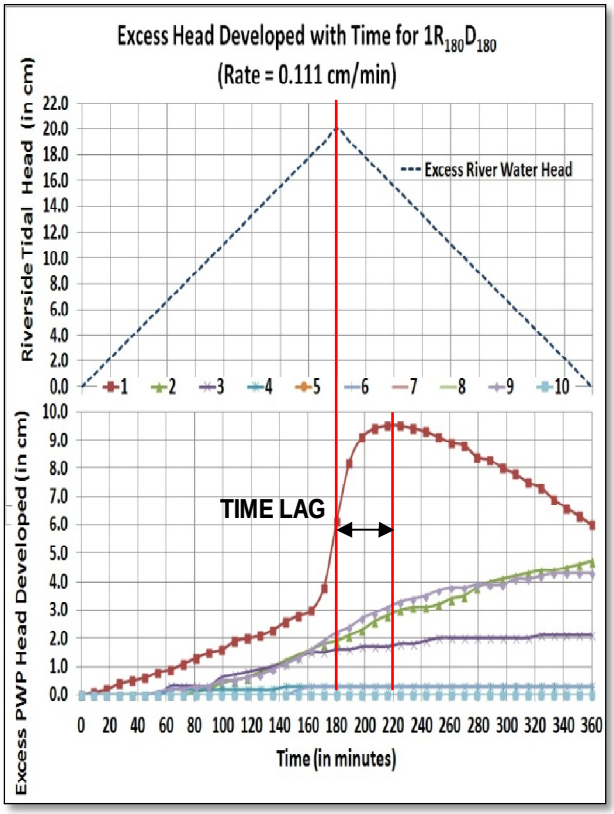

Figure 6.17 – Excess PWP Head v/s Tidal Cycle Time for $1R_{180}D_{180}$

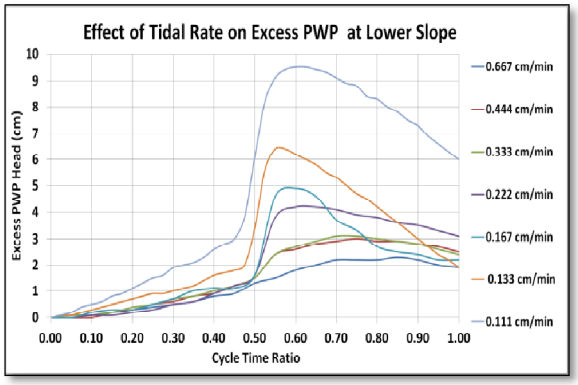

Figure 6.18 : Effect of Tidal Rate on the Excess PWP developed in the Lower Slope

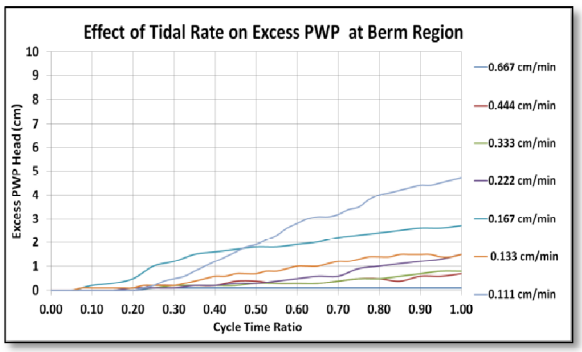

Figure 6.19 : Effect of Tidal Rate on the Excess PWP developed in the Berm Region

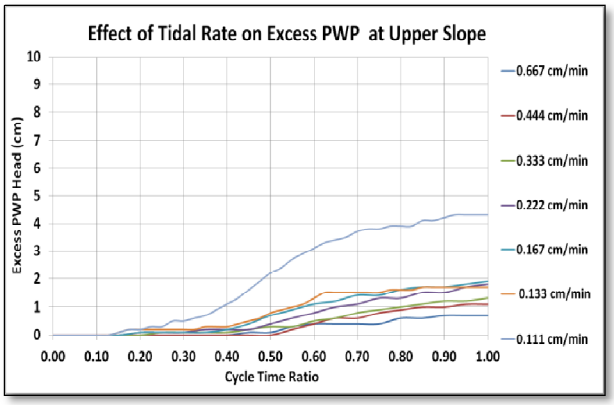

Figure 6.20 : Effect of Tidal Rate on the Excess PWP developed in the Upper Slope

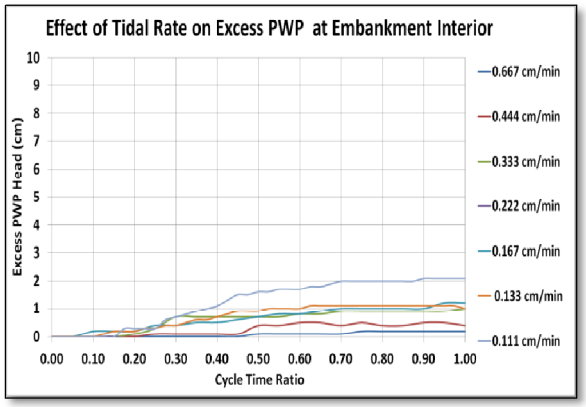

Figure 6.21 : Effect of Tidal Rate on the Excess PWP developed in the Embankment Interior

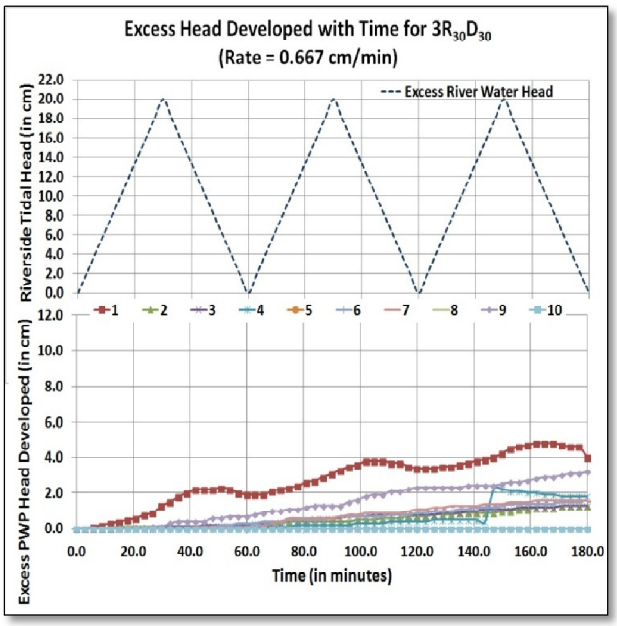

Figure 6.22 – Excess PWP Head during Multiple Cycles for $3R_{30}D_{30}$

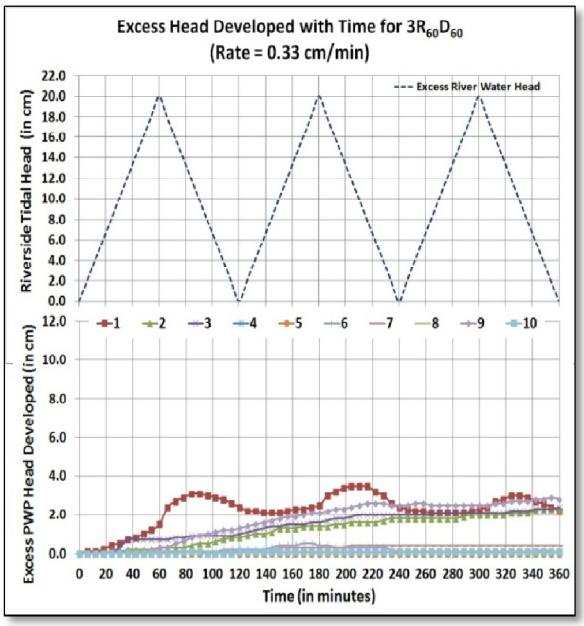

Figure 6.23 – Excess PWP Head during Multiple Cycles for $3R_{60}D_{60}$

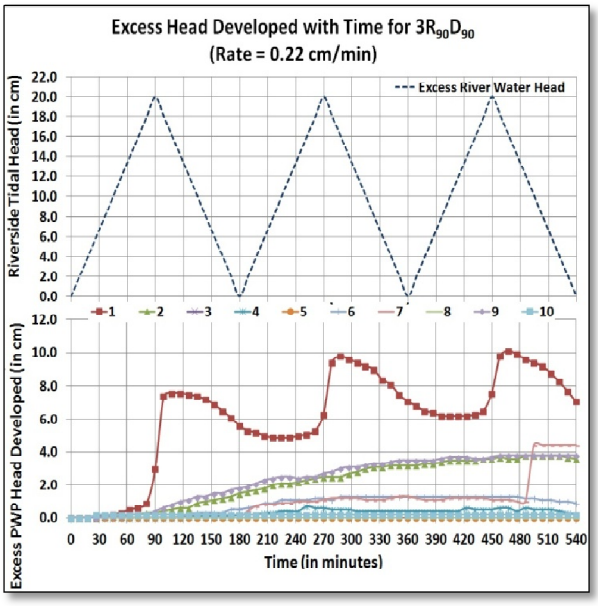

Figure 6.24 – Excess PWP Head during Multiple Cycles for $3R_{90}D_{90}$

Figure 6.25 : Low Tide Position with Excess River Water Head = 0 cm

Figure 6.26 : High Tide Position with Excess River Water Head = 20 cm

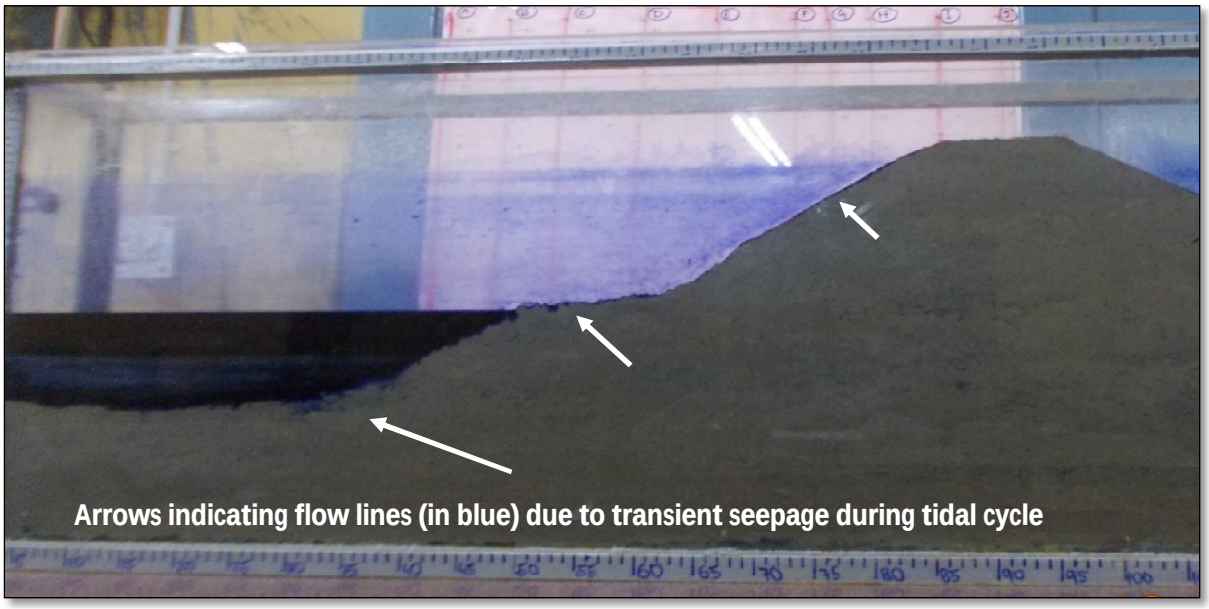

Figure 6.27 : The flowlines (shown in blue colour) due to Transient seepage during Tidal Cycle are visible. Maximum penetration has been seen in the Lower Slope Region

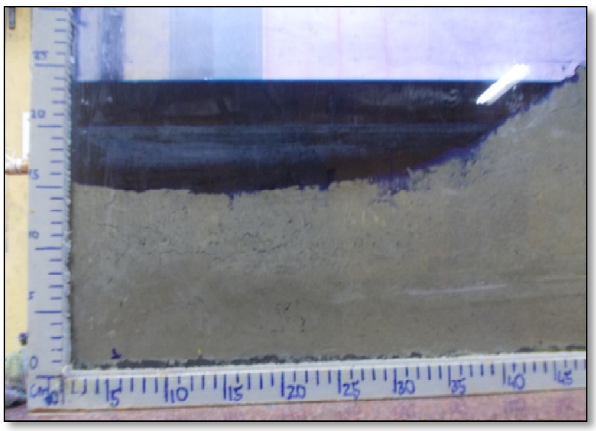

Figure 6.28 (a) : Magnified view of Lower Slope showing development of cracks after multiple tidal cycles

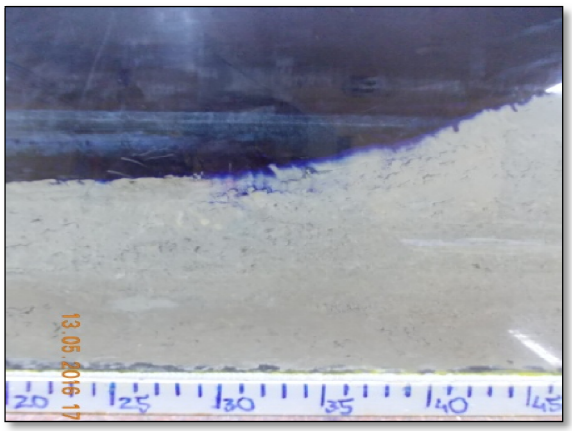

Figure 6.28 (b):Magnified view of Lower Slope showing development of deformation zone after multiple tidal cycles

CHAPTER SEVEN
VALIDATION AND DISCUSSIONS

CHAPTER SEVEN
VALIDATION AND DISCUSSIONS

7.1 : METHODOLOGY

An effort has been made to compare and validate the results obtained from the Numerical and Experimental Analysis. The suggestive patterns have also been compared with the field observations. It is to be mentioned that in the Numerical Analysis, the soil parameters were selected as per previous bore log data report from the Patharpratima site, whereas in the Experimental Analysis, the soil collected from site was separately analysed for basic properties.

A linear scaling was done to obtain the Laboratory model. A length scale ratio of L_r =20 was used in the construction of the model. As the major forces associated with both the prototype and model are the Gravity force and the Inertia force, the Froude Methodology for Scaling was adopted. On basis of the scaling ratio, the other important scale ratios are given in **Table-7.1** .

Table -7.1 : **Scaling Ratio as per Froude Scaling Methodology**

Length Scale Ratio	Time Scale Ratio	Velocity Scale Ratio	Discharge Scale Ratio	Pressure Scale Ratio
20	4.47	4.47	1788.85	20

The experimental results have been scaled for comparison purposes. As per Table-7.1, it was seen that using Froude methodology, the full cycle tidal rate in the model should be 0.249 cm/min (i.e. lies between 0.22 cm/min and 0.33 cm/min rate tests conducted in the laboratory) to simulate the field prototype tidal rate of 0.667 m/hr which has also been used in the full scale numerical analysis. The results selected from the numerical analysis are based on the model $SDBN_0$. The coupled analysis results were used for the comparison with the experimental results.

7.2 : VALIDATION

The results have been shown in **Figures - 7.1, 7.2, 7.3**. for the Lower Slope, Berm and Upper Slope region. The maximum and minimum rate of tide cycle used in the experimental scheme has also been shown in the above mentioned figures. It may be noted that the experimental observations for the different regions are based on representative number of piezometric points which were limited in number. The parameter wise discussions are given in the following sub sections

Pore Water Pressure Head Variation

The observations are given pointwise as -

(i) For the Lower Slope region, both the numerical and experimental analyses have shown that the pore water pressure increases during the Rise-Up half cycle and decreases during the Draw-Down half cycle. The maximum variation in the pore water pressure during a single cycle is encountered in this region, when compared with the Berm and Upper Slope portions. At the end of a single cycle, there is net build up of pore water pressure compared to the initial condition. It was observed that the numerical and experimental results showed close matching in the magnitude of excess pore water pressure head at the end of single tidal cycle (at Cycle Time Ratio = 0.80 – 1.0) for the scaled tidal rate. Experimentally, a non-linear variation pattern was obtained for lower rates and almost linear pattern was observed at higher rates. The variation pattern during each half cycle is obtained as linear in the numerical analysis, where a high tidal rate of 0.667 m/hr is simulated. A time lag was recorded between the High Tide Level occurring at exact half cycle time and the instant at which peak value was recorded for the Lower Slope region only. The magnitude of time lag decreased with increase in tidal rate. However, this time lag was not observed in the numerical analysis which may be attributed to the fact that the tidal rate in both field and numerical is 0.667 m/hr which is quite high, so the time lag magnitude is negligible.

(ii) In the Berm Region and Upper Slope, both the numerical and experimental results have shown a comparative lower variation in pore water pressure head when compared to the Lower Slope. The pore water pressure increases during the Rise-Up half cycle and decreases during the Draw-Down half cycle in the numerical analysis whereas the experimental results have shown gradual build up of the same without any decline. There was a net gain in pressure head after the end of the cycle with reference to their initial condition, which is indicated in both numerical and experimental analyses. Both analyses showed close matching in the magnitude of excess pore water pressure head at the end of single tidal cycle (at Cycle Time Ratio =0.75 - 1) for the scaled tidal rate.

(iii) The interior parts of the embankment lying outside the Zone of Influence of Rise-Up did not show any variation in pore water pressure during the tidal cycle. This was observed in both numerical and experimental results.

(iv) For Multiple Tidal Cycles**,** the experimental analysis has shown cyclic pore pressure build up and release, with a cumulative effect in pore pressure build up at the end of each consecutive cycle for the Lower Slope region. In other sections like Berm and Upper Slope, there was only cumulative build up of Pore Water Pressure throughout multiple cycles. The observation was made for 3

cycles. The numerical results have shown similar trends for the initial cycles and after a certain number of initial cycles, the pore water pressure became constant more or less for higher number of cycles. .

Deformation

The numerical analysis showed major settlement and rebound of several points lying in the Lower Slope and Berm region with cumulative action of permanent deformation after multiple tidal cycles. Such deformation and serviceability failure was observed in the laboratory with cracks and fissures developing in the Lower Slope region after multiple tests had been conducted. This is also in accordance with the field data where numerous failure zones have been identified in the Lower Slope region.

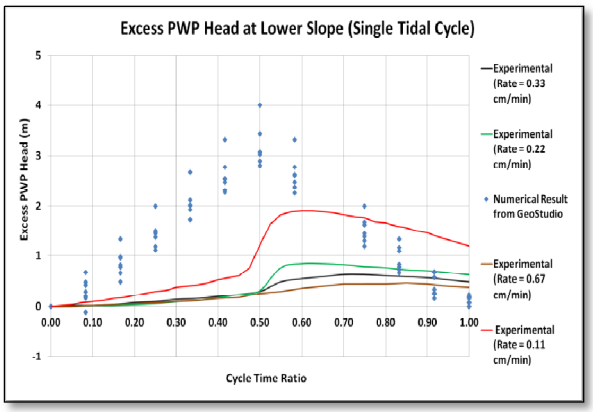

Figure 7.1 : Comparison of Results for Excess PWP in Lower Slope for Single Cycle

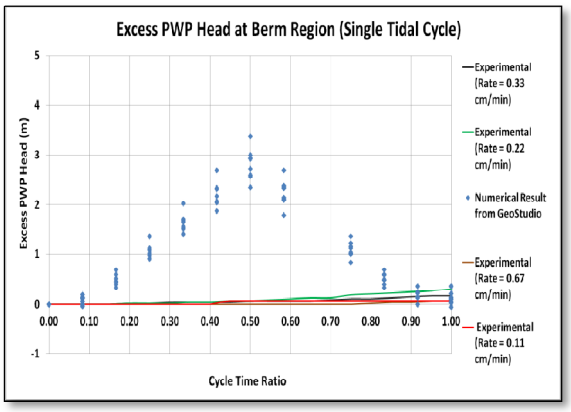

Figure 7.2 : Comparison of Results for Excess PWP in Berm Region for Single Cycle

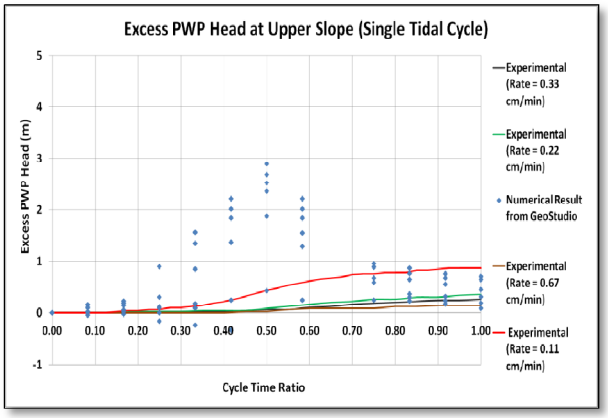

Figure 7.3 : Comparison of Results for Excess PWP in Upper Slope for Single Cycle

7.3 : DISCUSSION ON THE SUNDERBAN PROBLEM

At various sites of Sunderbans like Patharpratima, Gosaba, Namkhana, Sagar Bamankhali, Sonakhali, etc, deformation failure has been observed in the Lower Slope region of the embankment. The same has been shown in Figure-4.4. It is observed from numerical and experimental analyses that both pore water pressure and deformation variation is maximum for this region in comparison to others. Development of fissures and cracks have been observed in the lower slope region of the laboratory model during conduction of cycle tests. It has been seen that this region experiences both build up and release of pore water pressure during tidal cycles, thereby leading to cyclic settlement and rebound. Sunderban embankments face 720 tidal cycles approximately per year. As soil is predominantly clayey silt which is plastic in nature, it is evident that permanent deformation shall take place after multiple number of cycles. Hence considering the huge number of cycles to the tunes of 10^3 to 10^4 that these embankments are exposed to during their design life, there is a good probability of serviceability failure. It may be noted that major portions of other regions like Berm, Upper Slope only show a very slow build up in pore water pressure along tidal cycle and there is almost no pressure release, eliminating the rebound and overall settlement – rebound cycle, thus are less prone to serviceability failure.

CHAPTER EIGHT
CONCLUSIONS AND FUTURE SCOPE OF WORK

CHAPTER EIGHT
CONCLUSIONS AND FUTURE SCOPE OF WORK

8.1 : CONCLUSIONS

The following conclusions were drawn from this study –

(i) The position of the phreatic surface in a riverfront earthen embankment is affected by the transient seepage induced by tidal water. Multiple cycles have a cumulative effect on the phreatic surface, but within a certain zone from the river embankment interface.

(ii) Transient seepage induced by Cyclic Tidal Head has a dominant effect on the pore water pressure distribution within an earthen embankment. The pore water pressure becomes a function of time for areas lying within the Zone of Influence of Rise-Up. The areas lying outside the Zone of Influence of Rise-Up are un-affected by the cyclic tidal head.

(iii) Coupled Seepage Analysis of an earthen embankment involving the estimation of deformation and pore water pressure simultaneously is extremely important and gives field oriented results. The probability of Serviceability failure can be ascertained from this type of analysis.

(iv) Zones within an earthen embankment that experience both build up and release of pore water pressure within a tidal cycle are more prone to Serviceability failure, even though the Stability Factor of Safety may be quite adequate. This is due to the plastic nature of soil.

(v) The location of the Land Groundwater Table controls the initial conditions and the zone of saturation and unsaturation within the embankment and hence has an effect on the Transient seepage parameters.

(vi) In a typical Sunderban earthen embankment, the Lower Slope region is more prone to serviceability failure compared to the Berm region and Upper Slope region. This is due to tide induced cyclic hydrostatic loading on the riverside part of the embankment resulting in cyclic settlement and rebound of the plastic soil, leading to permanent deformation.

8.2 : FUTURE SCOPE OF WORK

The following work may be carried out in the future as a continuation of the present study.

(1) **Experimental programme**

(a) Higher number of cycles may be taken up. The set-up may be modified to record deformation and pore water pressure simultaneously.

(b) The effect of salinity may also be studied in the experimental scheme.

(2) **Numerical Analysis**

(a) A 3-D model may be developed for the Typical Sunderban Embankment and similar analysis carried out taking into consideration anisotropy.

(b) The role of precipitation may be included in future models, with inclusion of precipitation and infiltration parameter to investigate the stability of slopes of the Sunderban embankment during various seasons.

(3) The effect of groundwater - surface water interaction in Sunderban embankments during tidal cycles may be studied.

(4) An creek based analysis considering embankment on both sides, with upliftment of river bed may be modeled, for better results.

REFERENCES

- Aral Mustafa M., and Maslia Morris L. (1983), "Unsteady Seepage Analysis Of Wallace Dam", J. Hydraul. Eng.109, pp.809-826.

- Aubertin M., Ricard J. F., and Chapuis R. P. (1998), "A predictive model for the water retention curve: Application to tailings from hard rock mines", Can. Geotech. J., 35(1), pp.55–69

- Aubertin M., Mbonimpa M., Bussière B. and Chapuis R.P., (2003), "A model to predict the water retention curve from basic geotechnical properties", Canadian Geotechnical Journal, 40(6), pp.1104-1122

- Athania Shivakumar S. , Shivamanth , Solanki C. H. and Dodagoudar G. R. (2015), "Seepage and Stability Analyses of Earth Dam Using Finite Element Method" , International Conference On Water Resources, Coastal And Ocean Engineering (Icwrcoe 2015)), Elsevier , Aquatic Procedia 4, pp.876 – 883

- Bansal R.K. "A Textbook of Fluid Mechanics & Hydraulic Machines"

- Bhandari Gupinath, (2011), "Report on the Soil Investigation Work for Construction of Proposed G+3 Storied Multipurpose Cyclone Shelter (MCS) at Government 283 ICDS Centre, Kuimuri, Patharpratima, 24 Parganas (S), Paschimbanga"

- Bhandari Gupinath, (2011), "Report on the Soil Investigation Work for Construction of Proposed G+3 Storied Multipurpose Cyclone Shelter (MCS) at Bally Kamalachak F.P. School, Bally-II, Gosaba, 24 Parganas (S), West Bengal"

- Biot M.A., (1941), "General theory of three-dimensional consolidation", Journal of Applied Physics, Volume 12, pp. 155-164.

- Bishop, A.W., (1955), "The Use of the Slip Circle in the Stability Analysis of Slopes", Geotechnique V, No.1, pp.7-17

- Boufadel M. C., Suidan M. T., Venosa A. D., and M. T. Bowers J. (1999), "Steady seepage in trenches and dams : Effect of capillary flow", Hydraulic. Eng., ASCE, vol 125

- Boufadel Michel C., Suidan Makram T.,Venosa Albert D. (1999), "Effect of Unsaturated Flow on Steady Seepage"

- Chang Ching S , (1987), "Boundary Element Method In Drawdown Seepage Analysis For Earth Dams", J. Comput. Civ. Eng.1, pp.83-98.

- Cresswell, H. P., and Paydar, Z. (1996), "Water retention in Australian soil, description and prediction using parametric functions." Austral, J. Soil Res., 34_2, pp.195–212.

- Darcy, H. (1856), "Les Fontaines Publiques de la Ville de Dijon", Dalmont, Paris.

- Das. B .M , 'Advanced Soil Mechanics & Foundations'

- Das Barun Kr. (2005), "A Preliminary Study on Identification of Probable Causes of Failure of Existing Earthen Embankments around Sunderban" (Thesis submitted for Masters' Degree at Jadavpur University , Kolkata)

- Desai C.S, Abel John, (1987), "Introduction to the Finite Element Method – A Numerical Method for Engineering Analysis" , CBS Publications

- Desai C.S, (1988), "Case Studies through Material Modeling and Computation" , 2nd International Conference on Case Histories in Geotechnical Engineering, Missouri University of Science & Technology,

- Dey Jhumur, (2010), "Estimation of Pore Water Pressure Distribution and Saturated Zone in a Tidal Water Front Embankment" (Thesis submitted for Masters' Degree at Jadavpur University , Kolkata)

- Department of the Army Corps of Engineers, U.S.Army, "Engineering & Design : Seepage Analysis and Control for Dams"

- Dupont E., Dewals B.J, Archambeau P. Erpicum S, Pirotton M., "Experimental and Numerical Study of the Breaching of an Embankment Dam"

- Fredlund, D.G., Morgenstern, N.R., (1976), "Constitutive Relations for Volume Change in Unsaturated Soils", Canadian Geotechnical Journal, , Vol. 13, pp. 261-276.

- Fredlund, D.G., Morgenstern, N.R., (1977), "Stress State Variables for Unsaturated Soils", ASCE, Vol.103, pp. 447-464.

- Fredlund, D.G., Rahardjo, H. , (1993), "Soil Mechanics for Unsaturated Soils", John Wiley & Sons, Inc.

- Fredlund, D. G., Xing., (1994), "Equations for the soil-water characteristic curve", Canadian Geotechnical Journal. Vol. 31, pp.521-532.

- Fredlund, M. D., Fredlund, D. G., and Wilson, G. W., (1997), "Prediction of the soil-water characteristic curve from grain size distribution and volume-mass properties." Proc., 3rd Brazilian Symp. on Unsaturated Soils, Rio de Janeiro, Brazil

- Green, R.E. and Corey, J.C., (1971), "Calculation of Hydraulic Conductivity : A Further Evaluation of Some Predictive Methods", Soil Science Society of America Proceedings, Vol. 35, pp. 3-8.

- GEO-SLOPE International Ltd, (2012), "Seepage Modeling with SEEP/W, an engineering methodology"

- GEO-SLOPE International Ltd, (2012), "Stability Modeling with SLOPE/W, an engineering methodology"

- Hansen David and Roshanfekr Ali, (2012), "Assessment of Potential for Seepage-Induced Unraveling Failure of Flow-Through Rockfill Dams", Int. J. Geomech.12, pp.560-573

- Harr M.E., (1962), "Groundwater & Seepage" , Mcgraw Hill (USA)

- Huang Yang H., (1986), "Unsteady State Phreatic Surface in Earth Dams", Journal of Geotechnical Engineering, Vol. 112, No. 1

- Hutson J. L., and Cass, A., (1987), "A Retentivity Function For Use In Soil Water Simulation Models", Soil Sci., 38(1), pp.105–113,

- Janbu, N., (1954), "Application of Composite Slip Surfaces for Stability Analysis", Proceedings of European Conference on Stability of Earth Slopes, Sweden, pp-43-49

- Jia G.W, Zhan Tony L.T, Chen Y.M , Fredlund D.G, (2009), "Performance of a large-scale slope model subjected to rising and lowering water levels", Elsevier Engineering Geology 106, pp. 92-103

- Johari.A, Habibagahi. G., Ghahramani. A., (2006), "Prediction of Soil–Water Characteristic Curve Using Genetic Programming", J. Geotech. Geoenviron. Eng., 132(5), pp.661-665

- Khalilzad Mahdi , Gabr M. A., and Hynes Mary Ellen, (2014), "Deformation-Based Limit State Analysis of Embankment Dams Including Geometry and Water Level Effects", Int. J. Geomech 04014086,pp.1-11

- Krahn John, "Stress and Deformation Modeling with SIGMA/W – An Engineering Methodology"

- Lane P. A., Griffiths D. V , (2000), "Assessment Of Stability Of Slopes Under Drawdown Conditions", J.Geotech. Geoenviron. Eng.126, pp.443-450

- Li G. C., Desai C. S., (1983), "Stress And Seepage Analysis Of Earth Dams", Journal of Geotechnical Engineering, pp .946-960

- López, Acosta N.P., Fuente de la H.A., Auvinet G., (2013), "Safety of a protection levee under rapid drawdown conditions. Coupled analysis of transient seepage and stability", Proceedings of the 18th International Conference on Soil Mechanics and Geotechnical Engineering, Paris

- Marinho, A.M.F, (2005), "Nature of Soil Water Characteristic Curve for Plastic Soils" , Journal of Geotechnical & Geoenvironmental Engineering, ASCE

- Moayed R. Ziaie, Rashidian V., Izadi E., "Evaluation of Phreatic Surface in Homogenous Dams with different drainage systems", Innovative Dam & Levee Design and Construction, pp.619-626

- Morgenstern, N.R., and Price, V.E., (1965), "The Analysis of the Stability of General Slip Surfaces", Geotechnique, Vol. 15, pp. 79-93.

- Ozkan, Senda., Donald, D Adrian., (2008) "Analytical Construction of Transient Flow Nets in Homogenous and Isotropic Flow Medium" , J. Geotech. Geoenviron. Eng..134, pp.888-893.

- Ozkan, Senda., Donald D. Adrian., Sills George L., Singh Vijay P., (2008), "Transient Head Development due to Flood Induced Seepage under Levees", J. Geotech. Geoenviron. Eng.,134(6), pp.781-789

- Potts David M., Dravkovic Lidija, "Finite Element Analysis in Geo-technical Engineering – Theory", Thomas Telford Publishing

- Rakhshandehroo G. R., Pourtouiserkani A., (2013), "Predicting Doroodzan Dam Hydraulic Behavior During Rapid Drawdown", IJST, Transactions of Civil Engineering, Vol. 37, No. C2, pp. 301-310

- Sachpazis Costas I., (2014), "Experimental Conceptualization of the Flow Net System Construction inside the Body of Homogeneous Earth Embankment Dams", EJGE, pp. 2113-2136

- Simulia Abaqus, (2007), "Construction, Rapid Drawdown and Earthquake Simulation of an Earthen Dam", TB-03-DAM-1

- Singh .Bharat., Sharma .H.D., (1976) , "Earth and Rockfill Dams", 1st edition

- Spencer, E., (1967), "A Method of Analysis of the Stability of Embankments assuming parallel inter-slice forces", Geotechnique XVII, No.1, pp.11-26

- Thieu, N.M., Fredlund, M.D., Fredlund, D.G., Hung, V.Q. (2001), "Seepage Modeling in a Saturated / Unsaturated Soil System" , International Conference on the Management of Land and Water Resources, MLWR , Hanoi, Vietnam

- Tomasella, J., and Hodnett, M. G., (1998), "Estimating soil water retention characteristics from limited data in Brazilian Amazonia.", Soil Sci.,163(3), pp.190–202

- U.S Department of Agriculture, Soil Conservation Service Engineering Division, (1979), "The Mechanics of Seepage Analyses"

- VandenBerge Daniel R., Duncan J. Michael and Brandon Thomas L. , (2015), "Limitations of Transient Seepage Analyses for Calculating Pore Pressures during External Water Level Changes", J. Geotech. Geoenviront. Eng.141

- Van Genuchten, (1980), "A closed-form equation for predicting the hydraulic conductivity of unsaturated soils", Masters' Thesis, Soil Science Society of America Journal 44, pp.892-898.

- Xu G. M., L. Zhang and Liu S. S., (2005), "Preliminary Study of Instability Behavior of Levee on Soft Ground during Sudden Drawdown", Slopes and Retaining Structures Under Seismic and Static Conditions

- Zapata,Claudia E., Houston, William N. , Houston, Sandra L., Walsh , Kenneth D. , "Soil-Water Characteristic Curve Variability", Advances in Unsaturated Geotechnics, pp.84-124

- Zheng Y. R., Shi W. M., Kong W. X. , Lei W. J., (2005), "Determination of the phreatic-line under reservoir drawdown condition" , Slopes and Retaining Structures Under Seismic and Static Conditions